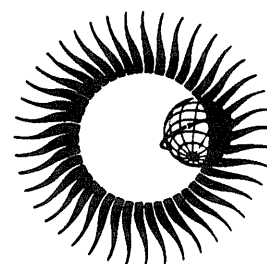# WORLD DATA CENTER A
for
Solar-Terrestrial Physics

IONOSONDE NETWORKS AND STATIONS

Proceedings of Session G6 at the
XXIVth General Assembly of the
International Union of Radio Science (URSI)
Kyoto, Japan, August 25-September 2, 1993

January 1995

NATIONAL GEOPHYSICAL DATA CENTER

POINT ARGUELLO   (35.6 N , 239.4 E)   0800 LT   03/06/73

WORLD DATA CENTER-A

COORDINATION OFFICE
World Data Center-A: Coordination Office
National Academy of Sciences
2101 Constitution Avenue, NW
Washington, D.C. 20418, U.S.A.
Tel: 202-334-3368
WWW: http://www.ngdc.noaa.gov/wdcmain.html

ATMOSPHERIC TRACE GASES
World Data Center-A: Atmospheric Trace Gases
Carbon Dioxide Information Analysis Center
Oak Ridge National Laboratory
Oak Ridge, Tennessee 37831-6335, U.S.A.
Tel: 615-574-0390 (fax:-2232)

GLACIOLOGY
World Data Center-A: Glaciology (Snow and Ice)
Cooperative Institute for Research in Environmental
Sciences, Campus Box 449
University of Colorado
Boulder, Colorado 80309, U.S.A.
Tel: 303-492-5171 (fax:-2468)
Email: brekke@kyros.colorado.edu
WWW: http://nsidc.colorado.edu

MARINE GEOLOGY AND GEOPHYSICS
World Data Center-A: Marine Geology and Geophysics
National Geophysical Data Center
NOAA, E/GC3
325 Broadway
Boulder, Colorado 80303, U.S.A.
Tel: 303-497-6141 (fax:-6513)
Email: info@ngdc.noaa.gov
WWW: http://www.ngdc.noaa.gov

METEOROLOGY
World Data Center-A: Meteorology
National Climatic Data Center
NOAA, E/CC
Federal Building
Asheville, North Carolina 28801, U.S.A
Tel: 704-271-4682 (fax:-4246)
WWW: http://www.ncdc.noaa.gov

OCEANOGRAPHY
World Data Center-A: Oceanography
National Oceanographic Data Center
NOAA/NESDIS, E/OC23
1825 Connecticut Avenue, NW
Universal Building, Room 409
Washington, D.C. 20235, U.S.A.
Tel: 202-606-4507 (fax:-4586)
Email: wdca@nodc.noaa.gov
WWW: http://www.nodc.noaa.gov

PALEOCLIMATOLOGY
World Data Center-A: Paleoclimatology
National Geophysical Data Center
NOAA, E/GC
325 Broadway
Boulder, Colorado 80303, U.S.A.
Tel: 303-497-6146 (fax:-6513)
Email: info@ngdc.noaa.gov
WWW: http://www.ngdc.noaa.gov

REMOTELY SENSED LAND DATA
World Data Center-A: Remotely Sensed Land Data
U.S. Geological Survey
EROS Data Center
Sioux Falls, South Dakota 57198, U.S.A.
Tel: 605-594-6142 (fax:-6150)

ROCKETS AND SATELLITES
World Data Center-A: Rockets and Satellites
National Space Science Data Center
NASA/Goddard Space Flight Center,Code 633
Greenbelt, Maryland 20771, U.S.A.
Tel: 301-286-6695 (fax:-0587)
WWW: http://nssdc.gsfc.nasa.gov

ROTATION OF THE EARTH
World Data Center-A: Rotation of the Earth
TSEO, U.S. Naval Observatory
Washington, D.C. 20392-5100, U.S.A.
Tel: 202-653-1509 (fax:-0587)

SEISMOLOGY
World Data Center-A: Seismology
National Earthquake Information Center
U.S. Geological Survey, P.O. Box 25046
Denver Federal Center, Mail Stop 967
Denver, Colorado 80225, U.S.A.
Tel: 303-273-8440

SOLAR-TERRESTRIAL PHYSICS
World Data Center-A: Solar-Terrestrial Physics
National Geophysical Data Center
NOAA, E/GC2
325 Broadway
Boulder, Colorado 80303, U.S.A.
Tel: 303-497-6324 (fax:-6513)
Email: info@ngdc.noaa.gov
WWW: http://www.ngdc.noaa.gov

SOLID-EARTH GEOPHYSICS
World Data Center-A: Solid Earth Geophysics
National Geophysical Data Center
NOAA, E/GC1
325 Broadway
Boulder, Colorado 80303, U.S.A.
Tel: 303-497-6521 (fax:-6513)
Email: info@ngdc.noaa.gov
WWW: http://www.ngdc.noaa.gov

World Data Center-A was established in the United States under the auspices of the National Academy of Sciences. WDC-A is operated with national resources, but follows ICSU guidelines. The National Academy of Sciences has overall responsibility through the Geophysics Research Forum and its Committee on Geophysical Data. WDC-A consists of a Coordination Office and nine sub-centers at scientific institutions in various parts of the United States. Most WDC-A sub-centers are at corresponding national data centers, whose large national collections are available through the WDC-A sub-centers.

Organizations wishing to contribute data or establish exchange agreements should contact the appropriate World Data Center-A.

WORLD DATA CENTER A
for
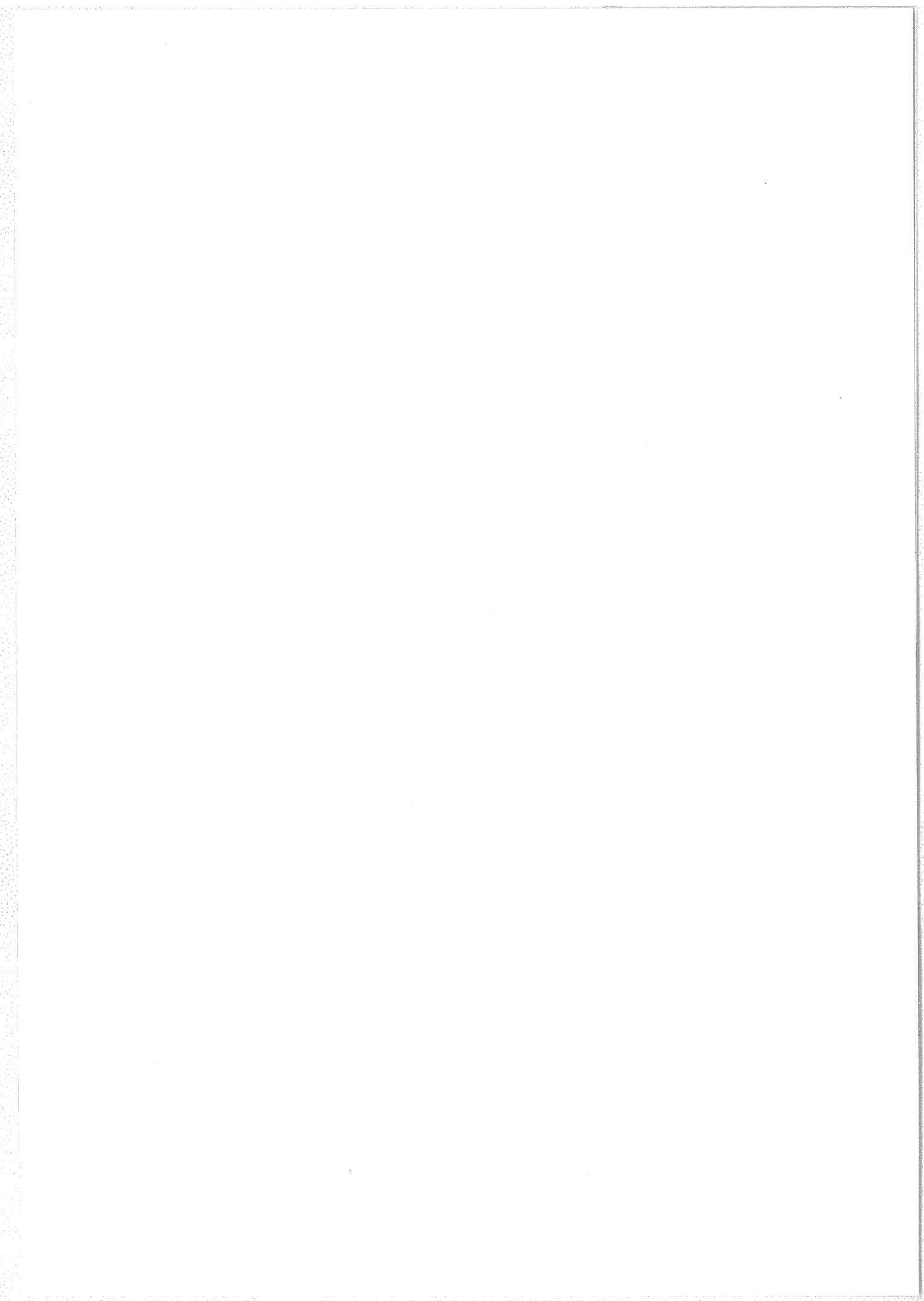## Solar-Terrestrial Physics

IONOSONDE NETWORKS AND STATIONS

Proceedings of Session G6 at the XXIVth General Assembly of the International Union of Radio Science (URSI) Kyoto, Japan, August 25-September 2, 1993

Edited by

Phil Wilkinson
IPS Radio and Space Services
P.O. Box 5606, West Chatswood
Australia

IONOSONDE NETWORKS AND STATIONS

Proceedings of Session G6 at the XXIVth General Assembly of the
International Union of Radio Science (URSI)

TABLE OF CONTENTS

Introduction

This collection of papers forms the bulk of the papers that were presented, either orally or as Poster papers, at the 1993 Kyoto URSI General Assembly session sponsored by the URSI Commission G Working Group INAG (Ionosonde Network Advisory Group).

The ionosonde has been used to measure ionospheric information for over fifty years. During much of this time it has been a routine instrument, data often being processed months after recording. For long term measurements of the climate of the ionosphere this is adequate. However, it is now inescapable that if ionosonde stations cannot offer a more timely service, so the data can be used in near real time, then they will cease to be funded. This situation has been developing over the last decade and has both positive and negative aspects to it. On the negative side, many ionosonde stations are now threatened with closure because upgrading of equipment to deliver real time data is economically unrealistic. Some indication of these problems are presented in the papers by Baker and Shirochkov.

On the other hand, more modern ionosondes, coupled with automatic scaling methods and a greater appreciation of the value of real time ionospheric data show this challenge can be met. The potential that can be realised with modern ionosondes is demonstrated in papers by Reinisch and Buchau et. al. New ionosondes are discussed in MacDougall et. al. and Akchyurin et. al. while Titheridge outlines a low cost method for upgrading a film based IPS-42 ionosonde to record digital records. Several papers (Pulinets, Igi et. al., Poole et. al., Vugmeister et. al. and Bakhitzhqan et. al.) discuss automatic processing of ionosonde records in varying degrees of detail accompanied by comments on applications for the data. Applications of ionosonde data for frequency management (Lynn) forecasting)Minullin et. al.), climate monitoring (Eliseyev) and as a new ionosonde site (Shaptev) are discussed. These papers offer views regarding the future deployment and use of ionosonde data in a range of applications.

Allied with these papers are papers on techniques, eg. Nozaki, and new analysis methods for the data recorded (Tsai et. al., Denisenko et. al. and Weixing Wan et. al.). Several papers report on the results of analysing ionosonde data to improve forecasting methods (Gulyaeva, Bowman and Igarashi et. al.) and for improving models (Chong et. al., Shun-rong Zhang et. al. and Bradley et. al.). Finally, two papers develop oblique propagation (Blagoveshchensky et. al.) and transionospheric propagation (Danilkin) ideas.

The ionosonde has already made a valuable contribution to our knowledge of the ionosphere and it is hoped it will continue to make an equally valuable and enlarged contribution in the years to come. This collection of papers offers an insight into the wide range of ways ionosonde collection and data use is changing in response to changing economic times.

Thank you to all the Referees!

I was assisted in the production of this report by several referees. In a number of cases the efforts of the referee could have earned them a place on the authorship list. The referees were:

Paul Argo, Cecelia Askew, Basil Briggs, John Bennett, Gordon Bowman, Peter Bradley, Mike Buonsanto, David Cole, Ray Conkright, Ken Davies, Peter Dyson, Anthony Finn, Matthew Fox, Yin-Nien Huang, John Kennewell, Ken Lynn, Kenro Nozaki, Bruce Paterson, Allon Poole, Allan Rodger, Haim Soicher, John Titheridge, David Whitehead, Zuo Xiao, K C Yeh, Bruno Zolesi

My thanks to all these people for the time they gave. I also would like to thank Lyn Vincent for entering several of the papers and dealing with formats that refused to cooperate.

Dr Phil Wilkinson
Chair, INAG
IPS Radio and Space Services
AUSTRALIA.
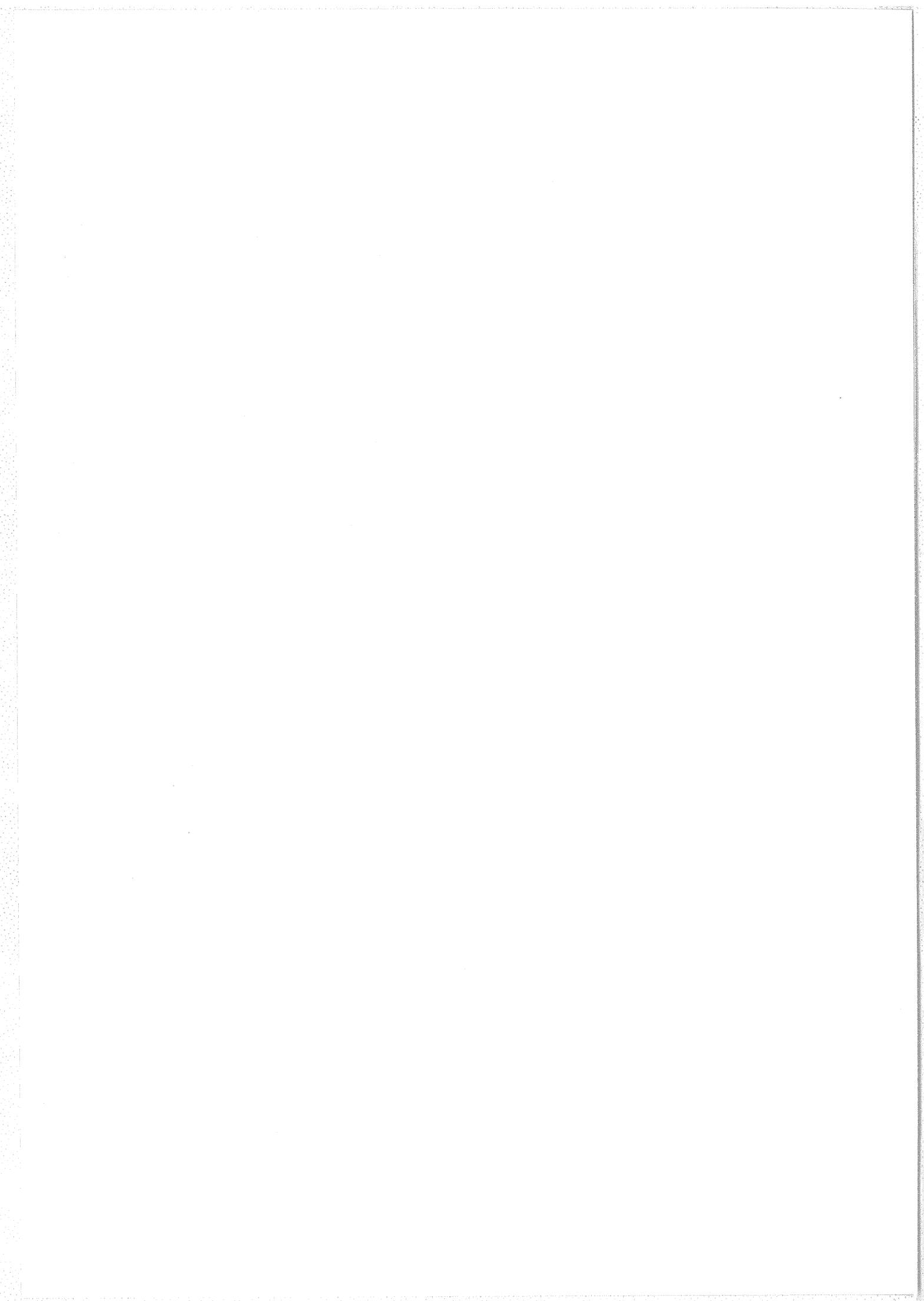
IONOSONDE STATIONS IN SOUTHERN AFRICA - A REVIEW OF CURRENT STATUS AND FUTURE PROSPECTS

Prepared by: Duncan C. Baker, Department of Electrical and Electronic Engineering, University of Pretoria, 0002 Pretoria, South Africa.
E-mail: duncan.baker@ee.up.ac.za

Introduction

This short note briefly sketches the history of the operation of ionosondes in South Africa and Namibia. It also discusses the various types of ionosondes used in the past and those available for use at present. The current situation is cause for concern to ionospheric researchers and local operators of HF communications equipment. A more optimistic long term scenario with mutually beneficial cooperation between states in Southern Africa, and possibly further North in Africa, is described.

One of the problems in preparing a review such as this is the paucity of information readily available on the establishment and subsequent history of ionospheric stations. It is believed that South Africa is not unique in this regard. Operators of ionosonde stations are urged to record the history and main events at the stations at the same time for future reference.

Historical Review
National Institute for Telecommunications Research (NITR)

The provision of HF predictions in South Africa dates back to the Second World War. The earliest published reference to a continuing HF prediction service during the post-war years is dated 1947 [1].
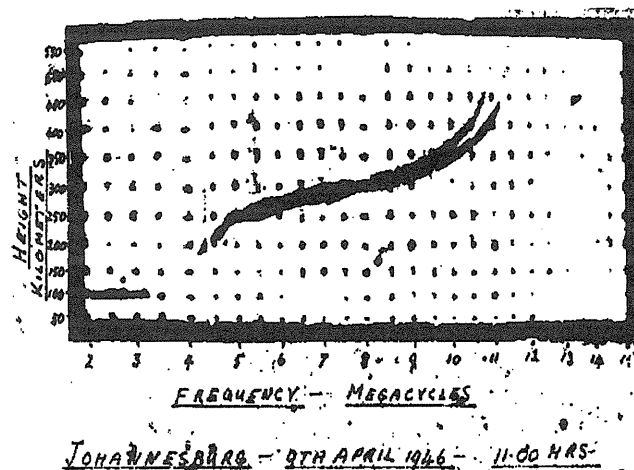
First ionogram recorded with the Wadley ionosonde [2] at the University of the Witwatersrand. After Mercer [3], courtesy of Rhodes University. Contrast enhanced using digital image processing.

The first ionospheric station in South Africa for synoptic studies was established near the Johannesburg city centre in May 1946. Regular ionospheric data were, however, recorded at Durbanville, near Cape Town, from September 1944 to January 1946 [1]. The equipment at Johannesburg was a single sweep pulse ionosonde which was developed locally [1,2] by Dr Trevor Wadley, the inventor of the Tellurometer, at the Telecommunications Research Laboratory (later the NITR) of the Council for Scientific and Industrial Research (CSIR). Figure 1 [3] shows the first ionogram recorded with the Wadley ionosonde at the University of the Witwatersrand, Johannesburg on the 9th of April, 1946. After several years this station

was moved to Frankenwald, about 18 kilometres to the north-northeast. A second station for regular synoptic studies was established near Cape Town during 1948 [2]. It was equipped with similar equipment to that at Johannnesburg. Antennas used at both stations were multiple vertical rhombics on a 60 metre lattice mast made of pieces of creosoted pine timber. Both stations were operated by the NITR of the CSIR. The NITR was recently incorporated into the MIKOMTEK Division of the CSIR in Pretoria during reorganisation of the Council.

At the beginning of May 1971, the station near Cape Town was relocated to the Magnetic Observatory at Hermanus, approximately 100 kilometres to the southeast. One of the reasons was that the original lattice mast had become unserviceable - this after about twenty years with minimal maintenance. Bearing in mind the coastal climate, this is a remarkable testimony to the durability of wooden creosoted masts.

During 1981 the ionosonde at Frankenwald, by now extensively modified but still retaining many of the old valve components and still operational after some 35 or so years, was replaced by a KEL 42 ionosonde. A BR Comms. chirp ionosonde (Chirpsounder) was purchased for use in a vertical incidence and oblique sounding program during the mid 1980's, but not implemented for various reasons. The ionosonde at Hermanus had been replaced by a locally developed transistorised one during the 1970's. During 1982 this station was also equipped with a KEL 42 ionosonde.

The Johannesburg and Hermanus stations continued in operation until March, 1993 when they were essentially mothballed due to lack of operating funds.

The NITR also established an ionospheric station on Marion Island, in the South Indian Ocean, during the IGY of 1957/1958. The ionosonde was manufactured by COSSOR of Canada. The station on Marion Island was temporarily re-opened sometime during 1972 using a locally developed transistorised ionosonde. The station operated with variable reliability till May 1980 when it was closed.

In addition to the above, NITR also took over some of the responsibilities for the running of the station at Tsumeb, in Namibia, during the 1970's.

Rhodes University, Grahamstown

As far as can be established, the first use of ionosondes for ionospheric research at Rhodes University, Grahamstown, dates back to the mid 1940's when a home-built instrument was used to study the partial eclipse of the sun on 14 January 1945 [4].

The Physics Department at Rhodes University in Grahamstown established an ionospheric research station there during the 1957/58 IGY. The equipment was built by members of the Department using plans for the original ionosonde developed by the NITR [2]. The station operated intermittently for a number of years for research purposes and has been operating on a regular synoptic basis since July 1972. Current equipment is a BR Comms. Chirpsounder which has been modified and improved under the guidance of Dr Allon Poole [5,6]. This station is currently the only one operating on a regular basis in South Africa.

During 1962 Rhodes University's Department of Physics began its Antarctic ionospheric research programme when a sounder was installed at Sanae Base in Antarctica by the author. Establishment of the station took place at the same time as the new base was being built. Consequently the first ionograms were only observed during June of that year using the refurbished COSSOR ionosonde, which had originally been installed by the NITR on Marion Island. This ionosonde was used until April 1975, when a BR Comms. Chirpsounder was installed. This made it possible to make oblique soundings between Sanae and Grahamstown. These oblique soundings were phased out during 1987. Ionospheric observations at Sanae were discontinued in February, 1990. Information on the Antarctic research program and a discussion of other local ionospheric research efforts can be found in articles by Gledhill [7] and Poole [8].

At present ionospheric research at Rhodes University is conducted by the Hermann Ohlthaver Institute for Aeronomy, with Dr Allon Poole as its Director.

Tsumeb, Namibia

From about 1964 an ionospheric station was operated at Tsumeb by the Max Planck Institute for Aeronomy in Germany. Apart from an involvement with the running of the station and data handling in the late 1970's by the NITR, this station operated independently. As far as can be established this station continued in operation until the mid to late 1980's.

Present Status

Operations of the Johannesburg and Hermanus stations were discontinued by MIKOMTEK in March, 1993 for financial reasons. The stations can be operated on request. At present the only active station which can be used for synoptic data, is the one at Grahamstown. Ionospheric research at both Rhodes University and the University of Pretoria are continuing, but at a relatively low level.

There are no modern fully automated ionosondes available in South Africa at present. Researchers are thus unable to participate in research requiring a reasonable level of sophistication. The manpower and funding situation is such that even reduction of ionograms to participate in the URSI Working Group G4 of Commission G on the Vertical Incidence Modelling (VIM) project, is out of the question.

There are many reasons for the declining support for and interest in ionospheric research. Some of the more obvious ones include the dramatic political changes in Southern Africa as a whole following changes in the USSR, and in South Africa itself as a result of new political initiatives here. There has therefore been a general rethink on the national scientific and social priorities pending a new political dispensation. Generally there also appears to be the perception that HF systems represent dated technology and as such it has fallen out of favour. It is also a fact that research and development funds in South Africa compare poorly with those of many other countries. Consequently competition for available funds is very keen.

Future Prospects

From discussions with various colleagues, it appears clear that ionospheric research can only be undertaken in future if this can be done in support of commercial ventures or political initiatives and cooperation in the subcontinent.

Commercial ventures include the development and evaluation of a variety of HF communications equipment, especially digital modems. Other possibilities are the support of near real-time frequency management systems, automatic HF link establishment and SSL HFDF systems. While some countries can also justify the continued operation of ionosondes in support of OTH HF radar systems, this option appears to be highly unlikely in the Southern African context.

With the rapidly changing political situation in South Africa comes a renewed awareness of the technological assistance which can be offered to neighbouring countries. Although HF communications are seen by many to be of limited use, this is probably still the cheapest means of communication in Africa. Many countries in Africa have a potentially viable HF communications infrastructure because of the amount of HF equipment already available for use by them. This offers an ideal opportunity for South Africa to assist these countries to maximise the potential benefits of such an HF infrastructure by providing advice on the whole spectrum of HF communications, including antennas and propagation.

Other options which could be explored in terms of cooperative ventures include SSL HFDF and improved HF predictions in support of policing and conservation activities. There is no reason why mutually beneficial initiatives aimed at search and rescue operations and reducing the smuggling of arms, drugs and products from endangered species, could not become a standard feature of the changing circumstances in Southern Africa.

Conclusion

The immediate future for ionospheric research in South Africa is not particularly bright. As with many other areas of research, priorities will ultimately be determined by the politics of the region and the potential visible benefits to the community at large. The higher priorities of social reconstruction are expected to impact directly on the amount of money available for research and thus to seriously test the levels of research commitment.

At present it is almost impossible for South Africa to make any contribution to international research programmes, such as the VIM program, with the currently available ionosondes.

As the political climate changes and more contact becomes possible with neighbouring countries, the possibility of cooperating with and providing these countries with technological expertise becomes a very real and exciting prospect. Perhaps if this could be achieved, even in some small measure, this will ensure the continued survival of ionospheric research activities at the Universities of Rhodes and Pretoria, and at the CSIR.

Acknowledgements

References

[1]   F J Hewitt, (Miss) J Hewitt and T L Wadley, "A frequency prediction service for South Africa", **Trans. SAIEE**, Vol. 38, pp. 180-197, July 1947.

[2]   T L Wadley, "A single-band 0-20-Mc/s ionosphere recorder embodying some new techniques", **Proc. Instn. Elect. Engrs.**, Pt. III, Vol. 96, pp. 483-486, 1949.

[3]   C C Mercer, "The search for an ionospheric model suitable for real-time applications in HF radio communications", MSc thesis, Rhodes University, Grahamstown, South Africa.

[4]   J A Gledhill and M E Szendrei, "The behaviour of the F-region of the ionosphere over Grahamstown during the solar eclipse of the 14th January 1945, **Trans. Roy. Soc. S. Africa**, Vol. 31, pp. 147-152, 1947.

[5]   A W V Poole, "Advanced sounding: (i) The FMCW alternative", **Radio Sci.**, Vol. 20, pp. 1609-1616, 1985.

[6]   A W V Poole and G P Evans, "Advanced sounding: (ii) First results from an advanced chirp ionosonde", **Radio Sci.**, Vol. 20, pp. 1617-1623, 1985.

[7]   J A Gledhill, "Thirty years of upper atmosphere research work at Rhodes", Part I, **The Radio Scientist**, Vol. 2, pp. 106-112, 1991.

[8]   A W V Poole, "Thirty years of upper atmosphere research work at Rhodes", Part II, **The Radio Scientist**, Vol. 2, pp. 112-114, 1991.

THE RUSSIAN HIGH-LATITUDE IONOSONDE NETWORK : ITS HISTORY, CURRENT STATUS AND PERSPECTIVES.

A. V. Shirochkov

Arctic and Antarctic Research Institute, 38 Bering Street, 199397 Saint-Petersburg, Russia.

Introduction

The Russian sector of Arctic includes a significant part of the Northern polar region. It covers territory from 30° E geographic longitude, on its Western frontier, to 190° E on its Eastern edge, which is equal to 10 hourly belts. The Arctic Ocean Route along the Siberian Coast - a very important sea-surface transport artery - is located well inside this region.

Ionospheric investigations in the Russian part of the Arctic, besides their purely scientific purposes, were motivated by some pragmatic values. The role of ionospheric polar research increased continuously with the complex industrial development of the Russian Far Northern territories.

This paper will briefly describe the major stages of the Russian ionospheric polar investigations - from their initial steps up to the present time, with special emphasis on contemporary problems.

History of the Russian ionosondes explorations of the polar ionosphere

The first sporadic ionospheric investigations in the Arctic were made by Russian scientists during the Second International Polar Year (1932 - 1933). Basically, quantitative instrumental measurements of the signals levels from remote HF radio transmitters were made (later this method became the A3 ionospheric absorption measurement). These measurements showed that auroral events create disturbance effects on HF radiocommunication in the polar regions. The irregular character of the occurence and intensity of these auroral events, in its turn, helped people to understand the need for regular measurements of the ionisation in the polar ionosphere. Consequently, one of the first Russian vertical ionosondes was installed for the regular observations in the Arctic in 1938.

The milestones of the development of the Russian high-latitude ionosonde network can be named as follows:

1938 - start of the first regular vertical ionospheric sounding at Tikhaja Bay (Franz-Josef Land Archipelago). The observations were performed annually.

1944 - start of the similar observations at Tixie Bay in Eastern Siberia (mouth of Lena river).

1950 - 1955. Three other vertical ionosondes were installed in the Arctic (Murmansk, Dixon Island, Cape Schmidt).

1954 - 1955. The first regular annual observations by a vertical ionosonde were performed at the Ice Drifting Station "North Pole-3", which drifted close to the North Geographical Pole. Perhaps they were the very first regular ionospheric observations ever made deep inside the arctic circle.

1956 - routine vertical ionospheric sounding in Antarctica (Vostok and Mirny).

1961 - the first airborne soundings of the polar ionosphere (Antarctica).

1963 - 1964 - routine operation of the Russian high-latitude riometer network, both in Arctic and Antarctica, started.

1969 - the first Russian regular oblique incidence bistatic ionospheric soundings between Saint-Petersburg and Murmansk (sweeping frequency range 3.5 - 27.5 MHz).

1969 - 1975 - establishment of the permanent oblique incidence ionospheric sounding network both in Arctic and Antarctica, closely connected with network of vertical sounders.

The formation of the Russian vertical ionosonde network in the Arctic region was completed towards the end of International Geophysical Year (1957 - 1959). The network was equipped throughout with the same type of ionosonde - the automatic ionospheric station, (AIS), similar to the U.S. C-4 ionosonde. Consequently, all ionospheric information collected in the Arctic had a uniform quality which was a great advantage in its interpretation.

The centres of ionospheric service and forecasting were organised simultaneously, originally under the auspices of the Academy of Science and afterwards the Hydrometeorological Service. Effective methods for both short-term and long-term ionospheric and radio-propagation forecasting were developed. The main purpose of all these actions was to organise a reliable radio-communication service for the Arctic Ocean Route - a very important transport link between European and Far Eastern parts of the Russian Arctic. Some other tasks including scientific ones were also solved by means of ionospheric information collected from this network.

The strategic ideas in the placement of the ionospheric stations was to make it possible to monitor the key regions of the polar ionosphere where the corpuscular radiation fluxes intrude into it: a nighttime part of the auroral oval and the polar cusp / cleft region. Subsequently the chains of ionosondes were organised along both geomagnetic meridians and parallels in order to cover all of the polar region.

The full list of the Russian high-latitude ionosondes which are in operation now is given in TABLE 1. The term "high-latitude" includes regions located above 60° of invariant latitude as geographically speaking the region is inside the North Polar arctic circle (66.7° N).

TABLE 1.

	Station	Geographic Latitude (N)	Geographic Longitude (E)	Invariant Latitude	Sponsor
1	Heiss Island	80.62°	58.05°	74.99°	Hydro - meteorological Service
2	Preobrazhenije Island	74.70°	112.90°	68.57°	Hydro - meteorological Service
3	Dixon Island	73.55°	80.57°	68.06°	Hydro - meteorological Service
4	Tixie Bay	71 .58°	129.00°	65.25°	Academy of Science
5	Amderma	69.46°	61.41°	64.58°	Hydro - meteorological Service
6	Murmansk (Loparskaja)	68.25°	33.08°	64.27°	Academy of Science
7	Cape Schmidt	68.92°	180.52°	64.07°	Academy of Science
8	Norilsk	69.20°	88.00°	63.81°	Academy of Science
9	Cape Wellen	66.17°	190.17°	62.25°	Hydro - meteorological Service
10	Salekhard	66.60°	66.70°	61.71°	Hydro - meteorological Service
11	Archangelsk	64.60°	40.50°	60.37°	Academy of Science

The list of the Russian high-latitude ionosondes in Arctica.

THE DIGISONDE NETWORK AND DATABASING

Bodo W. Reinisch

University of Massachusetts Lowell, Center for Atmospheric Research 450 Aiken Street, Lowell, MA 01854, USA

Abstract

The capabilities of modern ionospheric sounders are illustrated using results obtained with the Digisonde 256 and the Digisonde Portable Sounder. Unlike any other ionosonde, these instruments routinely perform a variety of complementary operations in real time: automatic ionogram scaling, calculation of electron density profiles, high resolution Doppler and angle of arrival, plasma drift velocity, polarisation, and precision group height.

Introduction

Today's advanced digital sounders[1] are digital HF radars with real time analysis capabilities. This paper shows results from selected stations of the Digisonde network (Fig. 1), including the Digisonde 256 (D256) and the Digisonde Portable Sounder (DPS). Since the D256 has previously been described[2,3] it suffices to present the main differences between the DPS and the D256 (Table 1). Low weight (40 kg), low power (500W peak) and pulse-to-pulse software control of the transmission waveforms make the DPS very attractive for routine monitoring and research.

Vertical Incidence Ionogram Sounding

The Digisondes measure all observables of the received signals at each of 128 or 256 ranges: Doppler spectrum (amplitude and phase), angles of arrival, and polarizations. The quiet daytime ionogram (Fig. 2) from El Arenosillo, Spain, illustrates the format applied for routine sounding: 100 kHz frequency steps, 128 x 5 km height increments. Small optically coded numbers represent the echo amplitudes: X polarisation in grey, O in black. The ARTIST-scaled[3] traces are marked by the letters E and F. Superimposed on the ionogram is the electron density profile.
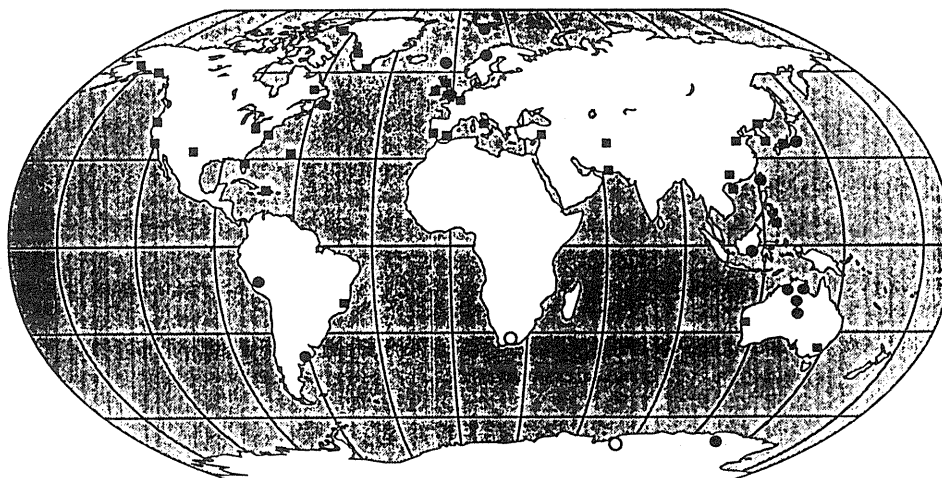
- ● **Digisonde Portable Sounder (DPS)**
- ■ **Digisonde 256**
- ○ **Digisonde Portable Sounder (DPS) Under Construction**

Figure 1: Global digisonde network
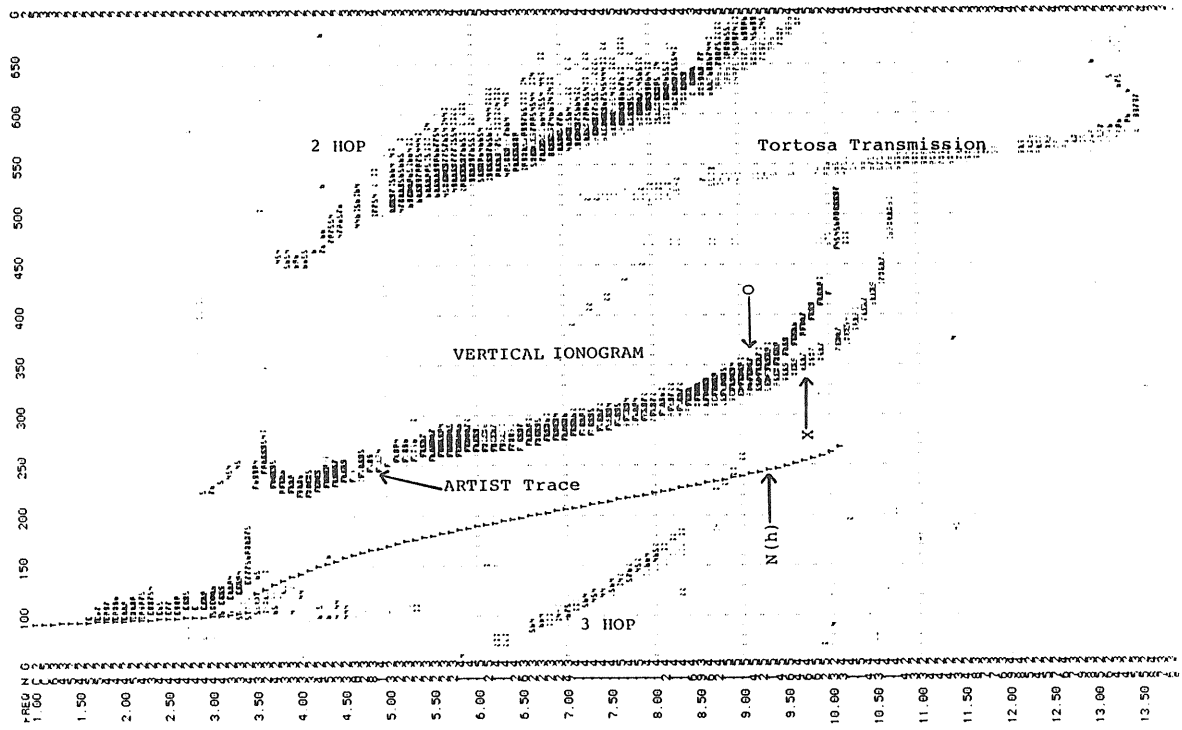
Figure 2: Simultaneous vertical incidence / oblique incidence soundings with D256s.

Figure 3: F layer patches observed with a DPS at Ny Alesund.

9
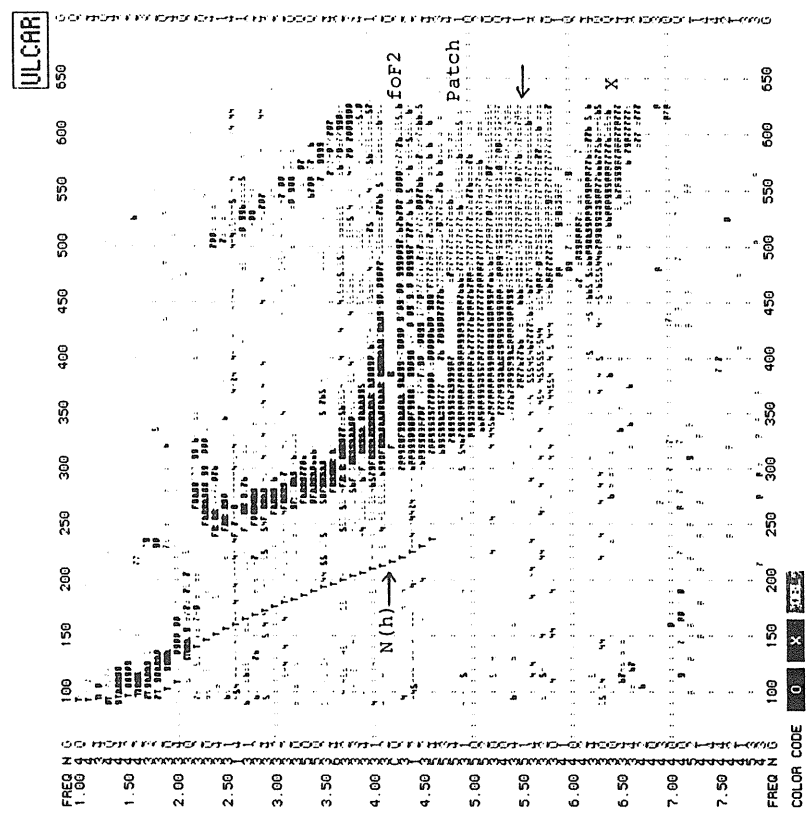
For each range, the DPS measures a full complex spectrum with 2^N Doppler lines (N = 1,2...7) for both O and X polarisation. This information is compressed into a standard ionogram, and for routine archiving each echo amplitude is amended by Doppler, polarisation and incidence angle. The Ny Alesund ionogram in Fig. 3 shows strong spread on the "overhead" echoes as well as an off-vertical patch of ionisation (light grey) with foF2 = 5.4 MHz, compared to 4.3 MHz for the overhead ionosphere.

Converting the sequence of measured electron density profiles to plasma frequency contours[5] gives the diurnal variations of the E and F layers, as in Fig.4 for two days at Jicamarca, Peru. Spread F developed in the first night when the F layer peak height rose above 500 km. The DPS also measures the three components of the F region plasma velocity, V_{vert}, magnetic V_{north} and V_{east} (Fig. 5); the vertical velocity measured by an incoherent scatter radar (ISR) is shown for comparison.

As one of the standard operating modes, Digisondes measure the Precision Group Height (PGH) by transmitting 2 frequencies separated by Δf. The phase difference $\triangle \Phi$ measured on the received echoes is proportional to the group path:

$$h' = \frac{c}{4\pi} \frac{\Delta\phi}{\Delta\phi} = \frac{c}{4\pi} \frac{2\pi n + \Delta\phi}{\Delta\phi}$$

where $0 < \triangle\Phi < 2\pi$. The range ambiguity introduced by the factor $2\pi n$ (30 km for Δf = 5 kHz) is resolved by the amplitude-versus-range profile in the ionogram. The DPS currently outputs PGH data with 1 km increments leading to the accuracy and resolution illustrated in Fig. 6.

Oblique Incidence Sounding

The same instrument can make vertical and oblique soundings synchronised by GPS receivers and special interface software to within 1msec. The oblique echo trace in Fig. 2 is an example for a 860 km link from Tortosa to El Arenosillo in Spain. For oblique sounding[6] the DPS can operate with 100% duty cycle, compared to $\approx$ 1% for the D256. A 127 bit binary phase code provides 67msec effective pulse width. Applying the PGH technique to the oblique echoes gives unparalleled group path resolution of 3msec. Fig. 7 shows a 620 km DPS ionogram received at Millstone Hill with only two polarised receiving loop antennas; the DPS at Wallops Island transmitted 200 W peak at10% duty cycle.

Digisonde Drift Measurements

Like the incoherent scatter radar the Digisonde measures the Doppler shifts of signals arriving from different directions. The line-of-site "Doppler velocity" is defined as $v_{r,i}$ = (c/2f)d_i, where c is the speed of light, f the sounding frequency and d_i the measured Doppler shift of a signal arriving at an angle of incidence, i. The wide beam transmit antenna illuminates a large area of hundreds of kilometers in the ionosphere and the different reflection points are resolved by combining Fourier transform and interferometry techniques[7,] producing so-called skymaps[8]. In Fig. 8 (Millstone Hill), small circles indicate the angles of arrival (zenith and azimuth)[9], the lines from the circles point toward the center (positive Doppler) or away (negative Doppler), and the line length is proportional to v_r. Since there are always more than 3 sources a least-squares error calculation[10,11] is used to determine the plasma bulk velocity[12,13] v = (v_x, v_y, v_z).

Table 1. D256 Vs. DPS

FEATURE	D256	DPS	COMMENTS
Vertical Inc. Ionog.	128/256 Height	128/256 Heights	2.5, 5.0 and 10km
Oblique Inc. Ionog.	Pulse	Pulse or CW	Binary Phase Coding
Peak Trans. Power	5kW	*500W*	
Beam Forming	Analog	*Digital*	
GPS Synchron.	Optional	*Standard*	[a] 1msec Accuracy
Phase Coding	Interpulse	Inter & *Intrapulse*	Pulse Compression in DPS
Waveform	67/133ms 50,100,200Hz PRF	*m x 67ms* 50,58,100,200Hz PRF	Pulse Compr. in DPS m=1,8,127 or 255
Transmit Antenna	Linear	Circular or Linear	
Receive Antennas	7 Loops	4 Loops	O/X Switching
Drift Measurements	2 Ranges, 2 Freqs. 128 Dopplers	*128 Ranges, 8 Freqs.* 128 Dopplers	Skymaps, Drift Velocity
Max. Doppler Range	±25 Hz	*±100 Hz*	
Doppler Resolution	0.025Hz	*0.006Hz*	
Prec. Group Height	Optional	1 km Accuracy	
Autoscaling	ARTIST	ARTIST	Real Time
N(h) Profile	ARTIST	ARTIST	Real Time
Output Storage	1/2" Tape, 30MB	QIC, 150MB	QIC also for DGS256
Volume	$1.1m^3$	$0.25m^3$	
Weight	475Kg	*55Kg*	
Input Power	110/220Vac, 2kW Avg	*24VDC, 300W Avg.*	Waveform dependent
Remote Control	Modem, Asynch.	Modem, Asynch.	
Data Editing	ADEP	ADEP	

STATION:JICAMARCA (LAT:12.0S LONG:283.1E) DENSITY PROFILE CONTOUR
TWO DAYS DATA AT 1992 MAR 30 (90) 16:00 (NOON:17:13 SSE:00:40 SSF:07:01)
DATA FROM J090092.ADP SMOOTH FIX LINK:120 PLOTTED AT FEB/22/1994
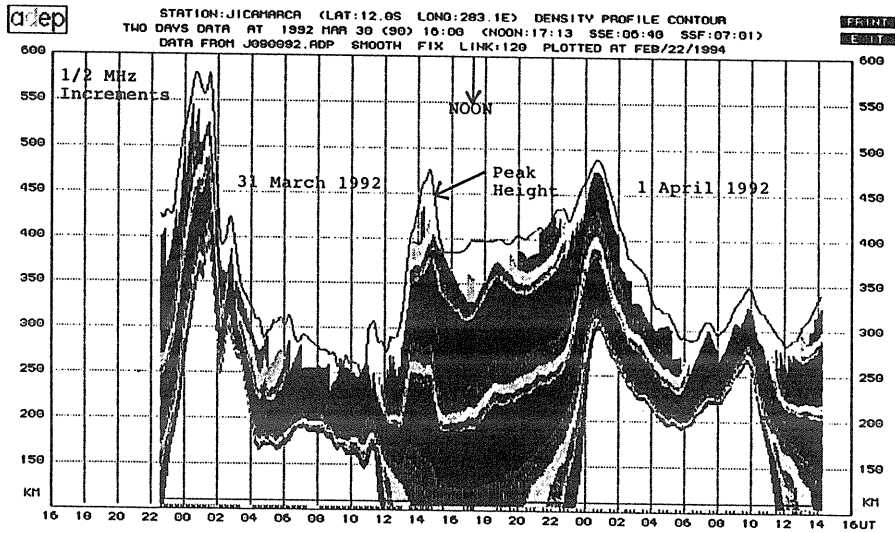
Figure 4: Palsma frequency contours at Jicamarca.

Figure 5: Vertical and horizontal F region drifts at Jicamarca.

Figure 6: A Precision Group Height (PGH) ionogram. The conventional amplitude versus range and frequency ionogram is shown on top. The PGH information (not shown in the ionogram) contained in each frequency/range pixel was used to make the high resolution plot at the bottom.
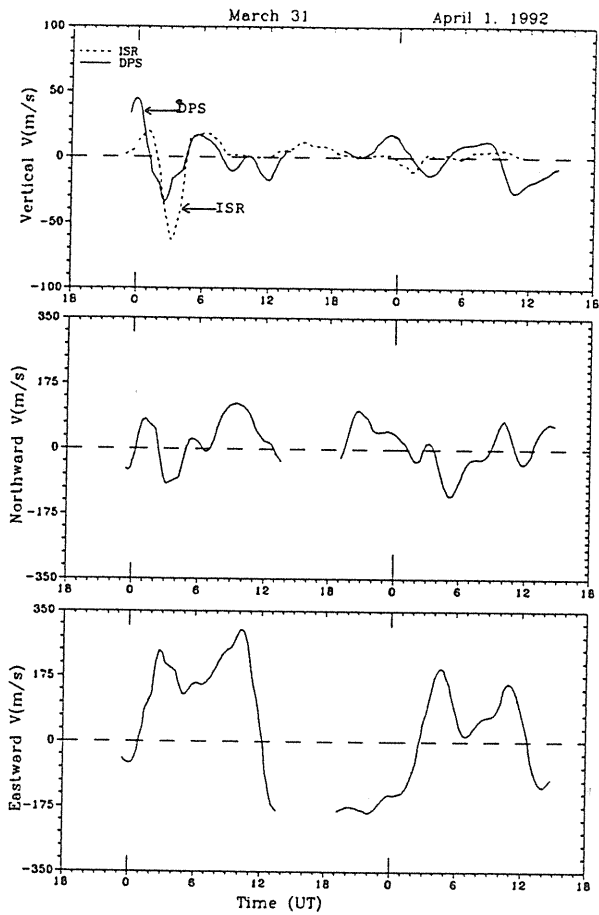
Figure 7: An oblique DPS ionogram over a 620km path.

Figure 8: A sample SKYMAP made at Millstone Hill.
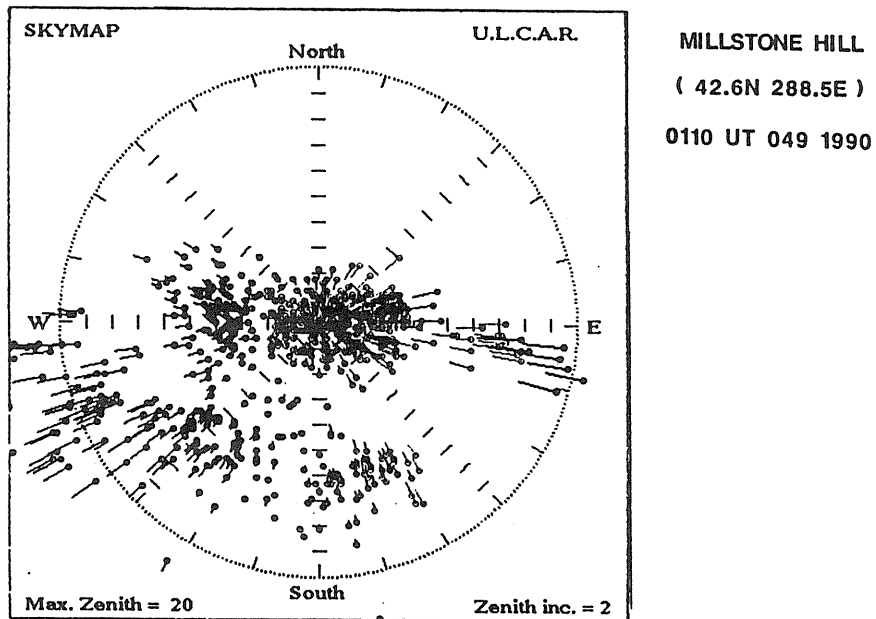
Databasing

Ionogram and drift data formats of the D256 and the DPS systems are compatible and all the software[14,15,16] for data editing and processing, archiving and dissemination developed for the D256 data is applicable to the DPS data.

Acknowledgments

References

1. Reinisch, B.W., "New Techniques in Ground-Based Ionospheric Sounding and Studies," **Radio Science, 21,** 3, pp. 331-341, May-June 1986.
2. Reinisch, B.W., "The Digisonde 256 System and Ionospheric Research," **URSI INAG Ionospheric Station Inf. Bulletin,** #48, 1986.
3. Reinisch, B.W., K. Bibl, D.F. Kitrosser, G.S. Sales, J.S. Tang, Z.M. Zhang, T.W. Bullett and J.A. Ralls, "The Digisonde 256 Ionospheric Sounder," World Ionosphere/ Thermosphere Study, **WITS Handbook,** Vol. 2, Ed. C.H. Liu, December 1989.
4. Reinisch, B.W. and X. Huang, "Automatic Calculation of Electron Density Profiles from Digital Ionograms, 3, Processing of Bottomside Ionograms," **Radio Science, 18,** 477, 1983.
5. Zhang, Z.M., "ARTIST Data Editing and Printing (ADEP) Manual", University of Massachusetts Lowell, Center for Atmospheric Research, 1992.
6. Reinisch, B.W., D.M. Haines and W.S. Kuklinski, "The New Portable Digisonde for Vertical and Oblique Sounding," **AGARD Proceedings** Number 502, pp. 11-1 to 11-11, 1992.
7. Bibl, K. and B.W. Reinisch, "The Universal Digital Ionosonde," **Radio Science, 13,** pp. 519-530, 1978.
8. Bibl, K., W. Pfister, B.W. Reinisch and G.S. Sales, "Velocities of Small and Medium Scale Ionospheric Irregularities Deduced from Doppler and Arrival Measurements," **Adv. Space Res,** XV, pp. 405-411, 1975.
9. Scali, J., "A Quality Control Package for the Digisonde Drift Analysis (DDA)," Version 2.0, University of Massachusetts Lowell, Center for Atmospheric Research, 1993.
10. Reinisch, B.W., J. Buchau and E.J. Weber, "Digital Ionosonde Observations of the Polar Cap F Region Convection," **Physica Scripta, 36,** 372-377, 1987.
11. Buchau, J., B.W. Reinisch, D.N. Anderson, E.J. Weber, J.G. Moore and R.C. Livingston, "Ionospheric Structures in the Polar Cap: Their Origin and Relation to 250 MHz Scintillation," **Radio Science, 20,** 3, pp. 325-338, 1985.
12. Cannon, P.S., B.W. Reinisch, J. Buchau and T.W. Bullett, **J. Geophys. Res.,** 96 (A2), 1239-1250, 1991.
13. Bullett, T.W., "Mid Latitude Ionospheric Plasma Drift: Comparison of Digital Ionosonde and Incoherent Scatter Radar Measurements at Millstone Hill," **Doctoral Thesis,** University of Massachusetts Lowell, 1994.
14. Gamache, R.R. and B.W. Reinisch, "Ionospheric Characteristics Data Format for Archiving at the World Data Centers," **Scientific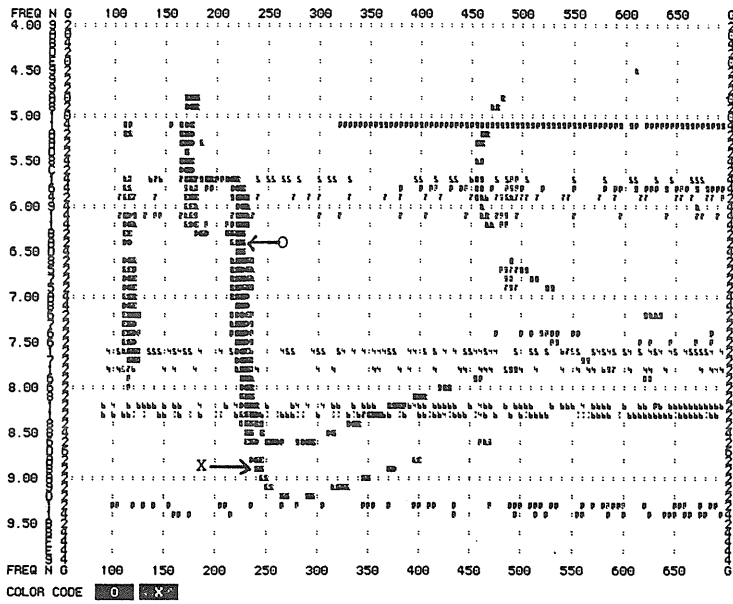 Report No. 3,** GL-TR-90-0215, Air Force Geophysics Laboratory, Air Force Systems Command, USAF, Hanscom AFB, Bedford, MA, 1990.
15. Gamache, R.R., T.W. Bullett, Z.M. Zhang, B.W. Reinisch and W.T. Kersey, "ADEP Database Record Structure," **ULRF-468/CAR,** University of Massachusetts Lowell, 1992.
16. Gamache, R.R., "Data Format for Station Monthly Characteristics Reports and Validation of Ionospheric Model Study," **ULRF-469/CAR,** 1992.

THE DIGITAL IONOSPHERIC SOUNDING SYSTEM NETWORK
OF THE US AIR FORCE AIR WEATHER SERVICE

Jurgen Buchau and Terence W. Bullett, Phillips Laboratory, Hanscom AFB, MA
Allan E. Ronn and Kevin D. Scro, Space Forecast Center, Falcon AFB, CO
Jeffrey L. Carson, Air Weather Service, Scott AFB, IL

A network of twenty Digital Ionospheric Sounding Systems (DISS) of the United States Air Force Air Weather Service (AWS) collects real-time ionospheric data on a global scale. The US Air Force Space Forecast Center (AFSFC) at Falcon AFB, Colorado, uses the real-time data to prepare ionospheric specifications and forecasts for communications, surveillance and navigation systems. Of the thirteen DISS currently deployed, six operate in the Arctic, six in the northern hemisphere mid-latitude region and one in Australia. The deployment of further DISS is in progress. The network is enhanced with three Digisonde 256s, the scientific version of the DISS. Both systems have identical data outputs provided by the DISS automatic ionogram scaling software. Twenty seconds after completion of the ionogram sounding the data become available in an output buffer as IONOS and IONHT messages. The AWS Automated Weather Net (AWN) polls the network's stations and transfers the IONOS and IONHT messages to SFC for direct use by the central data processing computer or further transfer to specific users, such as the Over-the-Horizon Backscatter Radars.

The DISS messages (together with other data) are used to provide an estimate of the effective sunspot number, R_{eff}, as driver for remotely operated models, and to update the AWS Parameterized Real-Time Ionospheric Specification Model (PRISM). Real-time PRISM updating using DISS, Defense Meteorological Satellite Program (DMSP) and magnetic activity data is under development. DISS data are typically acquired in half-hourly increments, and the full digital ionograms are tape recorded for quality control, scientific analysis and archiving. While scientific analysis of the global and specifically the high latitude data base is conducted at the Phillips Laboratory, all data are available within approximately six months at the World Data Center A, Boulder, Colorado, in charge of the quality control for the auto-scaled ionograms.

The US Air Force Space Forecast Center

The US Air Force Space Forecast Center is tasked to provide space environmental forecasts and warnings to the Air Force and to the other branches of the US Department of Defense (DOD), to enable the services to accomplish their global missions. A large array of satellite borne and ground based sensors provides in real or near real time the data base, which, used in conjunction with available models, provide the required support. Specifically, for the ionospheric area, this task involves the specification and forecasting of radio propagation conditions as they impact DOD systems which either require the ionosphere for their operation (High Frequency propagation) or which have to work through the ionosphere (satellite communication, Global Positioning Satellites), often against the background of a disturbed ionosphere (space surveillance radars).

The Digital Ionospheric Sounding System Network

To accomplish the task of specifying the global ionosphere in real time, the Air Force Space Forecast Center operates a network of fully automated digital ionosondes, the Digital Ionospheric Sounding System (DISS). Figure 1 shows the locations of the 13 deployed systems, and of six systems for which sites have been selected and deployment is expected by the end of 1995. The network is connected through a real time data network (Automated Weather Net - AWN, and Atlantic/Pacific Region equivalents ATMED and PACMED) operated by the US Air Force. The locations of the US Air Force Space Forecast Center (AFSFC), in Colorado, and of the hub of the AWN in Oklahoma are marked. Additional ionosondes which do not report in real time fill in the data base for requirements which do not rely on real time data, but which can live with 6 to 24 hours delayed summaries these stations provide.

AWS REAL TIME IONOSONDE NETWORK

▲ REAL TIME DISS   △ DISS TO BE DEPLOYED   ▣ REAL TIME OTHER   ◉ SUMMARY
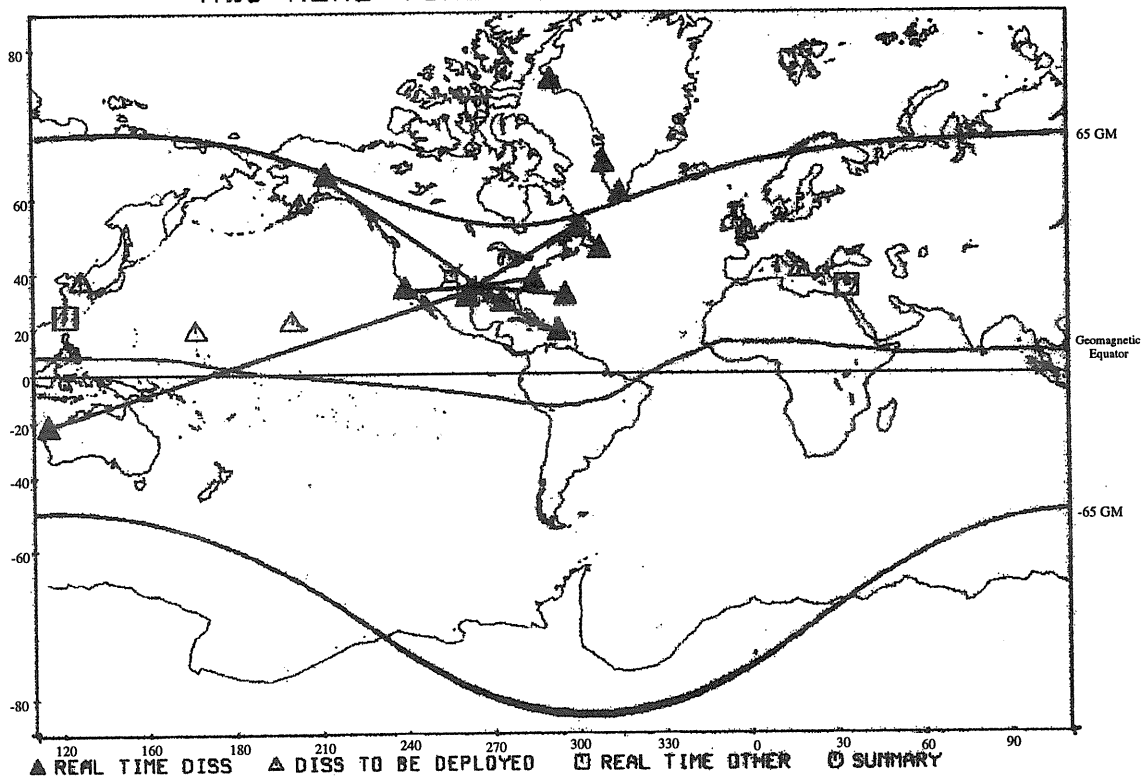
Figure 1 -- The Digital Ionospheric Sounding System network of the US Air Force Air Weather Service. Deployed and operational DISS are indicated by filled triangles, and those connected via the Automated Weather Network to the Air Force Space Forecast Center are connected with solid lines. Planned deployment sites for DISS are indicated by an open triangle. Other ionosondes which provide data in real time to the Air Force Space Forecast Center are shown with open squares. Also shown on this map are the geomagnetic equator and the 65° magnetic latitude lines. The DISS network is centered heavily in the northern hemisphere mid-latitudes, particularly on the continental United States.

The DISS is a fully digital ionosonde, derived from the well known Digisondes developed at the University of Massachusetts Lowell (UML) and almost identical to the Digisonde 256 *[Reinisch, 1986]*. Important features of the DISS include 10 kW of peak transmitter power, a low profile transmit antenna and an array of polarization sensitive receive antennas. In addition to distinguishing between ordinary and extraordinary polarization, the receive antenna array is phased using a delay cable network to discriminate between obliquely incident signals and those arriving from near zenith, with the latter used for ionogram scaling. Digital signal processing consists of real time discrete Fourier transforms and phase coherent integration.

Ionogram processing is accomplished by the ARTIST (Automatic Real Time Ionogram Scaler with True Height) software package, which scales the digital ionograms in real time, records raw and scaled ionogram data locally on digital magnetic tape, and generates the required data messages and transmits them to AFSFC via the AWN. These messages are called IONOS and IONHT, with the IONOS code providing a set of ionospheric parameters (e.g. foE, foF1, foF2, hminF, etc.) and the coefficients of a Tschebycheff polynomial to describe the automatically determined electron density profile, while the IONHT code provides the complete virtual height trace as identified by ARTIST. These messages are quite short, 140 characters for the IONOS code and typically less than 500 characters for the IONHT code. The global network is polled half-hourly through the AWN, ATMED, and PACMED networks, serving the US sector, the Atlantic/European sector, and the Pacific sector, respectively. The networks are controlled from Tinker AFB in Oklahoma, from which the data are sent on a single data link to the Air Force Space Forecast Center. The IONOS and IONHT messages are forwarded immediately after receipt to users such as the Over The Horizon Backscatter (OTH-B) Radars, which have a need for the actual station data rather then processed or derived

information.

The ARTIST's ionogram scaling accuracy is vitally important to the quality of the DISS data required by AFSFC. For high latitude stations 80% of all automatic foF2 measurements are required to be within 0.5 MHz while in the mid latitudes this performance has to be met by 85% of the data. Testing of the ARTIST was done at the Phillips Laboratory, using a total of almost 6000 ionograms from the DISS and Digisondes at Argentia, Goose Bay, Millstone Hill, Qaanaaq and Wallops Island. For this data set, the automatically scaled value of foF2 was within 0.5 MHz of the manually scaled value 91% of the time.

DISS Derived Space Forecast Products

The Air Force Space Forecast Center provides a wide range of space environment products to their customers. The ionospheric products which depend directly on the DISS inputs are shown in Table 1.

•

Primary HF Radio Propagation Report

Secondary HF Radio Propagation Report

Ionospheric Electron Density and Total Electron Content Products

HF Radio Usable Frequency Predictions

Ionospheric Scintillation

Environmental Assessments for Spacecraft Anomalies

Sunspot Number Prediction

Table 1 -- US Air Force Space Forecast Center products directly related to DISS inputs.

The HF Radio Propagation Reports, issued daily at 06 UT, provide information in four parts. Part I provides in quantized form the description of propagation conditions for the previous six hours and forecast for the next six hours for 20 regions organized in four longitude quadrants and five latitude regions (Polar, Auroral, Middle, Low and Equatorial) which contiguously cover the northern hemisphere and equatorial region.

Part II provides a clear text description of the impact of observed geomagnetic and ionospheric conditions on propagation, which may include the southern hemisphere.

Part III lists past solar flares which may have caused shortwave fades in the sunlit hemisphere, and a forecast of flare occurrence probability for next 24 hours.

Part IV provides solar and geophysical parameters which enable the users to run their own ionospheric and other models and forecasts. Due to current lack of real or near real time ionosonde data in the southern hemisphere, this region is currently not handled in Part I of the message.

Secondary propagation reports update parts I and II of the primary report at 12, 18 and 00 UT.

Data from the DISS and other instruments are used to determine daily or monthly median ionospheric electron density profile and total electron content products as well as link specific HF radio usable frequency predictions. Through the assessment of the deviation of observed foF2 and MUF4000 from monthly median values predicted by the ITS 78 model, computed using the Boulder sunspot number forecast, the persistence

of current conditions or change in ionospheric forecast can be determined.

In the near future, the Parameterized Real Time Ionospheric Specification Model - PRISM, will be updated directly with the DISS data. Recent validation of this updating scheme has shown a >50% improvement in accuracy over currently used models and techniques *[Daniell et al., 1993]*. The current products will then where feasible be derived from this best available ionospheric specification. In brief, PRISM is a physical, not a climatological, model which is parameterized in terms of geophysical quantities and reduced to a semi-analytical group of models. These models can be adjusted in near real time by data from both ground instruments such as DISS and total electron content products and satellite based ionospheric sensors on board the DMSP satellites. Model profiles of O^+ ion density are updated in peak concentration, altitude of the peak and bottom side profile using DISS data, while DMSP is used to alter the topside density profile and scale height. The PRISM adjustment method is a form of "multi-linear interpolation" using the angular great circle distance between any point and the location of the real-time data. This technique ensures that PRISM reproduces the real-time data it receives.

The DISS data base is also used to aid in the assessment of satellite and radar and scintillation anomalies.

Users of DISS Products

Users of the Air Force Space Forecast Center's products include various US Air Force Commands, the US Army, Coast Guard and Navy and the Unified Commands, the latter best known for their recent deployments in Kuwait (Desert Storm) and Somalia (Project Restore Hope). Scintillation advisories were especially important there since nighttime satellite links had to contend with equatorial region scintillation events.

Some customers make direct use of the individual DISS station data. The OTH-B radars use data from several DISS near the reflection region to update ionospheric models resident in the radar, improving target coordinate registration and identifying possible sources of propagation disturbances and anomalies which might reduce the performance of the radar. The NASA Wallops Island Flight Facility uses its DISS for ionospheric monitoring, sounding rocket launch criteria and diagnosis of chemical release effects on the ionosphere. The Arecibo incoherent scatter radar and HF ionospheric heating facility use the Puerto Rico DISS for radar electron density profile calibration, coordinated multi-sensor experiments and for diagnosis of high powered radio frequency heating effects.

The scientific community has general access to the DISS data base, recorded on magnetic tape at each station, after it has been used at World Data Center A (WDC-A) in Boulder, Colorado for quality control and has been archived. Ionogram data is available on request and in a variety of formats. Currently, the time lag of data availability is approximately six months to one year and is in the process of being improved. In addition to scientific research, this database is used to develop and test improvements to the automatic scaling programs and ionogram quality control techniques for use at the individual stations and by the Air Force Space Forecast Center. Recent budget cuts pose a serious threat to the continuation of this valuable database.

Future Developments

Since it is based on a full featured research ionosonde, the DISS is generally capable of a variety of sophisticated measurements and its potential to provide new types of data is being investigated. This effort deals primarily with the development of an automated ionospheric plasma drift measurement technique, which at high latitudes may provide a tool to monitor, together with DMSP, the convection pattern in the polar ionosphere. Also in the polar region, the possibility of a statistical summary of ionospheric patches is being investigated. Near the equator, similar measurement techniques may provide a short term forecast capability for the formation and transport of ionospheric scintillation regions associated with equatorial plumes.

From Figure 1 it is obvious that the current real time network is thin. In many areas PRISM will be data starved, especially in the equatorial and southern hemisphere regions. Due to funding limitations, no specific plans exist to expand the DISS network with additional systems. The current plan is to first deploy and link

up all DISS on hand, and get the network into full real-time operation. Data links costing less than the dedicated AWN lines, necessary to make practical the incorporation of additional ionosondes into the network, are being investigated, as is the possibility of including data from other sources such as the Southern Hemisphere Ionosonde Network. The feasibility to update and expand the DISS net with a more modern, low peak power ionosonde which uses modern pulse compression techniques to achieve the required signal-to-noise ratios is being pursued. In addition to making the ionosonde less expensive, more capable and more reliable, the lower transmitted power would minimize interference to neighboring users of the HF spectrum.

Jurgen Buchau, who died suddenly on August 9, 1993, was largely responsible for the existence of the DISS network. He spent his career supporting ionosonde development and promoting ionospheric science and remote sensing. This paper was one of his last projects and was kindly presented for him at the XXIV URSI General Assembly by his colleague and friend Dr. Bodo Reinisch and in his memory at the January 1994 National Radio Science Meeting in Boulder, Colorado.

References:

Daniell, R., et al., "PRISM Version 1.2 Validation Report", Computational Physics, Inc. Technical Report, June 1993.

Reinisch, B.W., New Techniques in Ground Based Ionospheric Sounding and Studies, *Radio Science*, v.21, p.331-341, 1986

THE CANADIAN ADVANCED DIGITAL IONOSONDE: DESIGN AND RESULTS

J. W. MacDougall, I. F. Grant, and X. Shen
Department of Electrical Engineering, University of Western Ontario, London, Ont.,
Canada N6A 5B9

Abstract

A new digital ionosonde called CADI is in use at 5 Canadian sites for scientific studies. The design of this instrument is briefly described. The measurement of ionospheric convection using digital ionosonde measurements is discussed and it is shown that at high latitudes convection measurements are usually relatively easy and a variety of techniques can be used, whereas at mid latitudes the irregularity structure which is required for good convection measurements is not observed.

Introduction

The Canadian Advanced Digital Ionosonde (CADI) was developed as a project of the Canadian Network for Space Research. There was a Network requirement to provide ionosonde support, at a number of sites, for collaborative experiments. These experiments involved observations by other Network instruments such as auroral radars or optical imagers and scanners. Since most of the Network sites were in the far north we needed a modern low-cost, digital ionosonde which could run essentially unattended, and had low power requirements.

In this paper the design of the CADI instrument will be briefly described. Following this description the remainder of the paper will be a discussion of our investigation of ionospheric structures to see if they provide a basis for convection measurements.

CADI Design

In this section a brief description of the CADI design is given. A more detailed design description will be published in a forthcoming issue of the Ionospheric Network Advisory Group bulletin.

The design philosophy of CADI was to make use of the capabilities of a modern PC as much as possible. Using the PC capabilities is very cost effective compared to providing similar capabilities using custom hardware. A PC can provide all the data storage, control, display and communications required by an ionosonde. The newer, faster, PCs can also do mathematical data processing, usually involving FFTs, with sufficient speed for 'real-time' data processing. This means there are also significant cost savings compared to satisfying these data processing requirements by means of dedicated processors.

Therefore we tried to utilise the PC capabilities as much as possible. The CADI design evolved over several prototype instruments. In the final design the receivers became PC plug-in boards, as did the frequency synthesiser. This had two advantages: the cost was decreased since no external cabinetry was required, and the system became very flexible and easy to maintain since one could plug in as many, or as few, receivers as required. In the CADI units we are using we have 5 plug-in boards: one control-and-frequency synthesiser board, and 4 receivers which are each one plug-in board.

The frequency synthesiser board uses a Qualcomm Direct Digital Synthesis 'chip' to generate the ionosonde transmitter frequencies. Frequencies can be specified to 1/100 Hz. There are a number of Motorola 68HC11 microprocessors which are used to control the system timing, and to sample the echoes. We usually use the system with 13 bit Barker pulse coding (an optional mode) and these 68HC11 microprocessors are used to generate the coded pulse, and to decode the echoes. Each receiver card has two of these microprocessors, one for the 'I' (in-phase) channel, and one for the 'Q' (quadrature phase) channel.

The radio frequency power amplifier is the only part of the basic system which is external to the PC. This produces 600W peak pulse power and is in a small chassis with a 'footprint' the size of a standard desktop PC and 95mm high.

Data storage uses standard PC backup tape units to which new data files are automatically transferred from hard disk once each day. The units we use store 120Mbytes. Storage capacity is increased by about 10% using the data compression provided in the backup software. Most of our CADI installations must operate for several weeks (typically 3) unattended so the system parameters are selected to give about 5 Mbytes of data per day.

The receiver antennas used at our field sites are based on an arrangement proposed by Wright and Pitteway [1979]. There are four receiver dipoles along the centres of the four sides of a 60m square. Each dipole is an untuned 'fat' dipole of overall length 19m and consists of a 'bundle' of 4 wires spaced approximately 30 cm apart. The centre of each dipole is fed to a balanced high input impedance wideband preamplifier. The transmitting antenna is a delta, using a relatively short mast (13m). The small size of the delta severely restricts performance at frequencies below about 2MHz, but is adequate for most of our studies.

Currently we have CADIs installed at Eureka (89$^{\circ}\Lambda$ magnetic latitude), Resolute Bay (84$^{\circ}\Lambda$), and Cambridge Bay (78$^{\circ}\Lambda$) . These form an approximate line from the centre of the (geomagnetic) polar cap to cusp latitude. The separation between these three stations is such that an F region feature moving along the line of these stations would become visible on the next station about the time it would become difficult to see from the adjacent station. Our experience is that dominant features can usually be tracked until they are of the order of 30-40° zenith angle.

Another CADI is at Rabbit Lake (68$^{\circ}\Lambda$) where it is used in support of auroral radar measurements. We also operate a CADI at a field site near our university (55$^{\circ}\Lambda$). This is used for studies of high midlatitude ionospheric phenomena.

Convection Measurements

In our routine measurements we usually record both ionograms and, interleaved, fixed frequency measurements on several frequencies. The fixed frequency measurements usually use a 64 point FFT data sample done every 30 seconds on each frequency. From these samples we have available the echo intensities, virtual height of reflection, Doppler shifts, phases, and calculated angles of arrival. Since a prime requirement of the CADI ionosondes is to measure ionospheric convection, in this section we will focus on some of the techniques which we have tried for convection measurements using the various measured parameters from the FFT samples.

For our stations in the polar cap region, convection measurements are usually relatively easy. As has been shown by Cannon et al. [1991], if the angles-of-arrival for significant peaks in the Doppler spectrum are plotted as a 'sky map', then the drift velocity can be obtained from this sky map by fitting of the equation:- $d_s = (1/\pi) \, v.k_s$ where s is an index number for the individual points on the sky map, d is their Doppler shift, v is the drift vector, and k is the wave number vector directed from the ionospheric reflection point towards the ionosonde.

This method works well for the polar cap measurements and for each of our polar cap stations we routinely produce plots of convection direction as a function of time that are similar to those shown in Cannon et al. [1991].
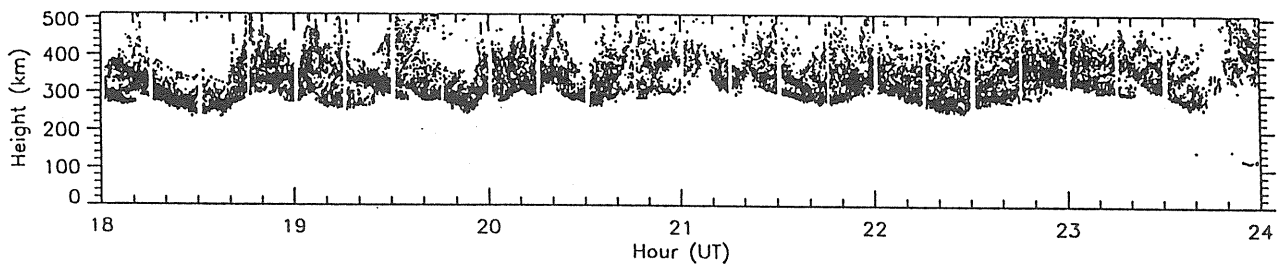
Fig. 1. A 6 hour sample of h't for Resolute Bay. The frequency was 4.012 MHz. Vertical white streaks are when the ionosonde was running in other modes. The figure show that the F region ionosphere is highly spread. 'U' shape features are signatures of moving patches.

The reason the 'sky-map method' works well for polar cap stations seems to be because the polar cap ionosphere is usually highly structured into various scale sizes rather than being just a relatively uniform medium with small density perturbations. The sensitivity of an ionosonde is usually set for specular (mirror) reflection. Therefore to get strong echoes from features at various sky positions requires large blobs of enhanced ionisation at these positions. These blobs must have surfaces that are comparable with the Fresnel zone size (a few kilometres) and these surfaces must be normal to the raypath. Figure 1 shows a plot of 4 MHz echoes recorded for 6 hours at Resolute Bay. This figure illustrates the spread nature of the polar cap echoes. In the spread can be seen occasional discrete echoes from the larger scale structures. The many 'U' shaped features are signatures of ionospheric perturbations that are convecting overhead. An apparent speed estimate is easily obtained just using the range versus time curves of these features, and for Figure 1 the speeds are about 180 m/sec. Thus when the ionosphere is highly structured, as it usually is in the polar cap, many techniques can be used for velocity estimates.

At midlatitude sites the ionosphere is usually not highly structured and therefore measurement of velocities is not as easy. Also the convection velocities are an order of magnitude smaller than they are in the polar cap, and this also makes measurement more difficult.

If, however, one could observe convecting discrete ionisation structures, even though weaker than those in the polar cap, then it should be possible to make reliable convection measurements. Therefore we used the capabilities of the digital ionosonde to look for evidence of convecting structures.

The most obvious evidence of some sort of structuring in mid latitudes is the spread-F which is commonly observed, particularly at night. However midlatitude spread-F may be due to 'corrugations' of a relatively flat surface rather than due to discrete structures [Bowman, 1991]. Thus even spread-F is not conclusive evidence that there are discrete structures.

Much of our search for discrete structures centred on searching for their signatures on plots of Doppler shift versus time. If a discrete reflector is convecting with a horizontal velocity, V, then its Doppler shift, f_D, as a function of time is will be, $f_D \approx -2V^2t/\lambda h$ (where λ is the radio wavelength, and h is the height: this result assumes the reflector passes overhead at time t = 0). Thus on a plot of Doppler shift versus time a discrete reflector would show as a negative sloping trace. We searched many hours of Doppler versus time plots for evidence of such sloping traces. Most of the plots looked like Figure 2 and revealed no evidence of any convecting reflectors. We tried varying the Doppler and time resolution but produced no better results.
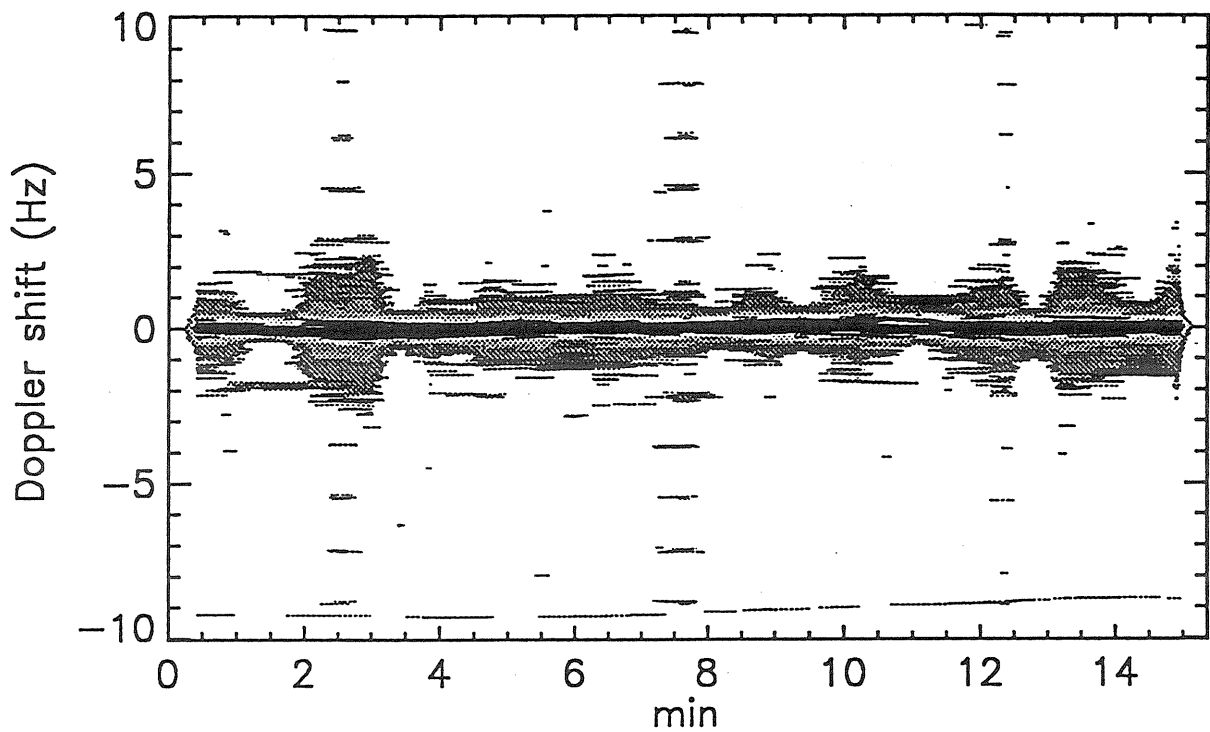
Fig. 2. A common Doppler plot for mid latitudes. This is an E region echo from height 112km. Minute 0 on the plot is 08:49 local standard time, July 14, 1993. Some 'noise' due to strong local interference can be seen. The main echo shows no features which would indicate that there are convecting ionospheric patches.
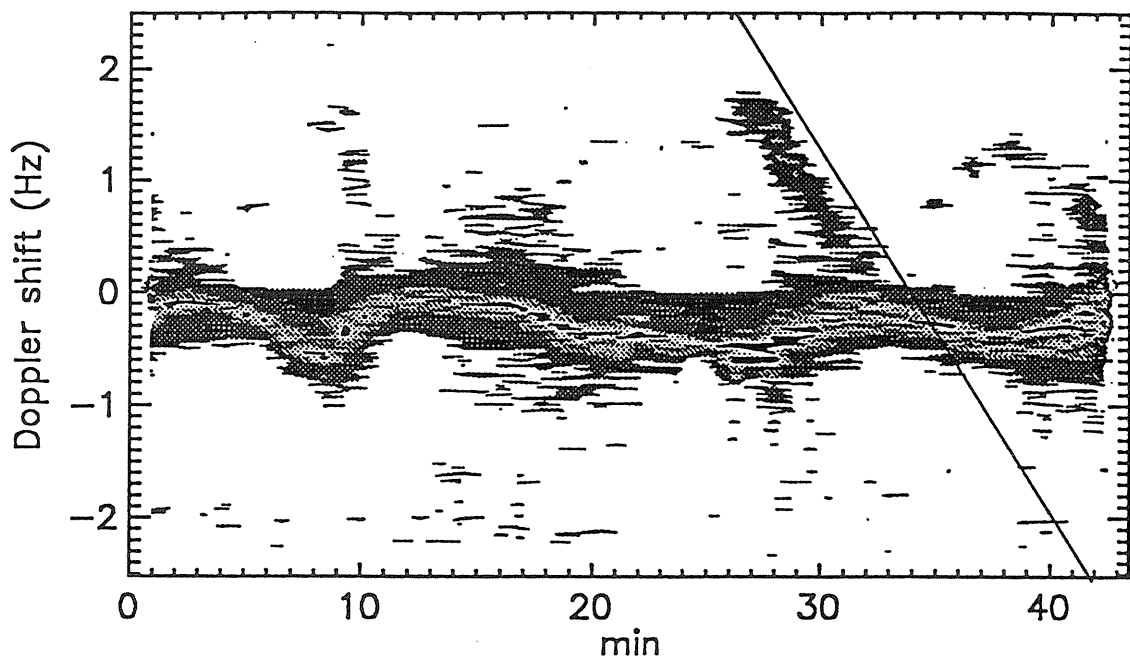
Fig 3. A 50 minute sample of the Doppler shifts observed at the London midlatitude station. This sample was recorded August 11, 1993 and starts at 15:00 local standard time. The virtual height was 264 km. The 'sinusoidal' band across the middle of the figure shows Doppler shifts due to gravity waves. The line drawn on the figure marks the edge of a sloping feature for which the calculated speed is 201m/sec.

Many of our plots showed features like those shown in Figure 3. Here there are 3 cycles of what is probably a gravity wave effect. The midlatitude ionosphere is continuously perturbed by gravity waves propagating from various sources. These gravity waves can cause large perturbations of the Doppler shift and angle-of-arrival of the echo. If there were weak convecting structures these gravity wave effects would make it difficult to observe them. For Figure 3 the peak-to-peak variation in Doppler shift is about 0.55Hz and using 20 minutes as the period of the wave, the variation in height is about ±1.8 km. This is not a large effect, and the maximum velocity perturbation corresponding to the Doppler shift is only about 10m/sec. However, because the perturbation is in vertical height, it is therefore in a direction that is easily detected by the ionosonde radar. A 10 meter per second horizontal speed would usually produce only a quite small Doppler shift if the reflector is near to overhead.

Before leaving Figure 3, note the slanting feature just to the left of the line which has been drawn on the figure. The apparent speed of approach of this feature can be determined from the slope of the Doppler shift versus time. For this feature the speed is 201 m/sec. This is a typical speed for gravity waves so
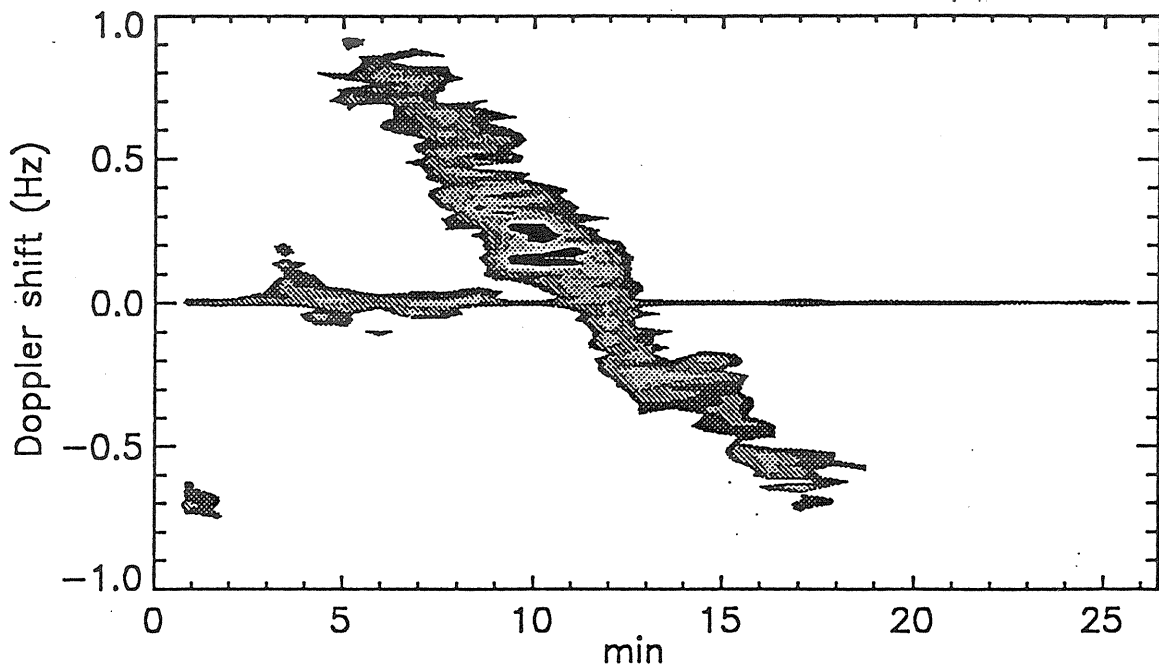
Fig. 4. Doppler shift versus time (in minutes) plot for a drifting E region patch observed from London on July 27, 1993 at 09:35 local standard time. Height of the patch was 109 km and the observing frequency was 3.85 MHz.

presumably this slanting feature is due to reflection from a part of the wave where the geometry is conducive to returning a reflection rather than from a convecting discrete structure.

The only strong convecting feature that we observed from many hours of recordings of Doppler shift versus time is shown in Figure 4. This is an E region feature at 110km height. From the slope of the trace the speed can easily be determined and is 102 m/sec. This result assumes that at closest approach the feature passed overhead. For this same feature a plot of position of the feature, using angle-of-arrival measurements as a function of time, gave another measure of the velocity, and this measurement gave the speed as 99 m/sec and the direction of motion was almost exactly towards magnetic south. These two measures of the velocity are in good agreement and confirm that if we could observe the signatures of convecting structures we could easily measure their velocity. We are suspicious that even the feature seen in Figure 4 is not a convecting structure but is associated with a wave. This is because the velocity is inconsistent with the known properties of convection at this location [MacDougall, 1981].

One reason why we were unable to observe evidence for convecting discrete structures in plots such as Figures 2 and 3 might be that the quite strong specular reflection, and its spread over neighbouring Doppler shifts, due to the finite sample length, might be obscuring the echoes if they are quite weak. We therefore looked to see if there might be weak partial reflection echoes in the ionosphere. To do this we chose a frequency a bit above the E region critical frequency, but usually below the F region critical frequency, and looked to see if, at a height between E and F region, there were any weak echoes. Although we used many samples and processed them using various techniques we found no evidence for partial reflections unless they were weaker than -40 dB with respect to specular reflection.

Discussion

From our measurements we concluded that there was no evidence that in mid latitudes there are readily observable discrete convecting reflectors in the ionosphere. Of course if the reflectors were extremely weak, or were short lived then we would not have been able to detect them. The lifetime of F region irregularities should be of the order of hours so it is unlikely that short lifetimes would be making them unobservable by the methods we used.

Mid latitudes scintillations are evidence that sometimes there are discrete irregularity structures present in the ionosphere. Unfortunately we were not making scintillation measurements during the time of this study, and therefore could not investigate whether there are observable discrete structures during intervals when scintillations are observed.

We conclude that discrete reflecting structures are, at best, rarely observable. Therefore methods of measuring convection based on the presence of such structures should not usually work. Both the standard methods of measuring convection are based on the assumption that convecting structures are present. The two methods are: correlation analysis [Briggs et al., 1950; Phillips and Spencer, 1955] and 'Doppler imaging' [Adams et al., 1986]. The second method is the same as the 'skymap' method used for the polar cap measurements mentioned earlier.

We have used both these methods to analyse many hours of data and both methods give reasonable velocity measurements a large fraction of the time. The Doppler imaging method works better than does the correlation method, but we suspect that this is because our antenna spacings favour the Doppler imaging method. Reinisch et al. [1989] also show reasonable ionospheric velocity measurements from mid latitudes using the Doppler imaging method. Thus although there is no evidence of discrete convecting structures, velocity analysis based on the assumption that such structures are present appears to often produce satisfactory results.

This immediately raises the question: Since the velocity measurements would not work unless there were convecting structures, why were we unable to detect such structures? Possible explanations are that reflections from the structures were either too weak to be observed by our methods, or that at any time there are such a large number of echo components that one cannot resolve individual reflectors. In hopes of solving this enigma we plan on repeating the search for convecting structures with increased resolution.

Conclusion

The CADI ionosonde is in use at a network of 5 Canadian stations. We now have more than a year's data from some of these instruments. Convection measurements at polar cap locations are usually possible using Doppler shift and angle-of-arrival data. This is because of the highly structured nature of the ionosphere at these locations. At mid latitudes our measurements fail to identify any signatures of discrete convecting structures. However standard convection measurements using methods based on the assumption that such structures are present work well a large fraction of the time.

Acknowledgments

References:

Adams, G. W., D. C. Brosnahan, D. C. Walden, and S. F. Nerney, Mesospheric observations using a 2.66 MHz radar as an imaging doppler interferometer: Description and first results, **J. Geophys. Res.,** 91A2, 1671-1683, 1986.

Bowman, G. G., Ionospheric frequency spread and its relationship with range spread in mid-latitude regions, **J. Geophys. Res.,** 96 (A6), 9745-9753, 1991.

Briggs, B. H., G. J. Phillips, and D. H. Shinn, The analysis of observations on spaced receivers of the fading of radio signals, **Proc. Phys. Soc. London Sect. B,** 63, 106, 1950.

Cannon, P. S., B. W. Reinisch, J. Buchau, and T. W. Bullett, Response of the polar cap F region convection direction to changes in the interplanetary magnetic field: Digisonde measurements in northern Greenland, **J. Geophys. Res.,** 96 (A2), 1239-1250, 1991.

MacDougall, J. W., Measurement of ionospheric electric field convection by the Long-Line technique, **J. Geophys. Res.,** 86(6), 4781-4789, 1981.

Phillips, G. J., and M. Spencer, The effects of anisotropic amplitude patterns in the measurements of ionospheric drift, **Proc. Phys. Soc. London Sec. B,** 68, 481, 1955.

Reinisch, B. W., K. Bibl, D. F. Kitrosser, G. S. Sales, J. S. Tang, Z. -M. Zhang, T. W. Bullet, and J. A. Ralls, The Digisonde 256 ionospheric sounder, **WITS Handbook Volume** 2, Ed. C. H. Liu, SCOSTEP, 1989.

Wright, J. W., and M. L. V. Pitteway, Real-time acquisition and interpretation capabilities of the Dynasonde 2. Determination of magnetoionic mode and echolocation using a small spaced receiving array, **Radio Sci.,** 14, 827-835, 1979.

COMPUTER--CONTROLLED OPERATION OF THE IPS-42 IONOSONDE.

J.E. Titheridge,
Physics Department, University of Auckland, New Zealand.

Sick of buying film for your ionosonde, processing it, scaling it -- and then finding (next month) that the exposure was wrong...? So was I. If you have the money, buying one of the new IPS-71 digital ionosondes from KEL Aerospace is the answer. This appears to be a very good and very flexible instrument. If you are poor, or just prefer doing things yourself, read on.

Our IPS-42 has proved very reliable, with camera problems being the main source of lost data. It would be nice to bypass the film, and have all information stored directly in a computer. With the rapidly decreasing cost of microcomputers, computer control has become quite inexpensive and for most experimental work we now use a digital system built round a cheap IBM--clone. We therefore began work (in 1987) on the development of a system to control the IPS-42, to collect the ionograms in digital form, and to store, display and scale these as required. This project was initially quite ambitious with facilities for choosing our own sounding frequencies, and for adjusting the number of soundings made on each frequency to get a reliable echo. After much interesting experimentation the equipment has now been reduced to a simpler form which fulfils all our current needs. This Version 3 of the Auckland "DIGION" system uses an optimised mix of hardware and software, as described below.

The Hardware

The IPS-42 is already, in essence, a digital instrument. Sounding occurs at a fixed sequence of 576 frequencies, logarithmically spaced from 1.0 to 22.6 MHz and set by a digitally-controlled synthesiser. Originally we read (and controlled) the lines driving the synthesiser. For routine operation, however, it has proved fully satisfactory to just store data as it comes, from each of the normal sounding frequencies.

The ionosonde pulses 3 times on each frequency. Echoes are detected using a comparator which gives a logical 1 when the amplitude exceeds the mean noise level by a fixed amount, and 0 otherwise. This binary signal is clocked into a shift register at a rate which stores data from the first 800 km of effective height. The data is re-circulated during the 2nd and 3rd soundings, on the same frequency, to zero any bits which do not correspond to a consistent return. The result is then passed out to the video display during a fourth (quiet) interval. For computer acquisition we intercept this final data stream, and the associated clock signal.

Figure 1 shows a block diagram of the overall "Digion" system. A small printed-circuit board is added at the rear of the IPS-42 ionosonde, drawing its power (1 Watt) from the ionosonde. 5 signal leads from this board are clipped on to edge connectors in the rear of the ionosonde, to extract the Data, Clock, Scan, Xmr (transmitter on) and Yb (display blanking) signals. As shown in Figure. 1, the Scan, Xmr and Yb lines are combined to give a single control line which contains all the necessary timing information. A "minute" signal is also extracted, so that the computer can synchronise itself to the ionosonde clock. One further lead is soldered to the "Monitor Sweep" push button inside the ionosonde; this is used by the computer to initiate a sweep when required.

Standard RS232 drivers are used to feed the ionosonde signals to a cable, which may be tens of metres long, connected to the computer. In the computer is an added printed-circuit board containing, in essence, the circuitry shown at the right of Figure. 1. The critical Y-control line is fed to the computer in both true and complementary form, to reduce noise. These two lines are processed by a circuit which records a transition (in the single Y output) only if both lines switch simultaneously over at least 75% of their full range. This completely avoids common mode interference from the transmitter pulses. A monostable is also used to eliminate rapid transitions. As a final safeguard, the computer keeps track of when the transmitter is on and
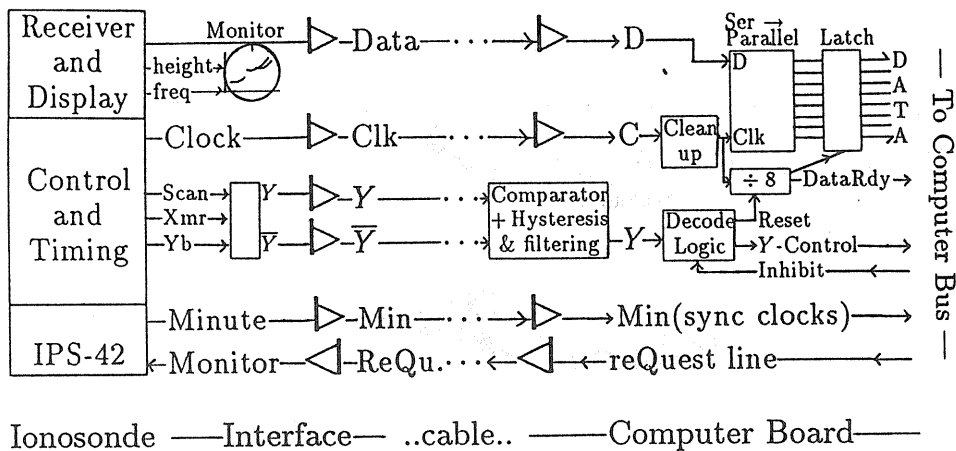
Figure. 1. Block diagram showing the signals extracted from the IPS-42, the general processing, and the signals connected to the computer bus (all fully buffered). Triangular symbols indicate RS232 drivers and receivers.

disconnects the Y signal at these times (using the `inhibit' line in Figure. 1). These precautions make the system fully immune to interference of any sort.

Data and Clock lines from the ionosonde enter the computer through normal RS232 receivers (with added hysteresis), and the Clock is cleaned up to remove any noise pulses. The Data line is then clocked into a serial to parallel converter, and a "Data-Ready" signal is activated when a full byte is available (in a latched register) to be read by the computer. The decoded Y signal is used to synchronise data collection with the transmitter pulses. 64 bytes are read by the computer at each frequency. This gives data bits at each of 512 heights in the range 0 to 800 km, for a height resolution of 1.56 km (double that available on film, or using the KEL DBD-43 controller for the IPS-42).

Within the computer an assembler subroutine is used to monitor the `DataReady' signal, and collect the 64 bytes of data at each frequency. After each byte the computer ignores further signals until the next byte is almost due. After 64 successive bytes, the program again shuts down (to avoid R.F.I.) until just before the time when data should be becoming available at the next frequency. This process is repeated until height scans have been collected at each of the 576 frequencies used by the IS-42 ionosonde. The ionogram is then displayed while the program waits for the next scheduled recording time. Any errors in the time, or in the number of heights or frequencies recorded, is flagged and recorded in a log file. However, with everything now double checked, we get error messages only during power failures. These record the time at which the mains power returns, when the equipment automatically does a full reset, resynchronising the clocks, and recommences recording.

Data Collection and Storage

When the computer is switched on (or reset) it connects to the ionosonde, and waits for a one-minute time signal. This is used to readjust the computer's clock to agree with the ionosonde. Synchronisation is also carried out after the first ionogram in each hour, so that the poor long-term accuracy of the typical computer clock is replaced by the good time-keeping of the IPS-42. The main recording routine is then entered to obtain ionograms at any required intervals. Collection of digital data uses only the `monitor' display on the ionosonde, and runs in parallel to any film recording program. Thus independent data sets are obtained; eg. digital data at 5 min intervals and film ionograms (if you still want them!) at 30 min intervals. Additional ionograms can be collected at any time by pressing `Enter' on the keyboard, or by activating a logic input to the computer. Holding this input low causes ionograms to be collected at an increased rate for periods of special interest.
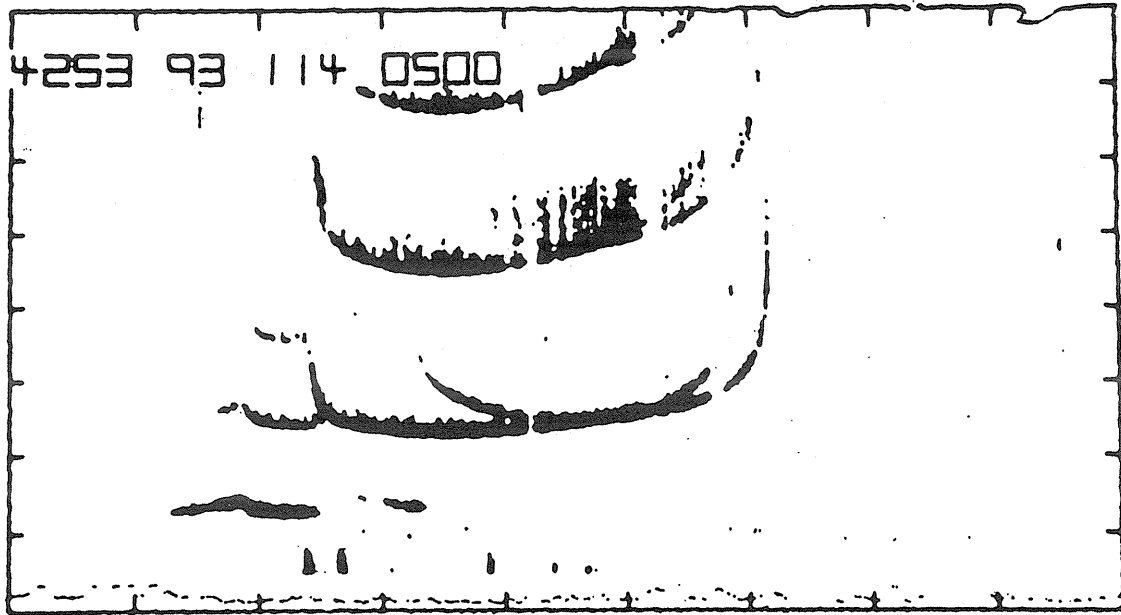
Fig. 2. A print from the film ionogram corresponding to the digital version in Fig. 3. Note that the film misses isolated points which are recorded digitally.
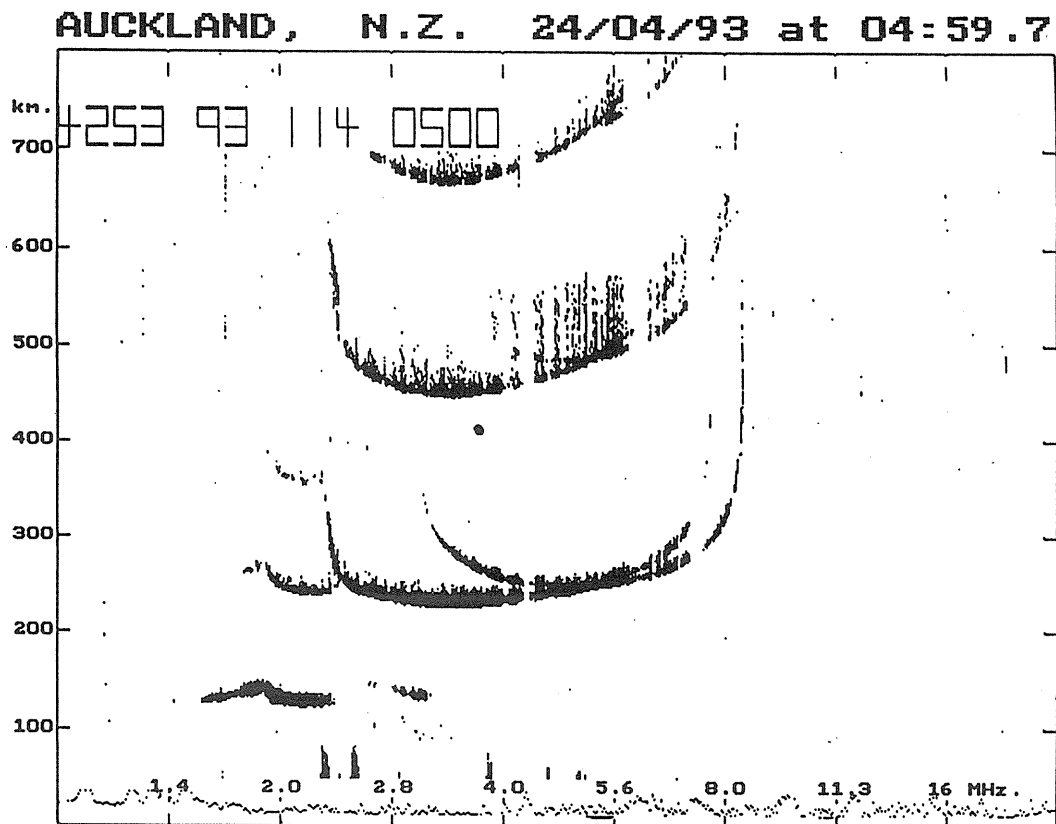
Fig. 3. A typical digital ionogram, as displayed by a computer with VGA monitor. Individual pixels are clearly visible and can be scaled exactly.

With a 1.56 km height resolution the digital ionograms occupy 37 kB. The binary data consists mainly of long runs of `0' (no echoes), with shorter patterns of `1' when echoes occurred. This is rapidly and

efficiently compacted using run-length encoding for the zeros (ie. a count of the number of zero bytes), and byte-long bit patterns for the echoes. This reduces the storage per ionogram to generally between 5 and 9 kB, depending on the echo density. Each ionogram is stored with header information giving the date, time, and the frequency and height ranges used. Each day's ionograms are stored in a different file with header information giving the date, time and station identification.

Storage requirements are reduced by `cleaning' the ionograms before they are compacted. This involves deleting the date-time numerals, all information below 75 km, and all of the graticules apart from 4 reference marks which serve to verify the frequency and height scales. We also normally delete data outside the range 1.3 to 16 MHz. Some isolated dots are deleted using a very conservative algorithm which retains any information which might be useful (as near a critical frequency). Hourly ionograms are left uncleaned to provide a full check on ionosonde operation, including the AGC trace. The negligible data loss is seen in Figure. 4, which gives the fully cleaned ionogram (with added scaling lines) taken 5 min after the uncleaned hourly record of Figure. 3. After this cleaning process, the modified run-length encoding reduces the size of the ionogram data by a factor of about 10--12.

For five-min ionograms, where one in 12 is not cleaned, the average size of the stored ionograms is typically about 3.5 kB. Data for one day (288 ionograms, with a 5--min recording program) then occupies 0.9 to 1.3 MB, depending on the density of spread echoes. This is stored in a separate file for each day, labelled according to the date (eg. FEB93.01, FEB93.02,..). Every five days a standard data-compression program (PKZIP) runs to reduce the files further, by a factor of about 1.8, and copy them to tape. Thus the final storage requirement for high-resolution ionograms, recorded every 5 mins, is about 15--20 MB per month or 180--240 MB per year. This fits comfortably on two 120 MB tape cartridges (costing less than $30 each) which are swapped monthly so that data can be scaled.
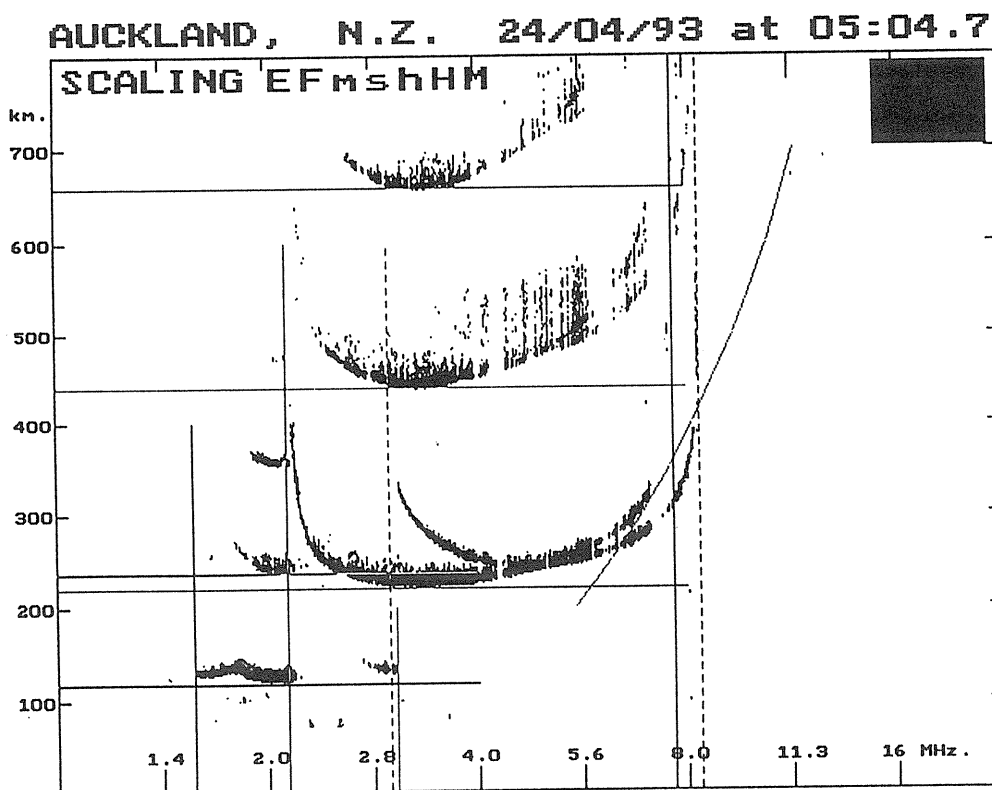
Figure. 4. A digital ionogram after `cleaning' to halve the size of the stored ionogram. Horizontal and vertical lines are added by the computer for scaling heights and frequencies; the curved line is for M(3000).

31

Results

A separate software package is used for display and scaling of the data. This is far more convenient than handling film ionograms. Several months' data can be stored on a hard disc, with any ionogram rapidly accessible. Holding down an arrow key gives a fast forward or backward scan of successive ionograms (`Movie' mode, at rates of about 2 per second) to dramatise changes and to select ionograms for further study. PageUp and PageDown keys are programmed to show only every sixth (half-hourly) ionogram, for a quick overview. Control--Page skips in two-hour steps for rapid access. We can also jump directly to the first or last ionogram in the current day, or on the preceding or following day. Another key will display, within one second, the ionogram at the same time on the preceding or following day. This feature, impossible with filmed data, is invaluable for studying unusual effects near sunrise and sunset. The display of digital ionograms is also much more detailed and accurate than anything available using films. This is seen by comparing Figure. 3, dumped from a computer screen, with the same ionogram printed from film (Figure. 2).

Scaling of data is carried out using a computer aided approach. Thoughts of fully automatic scaling were discarded because of the difficulty of identifying correctly the O and X traces. Also it is hazardous to use automatically scaled data without verification, so we may as well verify as it is scaled. The current display initially shows, as vertical or horizontal lines, the critical frequencies and minimum heights scaled from the previous ionogram (Figure. 4). Horizontal lines are shown simultaneously at h, 2h and 3h so that multiple echoes can be used to increase scaling accuracy. Similarly the critical frequencies for the x component, calculated exactly from the corresponding fo, are shown as broken lines. The MUF curve is also shown. Each line appears in a different colour, and coloured letters (following `SCALING' in Figure. 4) indicate the corresponding parameter. The rectangle at the top right in Figure. 4 is coloured to show the `current' parameter. (Original colour prints for Figures. 3 to 5 are available from the author.)

Figure. 5. A `Varion' plot, using 5-min ionograms to show the variations in echo height at a number of fixed frequencies, for four successive days in winter. The 4 frequencies used for this plot are listed at the top, coloured coded in the same way as the corresponding echoes.

Cursor keys are used to adjust the positions of the lines. Tapping `return' saves the scaled values and displays the next ionogram. Scaling is more accurate and very much faster than from film, and the results are fully checked and reliable. Simultaneous display of fo and fx for each layer, always at the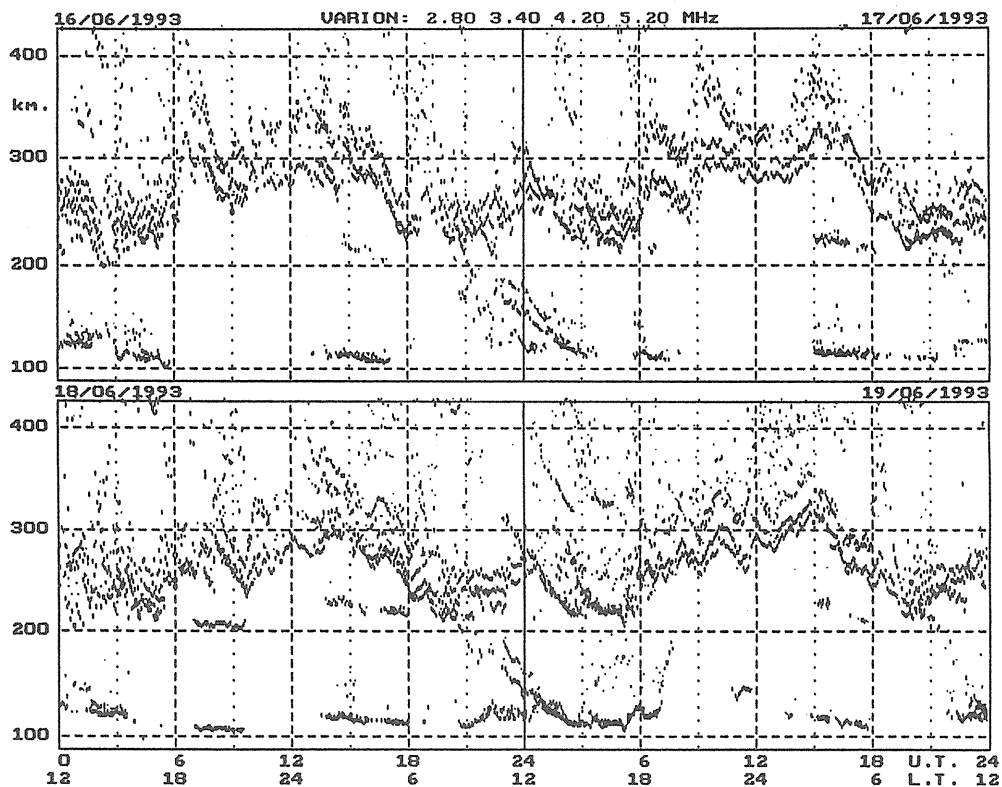 correct (calculated) separation, greatly increases the ease and accuracy with which critical frequencies can be determined. The vertical fo, fx lines will be replaced later by virtual-height curves calculated for a simple (adjustable) model ionosphere. This should provide maximum accuracy for foF2, and allow reasonable estimates of both the scale height and the peak height of the layer.

Summary

The ionosonde software is written primarily in C++, with assembler routines for the actual data collection, and occupies less than 200 kB. As a result it runs happily on the slowest and smallest IBM-compatible microcomputer. 10 Mb of free disk space will allow storage of up to one month of 15--min ionograms, using only the modified run-length compaction built in to the program. Further compaction (using PKZIP) fits a month's worth of 5--min ionograms into 15--20 MB. A cartridge tape drive is convenient for long-term storage.

An obsolete XT computer with a 40 MB hard disk is ideal for running the `Digion' system; these can be obtained for less than US$250, or $500 with a new tape drive. We can supply copies of our hardware (including plug-in printed circuit boards for the computer and the ionosonde, plus the cable and all programs) for about US$1,600. The new system has operated flawlessly for over two years at Auckland, and five copies have been provided to other satisfied users who have tried (and failed) to make the system `bomb'. Data is stored in a simple but efficient format, and source code is provided for all programs so that a user can get what he wants from the data, in whatever form he wants. It is hoped that cooperation between users will lead to an increasing amount of useful, freely available software for various purposes (such as the h'(t) plots shown in Figure. 5).

The main advantages of changing an IPS-42 to computer control, with digital data collection and storage, may be summarised as:

- **No Film**-- No more buying and processing film. Store ionograms for a decade in the space of one book. Share copies made cheaply in your computer.

- **No Hassles**-- Immediate display of final stored data to see that everything is correct. You don't have to wait a month to find the exposure was wrong.

- **Viewing**-- Scan data rapidly on your own computer. Skip through hourly ionograms for a quick overview. At the touch of a key, make rapid comparisons with data on adjacent ionograms, or at the same time on adjacent days.

- **Accuracy**-- Appreciably higher detail and resolution than film ionograms, and always in sharp focus. The height and frequency of each displayed dot is known exactly by the computer (with no calibration).

- **Scaling**-- is faster and much more accurate, without the eyestrain. Simultaneous display of both fo and fx, always at the correct separation, gives more accurate values of fc. For height measurements, rules at h, 2h and 3h allow convenient use of multiple echoes.

- **Savings**-- To store 5--min ionograms costs about $50 per annum. For 2--min ionograms it will cost you another $1 per week. Why be restricted by 15--min (filmed) ionograms?

- **New Uses**-- Plot h'(t) at any number of frequencies for a clear display of ionospheric changes, TID's and gravity waves (as in Figure. 5). Do real-height calculations with a simultaneous display of the full ionogram, the scaled data points, the calculated profile and the corresponding virtual heights.
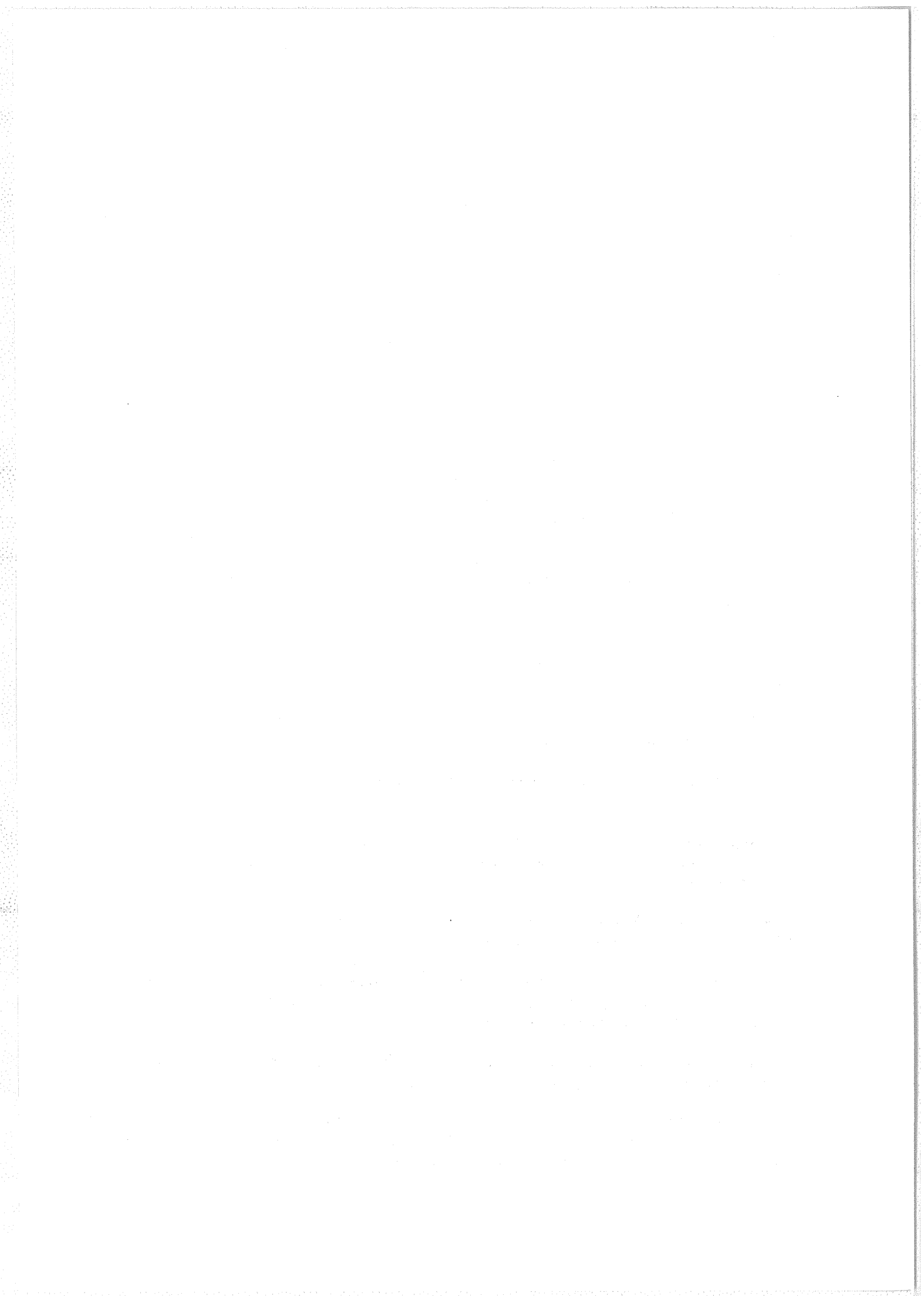
THE IONOSPHERIC COMPLEX "CYCLON"

A. D. Akchyurin, R. G. Minullin, V. I. Nazarenko, O. N. Sherstyukov, A. L. Sapaev and E. Yu. Zykov
Physics Faculty, Kazan State University, RUSSIA
email: root@scikgu.kazan.su

Development and manufacture of different types of ionospheric stations was started at Kazan University in 1977. In 1979 an analog ionospheric station (a mobile station) was made. Several cycles of measurements for investigating sporadic E layer peculiarities were made with the station.

Subsequently, a series of digital ionospheric systems, called "Cyclon", were started in 1983 utilising the radio receiving apparatus P-399, A ("Katran") and a computer, "Electronica D3-28". Further development of the ionosonde is continuing. At present, the seventh ionosonde model, Cyclon-7, and the tenth model, Cyclon-10, have been developed and produced with the following characteristics:

Sounding frequency band	1-32 MHz
Pulse width	50-200 mks
Pulse repetition rate	10-100 Hz
Pulse power	5-10 kW
Pulses per frequency	1-128
Receiver bandwidth	30 kHz
Receiver dynamic range	60 dB
Digitisation levels quantity of amplitude	512
Range increment	2,5 km
Range samples	400
Quantity of sounding frequencies	1-500 kHz
Minimum recording time of ionogram	2 s

The Cyclon-10 has a higher power output than the Cyclon-7.

The ionospheric complexes Cyclon-7 and Cyclon-10 were developed by Kazan University and are intended for digitally recording three dimensional ionograms (range, frequency, amplitude) from vertical, oblique and backscatter soundings of the ionosphere and to then calculate the electron density profile.

The complexes comprise a pulse transmitter, receiver, IBM compatible PC "Iskra-1030" and equipment for keeping and locking the time standard. A Pascal program controls the operation of the complex and allows automatic processing of ionograms and interactive modes, to determine and store the ionospheric parameters as well as calculate the electron density profile and determine the monthly average values of the ionospheric parameters. The ionograms and ionospheric parameters are displayed and stored, using international standards, on paper and floppy disks.

Both Cyclons can be applied in static and mobile situations for scientific research and in ionospheric networks. Both ionosondes are intended for operation in a regional network as a central and also as an outlying ionosonde. Ionosondes "Cyclon-7" and "Cyclon-10" can both handle vertical and oblique soundings and are equipped to maintain a time standard. Both ionosondes take records of ionospheric

parameters (critical frequency, virtual height) in the international standard form, and also the frequency and virtual height of every reflection point for any ionospheric layer.

As already mentioned, Cyclon-7 and Cyclon-10 may be to used for scientific investigations. It is possible to study any ionospheric layer or some regions of reflected traces. Frequency steps of 1 kHz can be used. The ionosondes can be used to study energy characteristics of reflected signals. Every reflected pulse can be displayed on the screen as an amplitude-time realisation where pulse distortion due to multi-ray interference is evident.

The Cyclon-7 and Cyclon-10 ionosondes are designed for making detailed investigations of the Es-layer and the characteristics just mentioned support this when analysing Es-layer reflections. It is possible to analyse multiple Es-layer reflections in both frequency and amplitude, to investigate the amplitude-time dynamics of Es-layer reflections, to watch the Es-cloud generation and destruction, to observe the rate of amplitude-frequency variation of Es-layer and so on. The Cyclon-10 ionosonde, unlike the Cyclon-7, has increased radiated power for detailed research of weak Es-layers, that are not always seen successfully with ordinary ionosondes.

Cyclon-7 was used to make over-all tests in three measuring cycles: June 1992 in Kazan, September - November 1992 in Moscow region. The tests have shown agreement between the calculated and real engineering characteristic of ionosonde. Cyclon-7 was used to make around-the-clock tests at different seasons in a mobile version. These tests were carried out successfully and confirmed the normal operation of the ionosonde in different unfavourable climatic conditions. The comparison of data obtained with the Cyclon-7 and those from the institute ionosonde, a distance of about 50 km away, were good. The critical frequency errors for ionospheric layers were no more 0.2 MHz in most cases. Routine operations were tested using Cyclon-10 during June 1993 at the experimental range in Kazan.

Thus, the over-all tests of Cyclon-7 have shown satisfactory, normal operation and good accuracy agreement with characteristics obtained with a network ionosonde. Consequently, Cyclon-7 may be used successfully in regional ionospheric networks as well as for scientific research on small scale irregularities.

By using the Cyclon-7 and Cyclon-10 ionosondes, we plan to test the principles of a regional ionospheric network described above. One of the ionosondes will be used as a central location and the others as outlying ionosondes, thus creating one arm of a regional ionospheric network. Using two ionosondes it will be possible to work out all regimes of ionosonde co-operation as well as support a regional ionospheric network.

AUTOMATING VERTICAL IONOGRAM COLLECTION, PROCESSING AND INTERPRETATION

S. A. Pulinets
IZMIRAN, Troitsk, Moscow Region, 142092, RUSSIA

INTRODUCTION

As a result of global scale and regional modelling of the Earth's ionosphere, international data exchange of the ionospheric data in the frame of international projects such as SUNDIAL or PRIME, creating of different data bases and data banks, there arises a need for fast data processing and recording in a standard format. One such format was elaborated by the URSI Working Group on the Ionospheric Informatics [1]. During the last years a lot of algorithms and computer programs appeared concerning the automatic scaling of vertical ionograms. At the same time we should keep in mind that the global network of ionospheric stations (especially in the previous Soviet Union) was created in the 50-60 years when the International Geophysical Year projects were carried out and a lot of stations continue their work with photo film or paper output. So the problem should be looked at more widely: not only from the point of view of modern hardware and digital ionosondes, but also how to include in the digital international data exchange these old stations and how to master the old data banks on photo films for the previous tens of years of regular observations.

This paper is an attempt to combine both the modern developments and modernisation of the old stations with the following description of the works carried out in the former Soviet Union (FSU).

The Short History

From the very beginning of vertical sounding activity in the Soviet Union IZMIRAN (Institute of Terrestrial Magnetism, Ionosphere and Radiowave Propagation of the Russian Academy of Sciences) was responsible. The present network of ionospheric stations was created mainly during the International Geophysical Year and the basic ionospheric station for the network was the station AIS (Automatic Ionospheric Station, see Fig.1) developed in IZMIRAN. Some of the central institutions like IZMIRAN, Moscow, were equipped by a more powerful station SP-3 made in Eastern Germany. All of them were tube stations with photo film output and manual processing of the ionograms. The majority of the stations still exist and are working within the network.
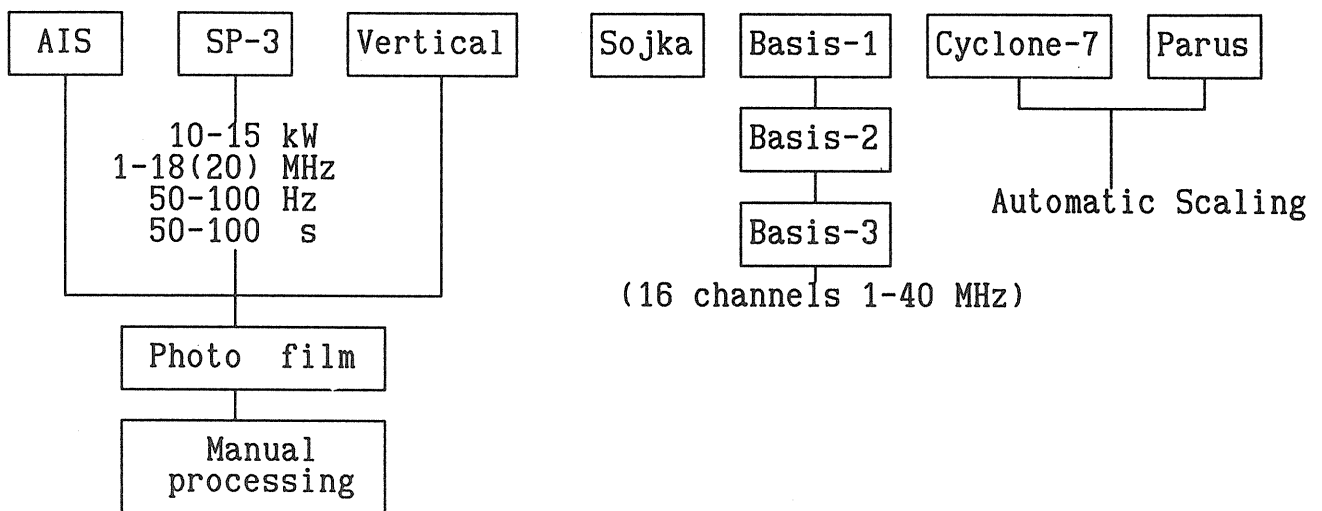
Fig.1 The hystory of Russian ionospheric stations
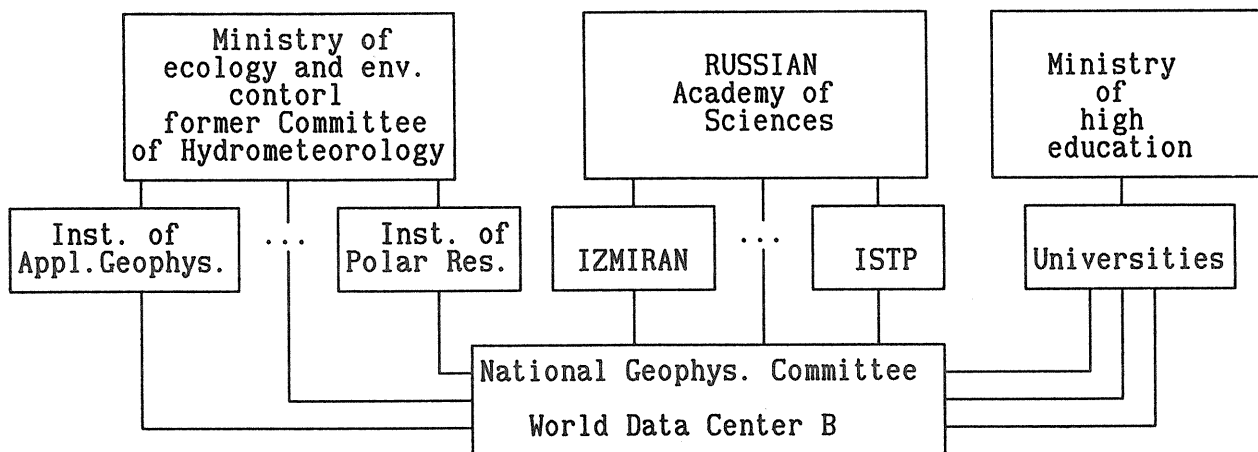
Fig.2 Schematic diagram of Ionospheric study management

When, after several transformations, IZMIRAN was included in the Academy of Sciences, the duty of ionospheric service and forecast was given to the Committee of Hydrometeorological Service where the special institutes were created such as the Institute of Applied Geophysics (Moscow), Institute of Arctic and Antarctic Research (St Petersburg), Institute of Polar Geophysics (Murmansk) etc. After this time coordination of ionospheric sounding was spread out and every institution tried to create its own ionosondes: "Vertical" station for service by Institute of Applied Geophysics, "Sojka" and "Basis" for scientific research by IZMIRAN (see Fig.1). If it is taken into account that some Universities which were subject to the Ministry of High Education (now Ministry of Science) had their own stations, the very complex system of ionospheric research in FSU can be understood. The centres which united the different institutions were the National Geophysical Committee and World Data Center B where the ionospheric data were accumulated (see Fig.2).
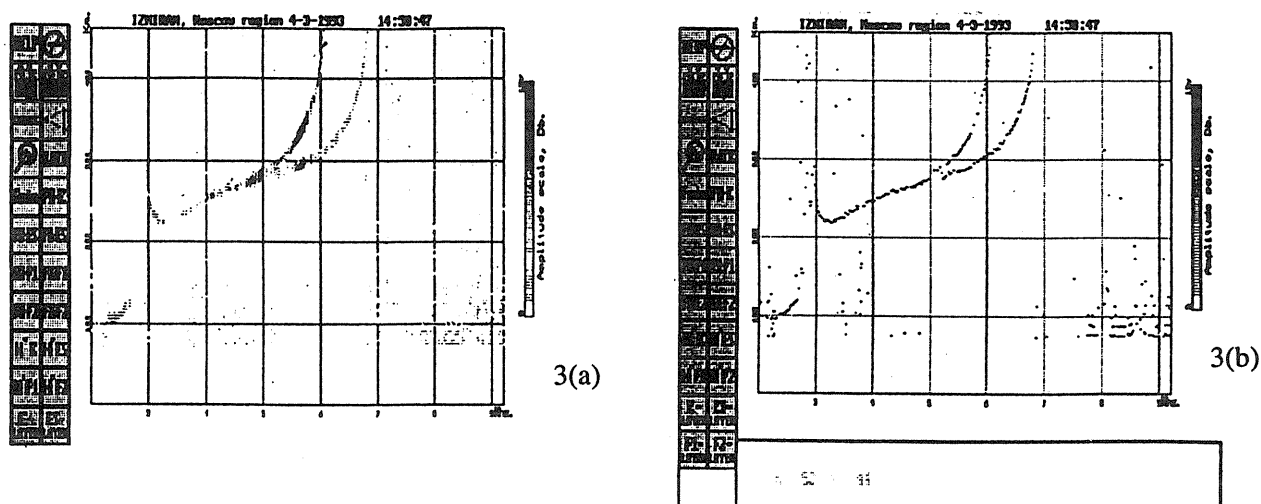
Figure 3: PARUS ionosonde ionogram before (a) and after (b) "cleaning" procedure.

The first station which used computer processing of ionograms was the "Sojka" station opened at IZMIRAN in the 70s. The first algorithms of ionogram "cleaning", extracting of traces and automatic scaling were created at this station.

The next family of ionosondes which should be mentioned are the "Basis" stations where for the first time multi-channel technology was used for the automatic extraction of O or X traces and Doppler measurements. Some of the ionospheric observatories in the FSU are equipped with Basis-1 or 2 stations. The latest version, the Basis-3 station, is a 16-channel station which could work within the frequency band 1-40 MHz in vertical or oblique sounding regimes and could be regarded as a HF Coherent radar station. The main deficiency of the station is the low degree of integrated electronic circuitry, which lowers its reliability.

The first stations where the fully automatic algorithms of ionogram processing were introduced are: Cyclon-7 station in Kazan' (Kazan State University, Tatarstan), Chirp station at Irkutsk (Institute of Solar-Terrestrial Physics) and Parus station at IZMIRAN (Troitsk, Moscow Region).

Automatic Scaling of Vertical Ionograms

First of all, in developing the principles for automatic scaling the input information for scaling algorithms needs to be taken into account. The most complex case is old ionograms stored on photographic film and currently working, old ionosondes with film output. In this case we have as input two dimensional frequency-time delay information (Fig.3a). The second step introduces the amplitude of the reflected signal into the processing procedure, which is possible if the output from the old ionosonde is taken before being photographed (for example with the help of a digitising card, taking the analogous electrical signal output).

The next step which increases the probability of automatic scaling is the use of polarisation measurements. In this case one can exclude from the processing algorithm one of the most complex procedures of the ionogram scaling: separation of O and X traces.

The last improvement which has now been made in most modern ionosondes is the Doppler measurements and measurements of the angles of the wave arrival. This is a very important feature, especially in high latitudes and during disturbed periods when non-vertical propagation traces could be registered.

Various possibilities are as follows:

Semi-manual scaling and digitising of vertical ionograms.

As the input for processing we have a two dimensional (frequency-virtual height) picture. The sources for such processing could be: digitised ionograms from photo films or from paper, a digitised ionogram directly from the analog output of an old ionosonde or a computer recorded ionogram without amplitude as in the Polish, KOS type, ionosonde. In the first two cases we need to introduce the procedure of screen scaling. It is implied that all ionograms under processing have the same scale and the procedure of screen calibrating is done once before processing any ionograms. The software, for ionogram scaling, was created at IZMIRAN by V. Zarubanov and S. Pulinets and includes the following procedures:

- Screen scaling
- Ionogram scaling and interpretation with recording of standard ionospheric parameters and their URSI codes
- Ionogram scaling and N(h) profile calculation based on algorithm of Gulyaeva [2]
- Formation of hourly tables of standard ionospheric parameters in URSI IIWG format

Ionogram processing could be done with the help of a mouse or keyboard. For good quality ionograms the procedure of automatic tracing could be introduced as it was produced for topside ionograms. In this case

it is necessary to indicate by hand the O and X traces.

Further utilisation of the data base in URSI IIWG format is possible using the IDIM (Ionospheric Data Illustrator) program developed at IZMIRAN [3]. This program makes the visualisation of any standard ionospheric parameter (monthly variations, daily variations or any selected period within one month) possible. The User can construct, with the help of this software, their own output format plot for any of the ionospheric parameters or several of them together. One can edit the ionospheric data files in the form of hourly tables. It is possible to use the external programs using the ionospheric parameters and results will be presented on the screen in graphical form. The hard copy of every plot could be done.

Semi-automatic scaling using the amplitude information

Amplitude information is used for ionogram processing in ionosonde systems "Parus" [4] and "Cyclon-7" [5]. In both systems a correlation analysis and adaptive filtration procedure is used to clean the ionograms before their interpretation. Wide-band noise, spread signals and non-trace points are removed from the ionogram with the help of a "cleaning" procedure and the maximum weighted amplitude points are kept as a trace. One can see on Fig.3a the example of an ionogram before and after the "cleaning" procedure. The automatic tracing procedure is then used. The role of the operator is to "show" the O and X traces to the tracing program. Such an algorithm is realised in the "Parus" system. The more advanced procedure of full automatic scaling of vertical incidence ionograms using only amplitude information, was developed at Irkutsk Institute of Solar-Terrestrial Physics [6] and is described in the next paragraph. The procedure is described in more detail because it does not demand advanced hardware and could easily be introduced into any ordinary ionospheric station.

Automatic scaling of vertical incidence ionograms

The program PACIFIC (Program for Autoscaling of Conventional Ionograms with Flexible Interpretation Control) was designed for a FMCW sounder but the algorithm could be used for any ionogram because the linguistic image analysis procedure was chosen for ionogram processing and is based on the final

$$\rho = \frac{\text{Minimum between } A_m \text{ and } A_{test}}{\text{Minimum of } A_m, A_{test}}$$

if $\rho < \rho*$, separate echoes

$\rho*$ - user-defined parameter
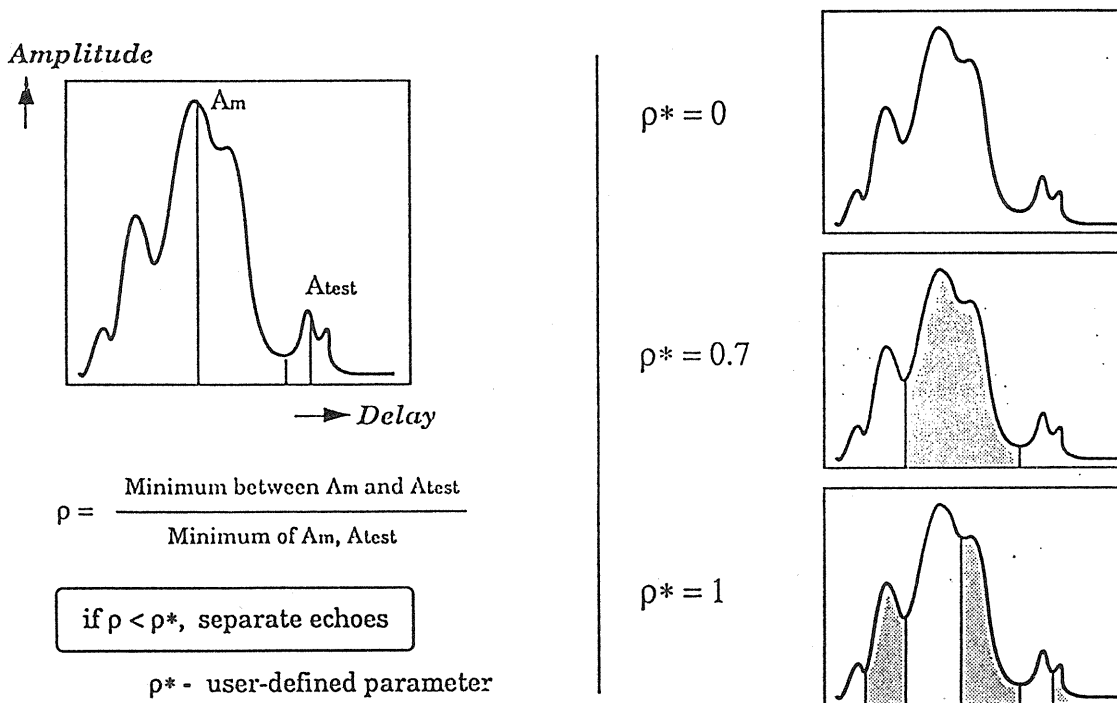
Figure 4: Illustration of the Separating Overlapping Echo procedure within the PACIFIC algorithm.

40
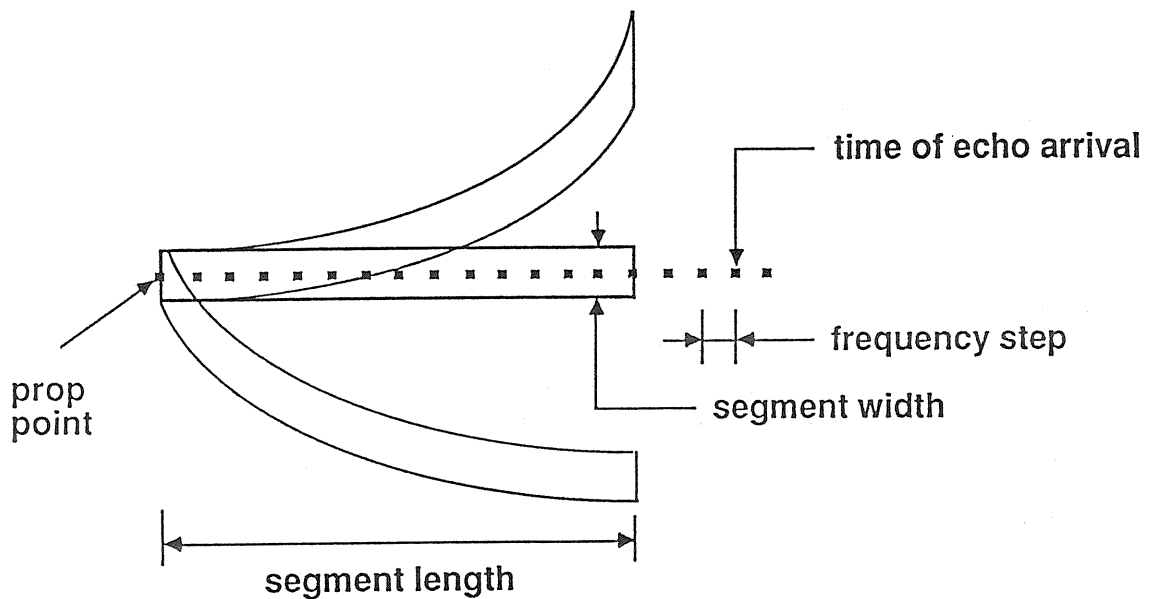
Figure 5: The Single Segment Fit procedure within the PACIFIC algorithm.

appearance of the ionogram pattern. The main processing steps are as follows:

- Separating Overlapped Echoes (adaptive separation based on significance of valley between peaks);

- Segment Fit (line tracing by fitting, combining and chaining trace segments);

- "E-Es-F2-F1" Interpretation Procedure (search for the fxF2 cusp after E-layer data has been identified);

- Inclination Check (interpretation of the traces with proper inclination).

The first step is illustrated in Fig.4. The special criterion developed is based on which signal of complex form is recognised as consisting of two or more overlapping signals. The control parameter p makes it possible to control the dividing threshold. One can see on the presented figure that, depending on the

1. E-layer parameters
2. Center of F-layer reflections
3. Es-line
4,5. Tracks close to critical frequencies of F2 layer
6. Intersection point of O- and X-tracks in F2 layer
7. O-line
8. Kinks and fractures of O-line
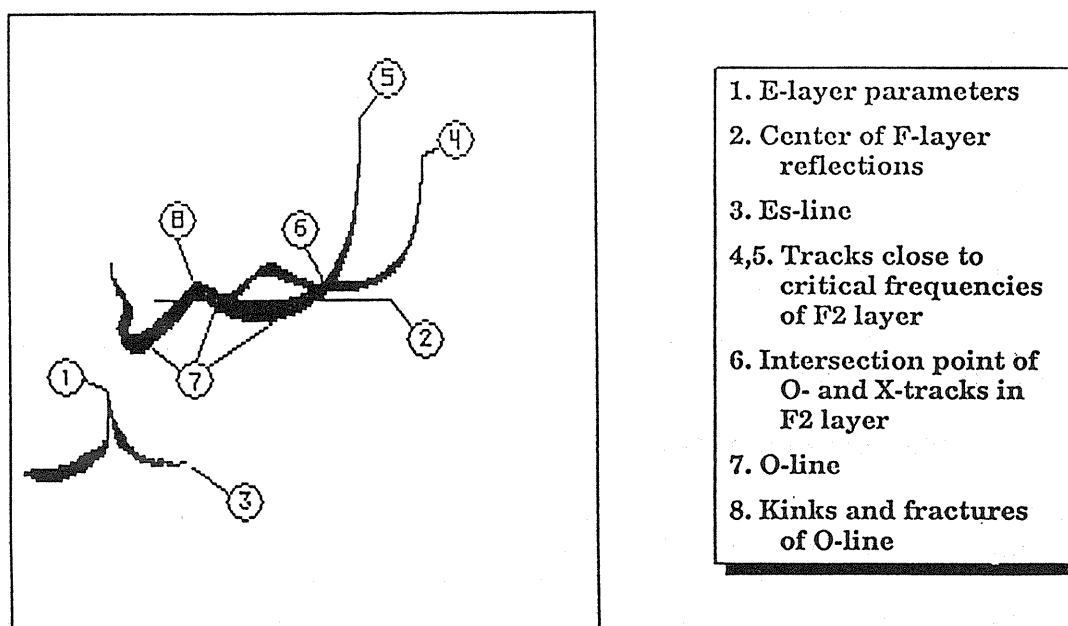
Figure 6: Schematic representation of the PACIFIC ionogram interpretation algorithm.

41

parameter value, the same signal could be recognised as one, three or six different signals.

The Segment Fit procedure is illustrated by Fig.5. It is based on the fitting mask algorithm. The left side of the mask is fixed on the processed point and different inclination angles are probed, and the best variants of mask orientation are stored. Then the selection and combining of stored masks is done to provide chaining of the ionogram elements. During the fitting procedure, information on the 9 neighbour frequencies is analysed to determine what makes the algorithm more stable.

After real trace selection, the interpretation procedure begins, which is shown in Fig.6. After separation of the E-layers, a search and identification of signals near the critical frequencies of both components is done making the algorithm more stable in relation to multiple layers and spread-F effects. The next step is the construction of the O-trace line between fmin and the O-X trace intersection point (6). This consists of the points of maximal amplitude. After its extraction, a search for kinks and fractures is made, which gives the F1 critical frequency.

Testing of this software gave the following results in comparison with the manual scaling of March 1987:

Total 162	ionograms	percentage
113	processed without errors	70.0%
22	F1 interpretation errors	13.5%
11	O-line problems	6.7%
6	Errors due to F-spread	3.7%
5	F2 critical frequencies errors > 0.2 MHz	3.1%
5	h'F1 incorrect estimation	3.1%
5	foE errors	3.1%
4	Erroneous identification of Es	2.5%
3	Loss of steep tracks	1.9%
1	General scheme failure	0.6%

This is a very promising result. It should be mentioned that correcting mistakes when scaling automatically is much easier than manual processing of the ionogram from the very beginning.

Advanced Processing and Perspectives

The outlook on the automatic scaling of ionograms is now more optimistic than a few years ago mainly due to progress in signal and image processing. Modern ionosondes such as D-256, IPS-71 or "Parus" have options such as O/X separation, Doppler, Angle and Direction of Arrival information that can be measured routinely. For such stations the main task now is to improve existing algorithms, especially for high latitudes and during strongly disturbed periods. Experts in the field of artificial intelligence should be encouraged to introduce into algorithms more sophisticated methods of pattern recognition. One can attribute a lot of complex cases for ionogram interpretation but there are still a finite number of cases and

they could be stored as samples in computer memory.

More complex is the situation with old film based ionosondes and utilising old ionospheric data stored on photographic film. The solution to the problem is seen in supplying old ionosondes with a digitising card connected to a computer. Photographic films could be processed by digitising devices based on CCDs or TV cameras. Both types of ionograms, from the old ionosondes and those digitised from films, could be processed then by software like PACIFIC or ISC.

Taking into account the very great importance of real time processing of ionospheric information in the light of new ideas of global ecology monitoring, the possibility of earthquake predictions and the necessity for old data utilisation from the point of view of Global Change, common international efforts should be undertaken to make automatic ionogram scaling a common feature of modern ionospheric science.

Acknowledgments

References

1. R. R. Gamache and B. W. Reinisch, Ionospheric Characteristics-Data Format for Archiving at the World Data Centres, Dec. 1990, Univ. of Lowell Centre of Atm. Res. Sci. Rep. No. 467

2. T. L. Guliaeva, Progress in ionospheric informatics based on electron density profile analysis of ionograms, **Adv.Space Res.** 1987, 7(6), p.39-48

3. K. F. Yudakhin and S. A. Pulinets, Ionospheric Data Illustrator (IDIM) program, Techn. Rep., 1993, No.2/35, TRONIS

4. A. E. Reznikov, A new ionosonde: the digital ionosonde-PARUS, **INAG Bulletin** No.56, Nov.1991, p.3-4

5. A. D. Akchurin, R. G. Minullin, V. I. Nazarenko, A. L. Sapaev and O. N. Sherstiukov, "Cyclon" ionospheric complex with automatic ionogram processing, **Proc. of Nat. Workshop on Ionospheric Monitoring**, 1991

6. I. A. Galkin, On the problem of automatic processing of back-scatter and vertical-incidence ionograms, **Proc.of ISAP'92**, Sapporo, Japan, p.1197-1200

AUTOMATIC IONOGRAM PROCESSING SYSTEMS IN JAPAN

S. Igi, K. Nozaki, M. Nagayama, A. Ohtani, H. Kato, and K. Igarashi
Communications Research Laboratory, Ministry of Posts and Telecommunications, 4-2-1
Nukui-kita, Koganei, Tokyo 184, Japan

Abstract

A new system has been developed that digitises, archives, and autoscales the ionograms obtained by the four observatories located throughout Japan. This paper describes an automatic ionogram processing system and a new display method that shows both ionospheric phenomena and propagation conditions of HF radio waves. The test of the automatic scaling algorithm, performed using nearly 7000 ionograms, indicates that the algorithm can successfully derive the values of foF2, fEs, and fmin within an error of 1 MHz or less, more than 80%, 90% and 99% of the time, respectively. However, the reliability for foF2 is poorer during the summer season because of the presence of the presence of blanketing-type Es. With regard to obtaining the median values of foF2, fEs, fmin, and h'Es, the automatic scaling algorithm is found to perform well. The automatic scaling codes were converted to a M-750V system (IBM compatible system) in 1991, and the UNIX system in 1993.

Introduction

Synoptic ionospheric measurements in the form of ionograms have provided valuable information both for the HF communicator and for studies related to the physics of the ionosphere. However, the scaling of ionospheric parameters is a laborious task because of complex structures that can often appear on an ionogram. Furthermore, the appearance of two echo traces, called the ordinary and extraordinary components, adds further complexity to ionogram scaling. For the reason cited above, scaling is routinely done by highly specialised experts at a majority of ionospheric observatories.

In recent years, automatic scaling systems have been developed by several organisations [1][2], primarily motivated by the following reasons: the difficulties involved in training skilled scalers; the requirement for the availability of real-time data, and; the elimination of human errors. The Communication Research Laboratory (CRL) has completed the development of a fully automatic system that can be attached to conventional ionosondes for the purpose of collecting and processing ionospheric data [3][4][5].

This paper describes an automatic scaling algorithm for those ionograms which do not distinguish between ordinary and extraordinary mode components. In order to evaluate the performance of this algorithm, automatically-scaled parameters are compared with those derived from manual scaling for some 7000 ionograms acquired over an interval of one year. Also, new plots are presented showing the diurnal variation in ionospheric characteristics for surveying ionospheric phenomena.

Automatic Ionogram Scaling

The CRL has completed the development of automatic scaling software to cope with the difficulty of training reliable scalers. In this section, each of the major steps invoked by the algorithm will be described.

Elimination of Multiple Traces

Multiple echo traces are eliminated from the original ionograms by using the criterion that they must be observed at two or more virtual heights at a given frequency. This process becomes important in determining whether or not the F trace is completely blanketed by Es. The details of this decision will be discussed later.

Selection of Areas Containing foF2, fmin, E-layer Region and F-layer Region

This step selects four regions, that is the foF2, fmin, E-layer, and F-layer, for the sake of being efficient and economic use of CPU time. The foF2 region is extracted by detecting those echo traces with a large gradient in frequency. As for the fmin region, the lowest frequency region containing echo traces is removed. The criteria used to remove E and F layers are the E and Es layer echoes observed below and the F layers observed above about 180 km are removed.

fmin Scaling

After applying a low pass filter to the fmin region extracted in the previous step, the scaling program searches for fmin by detecting the lowest frequency of each echo trace. If fmin cannot be found within the frequency range measured by the ionosonde, the program signals that a value fmin cannot be determined because of the presence of radio wave absorption. In this case, the subsequent procedures are terminated, because it is assumed that no ionospheric echoes are observed within the frequency range measured by the ionosonde.

Extraction of E Region Parameters

The echo traces observed in the E regions exhibit very complex structures on an ionogram, because both E and Es layers can exist at similar heights, a situation further complicated by the inability of the ionosonde to separate ordinary and extraordinary mode waves. As a result, the task of automatically scaling E-layer parameters is rather difficult. Therefore, the CRL method scales the top frequency of the Es (fEs) instead of the highest frequency of the ordinary mode component of the Es (foEs), which is often impossible to determine, even by experienced human scalers. Although fEs coincides with fxEs in general, fEs corresponds to foEs in those cases when the extraordinary mode echo is not present.

The first step in obtaining the parameters of the E region is to connect the edges of echo traces that are thought to belong to the same line. The layer (E or Es) and polarisation (O-mode or X-mode) of each line are identified by comparing the shape of the echo traces to patterns stored in the computer memory. The E region parameters are then scaled from each identified echo trace.

Recognition of Blanketing-type Es

To recognise whether or not the F-layer is completely blanketed by Es or not is a critical step. Fail here and the program, which searches for F-layer parameters regardless of the appearance of F-layer traces, will be in error. The main reason for adding complexity to this recognition process is that multiple Es and F-layer traces are frequently observed at similar heights. Thus, the multiple traces associated with Es are eliminated in the first step, so that no echoes except for F-layer echoes should be observed at F-layer heights. The presence of completely blanketing-type Es can be determined by detecting whether or not traces in the F region in addition to those associated with the Es layer. In this case, the parameters related to the F-layer are not scaled but symbolised as "blanketed" in case of completely blanketed-type Es.

foF2 Scaling

Only echo traces in the neighbourhood of the F2 cusp are extracted from the foF2 region identified in the second step. Next follows noise reduction with a low pass filter, extraction of the leading edge, and preliminary fitting to the F2 trace with a parabolic curve. The hyperbolic curve described is fitted to the leading edge of the echo traces using an "analysis-by-synthesis" method, which was first used in the pattern recognition of handwritten characters. The frequency of foF2 is derived from the asymptote of the hyperbola determined using this procedure.

VIRTUAL HEIGHT (km)

FREQUENCY (MHz)
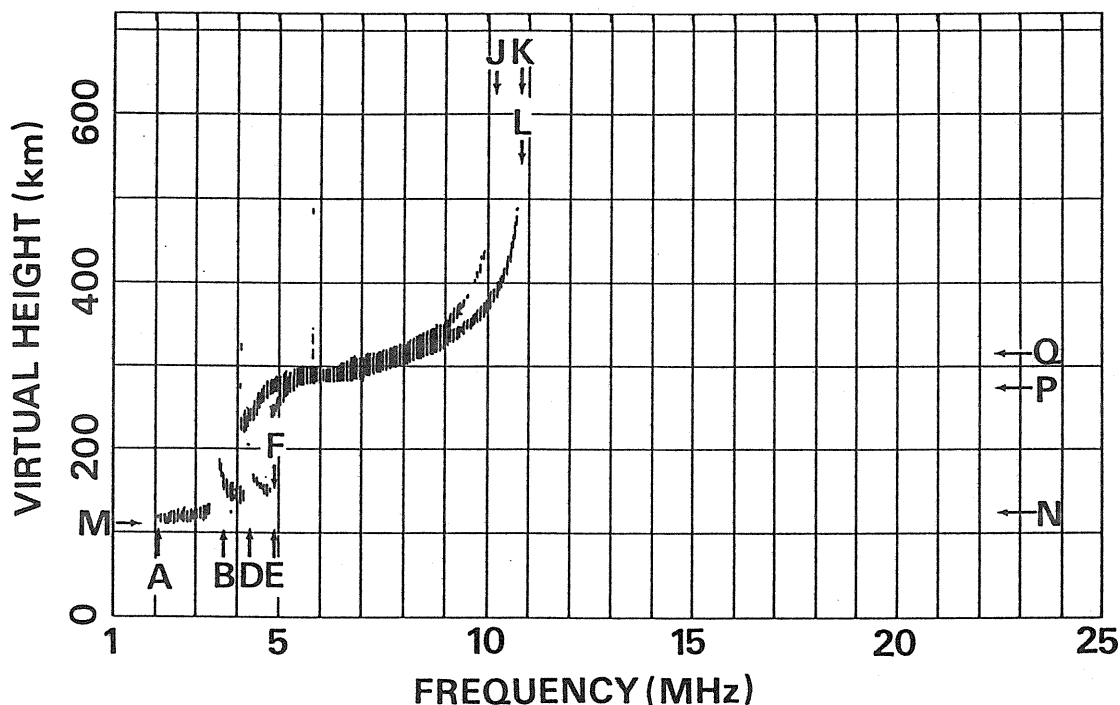
A; fmin=2.08   B; foE =3.66   M; h'E =110   J; foF2=10.2   P; h'F2=274
                D; foEs=4.28   N; h'Es=125   K; fxF2=10.8   Q; hpF2=316
                E; fxEs=4.88   L; fxl =10.8
                F; fEs =4.88

Figure.1 A typical example of the results obtained from the CRL automatic scaling method. The arrows in the figure indicate characteristic frequencies and virtual heights. The numerical values shown below the ionogram are the automatically-scaled values.

Scaling the Height of the F-layer

The parameters related to the F-layer are scaled using procedures identical to those applied for the detection of the E-layer parameters.

A typical example of automatic scaling is shown in Fig.1; the arrows indicate the characteristic frequencies and virtual heights that have been automatically scaled. The characteristic values are also shown at the bottom of Fig.1.

A Comparison Between Automatic and Manual Ionogram Scaling Methods

In order to evaluate the CRL method, the automatically-scaled parameters have been compared with the manually-scaled values using ionograms obtained every hour from April, 1986 to February 1987. Since the details are described by Igi et. al [4], only the results regarding foF2 are shown here.

Hourly Values and Medians of foF2

A histogram, showing the difference in foF2 between manually and automatically-scaled ionograms for April 1986, is presented in .2. It can be seen from this figure that the majority of the differences occur within 1 MHz of the manually scaled value. Figure 3 shows the percentage success for error limits of 1 MHz (solid line) and 0.5 MHz (broken line) obtained using the automatic scaling method extending over nearly one year. The increase in the failure rate during June, July, and August is due to the presence of a blanketing-type Es. This arises because the CRL algorithm frequently concludes that the F-layer is completely blanketed in spite
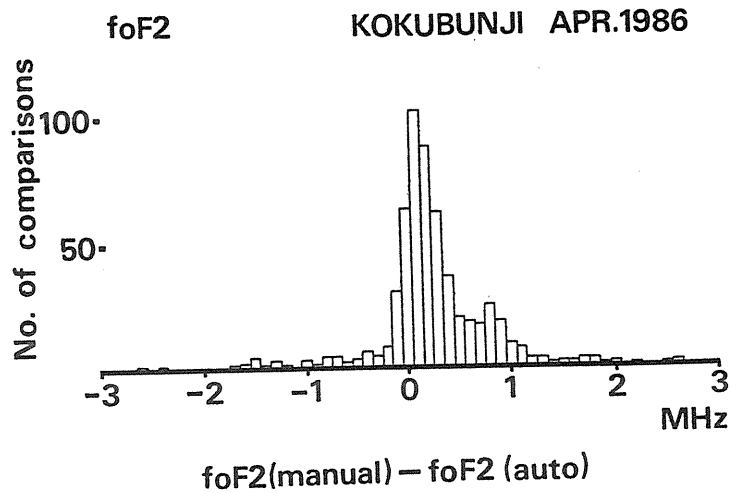
Figure.2 An error distribution for the foF2 between manually and automatically scaled ones. For this comparison, 608 ionograms recorded at Kokubunji station during April 1986 have been used.
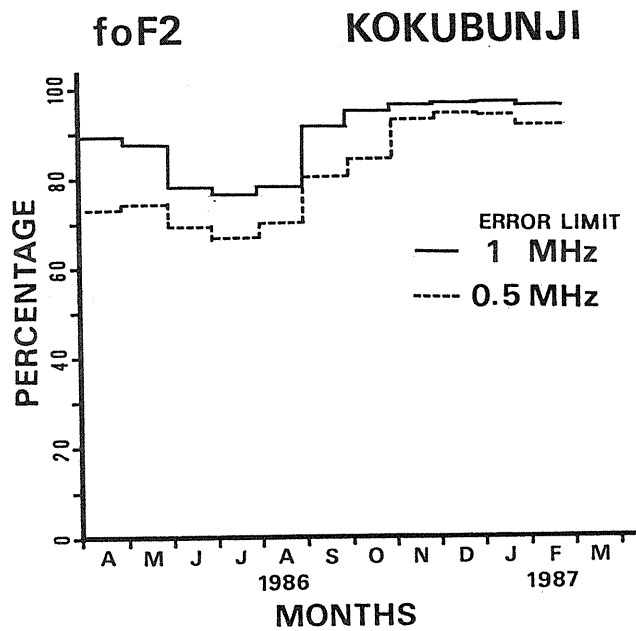
Figure.3 The seasonal variation of the "success rate" derived for automatic scaling of the foF2 for an eleven month period. The solid line and broken line indicate 0.5 and 1 MHz error limits, respectively.
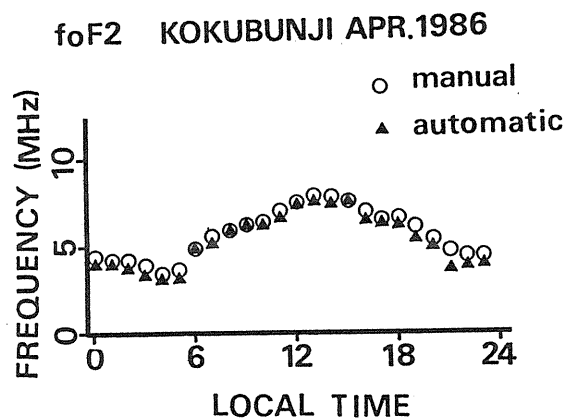
Figure.4 Comparison between medians by automatic scaling and medians by manual scaling for the foF2.

of the appearance of higher frequency traces near the F2 cusp. Generally speaking, the 1 MHz error limit test is passed by about 80% of all ionograms in June, July, and August, and by 95% of ionograms recorded at other times of the year. The median values of foF2 obtained by manual and automatic scaling are shown in Fig.4 as a function of local time. As can be seen in the diagram, there is good agreement except at the 21 hour LT.

Close agreement is also obtained in similar comparisons made for July and October 1986 and January 1987, which were selected to be representative of the other seasons.

Hourly Values and Medians of the other parameters

Similar comparisons to those made for foF2 have been made for the other parameters. The automatic scaling algorithm for fmin is nearly perfect throughout the one year period studied here and fEs can be automatically scaled with an error of 1 MHz or less in 90% to 95% of all ionograms studied.

A new method of displaying Ionospheric Characteristics

This section describes a new display method that clearly shows both ionospheric phenomena and propagation conditions of the HF radio wave. The new plots consist of three figures: (1) an fc_h'-t plot showing diurnal variations of ionospheric characteristics, (2) an MUF plot showing diurnal variations of the MUF, and (3) a Median plot showing variations of the median values of the ionospheric characteristics as a function of local time. Only the fc_h'-t plot is described here, because the details are shown in the paper by Igi [5].
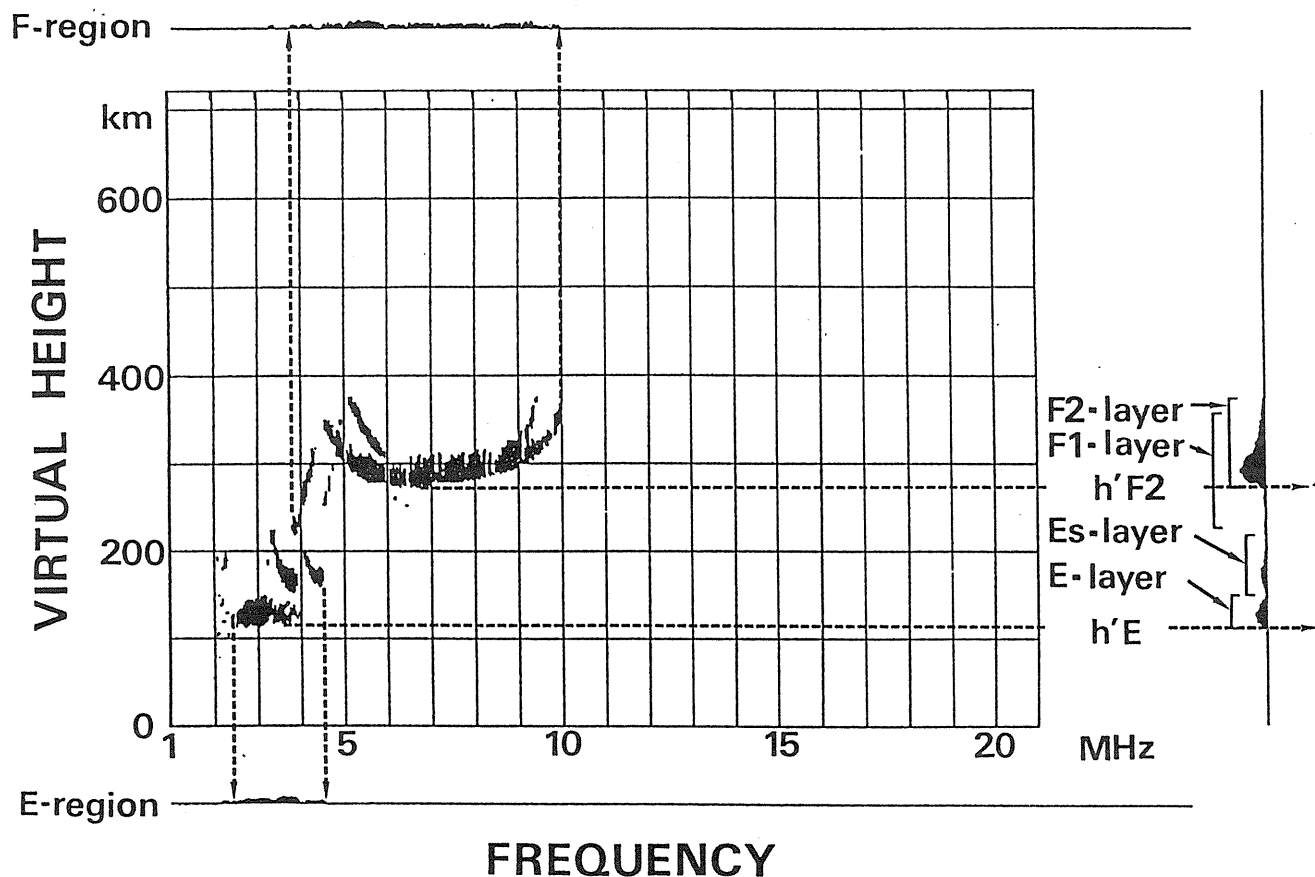
Figure.5 Noise-reduced ionogram and process for producing the fc_h'-t plot.

(a) histogram showing the frequency range of echoes reflected from the F-region. (b) same as (a) except for the E-region. (c) histogram showing the virtual height of echoes reflected from each ionospheric layer. (d) histogram showing virtual height of the lower edge of each layer.

STATION: KOKUBUNJI TOKYO
DATE: 4 NOV.1987 TIME ZONE: 135 E
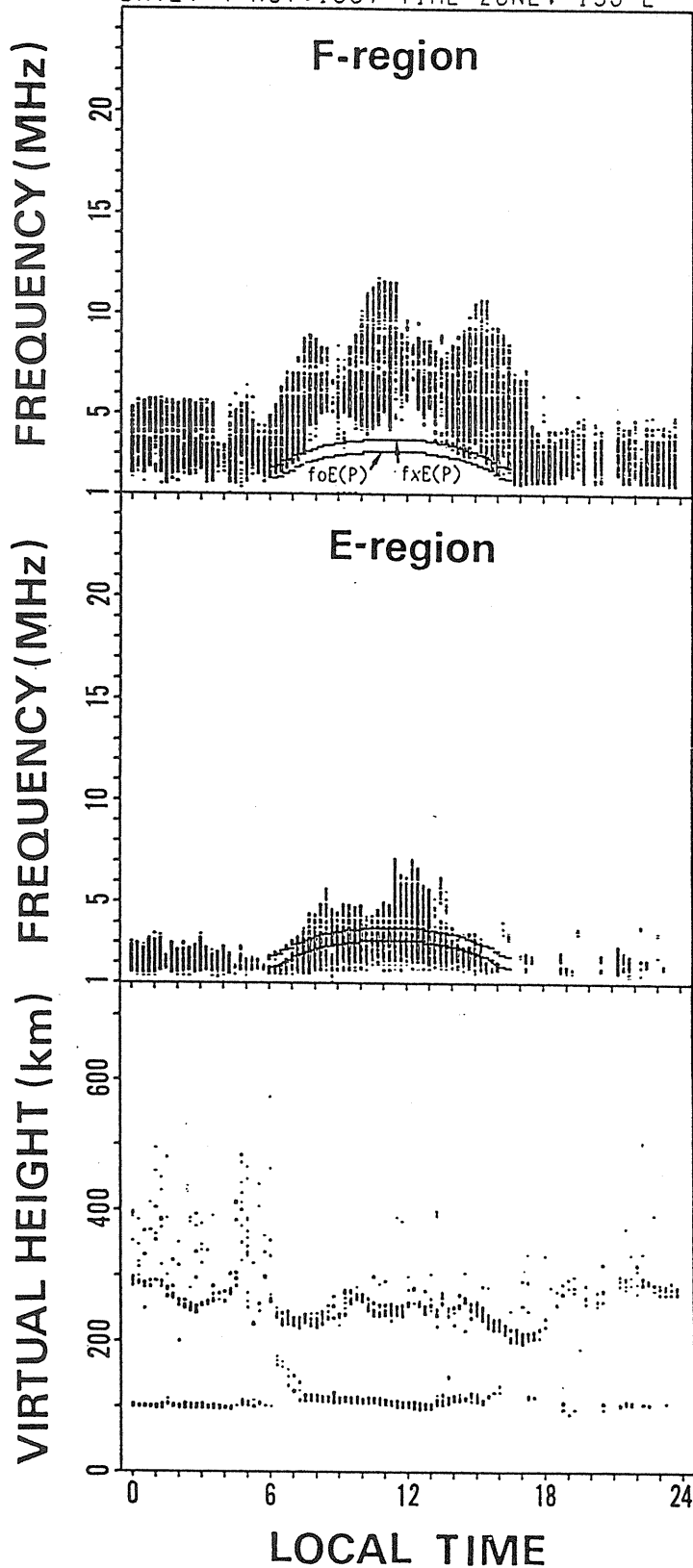
F-region

E-region

Figure.6 The fc_h'-t plot (top: F-layer, middle: E-region, bottom: virtual height). Two arching lines denoted fxE(P) and foE(P) indicate the predicted values of fxE and foE, respectively.

Ionospheric Phenomena - fc_h'-t plot -

A new plot is described showing the diurnal variation in ionospheric characteristics for surveying ionospheric phenomena. This plot indicates the time variations of the characteristic frequencies and virtual heights of each layer, this plot is termed the fc_h'-t plot. The fc_h'-t plot consists of three parts for the F region, the E region, and the virtual height.

Method

Figure 5 shows the process for producing an fc_h'-t plot. Noise and multiple echoes are eliminated from the original digital ionogram. Eliminating multiple echoes help to discriminate F-layer traces from multiple Es-layer traces, because the F-layer trace and the echo traces reflected twice between the Es-layer and the ground are observed at similar heights in the ionogram.

Next, the method of representing the F region and E region is described. The echoes reflected from the F region are plotted by summing up the pixels above 180 km along the virtual height axis at each frequency step from 1 MHz to 25 MHz (see (a) in Fig.6). The echoes for the E region are drawn by summing up the pixels below 180 km (see (b) in Fig.5). The F and E regions of the fc_h'-t plot are made by recording such histograms every fifteen minutes.

The top and middle panels of Fig.6 indicate the diurnal variation of the frequency range of the echoes reflected from the F and E regions, respectively. The two solid curves are the predicted values of fxE and foE calculated using the model recommended by CCIR (shown as fxE(P) and foE(P)).

The bottom panel of Fig.6 shows the diurnal variation of virtual height. First, a histogram of the virtual height is calculated by summing up the pixels along the frequency axis at each virtual height sample from 0 km to 719 km (see (c) in Fig.5). Since virtual heights are scaled from the lowest height of each layer, the differences between successive bars in the histogram (c) are calculated to detect the edge of each layer (see (d) of Fig.5). As positive values of the histogram (d) corresponds to the lowest height of each layer, the virtual height figure is made by sequentially recording positive values of the histogram (d) every 15 minutes.

The fc_h'-t plot aides in surveying ionospheric phenomena.

Conclusion

An automatic ionogram scaling algorithm incorporating a pattern recognition method has been developed at CRL. The CRL method is applicable to the data recorded by conventional type ionosondes, i.e., those that do not distinguish between ordinary and extraordinary mode echoes. Moreover, with a high degree of reliability, the CRL method is able to recognise Es layer blanketing, so that it is useful for scaling ionograms recorded at those latitudes where Es occurrence in dominant. Data obtained using the automatic ionogram scaling system has been routinely published since June 1988 for all Ionospheric observatories in Japan (Wakkanai, Kokubunji, Yamagawa, and Okinawa).

Ionospheric phenomena can be easily identified from the automatically-scaled parameters and also from sequential records of ionograms called Ionospheric Summary Plots. According to the URSI standard, most ionospheric observatories scale fourteen ionospheric parameters: fmin, foE, h'E, foEs, h'Es, type of Es, fbEs, foF1, M(3000)F1, h'F, h'F2, foF2, fxI, and M(3000)F2. The fc_h'-t plot displays parameters corresponding to fmin, foE, h'E, foEs, h'Es, type of Es, fbEs, h'F, h'F2, foF2, and fxI. The fc_h'-t plot provides an easy method to monitor ionospheric conditions. The examples of the fc_h'-t plot showing some ionospheric phenomena will be useful for users of fc_h'-t plot, which are published in the monthly bulletin from the CRL as "Ionospheric Data in Japan". However, users should check the original ionograms to confirm the phenomena displayed in the plot, since the fc_h'-t plot has slightly less information than the original ionogram.

References

[1] Reinisch, B. W. and X. Huang, "Automatic calculation of electron density profiles from digital ionograms, 3.Processing of bottomside ionograms", **Radio Sci.**, 18(3), 477-492, 1983.

[2] Fox, M. W. and C. A. Blundell, "Automatic scaling of digital ionogram", **Radio Sci.**, 24(6), 747-761, 1989.

[3] Nozaki, K., M. Nagayama, and H. Kato, "Automatic ionogram processing system 1. Data reduction and transmission of ionograms", **J. Commun. Res. Lab.**, 39(2), 357-365, 1992.

[4] Igi, S., H. Minakoshi, and M. Yoshida, "Automatic ionogram processing system 2. Automatic scaling of ionospheric parameters", **J.Commun.Res.Lab.**, 39(2), 367-379, 1992.

[5] Igi, S., "Automatic ionogram processing system 3. A new method of displaying ionospheric characteristics", **J. Commun. Res. Lab.**, 39(2), 381-402, 1992.

TOWARDS A SEMI-AUTOMATIC IONOGRAM SCALING PROGRAM TO PROVIDE MODEL PARAMETERS RATHER THAN TRADITIONAL SCALING PARAMETERS

Allon W. V. Poole

Hermann Ohlthaver Institute for Aeronomy, Rhodes University, Grahamstown 6140, Republic of South Africa.
Phone: (SA code) 461-318460; Fax (SA code) 461-25049;
e-mail PHAP@RUCHEM.RU.AC.ZA

Christopher C. Mercer
VODACOM, P. O. Box 335, Pretoria 0001, Rebublic of South Africa.

Abstract

At ionosonde stations where the raw ionograms are produced in digital form rather than on film, traditional manual scaling methods have given way to automatic computer based scaling algorithms. However, the output data still adhere to the scaling rules and parameters that arose historically with the evolution of the ionosonde and were appropriate for the manual scaling of film based ionograms. We have found that the standard ionogram scaling parameters are not well suited to the requirements of real time ionospheric modelling. We have therefore embarked upon the development of a PC-based program that will fit an ionogram synthesised from a simplified real height model to the ionogram by least squares and then report the parameters of this model rather than the standard URSI scaling parameters. We hope to build up an archive of these data, and produce monthly medians which will be more directly representative of the ionosphere.

Introduction

At the Hermann Ohlthaver Institute for Aeronomy our ionograms are captured digitally and can be displayed on a computer screen. We have developed a computer program to allow the manual scaling of 14 traditional ionospheric parameters (foF2, h'F2, foF1, h'F1, foE, h'E, foEs, h'Es, fbEs, Es types, fmin, MUF3000, M3000F2, fxI) by moving a cursor around the screen. These data are then stored, and monthly bulletins are produced that report the data as well as monthly medians in the traditional manner. These medians are an attempt to describe the average behaviour of the ionosphere for retrospective and for archival use.

Unfortunately, these parameters are not an efficient description of the ionosphere for communication purposes. This is because they describe the *ionogram* and not the *ionosphere*. They also contain descriptive and qualifying letters that require human interpretation to be useful and are thus not optimally designed for computers. It has become apparent that these parameters are of limited application to our main goal of developing a useful temporal and spatial ionospheric model for the South African region.

For a similar number of parameters, a simple ionospheric model can be described. If a model is chosen that is accessible to analytic (rather than iterative or numerical) raytracing, it has greater potential for communications applications and other purposes such as single site location (SSL). It thus seems reasonable to describe the average behaviour of the model ionosphere rather than the ionograms and to store this information for archival purposes.

The model

The model must therefore fulfil two important criteria:

(i) it must be analytical, as discussed above.

(ii) it must be described by parameters that can be meaningfully averaged over some time period, eg. a month.

Analytical requirement

In compliance with this requirement, we have chosen the Quasi-Parabolic (QP) layer as the basic building block of our model. Each layer is described by three parameters. The standard form for the "normal" QP layer is given by Hill (1979):

$$N = N_m \left[1 - \frac{(r-r_m)^2}{y_m^2} \frac{r_b^2}{r^2} \right]$$

$$= A + \frac{B}{r} + \frac{C}{r^2}$$

where

N is the electron density

r is the geocentric distance

r_m is the value of r at the layer peak

N_m is the value of N at the layer peak

r_b is the smaller value of r when $N = 0$ (bottomside)

y_m is the layer thickness

We then concatenate three such "normal" QP layers with two "inverted" QP layers to form a Multi-Quasi-Parabolic (MQP) model [Chen et al (1990)]. The three normal layers represent the E, F1 and F2 regions of the ionosphere. The form of the inverted layers is the same as that for the normal layers except that the signs of A, B and C are reversed.

Parameter averages

The three QP-layer parameters r_m, N_m and y_m specify the height of maximum ionisation, the maximum ionisation and the layer semi-thickness respectively. Thus monthly median values of these quantities will specify a median layer in an easily understood and uncomplicated way. It is proposed that archived, median values of these quantities will provide a reasonable basis from which each model layer can be reconstructed.

INPUT IONOGRAM

N-h PROFILE

MODEL

POLAN

COMPARE

OK?

NO

YES

CHANGE PARAMETERS

STORE

END

(a) STANDARD METHOD

INPUT IONOGRAM

MODEL IONOGRAM

MODEL

COMPARE

CONVERT

OK?

NO

YES

CHANGE PARAMETERS

STORE

END

(b) HOIA METHOD
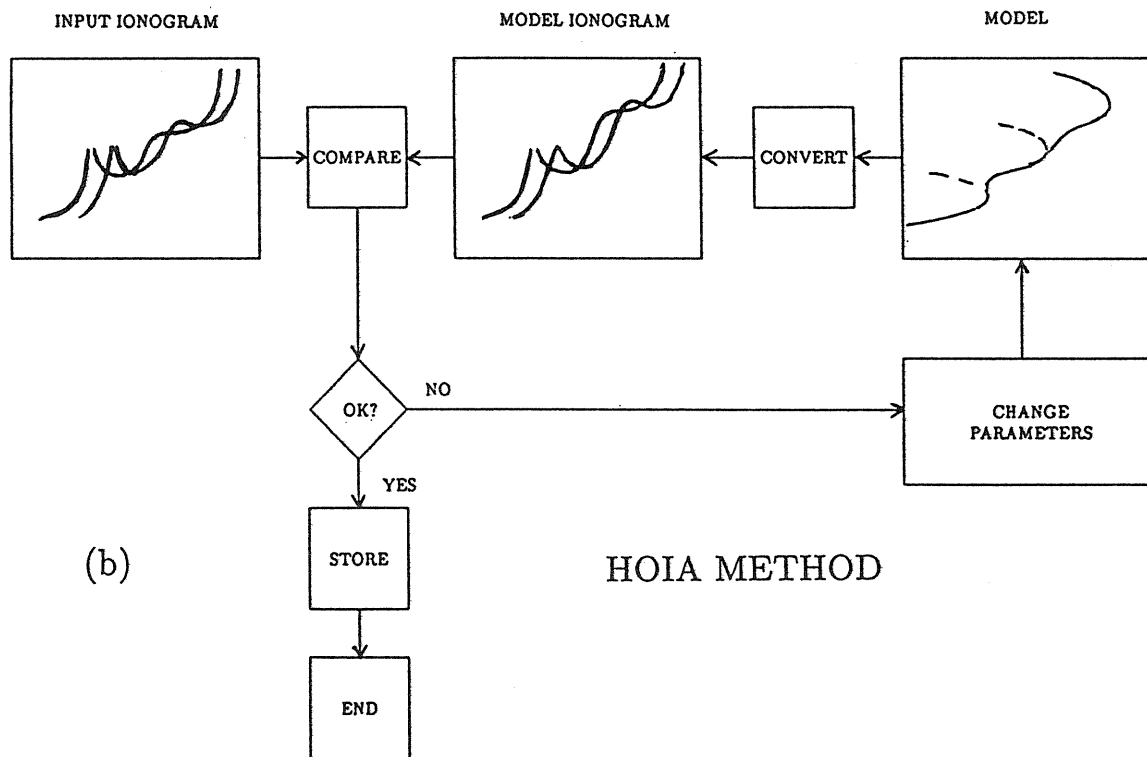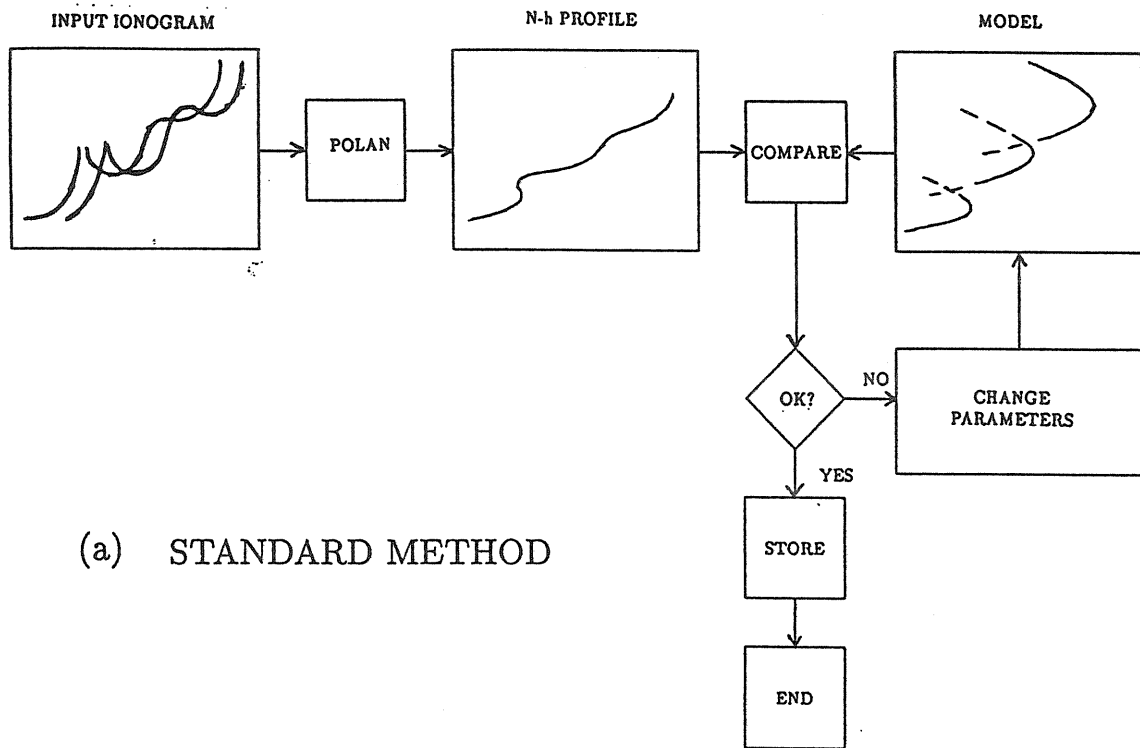
FIGURE 1: A comparison of (a) the standard method and (b) our method of fitting the model to the data.

Fitting the model to the ionogram

One standard way of doing fitting the model to the ionogram is to convert the ionogram to an N-h profile by means of some inversion program such as POLAN. Q-P layers are then fitted to this profile by, for example, least squares. We propose to iteratively adjust the QP layers by numerical, non-linear optimisation methods until the corresponding ionogram best fits the input ionogram. This task is simplified and speeded up by the fact that the model is analytic, allowing for the speedy calculation of the ionogram that would be associated with that model. This "model" ionogram is then compared with the "data" ionogram and the error signal used to iterate the model until the best fit is obtained. A comparison of the standard method and our proposed method is shown in Figure 1.

Conclusion

A synoptic, analytic model is required to describe the ionosphere in a manner that can be easily averaged for archival and prediction purposes. The MQP model is well suited to this purpose because it can be raytraced analytically at both vertical and oblique incidence. HOIA is writing an interactive PC-based program that will fit this model to digital ionograms without needing to convert to an N-h profile first.

References:

Hill R, **Radio Science**, 14, p885, 1979

Chen J, Bennett J A and Dyson P L, **J. atmos .and terrestrial Phys.**, 52, p277, 1990.

A SEMI-AUTOMATIC INTERPRETATION OF IONOGRAMS

B.O. Vugmeister and V.V. Radionov
Institute of Solar-Terrestrial Physics
664033 Irkutsk, Russia

Advances in ionospheric sounding techniques that made possible a variety of digital ionosonde designs and have helped researchers anticipate the possibility of a fully automated process of ionogram analysis and interpretation.

So far, however, these authors are unaware of any processing system capable of accurately scaling the 16 ionospheric characteristics endorsed by URSI. The main problems arising in ionogram analysis may be reduced to three:

- signal detection

- ray tracing

- ionogram interpretation

Usually, the first and second problems are resolved by choosing an appropriate value of ionosonde potential (high sensitivity of the receiver, adequate power of the transmitter, the use of a coded signal). Besides, such problems are tackled in related areas of knowledge (radar, nuclear physics, etc.).

Ionogram interpretation is accomplished following reasonably formalised rules (1); however, as our investigations and results [2,3] reported by other authors show:

a)   a correct determination of ionospheric parameters is possible in no more than 80 percent of cases,

b)   some parameters (type Es, for example) have not yet been automatically determined at all.

Obviously, large-scale computer treatment of ionograms would be followed by the transfer of the data to the WDC for storage. But no data would be preferable to storing incorrect data.

The above reasoning has led us to the idea that it would be premature to exclude man from the ionogram interpretation process. Based on this, it was possible to formulate a request for proposal (RFP) involving the development of a system for handling ionograms interactive .

The system's program software is implemented in FORTRAN and Macroassembler for micro-computers DVK-3M (PDP).

The system is designed to solve the following problems:

- signal processing to increase the signal/noise ratio

- ionogram interpretation in the interactive mode

- automatic transmission of an ionogram via telex.

The signal is processed through an post-detector accumulator with frequency averaging. The noise level is determined for every sounding frequency (normally in 5 kHz steps). For this purpose, the signal is analysed for those height ranges where an ionospheric reflection is obviously absent. A mean noise level is determined for the entire frequency range in which the signal amplitude (normally 5x5 kHz) is calculated.

The value of the mean noise level is used as the threshold when making a decision about the presence or absence of the signal.

In the interactive mode of ionogram interpretation, the height-frequency characteristic obtained by the above method, is displayed on the computer terminal, simultaneously with operator promptings (a list of allowable instructions that varies depending on operating conditions - according to the interpretation of the Es-layer or the E-, F1- and F2-layers) and with values of parameters to be determined. By moving the cursor along the ionogram, the operator detects the desired point and, by depressing an appropriate key, enters the name of the measured parameters and (if necessary) its signatures. In the process of interpretation, the operator is able to change the cursor step, erase incorrectly marked values of parameters and erase the data frame of a given size.

The points marked on the ionogram by the operator are displayed and maintained until the ionogram interpretation is terminated.

Data obtained are used to generate a series of (usually hourly) values of ionospheric parameters and a file-telegram in the IONKA BE code used by the Russian Agency on Hydrometeorology and Environmental Control.

The subsystem for data transmission via telex consists of the telegraphic line interface and the program software. The subsystem operates in active and passive (data transmission on request) modes. In the active mode, the subsystem performs the following functions:

- calling a telegraph office
- dialling the wanted party
- checking the answer-back of the wanted party
- transmitting the file-telegram
- handling and recording of the acknowledgement of data received.

The data transmission subsystem receives, handles and communicates to the operator the service information of the telegraph office.

The system for interactive processing of ionograms permits ionogram interpretation in real time (average processing time - 90 seconds) and the transmission of data obtained via telex.

References

1. Piggott W. R. and K. Rawer, URSI Handbook of Ionogram Interpretation and Reduction. **Report UAG-23A**, World Data Center A for Solar and terrestrial Physics, 1978.

2. Reinisch Bodo W. and Xuegin Huang. Automatic Calculation of Electron Density Profiles from Digital Ionograms. 3. Processing of Bottomside Ionograms. **Radio Sci.**, 1983, v. 18, No. 3.

3. Galkin I.A. The Program Software for Automatic Processing of Vertical-Incidence Sounding Ionograms. II. Interpretation of the Height-Frequency Characteristic. Preprint No. 22-88, SibIZMIR, Irkutsk, 1988.

IONOGRAM INTERPRETATION AS IMAGE RECOGNITION

Bakhitzhqan Dj. Chakenov and Alla P. Chakenova
Ionospheric Institute
Alma-Ata, 480068, Kazakhstan
(Phone: (8 3272 65-80-82, Fax: (7 3272) 63-12-07 (or 63-69-73))

Complicated visual image recognition is possible due to isolation contours, i.e. the high-frequency components present in the space-frequency spectrum of an image make it possible. Sudden disappearance of the image fragments and a distorted image perception occurs while the sensory signal is extinct. An image then becomes fixed relative to the retina. In this case, the eye movements not only refresh the perception, and help to see the more fine details due to arrival of information about high spatial image frequencies, but also suppress the previous stimulus signal. The highest keenness of sight then takes place, presenting the images for 400-600 ms. Perceptional organisation occurs in distinguishing between figure and background. Any groupings possessing special features can serve as "units". Similar element clots, or periodical pattern gaps, can be taken as "figures". The regions with homogeneous distribution of illumination intensity and different textures are singled out. A coherent picture comes out after sensory information integration. Contextual information using ionogram redundancy (particularly their availability for the subsequent time intervals) makes it possible to draw attention selectively to separate fragments of the height-frequency time-changed profile and to concentrate on key elements. If in an ionogram some details are absent, then conventional elements can be substituted, e.g. line segments of a suitable length. The shape, dimensions and orientation of these elements can be chosen from a typical ionogram image, which would relate to a given time, season, and solar activity level. More intensive usage of a short-term image memory (duration of an exact and full ionogram image lasts about 1s) gives an operator an additional advantages, while matching the two fast changing ionograms. Line orientation information retains fuller volume than the complicated figure shape and the complicated signs do not stay in short-term image memory. The inner observer's models formed according to logical criteria [1] are compared with visual information.

Conclusion

An operator's work quality depends much on images presenting parameters (sharpness, contrast range, brightness, exposure, colour, signal/noise relation, size, orientation). The operator has a section reference book at his disposal (E, E_s,...F1, F2). A sign reference book includes a slope of ionogram trace, an interval between 0- and X-mode critical frequencies. Data on trace dimensions, its general shape and context information can be combined. In addition, small parts of an ionogram should be analysed simultaneously and in detail [2].

References:

1. URSI Handbook of Ionogram Interpretation and Reduction, 1961.

2. B. Dj. Chakenov, Wave Processes in the Ionosphere, A.-A., 1987.

THE APPLICATION OF IONOSONDES TO HF REAL-TIME FREQUENCY MANAGEMENT IN NORTHERN AUSTRALIA

Kenneth J.W. Lynn,
Communications Division, Defence Science and Technology Organisation,
PO Box 1500, Salisbury, SA 5108, Australia

Abstract

The ability of networked ionosondes to provide accurate frequency management advice to HF communicators is being investigated. in northern Australia. Previous studies carried out in southern Australia have shown that the direct conversion of vertical ionograms to equivalent oblique ionograms was an accurate and effective means of providing Maximum Useable Frequencies for communication links up to 1000 km in length. The effect of spatial decorrelation as distances between control and reflection points increased was also investigated. The present program has extended the range of paths studied and demonstrated that oblique as well as vertical ionosondes can be used to provide the control point information for non-colocated links up to 2460 km in length. The importance of correcting for ionospheric gradients as the separation between the reflection and control point increases is confirmed and a method for so doing indicated.

Introduction

Trials carried out in southern Australia (Lynn and Malcolm, 1991) demonstrated that vertical ionograms could be accurately converted to equivalent oblique ionograms in real-time for the frequency management of HF circuits (up to 1000 km in length) with reflection points within some 300 km of the ionosonde. Decorrelation of foF2 with increasing control/reflection point separation was found to consist of two terms, one being associated with the short term time variability (<4 hours) of the ionosphere and the other being related to large scale geographic gradients in the ionosphere including the effects of the terminator (for recent European measurements of foF2 correlation and gradients see Soicher et al, 1993). In early 1992, this work was extended by demonstrating that a vertical ionosonde near the path mid-point could provide accurate values of MUF for a 2590 km path from Darwin to Melbourne (Lynn and Kelly, 1993).

The present paper describes work in progress involving a network of oblique ionosondes with transmitters in S.E. Asia for reception in Australia (known as LLISP - the Low Latitude Ionospheric Sounding Program; Clarke et al,1993; Wright et al, 1993) as well as transmitters within northern Australia. The network within northern Australia was set up as a temporary measure specifically to develop Real Time Frequency Management (RTFM) techniques for HF communications in anticipation of the major ionosonde deployment which is expected in 1995 in support of the Jindalee Operational Radar Network (JORN). Extended ionospheric sounding is the backbone of frequency management and range calibration for an OTH radar such as JORN but has seen little use in the management of HF communications. It is the aim of the present project to develop the latter application. The main objective of LLISP is to test and improve the modelling of the low latitude ionosphere. However it is hoped to expand the application of RTFM into the equatorial area as experience in such operations is developed. Initial results obtained to date in northern Australia relevant to the RTFM of HF communications are described.

Equipment

LLISP oblique chirp ionosonde transmitters are currently situated in Saipan, the Phillipines, Papua New Guinea and Cocos Island with receivers at Townsville, Darwin and Derby (see Figure 1(a)). These receivers also work in conjunction with chirp ionosonde transmitters at Townsville, Darwin and Tennant Creek in support of the north Australian RTFM program. In addition, there is a quasi-vertical ionosonde in operation at Darwin. A pulsed ionosonde (4B/IPS42 hybrid) and chirp receiver have also operated intermittently at

Tindal. The ionosonde network in northern Australia is shown in Figure 1(b). All oblique ionosondes were designed and built in DSTO and feature low power operation (some tens of watts on long paths), flexible computer control of operating parameters, fast sweep speeds (e.g. 500 kHz/sec) and a maximum sounding frequency in excess of 64 MHz (required over long equatorial paths at high sunspot number). All ionosondes operate from atomic frequency standards to minimise relative drift.
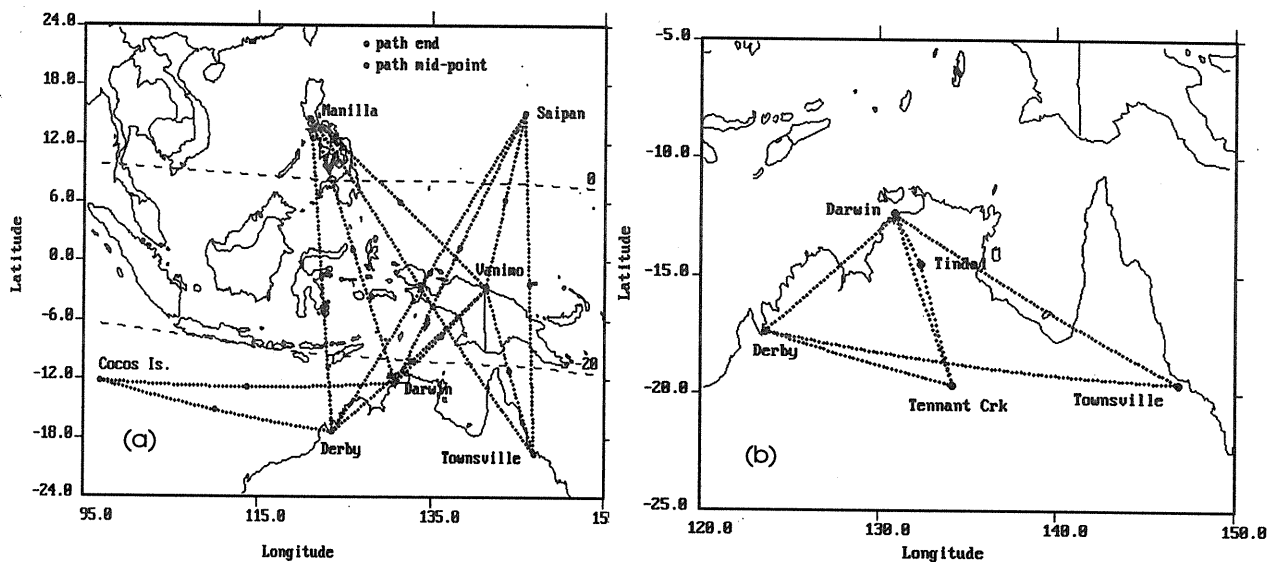
Figure 1. Sites and oblique ionosonde paths (a) LLISP (b) northern Australia.

A new vertical pulsed ionosonde (the IPS 71) has been developed by KEL Aerospace to DSTO specifications and employing DSTO concepts to obtain true high-resolution Doppler ionograms. The IPS 71 typically sweeps 171 frequencies in 3.5 minutes obtaining Doppler measurements over a bandwidth of ± 2.5 Hz to a Doppler resolution of 0.039 Hz for every 6 km range bin from 75 to 842 km at every frequency. The IPS71, now in operation in Adelaide, will be deployed in northern Australia to further investigate the dynamics of the ionosphere.

Technique

The technique pursued here is to directly convert the reference ionogram to an equivalent oblique ionogram for the required range by a well known method (Davies, 1990). The technique as used is based on a curved earth and flat ionosphere model. A bounded error develops as the flat ionosphere approximation fails, typically when the algorithm is used to convert a vertical to an oblique ionogram at ranges greater than about 1000 km. A correction for this error has long been known as the k factor. A simple linear dependence on distance for the k factor has been assumed here suitable for correcting the F layer peak value but more sophisticated models can be developed to make the k correction a function of height and sensitive to the ionogram profile. The basic conversion algorithms have been generalised and consolidated to operate from either vertical or oblique ionograms for conversion to either greater or lesser range (Lynn,1992).

The method is ideal for operating with a mixed network of vertical and oblique ionosondes since it always produces a result, is computationally quick enough for real-time operation even on simple computers and uses all the data inherent in an ionogram (automatically correcting for height variations, for example). However the method is applicable only to the o-ray and does not take into account the effect of the earth's magnetic field which may introduce directional asymmetry. As with all methods which fully utilise oblique ionograms, the ionosonde must provide an absolute measurement of time delay. To date, this has been accomplished by calibrating time delay over the oblique ionosonde path using Sporadic E as a known reference height (Lynn and Malcolm, 1992), however GPS absolute timing has now been added to all sites .

Another technique which could be directly substituted for that used here (though with much greater complexity) is to invert the ionogram and ray trace through the resultant electron density profile (Chen et al, 1992) to again obtain the equivalent oblique ionogram. For other approaches to providing real or near-real time frequency management see Reilly et al (1991), Goodman,1992.

The main scientific problem to be overcome in using networked ionosondes to control HF communication links is to determine the distance from a sounder reflection point for which the data remains valid i.e. the correlation distances of ionospheric parameters and the manner in which decorrelation occurs. Much statistical work bearing on this point has been done in the past to indicate that significant decorrelation for the F region occurs in the range 300 to 1000 km from the sounder reflection point (Rush, 1976; Rush and Edwards,1976). The present work has concentrated on determining the real-time errors which can occur at a 15 minute update rate and the manner in which the ionosphere spatially decorrelates. This has been done by comparing computed and observed MUF over a variety of oblique paths.
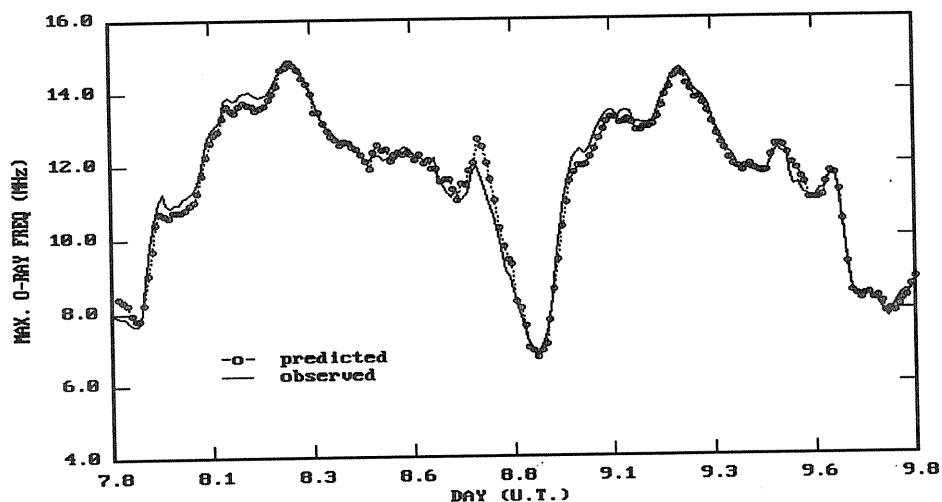
Figure 2. Observed MUF for Darwin to Tindal (281 km) and the spatial extrapolation based on the Darwin vertical values of foF2.

Results

The quasi-vertical ionosonde at Darwin was initially taken as the reference for spatial extrapolation. Figure 2 shows a comparison between the o-ray F region MUF at Darwin and that observed over a 281 km path to Tindal (no range conversion is required at this distance). The agreement is within the errors of measurement. Figure 3(a) provides a similar comparison between the converted Darwin ionogram MUF and that actually observed over a 874 km path from Darwin to Tennant Creek. Considerable decorrelation is now evident. Examination shows that two factors are at work. The short-term (<4 hr) variations continue to correlate well at the two sites but significant biases develop each day such that the predicted MUF is an overestimation. Darwin is at the edge of the equatorial anomaly region and considerable north-south gradients in foF2 develop. Accordingly the spatial predictions were corrected by multiplying each calculated value by the ratio of foF2 at the oblique path reflection point and at Darwin using values given by the ionospheric prediction program ASAPS.
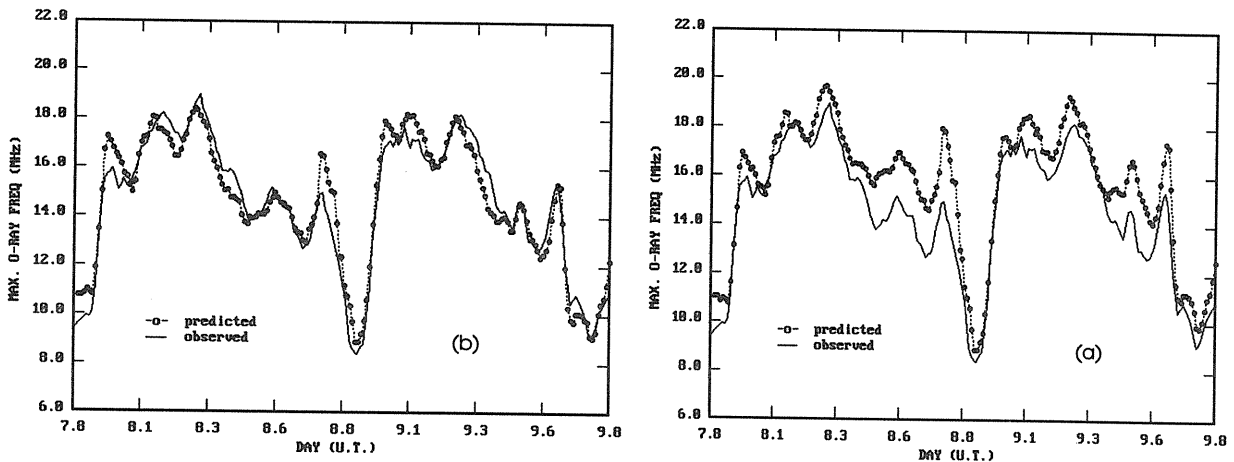
Figure 3 Observed MUF for Tennant Creek to Darwin (874 km) and the spatial extrapolation from Darwin with (a) gradient corrected (b) no gradient correction.

The result is shown in Figure 3(b). Here most of the decorrelation has disappeared confirming that the foF2 gradient was the main problem. A gradient in the height of the F layer could also be expected to occur but at this range appears to have made little contribution to the decorrelation. The question of the relative importance of gradients in foF2 and in height with increasing conversion range will be the subject of future investigation.

The results of Figure 3 are consistent with those previously obtained elsewhere in Australia (Lynn and Malcolm, 1992, Lynn 1992) in which vertical ionosondes were used as the reference for ionogram conversion. One of the main points in using the direct ionogram conversion technique was the expectation that both vertical and oblique ionosondes could be used. To test this, spatial extrapolations of expected MUF for a 2460 km path from Townsville to Derby were made using an oblique ionosonde operating from Tennant Creek to Darwin (874 km) as the reference in a period which included the major ionospheric storm
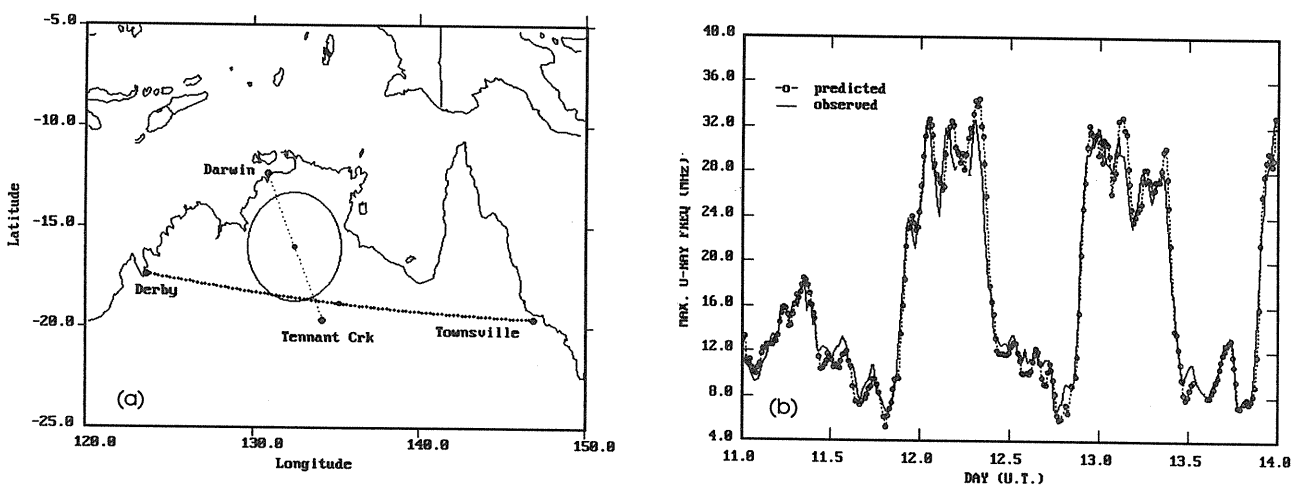
Figure 4 (a) The 300 km radius of high correlation expected around the Tennant Creek to Darwin control point relative to the Townsville to Derby mid-point. (b) Comparison of the observed MUF for Townsville to Derby (2459 km) with that computed from the Tennant Creek to Darwin oblique ionosonde (gradient corrected).

62

on 11 May 1992. Figure 4(a) shows the relative location of paths, reflection points and the region of expected high correlation about the ionosonde control point. The comparison between the calculated and observed o-ray MUFs for the 2460 km path is made in Figure 4(b) which also includes a minor foF2 gradient correction.

The computed MUF tracks accurately through the storm indicating that the ionogram conversion is automatically correcting for the major increase in ionospheric height which occurred. Thus the expectations of the technique were confirmed. The use of oblique ionosonde paths may be preferable in managing long one-hop circuits since any error in the k factor algorithm will be reduced because of the smaller disparity in length between the referenced and managed paths.

Real-Time Gradient Correction

The results to date have used gradient corrections taken from a standard propagation prediction program (ASAPS) to extend the distance for which control point data is accurate. A true real-time management system would derive its own gradient measurements thus allowing for the more extreme variations in large scale gradients which occur e.g. during ionospheric storms. At such times, predicted gradients can be greatly in error (Lynn and Kelly, 1993). Such corrections become possible within an area of networked ionosondes. Once again the problem arises as to how to combine data from both vertical and oblique ionosondes. The technique described here can be brought to bear by converting all ionograms to a common range (e.g. that of the circuit being managed). The gradient correction at the managed reflection reflection point then becomes an interpolation problem within the network of reference-point ionograms and is applicable to any ionogram parameter i.e. frequency or group range. Bradley and Dick (1993) have recently investigated methods for interpolating ionospheric data within a vertical ionosonde network. These methods would be equally applicable in our present application once all ionograms have been converted to a common range.

In a first attempt at normalising the ionograms, zero range was taken to verify that long path oblique ionograms (e.g. Townsville-Derby, 2460 km) could usefully be converted to the equivalent vertical. This did prove to be the case for the F region MUF for which good critical frequencies were derived from the high angle rays. Much of the E region structure was smeared by the process indicating that the fundamental problem with inverting long range ionograms is that structure at lower heights is not adequately resolved by current ionosondes because of the extreme time-delay compression which is present.

Summary

The present paper provides an update on a continuing project to develop and deploy practical real-time frequency management systems for HF communications both within and external to Australia. A technique has been demonstrated which will allow a mixed network of vertical and oblique ionosondes to provide frequency management to circuits of arbitrary one-hop length with reflection points within the area covered by the ionosonde network. Future work will aim at practical experience with users and the testing of the real-time ionosperic gradient-correction methodology.

References

Bradley P.A. and M.I.Dick, Use of real-time ionosonde data to improve regional ionospheric models for HF Over-the-Horizon radar and passive single site target location, **This Conference Proceedings**, 1994.

Chen J., Bennett and P.L. Dyson , Synthesis of oblique from vertical ionograms using quasi-parabolic segment models of the ionosphere, **J.Atmos.Terr.Physics**, 54, 23-331, 1992

Clarke R.H., Fyfe D.F., Kettler D.I., Lynn K.J.W., Malcolm W.P., Sprey B.M., Taylor D.P. and C.S.Wright, An ionospheric sounding program to investigate HF and low VHF propagation at low latitudes, **TENERP Conf. Proceedings**, June 22-24, NPS, Monterey, CA, 1993.

Davies K. , Ionospheric Radio, IEE Electromagnetic Wave Series 31, **Peter Peregrinus Ltd.**, IEE, London, 1990.

Goodman J.M., HF Communications - Science and Technology, **Van Nostrand Rheinhold**, New York, 1992.

Lynn K.J.W., Ionogram range conversion, **Proc. of the South Pacific STEP Workshop**, Melbourne, February, 1992.

Lynn K.J.W. and T.Kelly, A new real time frequency management technique based on vertical sounding demonstrated over a 2598 km circuit, **Proc.of the 7th International Ionospheric Effects Symposium**, Alexandria, VA, 4-6 May, 1993

Lynn K.J.W. and W.P. Malcolm, The spatial variability of foF2 and its relevance to HF real time frequency management, **Proc. of the South Pacific STEP Workshop**, Melbourne, February, 1992.

Reilly M.H., Rhoads F.J., Goodman J.M. and M.Singh, Updated climatological model predictions of ionospheric and HF propagation parameters, **Radio Sci.**, 26, 1017-1024, 1991.

Rush C.M., An ionospheric observation network for use in short-term propagation predictions, **Telecomm. J.**, 43, 544-549, 1976.

Rush C.M. and W.R.Edwards , An automated mapping technique for representing the hourly behavior of the ionosphere, **Radio Sci.**, 11, 931-937, 1976

Soicher H., Gorman F.J., Tsedilina E.E and O.V.Weitsman, Ionospheric foF2 values and their gradients at European longitudes, **Proc.of the 7th International Ionospheric Effects Symposium**, Alexandria, VA, 4-6 May, 1993.

Wright C.S., Kettler D.I., Trudinger P.L., Malcolm W.P., Sprey B., Taylor D.and R.H.Clarke., The LLISP data base of low-latitude oblique-incidence ionograms, **TENERP Conf. Proceedings**, June 22-24, NPS, Monterey, CA, 1993.

DEPLOYMENT OF A MODERN STANDARD IONOSPHERIC STATION

V. A. Shapstev, L. S. Terekhov

Russian Academy of Science, Institute for Informatics Technologies and Applied
Mathematics, 28 Andrianov str., 644077, Omsk, RUSSIA

Introduction

Nowadays the world community is moving from an armaments race to the solution of ecological problems. Some technological processes are accompanied with negative and even dangerous effects (eg. radio-active precipitation, ozone holes etc.) which have global effects. Strategic solutions to these problems are required for the future of humanity. In particular, fundamental ecological ways of thinking, such as being ecological professionals by means of international information exchange, national and international ecology education networks and international financial support for ecology projects via the NATO and European Community. A world-wide system of ecological monitoring is being created [1].

In this connection, a project for an optimised global ionospheric monitoring network is very important [2,3]. Often the ionosphere - the upper part of the Earth's envelope - is very sensitive to processes occurring on the Earth and in its atmosphere.

In addition to a global network [2], new arguments are suggested for the deployment of a model ionospheric sounding station in Omsk (55°N, 73°W) Russia as part of a global ionosonde network.

Unique geographical location of the city of Omsk

The geographical latitude of Omsk is 55° north, ie. the city is situated nearly in the middle of the latitude region 30°-70° north, where the D layer winter anomaly is observed. The phenomenon of the winter anomaly at this latitude is expected to manifest itself especially clearly. Omsk is situated at the bottom of a land plain, which is the greatest on our planet, far from sea and mountain discontinuities. If we start from the modern hypothesis that the ionospheric winter anomaly is formed by middle atmospheric processes, then this phenomenon can be investigated in the Omsk region free from terrain discontinuity effects which can create distortions in the regular transfer of atmospheric mass.

The background electro-magnetic noise level is relatively low at Omsk because it is situated far from powerful sources of atmospheric noise (eg. the Indian Ocean lightning centre) and far from radio transmission centres which are usually located at sea ports.

Scientific Potential of the City of Omsk

Ionospheric monitoring data are useful for both fundamentally scientific and practical applications. The fundamental investigations of ionospheric behaviour are carried out by geophysicists who specialise in predicting global environmental change. The practical applications of monitoring data are in the control of rising noise levels, seismic activity electromagnetic precursor detection [4] and ozone hole observation networks etc. Modern HF communication systems urgently need more detailed and timely information on ionospheric structure and dynamics.

Omsk is a large scientific Center in the field of radio investigations, with many scientific personnel in radio physics and radio engineering. There are several research and development enterprises and educational institutions in Omsk, eg. State Engineering University, Omsk State University and Institutions of the Russian Science Academy which need ionospheric sounding data while being themselves able to carry on the development and manufacture of ionosondes. Much high level ionospheric research has previously been carried out demonstrating the competence of Omsk engineers and scientists. For example, a theoretical

analysis of ionospheric sounding was carried out and a systematic error was revealed in virtual height h' measurements. Apparently, this error is a characteristic feature of all modern methods of radiowave sounding in a non-uniform plasma layer. This error is especially large in the vicinity of the layer critical frequency. But in the vicinity of the ionospheric F2 layer, the value of the virtual height h' itself is bigger and masks the h' measurement error. This diverted the attention of the researchers from this kind of error. Taking this into account, a procedure was suggested for ionospheric plasma sounding that provides the possibility of reducing the h' measurement errors in the vicinity of foF2 by an order of magnitude [5]. This theoretical research needs experimental confirmation using a research ionosonde.

Earlier (in one of the first Russian ionospheric laboratories in the city of Tomsk) a procedure for a more precise determination of critical frequency of a non-stationary foF2 layer was developed. This procedure was based on the Doppler effect and also needs confirmation by means of a research ionosonde [6].

The precise determination of both virtual height and foF2 will provide the basis for quick ionospheric prediction, including recognition within seconds if sudden ionospheric disturbances occur caused by solar flares. Secondly, it would be possible to determine the fine structure of an HF ionospheric communication channel which in turn will increase its carrying capacity.

Some investigations were carried out in Omsk to study the multiray structure of decametric wave propagation. For this purpose, the sounding of an Omsk-Moscow radio route with wide-band (40 kHz) signals was used [7]. As a result, a dynamic multiray propagation map was obtained over a typical latitude route about 3000 km long [8].

Substantial experience was accumulated concerning radiometer complex construction for the continuous measurement of interference and of propagation for decametric radio waves. The construction was also used for the mixed-level simulation of communication conditions to assist the computer-aided testing of radio receiving devices [9].

The continuous monitoring of the ionospheric D-layer is performed to register electromagnetic precursors of earthquakes [4].

For a long time, radio channel and network simulation has been carried out in Omsk. A subsystem for signal parameter calculation, based on sounding data, is a part of a programmed system for the hierarchal simulation of radio network information [10, 11]. There are several radio industry enterprises in the city HF-VHF communication systems, such as point-to-point radio receiver devices, frequency synthesisers and crystal oscillators.

Station Hardware

The functional circuit of an ionosonde which is supposed to decrease virtual height h' measurement errors by an order of magnitude cannot be published just now because it is the subject of a Patent Application which is now under consideration by the Russian Federation Inventions Committee.

The Omsk Ionospheric State (OIS) functional tasks and hardware structural composition are a matter for special design work. Our opinion is that the station should have the following component parts:

- a modern research ionosonde similar to the Dynasonde with programmed functions;

- a means for accumulating a data bank accessible at least in the Western Siberian Region;

- a computer work station intended for the simulation of ionospheric dynamics,

- ionospheric sounding procedure algorithms for adapting communications to ionospheric conditions;

- computer simulators or trainers for schoolchildren and students.

Conclusion

The Omsk community is interested in work associated with ionospheric parameter measurements. The following topics are investigated:

- HF radio communication systems simulation;

- experimental investigations of seismotectonic phenomena affecting the lower ionosphere and thus MF and LF propagation in order to develop earthquake prediction methods;

- new designs for prospective HF radio communication systems intended for underpopulated regions.

Obviously the deployment of a new but not very modern ionospheric station or the dislocation of an old one (eg. from Tomsk or Novosibirsk) is pointless. Those stations are at the end of their natural life and are obsolete.

Starting from zero makes it easier to create an effective work program for future years. That is why we are in favour of the creation of a new Center of fundamental geophysical investigation in Omsk, a place that is quiet in seismic terms.

The problem of obtaining personnel for a future Omsk Ionospheric Station is also worth a mention. We should begin the training of staff right now. For this purpose, it is expedient to begin a joint program of Dynasonde software development. In the course of program development, our research workers will master the new equipment. New creative and business relations will help to develop network operations using modern ionosondes.

References

1. XXI Century Agenda. An Environmental and Development Conference, Rio-de-Janeiro, 3-14 July 1992.

2. J. W. Wright and A. K. Paul. Toward Global Monitoring of the Ionosphere in Real Time by a Modern Ionosonde Network. NOAA ERL SEL, **US. Dept. of Commerce**, NOAA/ERL (Boulder, Colorado 80303), July 1981, 61p.

3. **INAG Bulletin** 48, August 1986.

4. I. L. Guffeld, V. F. Marenko, E. A. Ponomarev and V. S. Yampolskyi, Issledovaniya D-oblasti ionosferi metodom naklonnogo zondirovaniya na sverchdlinnikh volnakh **Poisk elektromagnitnikh predvestnikov zemletryasenii** - Moskow: Institute for Earth Physics, AS of USSR, 1988 - P.150-168.

5. L. S. Terekhov, V. E. Zelenkov and V. A. Shaptsev. Russian Federation Invention Claim N92004925/09. Data of priority - November 5, 1992.

6. L. S. Terekhov, B. B. Borisov, S. L. Sokolnikov and Y. E. Tarashchuk, USSR Invention Certificate N 1493938. Date of priority - July 7, 1987.

7. E. S. Poberezgskii, Optimalnaya filtraciya signalov zondirovaniya v nebelom shume **Radiotechnics** 1977, No. 5 - P.91-93.

8. E. S. Poberexgskii, Optimalnaya tipitschnikh korotkovolnovikh trass **Technika Sredstv svyazi, Technika radiosvyazi**, 1979, No. 8-P.86-92.

9. V. A. Shapstev. Ob odnoi funkcii raspredeleniya ogibayuschei summarnikh radiopomekh **Problemi kibernetiki** - Tomsk: University, 1963, No. 64 - P.166-173.

10. V. B. Shulman, V. A. Shaptsev, V. A. Filimonov, Y. P. Tokarev, T. S. Kolobanova and A. V. Elciov-Stelkov, Sovremennoe sostoyanie i napravleniya razvitiya modelioovaniya radiokanalov **Tecknika sredstv svyazi, Sistemi svyazi**, 1990, No. 6 - P.46-53.

11. Panov S. A., Y. P. Tokarev and V. A.Shapstev, Multi Level Modelling of Communication Networks Using Radio Channels **Proceedings of the Int. Conf. on Functionability Problems of Comm. Networks**, 2-6 Sept. 1991 - Novosibirsk, 1991 - P. 150-157.

EMPIRICAL MODEL USAGE IN IONOSPHERIC WEATHER MONITORING

Alexander Eliseyev, Nikolay Zaalov
Radiophysics Division, Research Institute of Physics, St. Petersburg State University,
198904 Petrodvoretz, RUSSIA

Antenna Besprozvannaya
Arctic & Antarctic Research Institute, Beringa 38, 199397 St. Petersburg, RUSSIA

Abstract

An Empirical model is proposed for the interpretation of experimental ionospheric data. The model represents the major large-scale characteristics of the sub auroral and auroral F2 layer as well as the temporal variations during the transition from quiet to disturbed conditions. The model is in FORTRAN code and the correction of predicted foF2 values is possible using satellite and vertical sounding data.

Introduction

A global network of ionospheric observatories provides the possibility of determining ionospheric "weather" at a given time. Ionospheric modelling is used for ionospheric forecasting and for the calculation of ionospheric parameters along a radio path. The data from ionospheric observatories as well as in-situ satellite measurements can be used for the correction of the model parameters. In this paper, an empirical model is proposed for ionospheric weather monitoring. The first part of the paper gives the outline of the model. In the second the results of calculations for quiet and disturbed conditions are presented and briefly discussed, and finally an example of a comparison with experimental HF doppler sounding data is presented.

The Main Principles of the Model

The idea of plasma tubes connecting the ionosphere with the conjugate region is proposed as the basis for computation of the level of noon ionisation. The latitude variations of foF2 are approximated by a product of two functions. One is determined by the solar zenith angle and the other by magnetic field geometry (for the model under consideration the inclined dipole approximation is suitable).

$$(1) \qquad \text{foF2}_{12} = A \cdot \cos^n \chi_{12} \cdot M$$

where foF2_{12} and χ_{12} are dependent on the noon values of the critical frequency and solar zenith angle and M is the factor of conjugation, dependent on the geographical latitude difference at the ends of the tube and hence on their illumination conditions.

Following Rothwell (1962): $M = (\cos \chi_c / \cos \chi_g)^{1/4}$, where χ_g and χ_c are values of the solar zenith angle at the given (g) and magnetically conjugate (c) points. The solar cycle variations of A and n are:

$$(2) \qquad A = a \cdot [1 + b \cdot (\log(F10.7) - 1.812)]$$

$$n = c + d \cdot R$$

where $F10.7$ and R are radio emission flux and sunspots number (3-month average) respectively; a, b, c, d are coefficients of the model (Besprozvannaya, 1991). Experience has shown that both indices of solar activity are to be employed in modelling solar activity effects in the ionosphere. Introducing their interdependence (eg. in the IRI model) generally worsens the results.
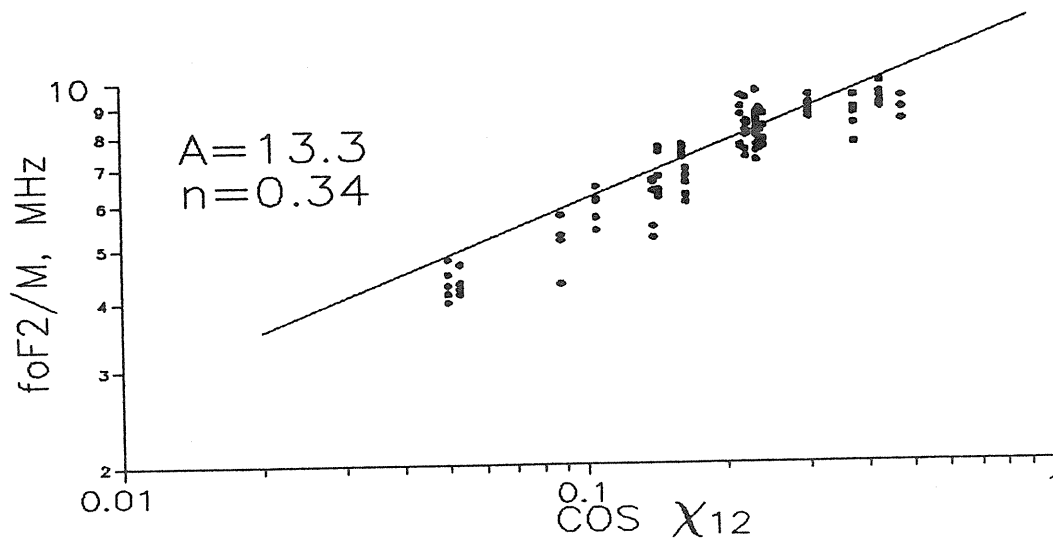
Fig.1

The relation (1) for an analyzed period (December 1988, $F10.7 = 108$, $R = 152$, $A = 13.3$, $n = 0.34$) is presented in Figure 1. In the same figure the noon values of $f{\circ}F2$ divided by the M-factor for 24 ionospheric observatories are shown (black dots). One can see that the experimental data agree closely with the model. Equation (1) gives the noon F2-layer critical frequency corresponding to an average undisturbed ionosphere for the invariant latitude belt from 35° to 75°, for any given solar activity level. This value is basic for further model calculations. Critical frequencies for other times are related with the noon values by the simple dependence:

Fig.2

70
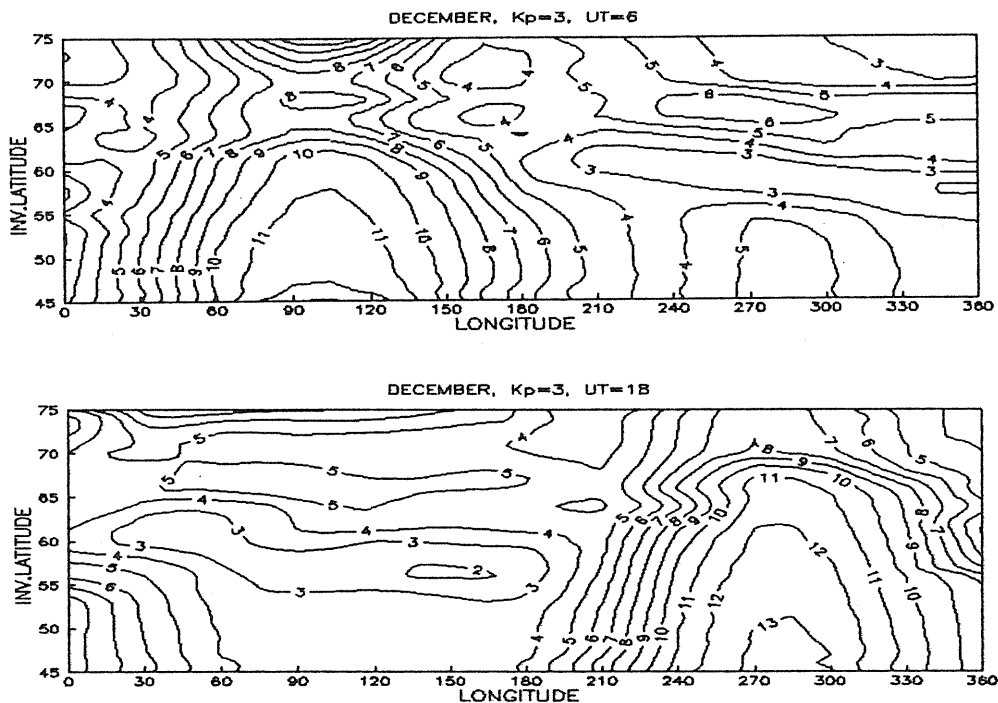
$$(3) \qquad f\circ F2 = K_i.\text{foF2}_{12}$$

Factor K_i shows how F2-layer ionisation varies with changes in magnetic activity and with the local time. The model incorporates a set of K_i -tables for four fixed UT periods; for three levels of magnetic activity (K_p = 0, 3, 5); for high ($F10.7 > 150$) and low ($F10.7 < 100$) solar activity; in winter, spring, summer and autumn. [A set of tables on diskette is available from the authors (A. E.)].

The K_i-value for a particular point at a given UT is obtained by interpolation between two tables of coefficients for the nearest fixed UT times. The longitude value, for which the coefficients are taken from the table, corresponds to the local time of the point under consideration at the given UT. Thus the interpolation is being made practically in longitude. The transition from one level of magnetic activity to another is made assuming that the movement of the mid-latitude trough is described by the Kohlein and Raitt (1977) formula:

$$(4) \qquad \Phi = 65.2° - 2.1° \cdot K_p - 0.5° \cdot t$$

where Φ is invariant latitude and t is the number of hours counted from local midnight.

To show the potential of the model for ionospheric reconstruction it is instructive to look at the calculated distribution of foF2 for selected universal times. This is done in this section.

Maps of $f\circ F2$ in the Northern hemisphere are shown in Figure 2 for two values of universal time (UT = 6 and UT = 18) for moderately disturbed (K_p = 3) conditions. One can see the dynamics of the high-latitude distribution of plasma density in F-layer. During disturbed conditions the maximum change takes place in the night sector which is connected with the main trough movement (Eq.4). The comparison of the maps for UT = 6 and UT = 18 shows notable longitudinal dependence.

Considerable computation efforts are required to incorporate longitudinal dependence into the ionospheric model (Sojka et al., 1979). But HF propagation forecasting needs a simple code which can be realised in real time. Our model was developed as FORTRAN code for IBM PC. Only a few minutes are required for the map calculation. Testing of the model (Besprozvannaya and Eliseyev 1992, Besprozvannaya et al., 1990) shows good agreement with experimental measurements.

Ionosphere Reconstruction and Data Interpretation

In the light of the above, it seems that for practical modelling some additional information about the input parameters of the model are needed.

First, for the noon value calculation we have to know A and n in Eq.1. One can use $F10.7$ and R indices of solar activity and Eq.2. Another way possible is that the analysis of the noon data from an ionospheric network for the preceding period (as in Figure 1) can give us the parameters of the regression line: gradient n and A. For further calculations we can also use the observed noon foF2 value.

During the night auroral and sub auroral stations fall into different regimes of large scale ionospheric structures. The time of transition from one structure to another is a complicated function of latitude, local time and geomagnetic activity level. In Figure 3, data (versus modelled values) for two ionospheric disturbances (December 6, 1988; December 10, 1988) are presented for 8 observatories of the Northern hemisphere. One can see that for disturbed conditions a great difference occurs between observed and calculated foF2 (Figure 3a). Analysis of the ionospheric network data showed that in one case (December 6) the ionospheric trough was 2° southward from the model position and in the second case (December 10) it was about 3° northward (Besprozvannaya et al., 1990). Using formula (4) we can calculate an "effective" Kp value. Results of this correction are presented in Figure 3b. The fitting was improved considerably.
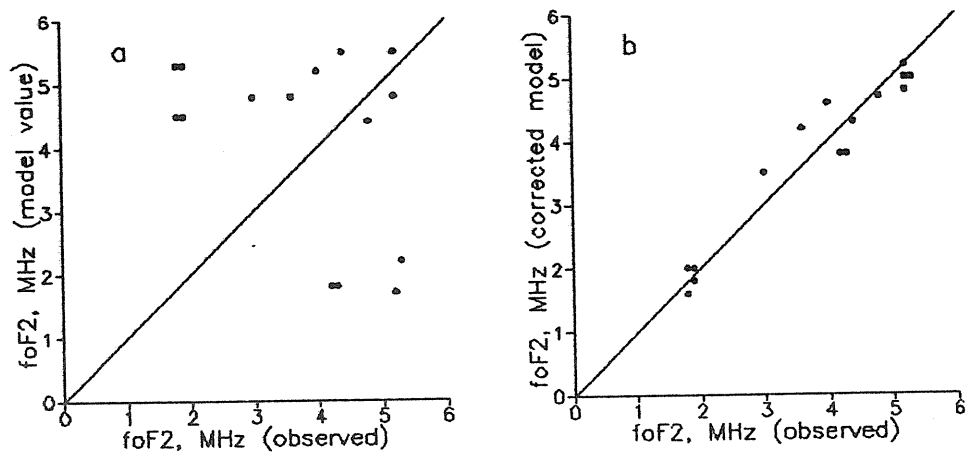
Fig.3

For probing regular and rapid changes in the ionosphere we used the oblique HF doppler technique. An observational multichannel receiver is situated at the St. Petersburg University ($60°N$, $30°E$) where it is a useful tool for investigations of solar flares effects, ionospheric gravity waves and natural and man-made ionospheric distortions. Doppler shift spectra (DS) can be obtained from the computer processing of the
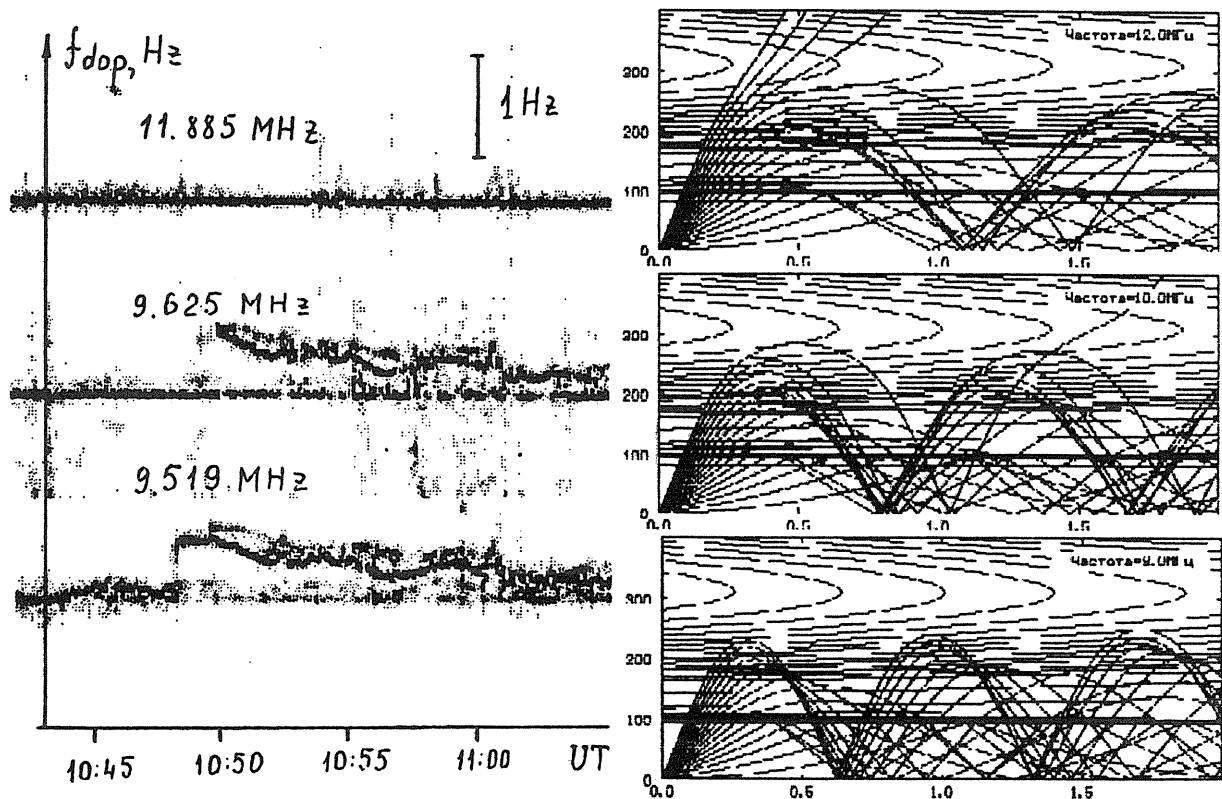
Fig.4

measurements on the ray paths between St. Petersburg and a network of broadcasting stations all over the world. DS usually show the frequency displacement of the signals reflected by different ionospheric structures.

72

The left side of Fig. 4 illustrates such DS spectra of the signal at the frequencies 9.519, 9.625, 11.884 MHz received on June 30, 1992 from transmitter situated in Germany (52°N, 10°, E). For 9.519 and 9.625 MHz, an additional model appeared at 10.47 UT and 10.49 respectively. No effect was observed for 11.884 MHz. In the right side of the figure the results of raytracing for 9, 10 and 12 MHz calculations are presented. From these results we can conclude that the new mode at 1580 km was a two-hope F2 mode for 9 and 10 MHz while only E mode could be observed for 12 MHz. Observed results agree well with the model calculations and show the transition of skip distance for 9.519 and 9.625 MHz in succession.

Discussion

The purpose of this paper is to demonstrate the capability of the empirical model to calculate and interpret foF2 and Doppler spectra. The model adequately describes the main features of foF2 distribution at auroral and sub auroral latitudes both for quiet and disturbed conditions. However, because the commonly used Kp-index is a poor quantitative measure of the ionospheric disturbance intensity, a real time data input is needed. As a replacement, an effective Kp value can be used which is estimated from the known position of the main trough.

Cambou and Galperin (1982) showed the possibility of monitoring the trough wall location. They used oblique incidence sounding at a chain of ionospheric observatories. The polar wall of the trough created by electron precipitation coincides with the equatorward diffuse auroral boundary. Monitoring of that boundary is possible from satellites (Gussenhoven et al., 1983, Gdalevich et al, 1986). To correct the model the measurements of interplanetary magnetic field are also desirable (Grib et al., 1985, Benkova et al., 1989).

The other way is to make a choice of Kp so that the model foF2 value equals the observed one at an ionospheric observatory in the trough region. It is necessary to allow for the operator experience because the direction of foF2 gradient depends on the location of the observatory (polar or equatorial wall of the trough). The effective Kp value found by either method (time resolution better than 3 hours is desirable) will be the main input parameter of the model.

In the future, we intend to propose our model as a FORTRAN subroutine for IRI to enable further comparison with experimental data as well as with other models. With ray-tracing calculations, the model can be used for near real-time interpretation of Doppler spectra observations and could be used for ionospheric weather monitoring over a wide region by passively receiving signals from broadcasting transmitters.

References

Benkova, N.P., A.S. Besprozvannaya, E.F. Kozlov, and S.A. Pullinets - IMF Influence on the Main Ionospheric Trough Position as Deduced from "Intercosmos-19" Satellite Data, **Geomagnetism i Aeronomiya**, 29, 863, 1989.

Besprozvannaya, A.S. - Empirical Modelling of the F2 Peak Density at 50x-70x Invariant Latitude Using Magnetic Conjugacy, **Adv. Space Res.**, 11, 23, 1991.

Besprozvannaya, A.S., A. Yu. Eliseyev - Empirical Model for foF2 Forescasting. **Proc. STPW. 1993** .

Besprozvannaya, A.S., P.N. Kishcha, E.V. Nepomniashchaya, S.A. Pulinets and T.I. Shchuka - Estimates of Accuracy and Correction of the Empirical Reference Ionosphere Model for Isolated Periods, XXIII **General Assembly URSI Abstracts**, Prague, 1, 163, 1990.

Cambou, F., and Yu. I. Galperin - Main Results of the Joint French-Soviet Space Project ARCAD-1 and ARCAD-2 for Magnetospheric, Auroral and Ionospheric Physics, **Ann. Geophys.**, 38, 83, 1982.

Gdalevich, G.L., A. Yu.Eliseyev, O.P. Kolomiytsev, V.V. Afonin, V.D. Ozerov, T.N. Soboleva - Ionospheric Plasma Density Variations at the Main Ionospheric Trough Zone Connected with IMP Changes for Magnetic Storm 18-19.12.1978, **Kosmicheskie Issledovaniyua**, 24, 79, 1986.

Grib, S.A., A. Yu. Eliseyev, O.P. Kolomiytsev - Ionosphere at the Main Ionospheric Trough Zone During Magnetic Storms, **Geomagnetism i Aeronomiya**, 25, 211, 1985.

Gussenhoven, M.S., D.A. Hardy and N. Heineman - Systematic of the Equatorward Diffuse Auroral Boundary, **J. Geophys. Res.**, 88, 5692, 1983.

Kohlein, W., W.J. Raitt - Position of the Midlatitude Trough in the Topside Ionosphere as Deduced from ESRO-4 Observation, **Planet. Space Sci.**, 25, 600, 1977.

Rothwell, P. - Charged Particles in the Earth's Magnetic Field and the Ionospheric F2 Layer, **J. Phys. Soc. of Japan**, 17, 263, 1962.

Sojka, J.J., W.J. Raitt and R.W. Schunk - Effect of Displaced Geomagnetic and Geographic Poles on High-Latitude Plasma Convection and Ionospheric Depletions, **J. Geophys. Res.**, 84, 9943, 1979.

THE ROUTINE DIAGNOSIS OF THE IONOSPHERE FOR THE SHORT-TERM FORECAST OF HF AND VHF PROPAGATION

R. G. Minullin, O. N. Sherstyukov, V. I. Nazarenko,SA. L. Sapaev, A. D. Akchyurin
Physics Faculty, Kazan University, RUSSIA

The routine diagnosis of ionospheric conditions can be accomplished by real-time measurements made within regional ionospheric networks. A proposed network design consists of seven digital ionosondes, one of which is at the centre of a region, the others being distributed around the periphery of the region. The ionosondes must be synchronised to operate alternatively in vertical and oblique mode.

The operating cycle of such a regional network starts with the operation of the central ionosonde in vertical sounding mode. At this time, the vertical sounding (VS) is also recorded at all peripheral stations. The same aerials may be used for VS and oblique incidence (OS) operation. Our experiments have shown that delta aerials, intended for vertical sounding, receive ionograms when oblique sounding at a distance of 1800 km. This was tested over the paths Moscow-Kazan (700 km) and Kaliningrad-Kazan (1800 km). Receiving oblique ionograms provides information about ionospheric conditions at the mid-point between the central and peripheral station.

In the next time interval, a vertical sounding is carried out by each peripheral stations in turn. The nearest neighbouring peripheral ionosonde, arranged in a large circle of radius 1400-1600 km, receive radiation from each peripheral ionosonde after reflecting from the ionospheric layers. Thus, OS ionograms are recorded in addition to each VS which characterise ionospheric conditions for points between peripheral stations at a distance of 700-800 km. Taking into account the correlation properties of the regular ionospheric layers (high within 700-900 km), the area of control may be equal to a circle with a diameter of approximately 5000 km.

Sounding data are processed at peripheral stations to reduce their content from 100 kBytes to 1kByte. If necessary, a further reduction by an order of magnitude can occur. After reduction, the results of the sounding are transmitted to the central station.

The main computer at the central site periodically calculates the present state of the ionosphere over the region, which is promptly corrected by data from the peripheral stations. On the basis of the corrected model, the forecast state of the ionosphere is determined. Consumers of ionospheric information entering into contact with the central station have information about the present as well as the forecast state of the ionosphere. An independent, autonomous communication link not subjected to ionospheric influence is then required.

The transmitters and receivers at the ionospheric stations may also be used for transmitting ionospheric information. After the transmission of the information, the transmitters and receivers then return to their usual function. Thus the sounding and transmission of information will alternate periodically in time.

Meteor burst communications [1] could be an alternative method for transmitting ionospheric information. Meteor communication is possible in the range 25-60 MHz over distances up to 1800 km and is a system of intermittent communication, where the duration of contact may be from part of a second to a few seconds with pauses which may run to tens of seconds. However, thanks to the wide bandwidth of a meteor radio channel (2 MHz or more) the rate of information transfer can be large during contact [2,3].

Daytime meteor radio communications have unfavourable conditions at 1800 LT. At this time, the number of meteor reflections is least with season, the minimum in meteor numbers occurs in spring. Calculations

for these worst conditions show that an ordinary ionogram of 1 kB may be transmitted via the meteor channel in individual contacts of a few tenths of a second.

Meteor communication is not subjected to ionospheric influence or a rise in radiowave absorption, because radio communication is carried out mainly in the meter wavelength range. Signals reflected from meteor trails may be received in a bounded zone of a few tenths of a km radius about a receiving station. Because reception outside the zone is not possible, peripheral stations may work at one carrier frequency without interfering with each other. At the central collection point of ionospheric information, special steps need not be taken to time-separate the stations because of the random nature of contact with the peripheral stations. Meteor communication selects the time and duration of a session of information transmission automatically.

For oblique sounding, the peripheral and central stations must be synchronised and locked to a common scale of time. Currently, synchronisers are locked via the transmission of exact time signals from radio stations in the decameter radiowave range. Such frequencies are subject to ionospheric influences, particularly in high latitudes, which may result in a complete loss of radio communication. Meteor communication makes it possible to solve this problem. Thanks to the broad band of transmission, exploratory experiments have shown that the meteor channel may provide a locked scale of time with errors of no more than tens of nanosecond. This is higher than the precision required for synchronising ionosondes, which need to be mutually locked within tens of microseconds. Thus, high precision timing within the given region may be provided by an ionospheric network which has a meteor communication system. Exact timing requires checking and correcting at intervals from tens of hours to a few days so that the communication channel access for this objective is low. Therefore, this channel may also be provided by the meteor communication system intended for ionogram transmission to the central station.

Central stations of regional networks may be mutually connected at key border points. As a result, regional centres may exchange data about the current ionospheric situation and maintain a routine ionospheric map for a large region of the Earth.

Thus, such a variant of the regional ionospheric network when based on meteor communication channels between central and peripheral stations, solves the problem of obtaining routine ionospheric information for the control and reliable short-term forecasting of HF and VHF propagation conditions.

A regional ionospheric network may allow the prompt recognition of the presence and movement of sporadic E-layers, as well as ionospheric disturbances and the ionospheric response to "heating" and surface and nuclear explosions etc. All this timely information may be immediately transmitted to the appropriate consumers. A network with such meteor channels of communication may also be used for the receipt and transmission of meteorological and geophysical information to consumers spread over a large geographic region, along with other low data rate information.

References

Minullin, R. G. The Variants of Regional Ionospheric Networks, **Ionosfernye issledovania**. Moscow, 1994. N50 (in the press).

Kazantsev, A. N. Meteor Radio Communication on Ultra-short Waves. Moscow. F.L., 1961. 286p.

Minullin, R. G., Palii, G. H., Sidorov, V.V. and another. Locking Scales of Time to a State Standard by Using Meteor Reflections. **Izmeritelnaya tekhnika**. 1971. N1. P.22.

Boikov, V. I., Zhulina, E. M., Minullin, R.G. and another. Influence of Proton Flares on Radiowave Propagation in the Subaurora Region. **Geomagnetizm in Aeronomia**. 1973 V.13, N6. P.1116.

Zhulina, E. M., Kurganov, R. A., Minullin, R. G. and another. Influence of Auroral Absorption on the Numbers of Meteor Reflections. **Geomagnetizm in Aeronomia**. 1978. V.18. N4. P.734.

APPLICATION OF FM/CW TECHNIQUES TO IONOSONDES

Kenro Nozaki
Hiraiso Solar Terrestrial Research Center,
Communications Research Laboratory
3601 Isozaki Nakaminato Ibaraki, 311-12 Japan

Abstract

In this paper, advantages of FM/CW techniques over the pulse radar are presented as they apply to ionosondes. The data processing gain that comes from a matched filter enables an FM/CW ionosonde to make observations with very low transmitting power. The frequency and height resolution of an FM/CW ionosonde can also be changed after an observation has been made. These make the FM/CW ionosonde particularly useful for some specific observations, while it also has functions equivalent to those of the pulse ionosonde.

Introduction

An FM/CW ionosonde (or a chirp sounder) has a high duty factor and narrow band width. So, compared to a pulse ionosonde, it has the advantages of:

(i) Low peak power, so, it creates less interference for other radio users.

(ii) Good noise and interference discrimination.

Doppler analysis, angle of arrival, polarization, and amplitude measurements can be performed equally as well by a chirp sounder as by a pulse ionosonde[1,2,3].

The high cost and laborious task in frequency sweep synthesizers and spectrum analyzers have prevented FM/CW radars from becoming popular for use in the field of the ionosphere observation. These obstacles to the use of chirp sounders, however, can now be easily overcome due to recent improvements in semiconductors and microprocessors.

Basic Equations

The transmitter frequency increases (or decreases) linearly with time as shown in Fig. 1. Frequency differences between the echo and the transmitting signal are proportional to the distance. De-chirped signals from the receiver are sampled at a constant rate while a chirp sounder sweeps from the starting frequency to ending frequency. Fast Fourier Transform (FFT) is generally used to analyze the de-chirped signal. We get echo amplitude vs. range in every FFT.

Frequency analysis of the de-chirped signal is known to be identical to a matched filter in pulse compression radar. The pulse compression ratio G is given by

$$G = BT \qquad (1)$$

where B is the frequency sweep range and T is the time duration for one spectrum analysis[4]. Range resolution Δr is given by

$$\Delta r = c / 2B \qquad (2)$$

where c is the velocity of light. Velocity resolution Δv is determined by

$$\Delta v = c/2f\sigma \qquad (3)$$

similar to that of pulse radar in a fixed frequency mode. Here f is the observation frequency and σ is the Doppler observation time.
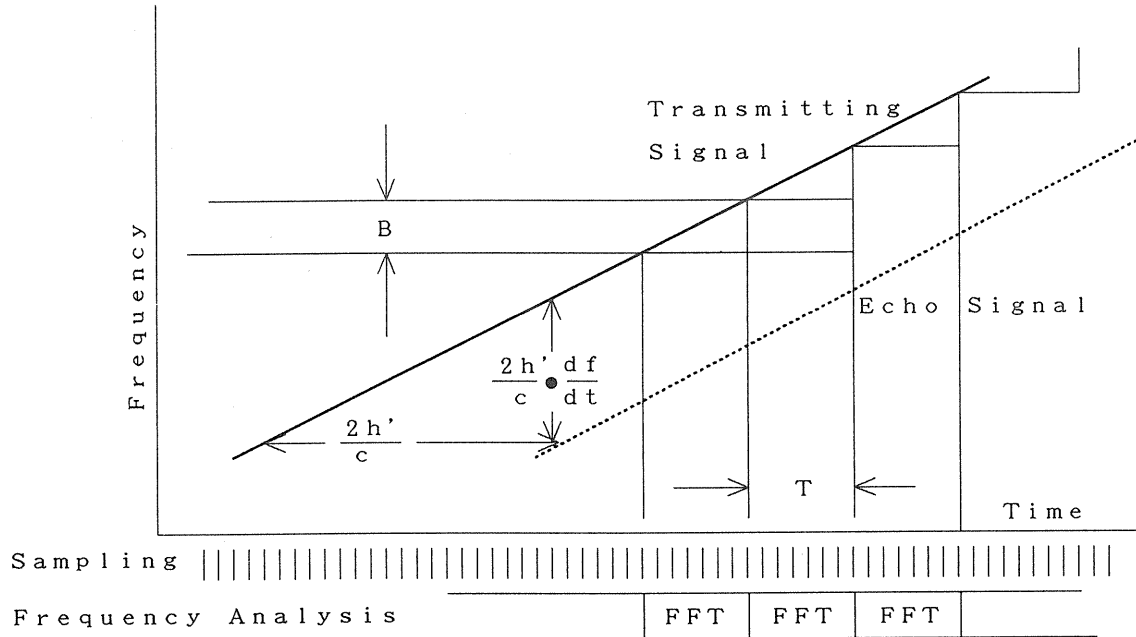
Fig.1 Frequency-time diagram of a chirp sounder.

Applications to Observations
Low Power Operation

Using eqs. (1) and (2), and considering that B=(df/dt)T, we obtain

$$G = \frac{c^2}{(2\Delta r)^2 \dfrac{df}{dt}}. \qquad (4)$$

G increases with fine range resolution and a slow sweep rate. Let the frequency sweep rate df/dt=100 kHz/s and the range resolution 5 km, for example, then we obtain a pulse compression ratio of about 10,000. A chirp sounder with an output of only 1 W is equivalent to a typical 10 kW output pulse ionosonde. Figure 2a shows an oblique incidence ionogram by means of a chirp sounder of 1 W transmitting power while Fig.2b shows a vertical incidence ionogram obtained by means of a conventional mono-pulse ionosonde near the chirp sounder.
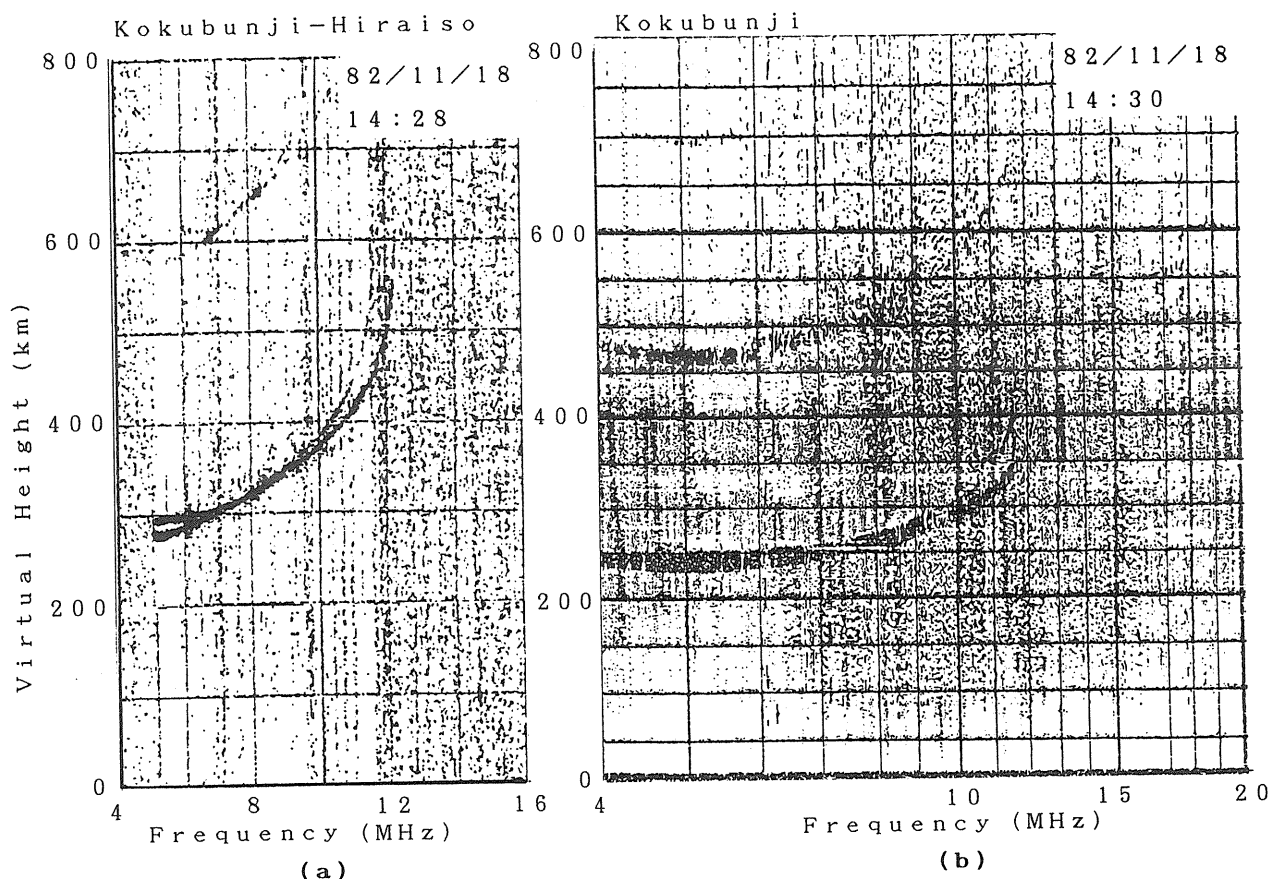
Fig. 2   Ionograms obtained at close time and location

(a) chirp sounder of 1 W, 100 kHz/s, and 150 km oblique

sounding

(b) pulse ionosonde of 10 kW and vertical sounding.

Variety in Observation Parameters

The equivalent power, range, frequency resolution, and time resolution (and velocity resolution in the fixed frequency mode) are closely related to each other in the chirp sounder.   By decreasing the frequency sweep rate, one can increase equivalent output power without increasing the actual output power.

Fine range resolution is accompanied some difficulty in pulse ionosonde because a narrow pulse needs high output peak power and wide frequency band allocation for the same signal to noise ratio as wide pulse observation.   However, figure 1 and eq. (2) indicate that the wide range of time domain (T) data provides wide frequency sweep range B, thus, fine range resolution.   There needs no change in the transmitting parameters.

Post Observation Analysis

When using a pulse ionosonde, range resolution and frequency resolution are defined by pulse width and frequency step which must be decided before the observation.   On the contrary, these resolutions can be

decided after an observation with a chirp sounder. A series of de-chirped signals can be stored in a memory and frequency analysis can be applied after the observing frequency scan has been completed.

Fine height resolution but coarse frequency resolution is required to detect the fine motion of a flat type Es, whereas coarse height resolution but fine frequency resolution is required to determine an accurate critical frequency of a normal layer. We can select any of these resolutions from a single observation according to the characteristics of the analysis after observation by recording the de-chirped signal in the time domain.

About 30 kBytes of sampling data is recorded by a chirp sounder with a frequency range of 1 - 30 MHz, a height range of 750 km, and 8 bit amplitude resolution. This is comparable to the amount of data in amplitude ionogram from a pulse ionosonde.

Conclusion

A chirp sounder has certain advantages of its own along with common functions with a pulse ionosonde. Actual transmitting power of a chirp sounder can be reduced while equivalent output power is kept as high as a pulse ionosonde. The ability to analyze the time domain data after observation makes the chirp sounder particularly useful in some specific observations.

References

[1]Davies K. Ionospheric Radio, Peter Peregrinus Ltd., pp.102-105, 1989.

[2]Barry G.H., IEEE Trans. Geosci. Electron. GE-9, 1609, 1971.

[3]Poole A.W.V., Radio Sci., 20, No.6, 1609, 1985.

[4]Skolnik M.I., Introduction to Radar Systems, 2nd ed., McGraw-Hill, pp.422, 1980.

VERTICAL IONOGRAMS AS A TOOL IN HF PULSE PROPAGATION ANALYSIS

Davorka P. Grubor and Zivko V. Jelic
Geomagnetic Institute, 11306 Grocka, Belgrade, Serbia, Yugoslavia

Abstract

The dispersive bandwidth, or the reciprocal parameter, ie. the rise time, is calculated for oblique propagation using vertical ionograms. A number of ionograms taken at equinox, noon and high solar activity conditions are chosen and used to estimate the first total derivatives of group path with respect to frequency. To this purpose the slopes dh'/df_v of the tangents drawn at the selected points of $h'(f_v)$ curves, corresponding to the E, F1 and F2 traces, are used. These points are selected so that the equivalent frequency of the oblique propagation over the great circle distance D=300 km is f_o=5 MHz for both the 1E and the 1F1 wave and f_o=11 MHz for the 1F2 wave. The obtained values for rise times are about 5 μs for the 1E wave, about 9 μs for the 1F1 wave and 10-15 μs for the 1F2 wave. The results are in fair agreement with the corresponding values obtained by the simulation method, based on the application of the raytracing program to the same propagation path.

Introduction

Recent aspects of HF communications have given rise to interest in the analysis of vertical ionograms in order to obtain some additional information apart from the commonly scaled parameters. One useful parameter characteristic of oblique HF pulse propagation, which can be obtained from vertical ionograms, is the value of the *dispersive bandwidth*. The procedure explained in [1] is applied here to nine quiet condition ionograms, taken in October 1988 at Grocka ionospheric observatory (44° 38' N, 20° 47' E, I=61°), where an IPS-42 ionosonde is operating.

The relationship between the first total derivative of the group path with respect to frequency and the first total derivative of the virtual height with respect to frequency, as obtained in [1], is given by:

$$\frac{dP'}{df_o} = \frac{4h'\frac{dh'}{df_v}\cos i_o}{p' - 2f_o\sin^2 i_o \frac{dh'}{df_v}} \quad \text{at } f_v = f_o\cos i_o \quad (1)$$

where P' is the group path, f_v is the frequency of a vertically incident wave reflected at the virtual height h', and f_o is the equivalent frequency of the wave propagating obliquely with the angle of incidence i_o. The expression is valid for mirror type reflections. Since the ionograms selected for the present analysis show continuous and unambiguous traces, the values of dh'/df_v are determined by simply drawing the tangents at the points of interest, instead of applying the computational process described in [1]. According to the theory developed in [1] and [2], the distortion of the obliquely propagating pulse through a stratified ionosphere, in the quadratic phase approximation, can be described by the dispersive bandwidth, given in the following form:

$$f_d = \frac{1}{t} = \left(\frac{1}{c}\frac{dP'}{df_o}\right)^{\frac{1}{2}} \quad (2)$$

where t is so called pulse rise time and c is the velocity of the electromagnetic wave in vacuum. From (1) and (2), the rise times can be determined.

The rise times were calculated previously by simulation of the multipath pulse propagation as proposed in [2]. To this purpose, the Jones-Stephenson raytracing program [3] was used, considering the 1E, 1F1 and 1F2 ray paths over the range of 300 km, with frequencies 5 MHz, 5 MHz and the 11 MHz, respectively. The procedure for numerical evaluation of dP'/df_o was developed and the values thus obtained were subsequently used in (2) for the determination of rise times. The IRI electron density profile data were inserted in the raytracing program in the form of an analytic function, applying Booker's method [4]. The results of this numerical simulation and the ones obtained by the analysis of the ionograms are compared in this paper.

An Analysis of Ionograms

The IPS-42 ionosonde range of sounding frequencies is 1-22 MHz and the maximum registered virtual height is 800 km. Ionograms taken in October 1988, starting with October 1 (day 275 of the year) are used in the analysis. As all ionograms are taken around noon hours, the average values of scaled parameters are: h'E=115 km, f_oE=3.6 MHz, h'F=206 km, f_{oF1}=5.5 (UL), f_oF2=12.4 MHz. Only the ordinary ray traces are considered. The transmission curves are drawn assuming the distance D = 300 km with the equivalent frequency f_o = 5MHz for 1E and 1F1 f_o=11 MHz for 1F2 propagation. The vertical frequencies are determined from the intersections of the transmission curves with the ionogram traces, related to the low ray. The values are spread within an interval 0.5 MHz wide around f_v = 2.99 MHz (E trace), 0.17 MHz around f_v = 4.27 MHz (F1 trace) and 0.35 MHz around f_v = 10.4 MHz (F2 trace). The tangents are drawn at the points of the $h'(f_v)$ curves, corresponding to these average f_v values and the slopes of the tangents are estimated. In Table 1 the vertical propagation frequencies, the corresponding virtual heights and the slopes dh'/df_v, at the selected points (f_v, h'), are given for each ionogram.

The values of group path derivatives calculated from (1) using the slopes estimated from the ionograms (Table 1), along with corresponding rise times calculated from (2), are given in Table 2. It can be seen from Tables 1 and 2 that both the variations in the virtual heights scaled at a given frequency and the dispersion of rise times values are the greatest for the E trace. The average values of group path derivatives and rise times for each of the three traces considered are also given in Table 2, in order to provide comparison with the results presented in Table 3 obtained using the simulation method.

A Simulation of Multipath Propagation

By this simulation method the rise times are determined for three cases of propagation considered, using the 3D Jones-Stephenson raytracing program. The ionospheric profile inserted in the program is constructed on the basis of IRI data for equinox, 1200 LT, R=100, applying the fitting method [4]. For all three cases the great circle distance was D=300 km. In the case of 1E propagation, D=300 km is obtained with f_o=5 MHz and with the elevation angle 35.50°. The proper 1F1 propagation could not be obtained with the IRI profile, since this does not include the F1 layer. Nevertheless, the wave with frequency f_o=5 MHz and elevation angle 58.52° reflected at the base of the F region will be here named as "1F1" wave. In the case of 1F2 propagation, D=300 km is obtained for f_o=11 MHz and with the elevation angle 70.35°. The azimuth angle providing the north-south propagation direction is chosen to be a=180° for all the three cases considered. The ray tracing calculations are performed by slightly varying the initial

Table 1. Estimations from ionograms: f_V (MHz), h' (km) and dh'/df_V (km/MHz).

Ionogram day	time LT	1E $f_V=2.99$ h'	dh'/df_V	1F1 $f_V=4.27$ h'	dh'/df_V	1F2 $f_V=10.40$ h'	dh'/df_V:
275	1130	112	10.4	212	14.7	359	29.4
276	1200	100	5.6	200	16.4	300	32.0
279	1000	124	0.7	212	20.0	324	27.1
279	1215	121	10.6	224	13.9	329	25.7
280	1200	100	6.2	209	33.4	335	26.0
286	1245	118	3.9	224	10.2	312	26.0
288	1000	129	14.3	215	12.1	347	38.1
290	1400	127	19.1	227	16.4	335	30.7
301	1000	112	28.9	206	18.6	268	18.3

Table 2.   The group path derivatives and rise times; dP'/df_O (m/Hz) t (µs).

Ionogram day, time LT	1E dP'/df_O	t	1F1 dP'/df_O	t	1F2 dP'/df_O	t
275, 1130	0.0074	5.0	0.0196	8.1	0.0501	12.9
276, 1200	0.0034	3.4	0.0210	8.4	0.0512	13.1
279, 1000	0.0006	1.4	0.0267	9.4	0.0446	12.2
279, 1215	0.0084	5.3	0.0192	8.0	0.0425	11.9
280, 1200	0.0038	3.6	0.0441	12.1	0.0433	12.0
286, 1245	0.0029	3.9	0.0141	6.9	0.0422	11.9
288, 1000	0.0122	6.4	0.0163	7.4	0.0642	14.6
290, 1400	0.0159	7.3	0.0228	8.7	0.0511	13.1
301, 1000	0.0207	8.3	0.0243	9.0	0.0279	9.6
Average :	0.0084	4.9	0.0230	8.7	0.0463	12.4

parameters. Consequently, the small variations in the distance, group path and azimuth of the received ray are produced. From the series of calculations, the dependence of the distance, the group path and the azimuth on the initial ray parameters is established, enabling the evaluation of the total derivative of group path with respect to frequency. The values of the total group path derivatives and the rise times calculated from (2) are given in Table 3.

Table 3. Total group path derivatives corresponding and rise times; dP'/df_0 (m/Hz), t (μs).

1E		1F1		1F2	
dP'/df_0	t	dP'/df_0	t	dP'/df_0	t
0.0144	6.93	0.039	11.40	0.164	23.3

By comparing the values from Table 3 and Table 2, it can be seen that the rise time values obtained from vertical ionograms and the ones following the numerical simulation, are in reasonable agreement. The difference is most evident for 1F2 propagation, as shown in Figure 2. In that case, the ray path calculated using the IRI profile, which assumes layer penetration, significantly differs from the ray path corresponding to a mirror type reflection.
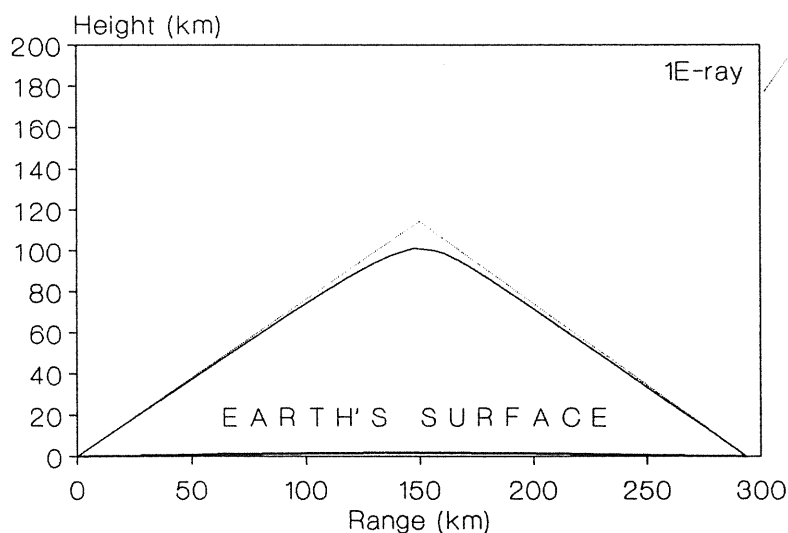
Fig. 1. The ray paths for 1E propagation: mirror type reflection - dotted line, reflection in the ionosphere described by IRI model - solid line.

In order to estimate the discrepancy between IRI profile and the real ionospheric profile corresponding to the ionograms, the real height of the F region base and the real height of the maximum electron density of the F2 layer are determined, following the procedure given in [5]. As can be seen from Table 4, the obtained real heights of the F region base, h_b, the real height of the F2 layer electron density maximum h_m with the corresponding scale height H, significantly vary from ionogram to ionogram.
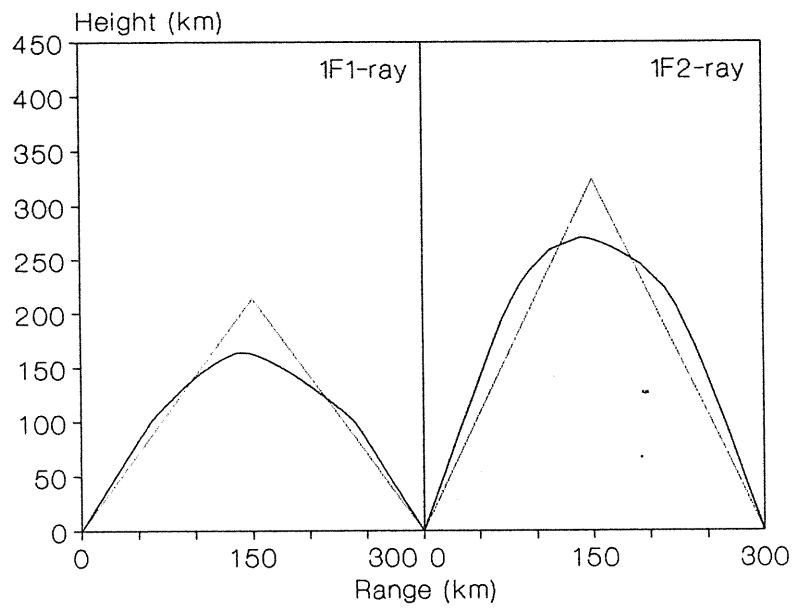
Fig. 2. The ray paths for 1F1 and 1F2 propagation: mirror type reflection - dotted line, reflection in the ionosphere described by IRI model - solid line.

Table 4. The real heights obtained using the parameters scaled from the ionograms.

ionogram day, time LT	scale height H (km)	base height h_b (km)	maximum F2 height h_m (km)
275, 1130	86.7	197.5	429.1
276, 1200	72.1	187.6	393.9
279, 1000	56.1	190.2	334.1
279, 1215	43.2	225.8	341.3
280, 1200	57.4	219.2	373.6
286, 1245	40.7	212.7	325.3
290, 1400	70.5	194.7	395.8
301, 1000	46.6	179.3	323.1
average values:	60.2	197.7	363.5

Conclusion

The average values of h_b and h_m following from Table 4 differ from the corresponding values described by the IRI model by about 30 km. The survey of Table 4, show that some of the ionograms could be described by the IRI model, while other indicate large deviations from it. Therefore, the comparison of the rise times values as determined from ionograms, with the ones obtained by the simulation method, is adequate only in cases where the real height analysis suggests the ionospheric profile close to the one described by the IRI model.

Further improvement in the determination of the rise times (or dispersive bandwidth) from vertical ionograms might be achieved by adopting a more realistic expression for the group path than the one describing the mirror type reflection, from which the group path derivative with respect to frequency could be estimated.

References

[1] Lin, K. H., Yeh, K. C., Soicher, H., Reinisch B. W. and Gamache, R. R., Vertical ionograms and dispersive bandwidths for an oblique path, **Radio Sci.** vol 24, No 4, pp. 521-526, 1989.

[2] Lundborg, B.,Pulse propagation through a plane stratified ionosphere, **J. atmos. terr. Phys.** vol 52, No 9, pp. 759-790, 1990.

[3] Jones, R. M. and Stephenson, J. J. A versatile three-dimensional ray tracing computer program for radio waves in the ionosphere, U. S. Department of Commerce, **OT Report** 75-76, 1975.

[4] Booker H., Fitting of multi-region ionospheric profiles of electron density by a single analytic function of height, **J. atmos. terr. Phys.**, vol 39, pp. 619-693, 1977.

[5] Krinberg, I. A., Vyborov, V. I., Koshelev, V. V., Popov, V. V., and Sutyrin, N. A., **Adaptive model of the ionosphere**, (in Russian), Nauka, Moscow, 1986.

SIMPLIFIED NUMERICAL PROCEDURES APPLIED TO THE TRUE-HEIGHT ANALYSIS OF IONOGRAMS

L.-C. Tsai
Space Dynamics Laboratory and Department of Electrical Engineering,
Utah State University, Logan, UT 84322-4120, USA
F. T. Berkey
Center for Atmospheric and Space Sciences, Utah State University,
Logan, UT 84322-4405, USA
G. S. Stiles
Department of Electrical Engineering, Utah State University,
Logan, UT 84322-4120, USA

Abstract

An efficient numerical process can enable true height calculations to be readily carried out on small computer systems. We have developed a numerical integration method termed "μ't-fitting", where μ' is the group refractive index and t is defined as $\sqrt{(1-f_N{}^2/f^2)}$ for the O-wave and $\sqrt{[1-f_N{}^2/(f^2-f f_H)]}$ for the X-wave. This method is best suited to the true-height analysis of digitally recorded ionograms. It can be used to analyze either the O- or X-waves in an ionogram and includes the effect of the Earth's magnetic field. For second order polynomial profile analysis, the μ't-fitting technique utilizes 38-62% fewer numerical operations than the Gaussian quadrature integration method. Applying 5 and 12 term μ't-fitting to 100 data points, the method completes a true-height analysis in 0.77 and 1.43 seconds, respectively, using a 80486/33 computer system. Furthermore, applied to the overlapping Chapman model profile adopted by U.R.S.I. Working Group G.6.2 [McNamara and Titheridge, 1977], the test results show rms errors of 8.3 and 7.0 meters for the O and X wave components (12-term μ't-fitting), over a set of 22 selected frequencies.

Introduction

Ionograms have provided the basis for much of our understanding of the physics of the ionosphere. Even more information can be obtained from these records by inverting the virtual height-frequency trace to obtain the ionospheric electron density profile, a process called true-height analysis. The proliferation of digitally recorded ionograms and the development of powerful microcomputers now enable true-height analysis methods to be readily implemented.

Titheridge [1985] developed one of the most widely used true-height analysis methods using polynomial equations to represent $h(f_N)$, where h is the true height and f_N is commonly expressed as plasma density. The POLynomial ANalysis program (POLAN) is a computer method that implements a generalized, polynomial analysis, the execution time of which is primarily dependent on the group refractive index calculation. In this paper, we describe an efficient method that can be used to derive the integral of the group refractive index μ', and enable true-height analysis of digital ionograms to execute in less than one second for 100 data points. A monotonic ionosphere is used for the purpose of a simplified comparison of the two true-height analysis methods described previously.

"μ't-fitting" technique

The electromagnetic field in the ionosphere is governed by Maxwell's equations. It is assumed that there is no permanent space charge and that all field variables vary sinusoidally with time at the same angular frequency ω. Ionospheric sounding utilizes radio waves transmitted vertically from the ground, which travel upward into the ionosphere, where they are reflected, and return to a ground-based receiver. The measured

virtual height h' and the true height h are related by $h' = \int_0^{h_r} \mu'dh$, where h_r is the height of the reflection, and μ' is the group refractive index, a function of the radio frequency f, the plasma frequency f_N, the magnetic gyrofrequency f_H, and the magnetic dip angle I.

The group refractive index μ' is a complicated function, as expressed in Shinn and Whale [1952], and approaches infinity at the reflection point. In order to avoid singular points in the integrations of μ', Shinn [1955] and Becker [1960] introduced the reduced frequency f_R. This quantity is defined to be f for the O-wave and $(f^2-f\times f_H)^{0.5}$ for the X-wave. By changing variables, we make the following substitution:

$$ t = \left(1 - \frac{f_N^2}{f_R^2} \right)^{\frac{1}{2}} . \qquad\qquad 1 $$

At the reflection point, the product $\mu't$ has a finite value, except for the ordinary component at 90° magnetic dip angle. Numerical methods permit approximation of the product $\mu't$ by an interpolating polynomial in t which fits a selected set of points $(t_i, \mu'_i t_i)$, where i = 0, 1, 2, .., n. Such a polynomial is unique, because there is only one polynomial of degree n passing through n+1 points. The Newton-Gregory interpolating polynomial [§5 of Cheney and Kincaid, 1980] can be used to find the polynomial that passes through a group of equispaced points for $t \in [0,1]$. Hence, the product $\mu't$ can be derived as a function of t as follows

$$ \mu't(t) = (\mu't)_{t=0} + \binom{s}{1}\Delta(\mu't)_{t=0} + \binom{s}{2}\Delta^2(\mu't)_{t=0} + \binom{s}{3}\Delta^3(\mu't)_{t=o} + \ldots + \binom{s}{n}\Delta^n(\mu't)_{t=0} \qquad 2 $$

$$ = \sum_{j=0}^{n} c_j t^j , $$

where s = t/d, and d is the uniform difference between the t-values. With this $\mu't$-fitting technique, the series terms of the group refractive index μ' can be calculated by the Shinn-Whale formula, and each coefficient of the Newton-Gregory forward interpolating polynomial can be derived. We assume that the variation of plasma frequency f_N with true height h is given by

$$ h - h_a = \sum_{k=1}^{N_T} q_k (f_N^2 - f_a^2)^k , \qquad\qquad 3 $$

where the point (f_a, h_a) is the origin for the real-height region under consideration, and the value of N_T defines the order of the analysis. This model yields

$$h'' - h_a = \sum_{k=1}^{N_T} \left[2q_k k \int_{f_a}^{f_R} \mu'(f_N^2 - f_a^2)^{k-1} f_N df_N \right],$$ 4

where h" is the reduced virtual height, equal to h' minus the group retardation due to those parts of the profile below the point (f_a, h_a). Therefore, by the μ't-fitting technique and replacing f_N^2 with ϕ, we can express the integral in equation (4) in terms of this known polynomial as

$$\int_{\phi_a}^{\phi_b} \mu'(\phi - \phi_a)^{k-1} d\phi = 2 f_R^{2k} \int_{t_b}^{t_a} \mu't(t_a^2 - t^2)^{k-1} dt = 2 f_R^{2k} \sum_{i=0}^{k-1} (-1)^i \binom{k-1}{i} t_a^{2(k-1-i)} I_i,$$ 5

$$I_i = \int_{t_b}^{t_a} \mu' t^{2i+1} dt = \sum_{j=0}^{n} \frac{c_j}{2i+j+1} t^{2i+j+1} \Big|_{t=t_b}^{t=t_a}.$$ 6

Complexity analysis

Titheridge [1985] developed the FORTRAN program POLAN that implements a generalized polynomial method which can be applied to the true-height analysis of ionograms. Ten standard modes of analysis are provided in POLAN, dependent on: 1) N_T, the order of the polynomial invoked for real-height analysis; 2) N_V, the number of virtual heights; 3) N_R, the number of known true heights and; 4) N_H, the number of new true heights calculated in each step. The coefficients of true-height polynomials yield an exact solution if $N_T = N_V + \_N_R\_$, or a least squares solution if $N_T < N_V + \_N_R\_$. Calculations normally proceed in a stepwise fashion to obtain successive, overlapping sections of the real-height profile. POLAN invokes a five- or twelve-term Gaussian quadrature integration, depending on the desired accuracy. In the case of the N_G-term used in the Gaussian quadrature method, since all N_T values of integration for equation (4) are obtained from the same N_G values of μ', there are a total of {($N_T + 11$) $N_G - 1$} additions and {($N_T + 19$) $N_G + 2 N_T$} multiplications required to calculate these integration terms.

For the μ't-fitting technique, since the gyrofrequency f_H, the magnetic dip angle I, and all radio frequencies are known, the coefficients of the Newton-Gregory interpolating polynomial for the product μ't as a function of t can be precalculated. If we assume N_G terms $(n = N_G - 1)$ for the Newton-Gregory interpolating polynomial, there are a total of $\{3\ N_T N_G + 0.5\ N_T^2 + 1\}$ additions and $\{(2\ N_T + 2)\ N_G + 2.5\ N_T^2 + 8\ N_T - 1\}$ multiplications required to calculate N_T values of integration for μ'.
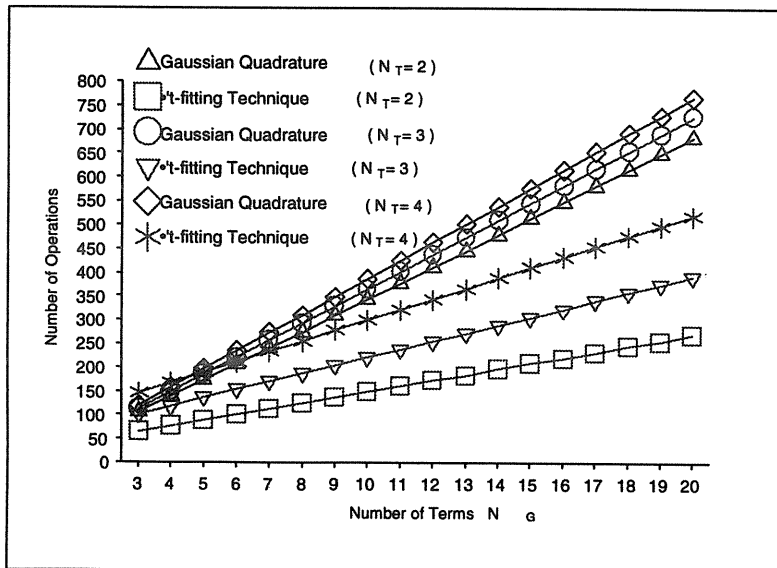
Figure 1 shows the number of mathematical operations (addition and multiplication) required for the two integration techniques, as a function of N_G between 3 and 20. With increasing the polynomial order, this diagram shows that the number of operations increases proportionally more for the μ't-fitting technique (100% for $N_T = 4$) than for the Gaussian quadrature method (13% for $N_T = 4$) at a N_G value of 12. The smaller increase in the number of numerical operations

Figure 1

for the Gaussian quadrature method results from using the same N_G values of the group refractive index μ' for every integration in equation (17). None-the-less, except for small values of N_G in the fourth order case, more mathematical operations are used by the Gaussian quadrature method since more complex calculations are required to derive the group refractive index μ'. For the parabolic lamination method ($N_T = 2$), the μ't-fitting technique utilizes 38-62% fewer numerical operations than the Gaussian quadrature method. For second order polynomial profile analysis, Figure 5 shows the execution times of the 5-term and 12-term μ't-fitting techniques as a function of echo number N, as implemented on an 80486/33 computer.

As expected, the execution times of these methods are approximately proportional to the square of the number of echoes N. They range from 0.77 (1.43) seconds for 100 data points to 3.14 (5.63) seconds for 200 data points when the 5(12)-term μ't-fitting techniques are applied.

Accuracy analysis

In general, the Newton-Gregory interpolating polynomial does not produce results which are identical with the real product μ't derived from the Shinn-Whale formula, even though common values can be found. The non-matching values obtained from the interpolating polynomial are subject to error, which decreases (as expected) as the

Figure 2

order of the interpolating polynomial is increased. A convergence test for various orders of the interpolating polynomial reveals the accuracy which can be expected and provides a basis for selection of the order of polynomial. The errors are computed relative to results derived using an 18-term Gaussian quadrature integration with 10^3 intervals over $t \in [0,1]$, in which all abscissas and weights were obtained from Love [1966] and have an error less than 1.5×10^{-23}. From the results, the worst case error of the X-wave is two orders of magnitude smaller than that of the O-wave; i.e. the interpolating polynomial for the $\mu_x't$ curve has smaller error than that derived for the $\mu_o't$ curve. The magnitude of relative error is less than 1.2×10^{-3} for a 5-term $\mu't$-fitting integration and less than 2.2×10^{-6} for a 12-term $\mu't$-fitting integration in the case of the X-wave, I=65°, and Y≥0.1. In order to decrease the error associated with the O-wave, we simulate the product $\mu_o't$ by using three non-overlapping polynomials instead of one over the interval $t \in [0,1]$. The points of intersection can be obtained by trial and error or found approximately from the curve for I = 65°, which varies by a factor of 2 between t=0.1 and 0.3. In this analysis, we chose the points of intersection at 0.1 and 0.3. The relative errors for this approach are less than 8.5×10^{-4} for 5 terms in each polynomial section and less than 2.5×10^{-6} for 12 terms in the case of I=65° and Y≥0.1. The associated execution time, which is the same as that of adding two more data points to the single-$\mu't$-fitting method, is increased slightly but is still a factor of 2 faster relative to the Gaussian quadrature integration method, when the number of data points exceeds 10.

Inadequate starting height data is a main source of error in most methods of true-height analysis. The simplest analysis makes the assumption that the virtual height of the lowest observed frequency is the first point of the electron density profile. Thus, the presence of underlying ionization is ignored. This is generally a good approximation, especially when the first observed frequency occurs below the critical frequency of the E layer and when the D layer is not present. A different method can be applied when there is no critical frequency below the lowest observed frequency. Here, we assume that the true heights of the starting region in an ionogram vary linearly with ϕ and that the higher order derivative is equal to zero. Therefore, the starting equations can be expressed as

$$h_{i'} = h_o + 2z' f_R^2 \int_0^1 \mu't dt , \qquad\qquad 7$$

where z' is constant over the starting range. Since there are two unknowns, h_o and z', in equation (7), the value of i must be at least two. If i is greater than two, we have more than two equations and must solve for the two unknowns by a least squares method.

A model profile adopted by U.R.S.I. Working Group G.6.2 [McNamara and Titheridge, 1977] consists of two overlapping Chapman layers, in which the Chapman tail has been cut off at 0.8 MHz. Virtual heights were calculated using a 40-point Gaussian integration applied over five successive height ranges, yielding errors of less than 1 m. We have used the 5- and 12-term $\mu't$-fitting techniques to analyze 150 data points in which the frequency interval is ≥ 0.02 MHz as recommended by McNamara and Titheridge [1977]. Table 1 shows true-height errors (in meters) obtained for the O- and X-wave components at 22 selected frequencies. Application of the 12-term $\mu't$-fitting technique to these profiles yields a difference error for the O-wave component that is a factor of ~5 smaller than that obtained with the 5-term $\mu't$-fitting technique. However, when either the 5- or 12-term $\mu't$-fitting technique is applied to the X-mode data, the difference error is essentially the same for each frequency-height data pair. This result is consistent with a smaller error in the interpolating fitting polynomial for the $\mu_x't$ curve than that derived for the $\mu_o't$ curve. The rms deviations of 23.5 and 7.0 meters for the X-wave component are the result of the approximation techniques that are employed.

Table 1. The errors in true-height analysis of the overlapping Chapman profiles as presented by McNamara

Gyrofrequency = 1.200 MHz Dip = 65.00 degrees										
f_R (MHz)	True height (km)	Errors (meter) O-wave		X-wave		f_R (MHz)	True height (km)	Errors (meter) O-wave		X-wave	
		5-term	12-term	5-term	12-term			5-term	12-term	5-term	12-term
0.905	93.133	-22	-23	3	3	4.256	135.725	-15	-3	-5	-5
1.505	99.305	-15	-10	-2	-2	4.303	138.306	-18	-3	12	12
2.002	102.386	-11	-7	-4	-4	4.355	140.667	-25	-3	-6	-7
2.503	105.269	-5	-5	-2	-2	4.501	145.906	-50	-3	5	5
3.004	108.397	-0	-3	-4	-4	5.002	159.030	-62	-1	4	3
3.505	112.406	-1	-3	-2	-2	5.503	170.685	-56	-1	8	8
4.005	120.144	-5	-2	6	6	6.004	183.298	-60	-1	3	2
4.056	121.860	-5	-1	-4	-4	6.505	199.363	-64	0	10	9
4.105	124.165	-6	-0	3	3	6.606	203.545	-64	1	-5	-5
4.156	127.814	-10	-3	-1	-1	6.707	208.358	-63	1	12	11
4.207	132.270	-15	-6	4	4	6.808	214.194	-59	6	-20	-20

Discussion and summary

In POLAN, a polynomial representation of the true-height profile is used to the inversion of ionograms. Although Gaussian quadrature integration is a very accurate numerical integration method, the computational overhead of this method is large due to the complicated mathematical calculations required to derive the various group refractive indices. However, in most instances of ionospheric sounding, the transmitted frequencies are well known. Using the characteristics of polynomial analysis, we can also express the product of the group refractive index and the variable t (defined in equation (1)) as a polynomial of t at a given radio frequency. Since all of the integrations can be expressed as polynomial integrations and because the precalculation step for the coefficients of the μ't fitting polynomial saves significant computational time, the μ't-fitting technique can utilize 38-62% fewer numerical operations than the Gaussian quadrature integration method for second order polynomial profile analysis. We note that echoes are not obtained at every transmitted frequency for a variety of reasons (interference, absorption, etc.). The Gaussian quadrature method cannot readily utilize a precalculated step, since it requires knowledge of the start and end frequencies of each interval. However, in the μ't fitting technique, we can precalculate the polynomial at every sounding frequency and calculate the integral of the product of μ' and t later, at any

interval or for any combination of echo frequency. We have demonstrated that the Newton-Gregory interpolating polynomial can be used to derive a polynomial that passes through a group of equispaced points. Furthermore, utilizing a technique whereby three interpolating polynomials intersect, the inherent error of the derived product $\mu't$ can be decreased. Applying this method to model ionospheric data, the test results indicate that an error of a few meters can be obtained in the true-height analysis of an overlapping Chapman profile.

Acknowledgements

References

Becker, W. (1960), Tables of ordinary and extraordinary refractive indices, group refractive indices and h'_o, $x(f)$ curves for standard ionospheric layer model, in Mitteilungen aus dem Max-Planck-Institut für Aeronomie, 4, 25 pp., **Springer-Verlag**, New York.

Cheney, Ward and David Kincaid (1980), Numerical mathematics and computing, **Brooks/Cole Publishing Company**, California.

Love, Carl H. (1966), Abscissas and weights for Gaussian quadrature, **National Bureau of Standards**, Monograph 98.

McNamara, L. F. and J. E. Titheridge (1977), Numerical ionograms for comparing methods of N(h) analysis, **IPS Series R Reports** X-5.

Shinn, D. H. and H. A. Whale (1952), Group velocities and group heights from the magneto-ionic theory, **J. Atmos. Terr. Phys.**, 2, 85-105.

Shinn, D. H. (1955), Tables of group refractive index for the ordinary ray in the ionosphere, in **Physics of the Ionosphere**, pp. 402-406, Physical Society, London.

Titheridge, J. E. (1985), Ionogram analysis with the generalised program POLAN, World Data Center A for Solar-Terrestrial Physics, **Report UAG-93**.

Titheridge, J. E. (1988), The real height analysis of ionograms: A generalized formulation, **Radio Sci.**, 23, 831-849.

POSSIBILITY OF USING IONOSONDES FOR REGULAR OBSERVATION OF IRREGULARITIES OF ELECTRON DENSITY

P.F. Denisenko, N.V. Nastasyina, V.I. Vodolazkin
Institute of Physics, Rostov State University, RUSSIA

INTRODUCTION

Recently it was ascertained that high frequency radio waves, reflected from the ionosphere by vertical sounding, experience additional collisionless attenuation in the F-region. Two mechanisms were revealed which apply in the mid-latitude ionosphere. One of them, anomalous absorption, occurs only for ordinary (o) waves. The additional losses of energy arise near the level of reflection through the conversion of o-waves into slow extraordinary (z) waves through scatter by small-scale (1–10m) fluctuations of electron density n_e [1]. The second mechanism is connected with scattering of both ordinary and extraordinary (x) spherical waves by large scale (10^2–10^4m) irregularities in n_e [2]. As it turns out, the decrease in the energy of the rays reflected vertically is not compensated for by the energy of the waves undergoing small angle scatter [3].

Thus, the possibility arises of developing a diagnostic method for the determination of the parameters of various scale irregularities, according to the following scheme. The total weakening of o- and x-waves is decomposed into into two parts: collisional and collisionless. The parameters of the large-scale irregularities are found with the help of the collisionless attenuation of the x-waves. These results are used for the appraisal of the weakening of the o-waves in the scatter process, and for the definition of the anomalous absorption [1]. The realization of this scheme at present is limited by the lack of diagnostic methods for the detection of the irregularities making use of the collisionless attenuation of the x-waves. Only first steps have been made in this direction [3]. Therefore, at this stage information on the efficiency of the influence of irregularities on the process of collisionless attenuation can be obtained as follows.

By interpretation of measurements of radio wave absorption by method A1 in terms of an effective electron collision frequency v_e for the F-region, values were obtained which differed substantially from gas-kinetic (theoretical) values v_e^{gk} [4,5,6]. Owing to the scatter of x-waves $v_e^x > v_e^{gk}$ [6,7]. Since o-waves are involved in the scatter and experience anomalous absorption $v_e^o > v_e^x$ [6,7].

Thus, the differences $\Delta v_e^x = v_e^x - v_e^{gK}$, $\Delta v_e^o = v_e^o - v_e^{gK}$ and their height dependencies are an important indicator of the influence of irregularities on radio wave attenuation. Therefore, development of methods of determining detailed height dependencies are of great interest. In this paper it is shown that this problem is solvable, if special regularizing algorithms are used for the processing of modern ionosonde data.

THEORY

Determination of the $v_e(h)$ profiles by measuring frequency dependent radio wave absorption $L(h)$ is an improperly posed inverse problem [8]. It is shown below that by employing special regularization algorithms detailed information on height dependence of can be obtained. The modelling was preformed for the night-time conditions when we can disregard the influence of D- and E-regions.

The direct and inverse problems were solved with the help of linearizing the dependence of the index of absorption on v_e [8]. The absorption was represented in the form

$$L^{o,x}(f) = \frac{2}{c} \int_{h_o}^{h_r(f)} K^{o,x}(X,Y,\theta)\, v_e\, dh, \qquad (1)$$

where c is the speed of light in vacuo, h_o the height of the sounding transmitter, h_r the level of reflection of the waves, X, Y, θ standard parameters of magneto-ionic theory [9], and the expressions for the kernels $K^{o,x}(X,Y,\theta)$ are not shown since they are very unwieldy.

The height dependence of electron density $n_e(h)$, and consequently of the parameter X, was set by the expression

$$X = X_m \left[1 - \left(\frac{h_m - h}{H} \right)^2 \right], \qquad (2)$$

where $X_m = (f_m/f)^2$, f_m and h_m are the critical frequency and height of the maximum of the F-region, and H is the half thickness of the parabola. The dependence of $v_e(h)$ was set in the form

$$v_e^{o,x}(h) = v_e^{gK}(h) + v_2^{o,x} + v_3^{o,x} \frac{h_m - h}{H}, \qquad (3)$$

where $v_2^{o,x}$ and $v_3^{o,x}$ are constants, differing for the o- and x-waves. In the gas-kinetic model embodied in v_e^{gK}, only electron-ion collisions were taken into account. Therefore, [10]

$$v_e^{gK} = \frac{M_1 n_e}{T_e^{3/2}} = v_e^m = \frac{X}{X_m}, \quad v_e^m = \frac{M_2 f_m}{T_e^{3/2}}, \qquad (4)$$

where v_e^m is the collision frequency at the maximum of the F-region, M_1 and

95

M_2 are constants, and T_e is the electron temperature, assumed constant. Let us transform to a new integration variable x in (1), and take into account (3). Then the following is obtained:

$$L^{o,x}(f) = \frac{H}{c}\left\{ v_e^m A_1^{o,x}(f) + v_2^{o,x} A_2^{o,x}(f) + v_3^{o,x} A_3^{o,x}(f) \right\}, \qquad (5)$$

where $A_i^{o,x}(f)$ (i=1,2,3) are determined.

Let us introduce dimensionless variables

$$x_1 = v_e^m \frac{H}{c}, \quad x_2 = v_2^o \frac{H}{c}, \quad x_3 = v_3^o \frac{H}{c}, \quad x_4 = v_2^x \frac{H}{c}, \quad x_5 = v_3^x \frac{H}{c}.$$

Suppose the measurements on n frequencies $(f_1^o, f_2^o, \cdots f_n^o)$ for o-waves and on m frequencies $(f_1^x, f_2^x, \cdots f_m^x)$ for x-waves are given. For the set of $n + m > 5$ frequencies the expression (5) can be arranged in the form of a system of over-determined equations

$$y_1 = L^o(f_1^o) = x_1 A_1^o(f_1^o) + x_2 A_2^o(f_1^o) + x_3 A_3^o(f_1^o) + x_4 \cdot 0 + x_5 \cdot 0,$$
$$\vdots$$
$$y_n = L^o(f_n^o) = x_1 A_1^o(f_n^o) + x_2 A_2^o(f_n^o) + x_3 A_3^o(f_n^o) + x_4 \cdot 0 + x_5 \cdot 0,$$
$$y_{n+1} = L^x(f_{n+1}^x) = x_1 A_1^x(f_{n+1}^x) + x_2 \cdot 0 + x_3 \cdot 0 + x_4 A_2^x(f_{n+1}^x) + x_5 A_3^x(f_{n+1}^x),$$
$$\vdots$$
$$y_{n+m} = L^x(f_{n+m}^x) = x_1 A_1^x(f_{n+m}^x) + x_2 \cdot 0 + x_3 \cdot 0 + x_4 A_2^x(f_{n+m}^x) + x_5 A_3^x(f_{n+m}^x),$$

which can conveniently be formulated in matrix form

$$\vec{y} = \widehat{A}\vec{x}$$

where $\vec{y}$ is a vector of dimension $n + m$, $\vec{x}$ is a vector of dimension 5, and $\widehat{A}$ is a matrix of dimensions $(n + m) \times 5$. In practice, the exact vector $\vec{y}$ is not known and it is necessary to work with the approximate value $\vec{y}_\varepsilon = \vec{y} + \vec{\varepsilon}$ where $\vec{\varepsilon}$ is the vector of errors. Let us consider that all its components ε_i have a null mathematical expectation $\langle \varepsilon_i \rangle = 0$, identical variance $D(\varepsilon_i) = \langle \varepsilon_i^2 \rangle = \sigma^2$, and are un-correlated, $\langle \varepsilon_i \varepsilon_j \rangle = \sigma^2 \delta_{ij}$. As the inverse problem is incorrectly posed, to obtain a solution of the equation

$$\vec{y}_\varepsilon = \widehat{A}\vec{x} \qquad (6)$$

it is necessary to minimize the functional [11]

$$\Phi(h) = \left(\vec{y}_\varepsilon + \widehat{A}\vec{x}\right)^T \left(\vec{y}_\varepsilon + \widehat{A}\vec{x}\right) + \alpha \vec{x}^T \widehat{C}\vec{x}, \qquad (7)$$

where the symbol $\cdot^T$ means transposition. If $\alpha = 0$, then the solution obtained from (7) corresponds to the result of the root mean squares method [12]

$$\vec{x}_R = \widehat{B}^{-1}\widehat{A}^T \vec{y}_\varepsilon, \quad \widehat{B} = \widehat{A}^T \widehat{A}. \qquad (8)$$

If $\alpha > 0$, then the approximate solution takes the form

$$\vec{x}_\alpha = \left(\widehat{B} + \alpha \widehat{C}\right)^{-1}\widehat{A}^T \vec{y}_\varepsilon. \qquad (9)$$

As the determinant of matrix $\widehat{B}$ may be very small, errors in $\vec{x}_R$,

$$\delta\vec{x}_R = \widehat{B}^{-1}\widehat{A}^T \vec{\varepsilon}$$

may be extremely large. For the vector $\vec{x}_\alpha$, errors are considerably smaller,

$$\delta\vec{x}_\alpha = \left(\widehat{B} + \alpha \widehat{C}\right)^{-1}\widehat{A}^T \vec{\varepsilon}.$$

The approximate solution (9) was evaluated taking $\widehat{C} = \widehat{B}^{-1}$. The optimal value of the regularization parameter α was determined from the condition that the function

$$F(\alpha) = \frac{1}{2}\left(\frac{\|\widehat{A}\vec{x}_\alpha + \vec{y}_\varepsilon\|^2}{\|\widehat{A}\vec{x}_R + \vec{y}_\varepsilon\|^2} + \frac{\langle\|\delta\vec{x}_\alpha\|^2\rangle}{\langle\|\delta\vec{x}_R\|^2\rangle}\right),$$

where $\|\vec{z}\| = \sum_i z_i^2$, be a minimum.

THE RESULTS

Numerical calculations were carried out with the following values of the parameters: $n = m$, $x_1 = 0.19$, $x_2 = 1.25$, $x_3 = -0.5$, $x_4 = 0.63$, $x_5 = -0.25$, $f_m = 6$ MHz, $H = 75$ km. The components of the vector $\vec{\varepsilon}$ were set with the help of a random number generator for various values of the mean relative error $\eta = 2n\,\sigma/\sum_i y_i$.

As it turned out, without the application of regularization, the worst results were obtained for spherical wave scatter.[?] Therefore modelling was carried out for the magnetic equator. Various values of n (5,10,25) and various levels of of relative error η (1%,5%,10%) were used. It turned out that the solutions obtained from the formula (8) were not satisfactory even with $\eta = 1\%$ and $n = 25$. The approximate solutions (9) were acceptable with $\eta = 10\%$ and $n = 5$.

The advantage of the of the application of the regularization method are illustrated in the figure for the case where $\eta = 5\%$ and $n = 10$. As is shown in the graph, the root mean square method does not determine even the sign of the height gradient of collision frequency. The associated errors are so large that the confidence intervals for the o- and x-waves intersect. The application of the regularization method allows the errors in $v_e(h)$ to be substantially decreased, and the sign of height gradient to be correctly determined. The errors in the diagnostic [??] v_e do not exceed 20% for the o-wave and 30% for the x-wave.

CONCLUSIONS

The application of the regularization method makes possible a determination, which is stable with respect to random errors in absorption, of the height dependence of the effective electron collision frequencies. This height dependence is an indicator of the influence of irregularities on the additional attenuation of radio waves in the F-region of the ionosphere. Thus the possibility of continuous monitoring of ionospheric irregularity conditions with the assistance of an ionosonde has been demonstrated.
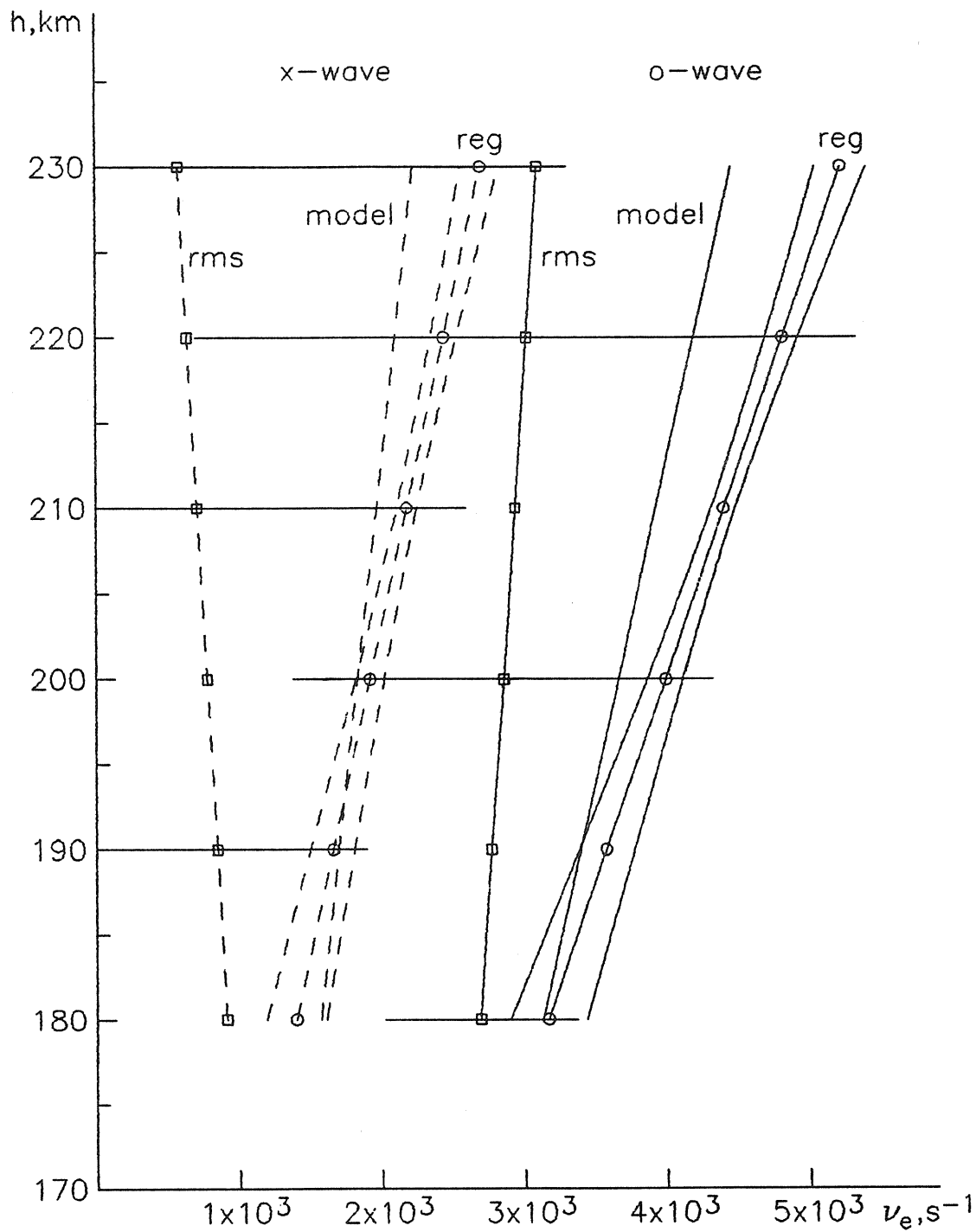
Fig. The results for modelling the inverse problem with $\eta = 5\%$, for the height interval in which reflection of the radio signal occurs. Full lines mark the results for the o-wave, and dashed lines the x-wave. The $v_e(h)$ profiles and their errors are marked by the symbol "rms" for root mean squares method, and by the symbol "reg" for the method of regularization.

REFERENCES

1. Vodolazkin V.I., Denisenko P.F., Faer YU.N., Determination of the parameters of small-scale natural electron concentration inhomogeneities in the F-region of the ionosphere from data on the anomalous absorption of the ordinary waves // Geomagnetizm i aeronomiya. 1989. T.29. N 2. p.329-332. (in Rus.)

2. Beley V.S. , Galushko V.G., Vodolazkin V.I., Denisenko P.F., Kiyanovsky M.P., Sotsky V.V., Faer YU.N., Iampolsky YU.M. Collisionless losses from ionospheric propagation of decametre radio waves // Geomagnetizm i aeronomiya. 1990. T.30. N 6. p.979-985. (in Rus.)

3. Zabotin N.A., Bronin A.G. Transfer of radiation energy through the turbulent magnetoplasma. Spatio-temporal Analysis for Resolving Plasma Turbulence. Aussois, France. 31 January - 5 February 1993. p.59-62.

4. Setty C.S.G.K. Electron collision frequency in ionospheric layers // Indian J. Radio Space Phys. 1972. VI. p.38-51.

5. Newbery S.M., Dyson P.L., Singh A. An inversion procedure for obtaining collision frequency profiles from swept-frequency absorption measurements // J. Atmos. Terr. Phys. 1989. V.51. N 5. p.425-432.

6. Vodolazkin V.I., Denisenko P.F., Rjanitsin V.P., Sotsky V.V., Faer YU.N. Absorption of radio waves and effective electron collision frequency in the ionosphere // Geomagnetizm i aeronomiya. 1993. T.33. N 3. p.74-83. (in Rus.)

7. Setty C.S.G.K., Jain A.R., Vyawahare M.K. Collision frequency of electrons in the F region // Canadian J. Phys. 1970. V.48. p.653-658.

8. Denisenko P.F., Sotsky V.V. Peculiarities of inverse problems vertical sounding of ionosphere (survey) // Izvestiya SKNC VS / Proceeding of NCSC HS .Natural Sciences. 1987. N 2. p.59-71. (in Rus.)

9. Ratcliffe J.A. The magneto-ionic theory and its applications to the ionosphere. Cambridge University Press: London 1959.

10. Ginsburg V.L. Spreading of electro-magnetic waves in plasma. M.,"Nauka/Science" 1967. (in Rus.)

11. Tickhonov A.N., Arsenin V.I. Methods for solution of uncorrect problems M., "Nauka/Science" 1979. (in Rus.)

12. Derek J. Hudson. Statistics Lectures on Elementary Statistics and Probability. Publisher?? Geneva, 1964.

ESTIMATION OF PROPAGATION PARAMETERS OF NON-UNIFORM IONOSPHERIC DISTURBANCES FROM HF PHASE MEASUREMENTS

Weixing Wan and Jun Li
Wuhan Ionospheric Observatory
Wuhan Institute of Physics
the Chinese Academy of Sciences
Wuhan 430071, P.R. China

Abstract:

This paper develops a new technique used to estimate the phase velocities of non-uniform ionospheric gravity waves from single station observation of both HF Doppler frequency shifts and angles of arrival. Based on the time-frequency analysis, we first derive the observation equations which reveal the relationship between the observables and the propagation parameters of the ionospheric disturbances. Then, the detailed calculation procedure of the new method is proposed to separate the individual gravity waves from the non-uniform disturbances, and to estimate the phase velocities and azimuth angles of horizontal propagation of each separated gravity wave packets. As an example, the new method is used to the data analysis of Digisonde drift measurements. The results show that the suggested technique is useful in the study of the propagation, evolution and dispersion of the causative gravity waves.

Introduction

The ground-based phase measurements of ionospheric HF echoes, known as the observation of the Doppler frequency shifts and the angles of arrival, have been widely used in the experimental study of large scale ionospheric disturbances such as gravity waves. It is believed that the simultaneous observation of both Doppler shifts and arrival angles, even at a single station, can be used to determine the horizontal propagation parameters of ionospheric gravity waves. Accordingly, in the data analysis, two kinds of methods have been proposed. The first may be called the time domain method[1,2]. In this analysis the measured Doppler shift and two arrival angles at any certain time t are directly used to estimate the horizontal phase velocity, $V_{ph}(t)$, and the azimuth angle, $\sigma(t)$, of the horizontal propagation of the gravity waves. The second method is the frequency domain method[3]. In this analysis the time sequences of the observables are transformed into their frequency spectra, then for certain frequency the spectral components are used to estimate the phase velocity, $V_{ph}(\Omega)$, and $\sigma(\Omega)$ as functions of frequency Ω.

It is easy to confirm that the above two methods are equivalent when there exists only one gravity wave, which is called the uniform ionospheric disturbance. While in the case of non-uniform ionospheric disturbances, the results of the two methods may be quite different. We assume that the non-uniform ionospheric disturbances consist of several individual gravity waves, so the time domain method is suitable for the case that the individual gravity waves are not overlapped each other in time domain. On the other hand, the frequency domain method is useable if the gravity waves are not overlapped each other in frequency domain. While the gravity waves contained in the non-uniform disturbances are overlapped in both time and frequency domain, as is the real case in most time, the above two methods may both lead to mistakes.

The purpose of the present work is to develop a new technique to separate the individual gravity waves from non-uniform ionospheric disturbances, and to estimate the phase velocities and azimuth angles of horizontal propagation of each separated waves. Unlike both the time domain method and the frequency domain method, the present method is really a time-frequency method based on the theory of time-frequency analysis of Signal Processing. In the following part of this paper, we first derive the observation equations which connect the observables and the propagation parameters of non-uniform ionospheric disturbances. Then we give the detailed analysis procedure, as well as the calculated results of the new method when applied in the data analysis of the Digisonde drift measurement. Finally a brief summary for this work is given.

Method

We first introduce the normal velocity V, of the radio reflection surface (an iso-electron density surface in the ionosphere). The amplitude, V, of V, and the horizontal components, n_x and n_y, of the unit vector along V are defined and connected with the HF Doppler frequency shifts, $\delta\omega$, and the angles of arrival (indicated by the deviation, δk_x and δk_y, between the wave number vectors of the received and transmitted radio waves) as[4]

$$V = -\frac{\partial N/\partial t}{|\nabla N|} = -\frac{c}{2\omega}\delta\omega \qquad n_x = \frac{\partial N/\partial x}{|\nabla N|} = -\frac{c}{2\omega}\delta\kappa_x \qquad n_y = \frac{\partial N/\partial y}{|\nabla N|} = -\frac{c}{2\omega}\delta\kappa \qquad (1)$$

where N is the electron density on the reflection surface, ω is the radio frequency.

Here it is assumed that the reflection point does not itself move along the reflection surface. This requires this distance moved to be much less than the smaller horizontal structure present. The problem of analysis when this assumption is not valid has been dealt with by From et al (1988). Unfortunately the requirement for this assumption means that the ionosphere has to be rather quiet. It can be recognised by the saw-tooth appearance of V, as a function of time, and is clearly evident in figure 1. Then only the dominant features of the ionospheric disturbances can be deduced by this method.

We assume that, (1) the non-uniform ionospheric disturbances are composed of many individual gravity wave packets; (2) the time-frequency spectra of each individual gravity wave packets are not overlapped each other in the time-frequency plane (t,Ω), that is, each wave packet occupies a certain sub-region. These assumptions make possible for us to adopt the following model to express the time-dependent spectrum, $N(\Omega, K_x, K_y, t)$, of the electron density fluctuation,

$$N\left(\Omega, K_x, K_y, t\right) = N(\Omega, t)\delta[K_x - K_x(\Omega, t)]\delta[K_y - K_y(\Omega, t)] \qquad (2)$$

where the time-frequency functions $K_x(\Omega, t)$ and $K_y(\Omega, t)$ indicate the time-dependent dispersion relations, and $N(\Omega, t)$ is the time-dependent frequency spectrum of electron density in the observation point which is assumed to be the original point of our coordinate system. It is obvious that the model of Eq.(2) satisfy the definition of $N(\Omega, t)$ as,

$$N(\Omega, t) = \int N\left(\Omega, K_x, K_y, t\right) dK_x, dK_y \qquad (3)$$

We assume that the ionospheric disturbances are so weak that the departures of the reflecting point from overhead of the station is negligible. Then, by using equations.(1), (2) and ignoring a factor $1/|\nabla N|$ which is approximately a constant, $N(\Omega, t)$ can be used to express the time-dependent frequency spectra of $V(t)$, $n_x(t)$ and $n_y(t)$,

$$V(\Omega, t) = i\Omega N(\Omega, t) = -iK_x(\Omega, t)N(\Omega, t), n_y\Omega, t) = -iK_y(\Omega, t)N(\Omega, t) \qquad (4)$$

or equivalently, the time-dependent auto spectrum, $\Phi_{NN}(\Omega, t) = N(\Omega, t)N^*(\Omega, t)$, can be used to express the time-dependent auto and cross spectra of $V(t)$, $n_x(t)$ and $n_y(t)$,

$$\begin{cases} \Phi_{vv}(\Omega,t) = V(\Omega,t) = \Omega^2 \Phi_{NN}(\Omega,t) \\[4pt] \Phi_{xx}(\Omega,t) = n_x(\Omega,t)n_x^*(\Omega,t) = K_x^2(\Omega,t)\Phi_{NN}(\Omega,t) \\[4pt] \Phi_{yy}(\Omega,t) = n_y(\Omega,t)n_y^*(\Omega,t) = K_y^2(\Omega,t)\Phi_{NN}(\Omega,t) \\[4pt] \Phi_{vx}(\Omega,t) = V(\Omega,t)n_x^*(\Omega,t) = -\Omega K_x(\Omega,t)\Phi_{NN}(\Omega,t) \\[4pt] \Phi_{vy}(\Omega,t) = V(\Omega,t)n_y^*(\Omega,t) == \Omega K_y(\Omega,t)\Phi_{NN}(\Omega,t) \\[4pt] \Phi_{xy}(\Omega,t) = n_x(\Omega,t)n_y^*(\Omega,t) = K_x(\Omega,t)K_y(\Omega,t)\Phi_{NN}(\Omega,t) \end{cases} \tag{5}$$

In the above equations (Equations.(4) and (5)), the terms on the left hand side, i.e, the time-dependent frequency spectra, $V(\Omega)$, $n_x(\Omega)$ and $n_y(\Omega)$, and the auto and cross spectra, $\Phi_{vv}(\Omega,t)$, $\Phi_{xx}(\Omega,t\Phi_{yy}(\Omega,t)$, $\Phi_{vx}(\Omega,t)$, $\Phi_{vy}(\Omega,t)$ and $\Phi_{xy}(\Omega,t)$, may be experimentally obtained by the time frequency analysis (such as wavelet analysis and the short time Fourier analysis). On the right hand side, the time-frequency functions, $K_x(\Omega,t)$, $K_y(\Omega,t)$, $\Phi_{NN}(\Omega,t)$ and $N(\Omega,t)$ are all the parameters to be found. So these equations are called the observation equations.

In the present work the two-dimensional distribution of the auto spectrum $\Phi_{NN}(\Omega,t)$, or the frequency spectrum $N(\Omega,t)$, is used mainly to separate the individual gravity waves from the non-uniform ionospheric disturbances. To do so, we divide the whole time-frequency plane into several sub-regions so that each sub-region contains only a single peak of $\Phi_{NN}(\Omega,t)$. We suppose that any peak of $\Phi_{NN}(\Omega,t)$ is corresponding to only one individual gravity wave packet. Therefore any of the sub-regions is mainly occupied by one individual wave packet, this implies that the individual gravity waves are separated in (Ω,t) plane from the non-uniform ionospheric disturbances.

Furthermore, limited to any certain sub-region mentioned above, $K_x(\Omega,t)$ and $K_y(\Omega,t)$ indicate the time-dependent dispersion of a individual gravity wave packet, and can be used to determine the phase velocity $V_{ph}(\Omega,t)$ and azimuth $\sigma(\Omega,t)$ of the wave packet as functions of both frequency and time.

For a certain individual gravity wave packet, the determined $K_x(\Omega,t)$ and $K_y(\Omega,t)$, or $V_{ph}(\Omega,t)$ and $\sigma(\Omega,t)$, can be directly used to study both the frequency dispersion and temporal evolution of the wave packet. And, if necessary, we can obtain uniform phase

$$V_{ph}(\Omega,t) = \frac{\Omega}{\sqrt{K_x^2(\Omega,t)+K_y^2(\Omega,t)}} \ , \ \tan\sigma(\Omega,y) = \frac{K_x(\Omega,t)}{K_y(\Omega,t)} \tag{6}$$

velocity and azimuth angle of the wave packet from the mean values of Ω, $K_x(\Omega,t)$ and $K_y(\Omega,t)$ averaged in the sub-region with $\Phi_{NN}(\Omega,t)$ as the power. In this paper, as an example, we take the average of Ω, $K_x(\Omega,t)$ and $K_y(\Omega,t)$ in only the frequency domain to yield the temporal variation, $\Omega(t)$, $K_x(t)$ and $K_y(t)$,

$$\Omega(t) = \frac{\int \Omega\Phi_{NN}(\Omega,t)d\Omega}{\int \Phi_{NN}(\Omega,t)d\Omega}, K_x(t) = \frac{\int K_x(\Omega,t)\Phi_{NN}(\Omega,y)d\Omega}{\int \Phi_{NN}(\Omega,t)d\Omega}, K_y(t) \frac{\int K_y(\Omega,t)\Phi_{NN}(\Omega,t)d\Omega}{\int \Phi_{NN}(\Omega,t)d\Omega} \tag{7}$$

The integrations are carried in the frequency region contains only one spectral peak. Then similar to Eq.(6), the quantities $\Omega(t)$, $K_x(t)$ and $K_y(t)$, are used to determine the phase velocity $V_{ph}(t)$ and azimuth $\Omega(t)$ as functions of time,

$$V_{ph}(t) = \frac{\Omega}{\sqrt{K_x^2(t) + K_y^2(t)}}, \sigma(t) = \frac{K_x(t)}{K_y(t)} \tag{8}$$

Examples

In order to exhibit the usage of the new method, we treated the Digisonde drift data observed at Millstone Hill Station. The procedure used and the results obtained are as follows.

First, we draw the Doppler frequency shifts and angles of arrival from the row data of drift measurement by the regression method[5], and then calculate the time sequences $V(t)$, $n_x(t)$ and $n_y(t)$ by using equation.(1).
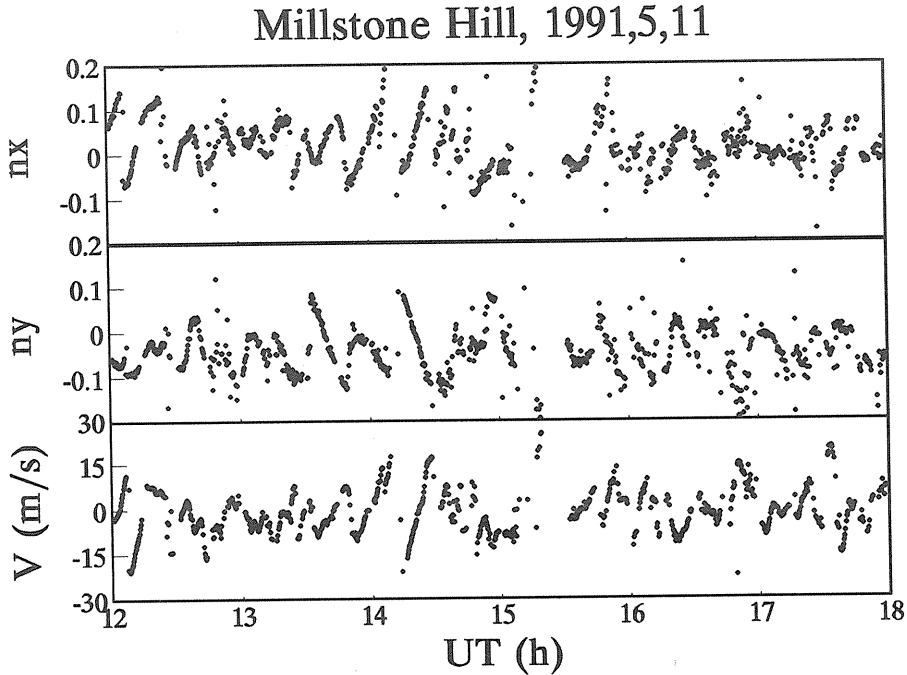

Figure 1. The temporal variation of $V(t)$, $n_x(t)$ and $n_y(t)$ deduced from the Digisonde observation of Doppler shifts and arrival angles.

Fig.1 is a segment of the curves of $V(t)$, $n_x(t)$ and $n_y(t)$ obtained from the Digisonde drift measurements. It can be seen from this figure that the fluctuations of the curves are not very sinusoidal as in the case of a single wave, so the disturbances may be non-uniform and consist of several individual gravity waves.

Second, the time sequences $V(t)$, $n_x(t)$ and $n_y(t)$ are used to estimate the time-dependent auto and cross spectra, $\Phi_{vv}(\Omega,t)$, $\Phi_{xx}(\Omega,t)$, $\Phi_{yy}(\Omega,t)$, $\Phi_{vx}(\Omega,t)$, $\Phi_{vy}(\Omega,t)$ and $\Phi_{xy}(\Omega,t)$, by the dynamic spectrum analysis (a kind of time-frequency analysis developed from the short time Fourier transformation). In the practice calculation, these spectra are estimated by using the multi-channel maximum entropy method in a 2-hour time window advanced in 6-minute time steps.

Then by using the observation equations (Equation.(5)) we calculate the spectrum $\Phi_{NN}(\Omega,t)$ and the dispersion relations $K_x(\Omega,t)$ and $K_y(\Omega,t)$ from the auto and cross spectra estimated in the previous procedure. The contours of $\Phi_{NN}(\Omega,t)$ corresponding to the data of Fig.1 is shown in Fig.2. Then sub-regions corresponding to individual gravity wave packets are obtained on the (Ω,t) plane according to the peak distribution of $\Phi_{NN}(\Omega,t)$. In these sub-regions $V_{ph}(\Omega,t)$ and $\sigma(\Omega,t)$ are calculated by using Equation.(6). The boundary of each sub-regions and the vector phase velocity (formed by both $V_{ph}(\Omega,t)$ and $\sigma(\Omega,t)$) are also overlaid in Fig.2. From this illustration it is clear that the estimated phase velocities and azimuth angles

are quite similar in any certain sub-region, while those in different sub-regions may be much different. Again this demonstrates that the sub-regions are mainly occupied by only one individual wave packet.

Finally, by using Equations.(6) and (7), we take the frequency average, $\Omega(t)$, $K_x(t)$ and $K_y(t)$, and then find the phase velocity $V_{ph}(t)$ and azimuth $\sigma(t)$ of each individual gravity waves. As shown in Fig.3, both the phase velocity $V_{ph}(t)$ and azimuth $\Omega(t)$, as well as the average frequency $\sigma(t)$, are all continuously varied in the time domain. This makes possible to study in detail the temporal evolution of the individual gravity wave packets.

Millstone Hill, 1991,5,11
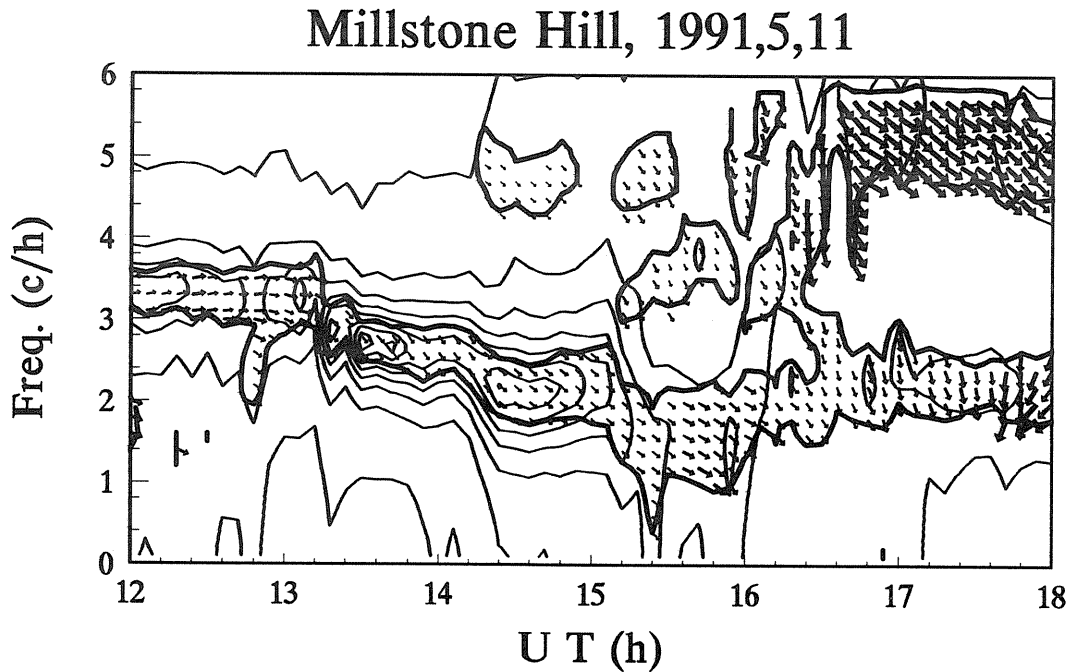

Figure 2. The estimate spectral contours (fine lines), the wave packets boundary (bold lines) and the Phase velocities (arrows).
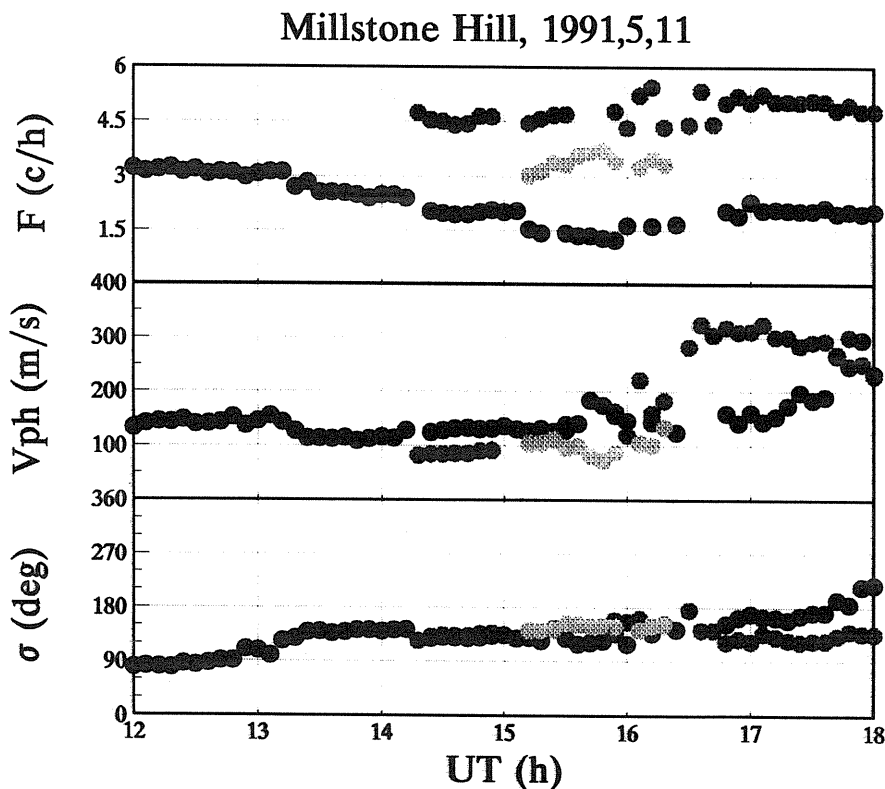
Millstone Hill, 1991,5,11

Figure 3. The temporal evolution of frequency, phase velocity and azimuth of different gravity wave packets.

Summary

This paper proposes a new technique to separate individual gravity wave packets from non-uniform ionospheric disturbances, and estimate the phase velocities and the azimuth angles of the horizontal propagation of the separated wave, from single station observation of both HF Doppler frequency shifts and angles of arrival. As the key technique and the theoretical base of the new method, the time-frequency analysis makes it possible to separate each individual gravity waves in the time-frequency plane, and to estimate precisely the propagation parameters of the separated gravity waves. As an example, the new method is used to the data analysis of Digisonde drift measurements. The experimental results shows that the suggested technique is useful in the experiment study of both the propagation and the evolution of ionospheric gravity wave disturbances.

Acknowledgment

References

[1] W. Pfister, **J. atmos. terr. Phys.**, 33, 999, 1971.

[2] P. L. Dyson, **J. atmos. terr. Phys.**, 37, 1151, 1975.

[3] W. R. From, E. M. Sedler and J. D. Whitehead, **J. atmos. terr. Phys.**, 50, 153, 1988.

[4] W. Wan and J. Li, **J. atmos. terr. Phys.**, 55, 47, 1993.

[5] W. Wan, J. Li, Z. M. Zhang and B. W. Renisch, "Study of ionospheric gravity wave disturbances from drift measurement of a digisonde", **Chinese J. Geophys.**, 36, (in press), 1993.

VERTICAL-INCIDENCE SOUNDING DATABASE AND ITS PRODUCTS

T. L. Gulyaeva

Institute of Terrestrial Magnetism, Ionosphere and Radio Wave Propagation, Academy of Sciences,142092, Troitsk, Moscow Region, Russia

Abstract

Long-term VI sounding observations present a unique database suitable for determining quiet and disturbed ionospheric conditions. Based on proposed criteria, local and regional catalogues of ionospherically disturbed and quiet days are developed from an analysis of vertical-incidence sounding data over the European area during 1964-1990. Comparison of ionospherically quiet days with geomagnetic quiet periods for 1976-1988 shows coincidence for no more than 30% of the days considered. The conventional practice of defining the state of the ionosphere by comparison with geomagnetic conditions should be replaced by specification of the proper ionospheric quiet and disturbed periods.

Satellite and rocket borne observations of the ionosphere yield a mix of quiet and disturbed ionospheric parameters. Similarly the short-term series of incoherent scatter observations don't allow results to be sorted by their degree of disturbance. At the same time there are long-term ground-based vertical-incidence sounding observations which provide a unique opportunity to separate the above conditions. Needless to say the development of ionospheric models requires clear specification of quiet conditions, with the degree of disturbance quantified by a proper system of indices.

At the URSI-COST238(PRIME) Workshop on Verification of Ionospheric Models and maps at Roquetes, Spain, May 1992, there were no publications, reports or presentations on criteria for defining quiet days in the ionosphere [Hanbaba, 1993]. Nevertheless there is an urgent need to clear up this problem since most available models and maps are built up just for quiet conditions. Specification of conditions in the ionosphere is often made by reference to geomagnetic quiet or disturbed conditions. To what extent are available iono-spheric models and maps valid in the real ionosphere? How should ionospheric conditions be ranked to show the degree of disturbance and quietness? Which steps should be taken first in analysis of the ionospheric data? These and other items need to be resolved immediately.

In response to that urgent need, work projects have been planned and cataloguing of ionospherically quiet and disturbed conditions has begun. During the year which has passed since the Roquetes meeting, criteria were developed and the first catalogues produced for ionospheric quiet and disturbed days [Cooper et al, 1993]. A general statistical approach for determining the weighted skewness of the histogram was introduced, to obtain the occurrence frequency of deviations of the current values of a specified parameter from its median or other background level [Gulyaeva, 1993a,b]. A mean-weighted measure of the histogram distortion, with an increasing contribution of the more disturbed sections of the histogram, serves as a measure of the disturbance of the particular parameter.

We have applied the proposed criteria to the long-term database of the VI sounding ionospheric observations currently available on optical disks [Allen, 1991; Hanbaba, 1993], to produce a second generation data base of ionosphere disturbance indices. As a result we obtained hourly, semi-diurnal, diurnal, monthly and annual indices of the negative Dm- and positive Dm+ ionospheric disturbances. Each annual collection of results, for each ionospheric station, includes 10 files originating from a set of 12 monthly tables of ionospheric characteristics in URSI format (routinely presenting parameter MUF3000F2, re-evaluated from two initial tables of critical frequency foF2 and the height equivalent M3000F2; or missing the latter the initial table of foF2 is used). From the initial tables the hourly values of indices of deviations from the monthly median are calculated. Note that the weights are increased when descriptive or

qualifying letters are provided with the numerical hourly value, and missed observations are taken into account as disturbed conditions. So the hourly disturbance indices of the negative and positive deviations, Dm- and Dm+, are obtained. Similarly the histograms of frequency of occurrence of different hourly Dm- and Dm+ indices are analysed with various temporal filters (semi-diurnal to annual scales).

TABLE 1 Part of the catalogue of 5 ionospherically disturbed days (D1 = the most disturbed day) and 10 quiet days (Q01 = the quietest day) at Moscow (MO) and Tokyo-Kokobunji (TK) during the 3d VIM period, for 4 seasons of 1988-1992.

STYRMN	D1	D2	D3	D4	D5	Q10	Q09	Q08	Q07	Q06	Q05	Q04	Q03	Q02	Q01	
MO9111	09	08	10	22	02	15	03	19	29	21	23	25	17	26	12	FALL
MO9112	18	30	05	24	23	21	22	12=	15	10	20	17	31	06	19	WNT
MO9203	29	01	30	05	25	06	07=	12	02	16	17	03	08	10	15	SPR
MO8807	11	22	23	27	21	20	07=	28	14	17=	26	16	04	15	24	SMR
TK9111	09	02	19	05	24	22	03	28	29	16	10	14	04	07	11	FALL
TK9112	1	05	23	28	30	15	10	11	31	12	07	26	09	03	22	WNT
TK9203	18	07	30	06	29	26	01	04	11	02	22	10	27	05	19	SPR
TK8807	01=	02	20	11	04	05	08	15	29	31	24	18	27	13	30	SMR

Specific criteria for obtaining a catalogue of quiet and disturbed days are proposed [Gulyaeva, 1993c]. Three signatures of disturbance are taken into account (diurnal indices Dm- for negative deviations from the median, diurnal indices Dm+ for positive ionospheric disturbances with ionisation input into the F region, and their range Rm for each day of the month). These indices are analogous to the well known three types of auroral electrojet indices - the lower hourly value Al, the upper value Au, and the range AE-index [Mayaud, 1980]. To define 5 ionospheric disturbed days and 10 quiet days per month, similar to those obtained from the planetary geomagnetic Kp index, the diurnal values of Dm-, Dm+ and Rm are ranked in decreasing order and the sum of current ranks is calculated for each day of the month. The most disturbed day is identified by the greatest sum of current ranks (as used to judge sport competitions), and the quietest day has the least sum of current ranks. An example of these results is presented in Table 1 for the third VIM period [Reinisch, 1993].

Ranking by 5 disturbed days and 10 quiet days is carried out independent of the mean monthly or annual level of disturbance within the solar cycle. But those important factors are crucial for a study of the consistency of parameters for different geophysical fields. Evidence of different levels of disturbance at Tokyo (Kokobunji) and Moscow for the third VIM period (see Table 1) is presented in Figure 1, where histograms show the frequency of occurrence of the hourly indices Dm- and Dm+ for 4 reasons. For convenience of computer analysis we can denote every day as quiet (0) or disturbed (1), separating these daily Dm indices with floating thresholds equal to the monthly index of Dmm- or Dmm+ provided with Figure 2. This is an example of a Bartels diagram for ionospheric semi-diurnal negative and positive disturbances, from the monthly mean levels at Moscow during 1991, which could be compared with a simple voting procedure with relevant diagrams for the geomagnetic indices.

Further selection of really quiet days is made within one standard deviation from Dm=1 (the least value of Dm by definition) among those days when diurnal Dm- and Dm+ do not exceed the monthly threshold. The results of such a selection of Q and D days (0 or 1) for each month of 1991 at Moscow are presented in
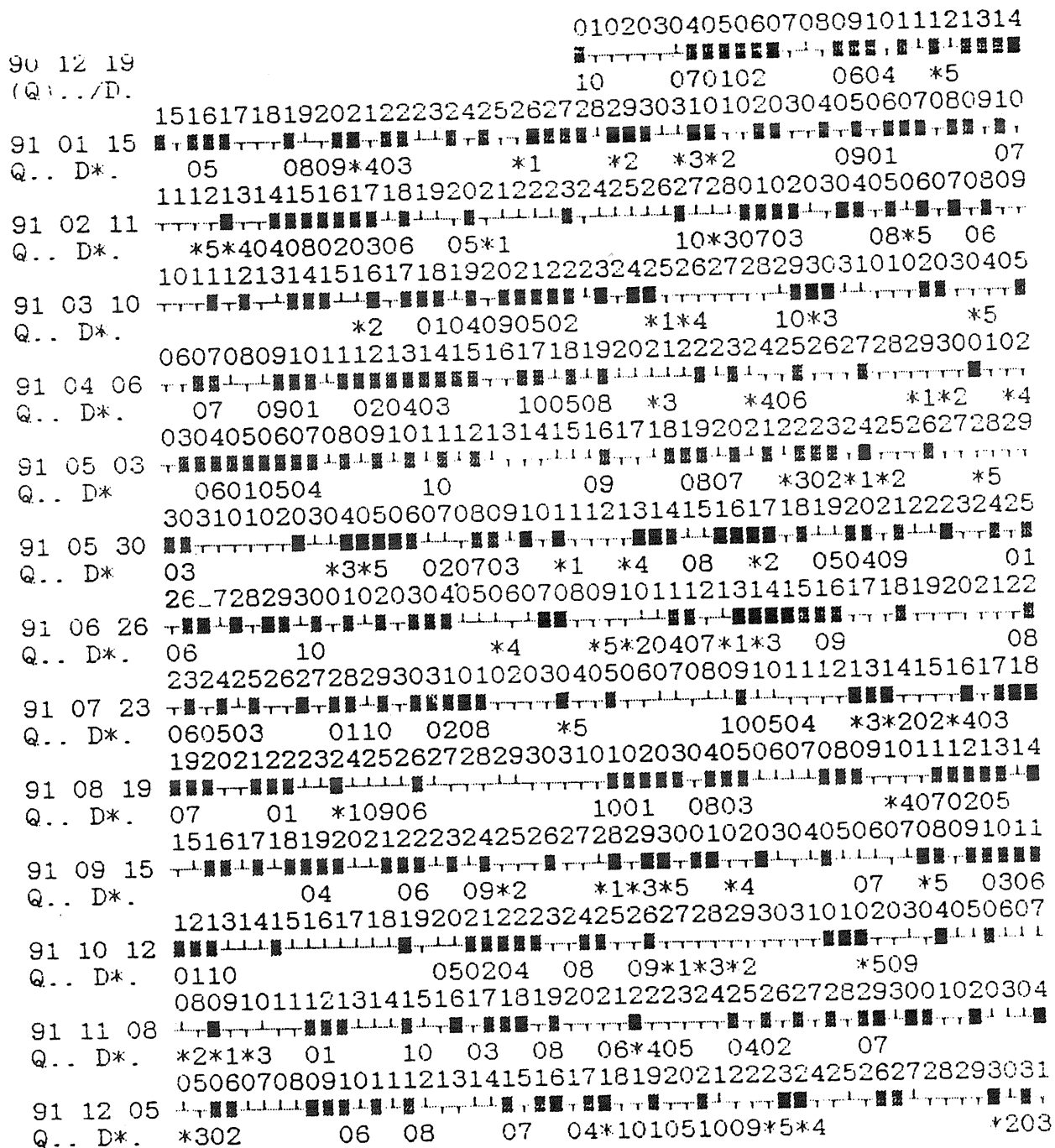
TABLE 2. Disturbed (1) and quiet (0) days in the ionosphere at Moscow during 1991.

STYRMN _	2 _ 4 _ 6 _ 8 _ 0 _ 2 _ 4 _ 6 _ 8 _ 0 _ 2 _ 4 _ 6 _ 8 _ 0 _	Q-DAYS
MO9101 1	1 1 1 0 0 1 1 1 1 1 1 1 1 1 1 1 1 1 1 1 0 1 1 1 1 1 1 1 1 1	3
MO9102 1	1 1 1 1 0 1 1 1 1 1 1 1 1 1 1 1 1 1 1 1 1 1 1 1 1 1 1	1
MO9103 0	0 1 1 0 1 1 1 1 1 1 0 1 0 1 1 1 1 1 1 1 1 1 1 1 1 1 1 1 1 1	5
MO9104 1	1 1 1 1 1 0 1 1 0 1 1 0 1 0 1 1 1 1 1 1 1 1 1 0 1 1 1 1 1	5
MO9105 1	1 1 0 0 1 0 1 1 1 1 1 1 1 1 1 1 1 1 1 1 1 0 1 1 1 1 1 1 0 1	5
MO9106 1	1 1 1 1 1 1 1 1 1 1 1 1 1 1 1 1 1 1 1 0 1 1 1 1 0 0 1 1 1 1	3
MO9107 1	1 1 1 1 1 1 1 1 1 1 1 1 1 1 0 1 1 1 1 1 1 1 1 1 1 0 1 1 0	3
MO9108 1	1 1 1 1 1 1 1 1 1 1 1 1 1 1 0 1 1 1 1 0 1 1 1 1 1 1 1 1 1	2
MO9109 1	0 1 1 0 1 1 1 1 1 1 0 0 1 1 1 1 1 0 1 1 1 1 1 1 1 1 1 1	5
MO9110 1	1 1 1 1 1 1 1 1 0 0 0 1 1 1 1 1 1 1 1 1 0 1 1 1 1 1 1 1 1	4
MO9111 1	1 1 1 1 1 1 1 1 1 1 0 1 1 1 1 1 1 1 1 1 1 1 1 1 1 1 0 1	2
MO9112 1	1 1 1 1 1 1 1 1 1 1 1 1 1 1 1 1 1 1 1 1 1 1 1 1 1 1 1 1 1 1	0

11.1991   FALL   HRS   12.1991   WNT

150

50

03.1992   SPR   07.1988   SMR

200

100

-6 -4 -2 0 2 4 6   -6 -4 -2 0 2 4 Dm-+

Fig. 1. Monthly histograms of frequency of occurrence of negative Dm- and positive Dm+ hourly ionosphere disturbance indices at Moscow (solid line) and Tokyo-Kokobunji (circles) for four seasons of 3d VIM period. The number of quiet days are greater at Moscow than at Tokyo during summer 1988, and vice versa at other periods.

010203040506070809101112131314

90 12 19
(Q../D.)
```
                              10      070102       0604      *5
   1516171819202122232425262728293031010203040506070809010
91 01 15
Q.. D*.    05    0809*403         *1     *2    *3*2           0901        07
   111213141516171819202122232425262728010203040506070809
91 02 11
Q.. D*.    *5*40408020306   05*1                10*30703        08*5    06
   1011121314151617181920212223242526272829303110102030405
91 03 10
Q.. D*.           *2   0104090502        *1*4        10*3          *5
   060708091011121314151617181920212223242526272829300102
91 04 06
Q.. D*.    07   0901    020403         100508   *3      *406        *1*2   *4
   030405060708091011121314151617181920212223242526272829
91 05 03
Q.. D*     06010504         10           09      0807   *302*1*2       *5
   303101020304050607080910111213141516171819202122232425
91 05 30
Q.. D*    03         *3*5    020703   *1   *4   08   *2   050409          01
   26_7282930010203040506070809101112131415161718192021 22
91 06 26
Q.. D*.    06        10             *4    *5*20407*1*3   09               08
   232425262728293031010203040506070809101112131415161718
91 07 23
Q.. D*.    060503      0110    0208      *5          100504   *3*202*403
   1920212223242526272829303101020304050607080910111213 14
91 08 19
Q.. D*.    07     01   *10906          1001    0803           *4070205
   151617181920212223242526272829300102030405060708091011
91 09 15
Q.. D*.         04    06    09*2     *1*3*5    *4          07    *5    0306
   121314151617181920212223242526272829303101020304050607
91 10 12
Q.. D*.    0110           050204   08    09*1*3*2          *509
   0809101112131415161718192021222324252627282930010203 04
91 11 08
Q.. D*.    *2*1*3   01       10    03    08    06*405    0402        07
   050607080910111213141516171819202122232425262728293031
91 12 05
Q.. D*.    *302       06    08      07   04*101051009*5*4              *203
```

Fig. 2. A mixed Bartels diagram for MUF3000F2 during 1991 at Moscow, with the date of the calendar month above each pixel. The 5 most disturbed days *1,...,*5 and the 10 most quiet days 01,...,10 are marked under the pixels. The thresholds used are:

MN:	01	02	03	04	05	06	07	08	09	10	11	12	YR
L3MO91 Dm-	19	21	25	25	25	27	26	24	21	30	24	20	239
L3MO91 Dm+	20	18	20	19	21	23	20	23	20	24	25	21	211

TABLE 3 Ionospherically quiet days coincident with part of the 7-day geomagnetically quiet periods during 1976-1988.

Year	Month	(a) Gulyaeva's Catalogue	(b) Stanislawska's Catalogue.
1976	May		12,18
	Jul.	19,20	18,19
	Aug	11,12,19	12,13,15,18,19
	Oct	21	21
	Nov	4	5,6
1977	Jun.	7	4
	Nov	21,22,23	19
1978	Jul	29,31	
	Dec		6
1980	Jan	18,23	
	Mar.	11,13,15,16,17	8,11,13,15,17,18
1985	Jun.		13,14
	Aug		3,4,5,7,9
1986	Jan	14	11,12,14,19
	May	12,13,14,15	9,10,11,12,13,14,15
	Jul	6,7,12,13,20	4,5,12
	Dec	9 3,4,7,8,9	
1987	Apr		29,30
	May	15,20,21	1,2,4,5,6; 20
	Dec	30	27,28,30
1988	Jan	28,29	28,29
	Mar		20,22,23,24
	Sep	10	4,10
	Nov	19	19,22,23,24,25

Table 2, as part of a local catalogue of ionospheric disturbed and quiet days. Note that while 0 means a really quiet day, 1 implies both moderate and heavy disturbances. To distinguish further the degree of disturbance one should look at the hourly Dm- and Dm+ indices. Similar results have been obtained using data from European and other world-wide ionospheric stations, comprising so far about 10% of the available planetary archive of VI sounding data.

The present average European Catalogue of ionospheric disturbed (1) and quiet (0) days is compared in Table 3 with an Ionospheric Catalogue for the same area [Stanislawska, 1993] and with the geomagnetic quiet 7-days periods [from Joselyn, 1990]. We have 39 Q-days by our criteria, 71 Q-days by Stanislawska, giving 21 common Q-days in the two ionospheric Catalogues, against 225 geomagnetic quiet days for the

same periods. Thus, only 10 to 30% of quiet days are common in the ionosphere and the geomagnetic field simultaneously. This means that the conventional rules for analysing ionospheric data based on available geomagnetic indices require re-examination. We need criteria and catalogues of ionospheric quiet, moderately disturbed and heavily disturbed conditions, to permit analysis of ionospheric data based on the ionosphere disturbance and quietness. To speed up and broaden such studies we have published the main subprogram for producing hourly, monthly and annual ionospheric indices [Gulyaeva, 1993b]. Exchange of results from such analyses through the relevant projects of URSI and other international bodies would stimulate progress in ionosphere research.

Acknowledgments

References

Allen J. (1991), Selected geomagnetic and other solar-terrestrial physics data of NOAA and NASA, **CD-ROM**, WDC-A-STP, Boulder, Co., USA,

Cooper J., K. K.Barbatsi, T. L. Gulyaeva, G. A. Moraitis, T. A. Th. Spoelstra, I. Stanislawska, S. M. Radicella, M. -L. Zhang (1993). PRIME Catalogue of undisturbed days No. 1 (April 1993). In: **Proc. of PRIME COST 238 Workshop**, University of Graz, Austria, 145-149.

Gulyaeva T. L. (1993a), Voting procedure for distinction of geomagnetic quiet and disturbed conditions at the ionosphere data analysis and modelling, in: Proceedings of the PRIME/URSI joint Workshop on "Data validation of ionospheric models and maps (VIM)", Roquetes, Spain, May 1992, **Memoria No.16**, Ed. by L.Alberca, pp.352-367.

Gulyaeva T. L. (1993b), Development of database of the ionosphere disturbances, **Adv. Space. Res.**, in press (1993)

Gulyaeva T. L. (1993c). Criteria for the definition of the quiet ionosphere. In: **Proc. of PRIME COST 238 Workshop**, University of Graz, Austria, 129-136.

Hanbaba R. (1993), Catalogue No.3 of European ionosonde data in the COST238 databank, in: Proceedings of the PRIME/URSI joint Workshop on "Data validation of ionospheric models and maps (VIM)", Roquetes, Spain, May 1992, **Memoria No.16**, Ed. by L.Alberca, pp.305-324.

Joselyn J. A. (1990). Forecasting magnetically quiet periods.In: **Solar Terr. Predictions: Proc. of Leura-1989 Workshop**, Australia. Ed. R.J.Thompson et. al., NOAA, Boulder, CO, USA, pp. 102-107.

Mayaud P. (1980), Derivation, meaning and use of geomagnetic indices, **Geophys. Monogr. Series 22**, AGU, Washington, D.C., USA.

Reinisch B. W. (1993), Chairman's Report, in: Proceedings of the PRIME/URSI joint Workshop on "Data Validation of ionospheric models and maps (VIM)", Roquetes, Spain, May 1992, **Memoria No.16**, Ed. by L.Alberca, pp.13-16.

Stanislawska I. (1993), Catalogue No.2 of European quiet ionospheric days 1966-1991. In: **Proc. of PRIME COST 238 Workshop**, University of Graz, Austria, 137-143.

SOME EVIDENCE SUPPORTING SHORT-TERM FORECASTING OF MID-LATITUDE IONOSPHERIC DISTURBANCE CONDITIONS

G. G. Bowman

Department of Physics, The University of Queensland, Brisbane, Qld 4072, Australia

Abstract

The relationships (determined statistically) which have been reported in recent papers between auroral-zone geomagnetic activity and spread-F occurrence in mid-latitude regions, are illustrated by a few specific events. These relationships include a 3 day delay as well as delays measured in hours, thought to result from upper-atmosphere neutral-particle density (UA-NPD) changes which occur in mid-latitudes following geomagnetic activity. Increased geomagnetic activity in the early-evening hours results in a suppression of spread-F occurrence in the hours which follow, while reduced activity produces the opposite effect of enhanced spread-F occurrence. It is suggested that these short-term delays may be useful in forecasting ionospheric disturbance conditions.

Introduction

A considerable amount of experimental evidence has accumulated over the years to support the idea that the primary cause of mid-latitude spread-F traces on ionograms is the existence of medium-scale travelling ionospheric disturbances (MS-TIDs) (see review by Bowman, 1990). It seems likely that these MS-TIDs are produced by the passage of ionospheric-level atmospheric gravity waves (IL-AGWs) (Dyson et al., 1970). Commenting on IL-AGWs Hines (1963) states "Because of their increase in amplitude with height (in the absence of strong dissipation) these waves would be more effective in the production of spread-F when the F layer is high." Of course the reason for this is the reduction with height of the upper-atmosphere neutral-particle density (UA-NPD). However, a reduction (or increase) in the UA-NPD at any specific height can also be expected to influence the IL-AGW wave amplitudes (and the corresponding MS-TID wave amplitudes). Recent results (Bowman 1992, 1993a) have shown that for mid-latitudes the diurnal, annual and sunspot-cycle variations of spread-F occurrence, as well as the annual and sunspot-cycle variations of equatorial spread-F, are closely related to UA-NPD changes. These associations are completely consistent with the concept of wave amplitudes (which need to exceed certain values for spread-F to be recorded) being modulated by UA-NPD changes.

Thus, it was not surprising to find from more recent analyses (Bowman, 1993b) (confirmation of earlier results - Bowman, 1984) that UA-NPD increases in mid-latitude regions which are expected approximately 6 hours after enhanced geomagnetic activity, seem to be effective in suppressing the level of spread-F occurrence. The reverse situation is also noted (at least statistically) where high levels of spread-F occurrence are found to be associated with low levels of geomagnetic activity (Bowman, 1993b). Since mid-latitude daytime disturbances are found to be associated with nighttime spread-F (Bowman, et al., 1987; Bowman, 1993c) the fact that these disturbances also appear to respond to geomagnetic activity a few hours earlier, is consistent with the spread-F results. An additional result indicates that UA-NPD changes directly associated with changes in the level of the 10.7 cm solar flux, also appears to influence the level of mid-latitude spread-F occurrence when considered on a world-wide scale (Bowman, 1993b). Another result involving delays of days rather than hours indicates that mid-latitude spread-F is enhanced after a delay of about 3 days following increased geomagnetic activity around midnight and also in the early morning hours around 0400 (local time) (Bowman 1993c). It has been proposed that delayed D-region absorption events in sub-auroral regions seem likely to be responsible, resulting in the generation of IL-AGWs with appropriately large wave amplitudes (Bowman, 1991a,b). These IL-AGWs are responsible in turn for the MS-TIDs which are associated with spread-F occurrence.

The Possibility of Short Term Forecasting

These results which have just been explained briefly, may allow estimates to be made of mid-latitude disturbance conditions a few days and also a few hours after noting the level of geomagnetic activity at particular local times. Thus short-term forecasting becomes a possibility. These recent results (Bowman, 1993b) have used spread-F controls to look for associated geomagnetic-activity levels. However, to obtain reasonable estimates of the reliability of these relationships for forecast purposes, the controls need to be obtained from geomagnetic-activity levels. With these controls the anticipated changes in spread-F occurrence levels can then be investigated. The statistical significance of these relationships using geomagnetic-field controls is indicated in Figure 4(b) of Bowman (1984). Spread-F occurrence levels at Moggill (35.7°S, 226.9°E geomagnetic (Gm) - near Brisbane, Australia), Norfolk Island (34.7°S, 243.2° E Gm) and Wakkanai (35.3°N, 206.0°E Gm) are considered. It is shown that for K indices at Macquarie Island (61.1°S, 243.2°E Gm) having values of 5 or 6, significantly suppressed spread-F activity after midnight is specifically related to this level of geomagnetic activity for interval 3 (1600 - 1900 Moggill local time, LT = UT + 10h). Furthermore, enhanced spread-F activity with a delay of 3 days is associated with interval 6 (0100 - 0400 Moggill local time). For very-low geomagnetic activity (ie. for K indices equal to 0 or 1) Figure 4(a) of Bowman (1984) records significantly enhanced post-midnight spread-F occurrence when using the K-index interval 4 (1900 - 2200 Moggill local time). It should be noted that minor time adjustments are needed for the local times of Norfolk Island and Wakkanai. Macquarie Island is in the same longitude zone as the spread-F stations.

The statistical significance of relationships between geomagnetic activity and mid-latitude spread-F occurrence has been discussed in the previous paragraphs. However the primary aim of this present paper is to consider a couple of specific examples which on some occasions illustrate clearly these relationships.
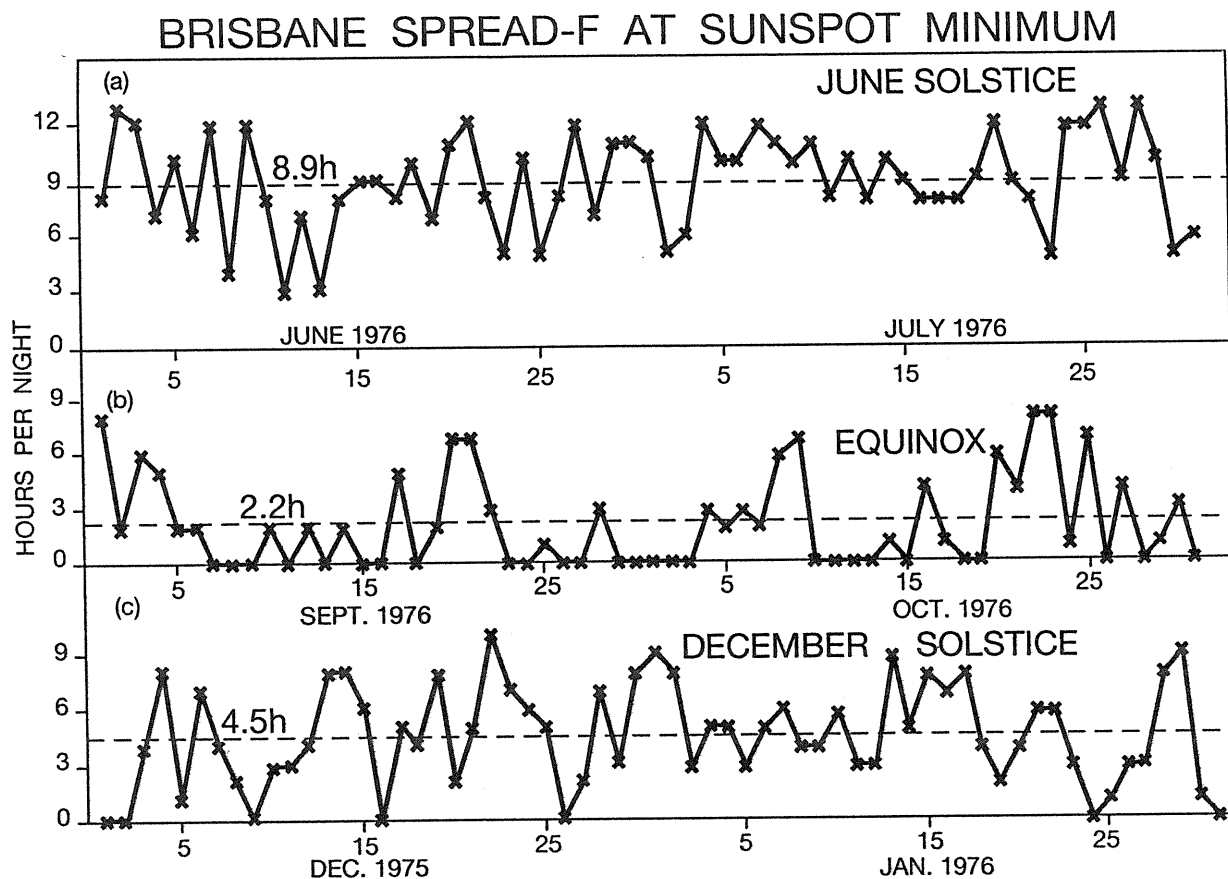
FIGURE 1. Brisbane spread-F occurrence levels for 3 different periods.

Results

The most favourable conditions for the increased recording of spread-F traces in mid-latitudes would seem to be enhanced geomagnetic activity in the early-morning hours on a specific date coupled with conditions of low-level activity in the early-evening hours on the nights the delayed spread-F occurrence is expected (ie. after a delay of 3 days for Brisbane (Moggill)). When geomagnetic activity is low the associated UA-NPD levels will be lower than average levels for the particular time of the year being considered. Therefore the probability of spread-F being recorded should be increased due to the anticipated MS-TID wave-amplitude increases. Since for any location the date changes at midnight, each nighttime recording of spread-F involves two dates in local time (LT). Consequently since for Brisbane LT = UT + 10h it has been found more convenient to use Universal Time, thus assigning the same date to pre-midnight and post-midnight spread-F occurrence. On any night 1800 to 0600 in local time becomes 0800 to 2000 in Universal Time. Similarly for geomagnetic activity early-evening levels are recorded in Universal Time on the same date as early-morning levels the following day in local time.

Figure 1 indicates (see dashed lines) average levels of spread-F occurrence at Brisbane for sunspot-minimum periods for (a) June-solstice months (b) equinoctial months and (c) December-solstice months. Average occurrence levels (quoted in hours per night) are found to be consistent with an inverse relationship with the semi-annual variation of the UA-NPD (Bowman, 1992). In Figure 1(a) the average level is 8.9 hours per night, in Figure 1(b) it is 2.2 hours while in Figure 1(c) it is 4.5 hours. However it can be seen that, from night to night, significant changes can occur in this level of activity due, it seems likely, to the short-term effects which have been discussed. Figure 2 illustrates two examples of enhanced spread-F occurrence at both Brisbane and a higher latitude station, Canberra (44.0S, 224.3E Gm) relative to geomagnetic activity levels at Macquarie Island as recorded by K indices. The spread-F is recorded a few days after early-morning (0100 to 0400 LT) enhanced geomagnetic activity (see labels C and H) combined with suppressed activity (see labels D and I) in the early-evening (1900 to 2200 LT) a few days after the early-morning increases. Also, the 10.7 cm solar flux (see Figures 2(e) and 2(j)) is shown to be below the average monthly levels for both examples. The observation from the diagrams in Figure 2 that Canberra spread-F occurrence precedes the occurrence at Brisbane (see labels A,B and F,G) by about a day is consistent with earlier results which indicated that following enhanced geomagnetic activity, the delays recorded increase for stations further from auroral-zone regions. (Bowman, 1979, 1982). Figure 3 illustrates two occasions when the level of Brisbane spread-F occurrence is reduced significantly. Associated AE indices and Macquarie Island K indices are both plotted. For the Macquarie Island records, the highest index for the local time interval 1600 to 0100 has been plotted for each day. Since the UA-NPD can increase to several times its initial value in the hours following severe geomagnetic conditions (Jacchia, 1965) it is not surprising that at these times the IL-AGWs wave amplitudes (and the corresponding MS-TID wave amplitudes) are not able to increase significantly at F2-layer levels to allow spread-F to be recorded. Consequently although, as Figure 1 shows, during some months of the year in a sunspot-minimum period spread-F at Brisbane is frequently recorded all night long, nevertheless even at these times increases in the UA-NPD can reduce the occurrence rate to a very-low level (Figure 3) on some nights.

Discussion

If it is important to know in advance what the level to mid-latitude spread-F occurrence might be (relative to the expected level for the season - see Figure 1) on any particular night, it is proposed that real-time monitoring of geomagnetic activity at an auroral-zone station in the same longitude zone, should be helpful. Reasonable estimates can then probably be made of expected changes in nighttime disturbance conditions. Of less importance, but still exerting some measure of influence, is the 27-day variation of the 10.7 solar flux, because of its effect on UA-NPD levels (Jacchia, 1965).

SPREAD-F - K INDICES - 10.7cm SOLAR FLUX
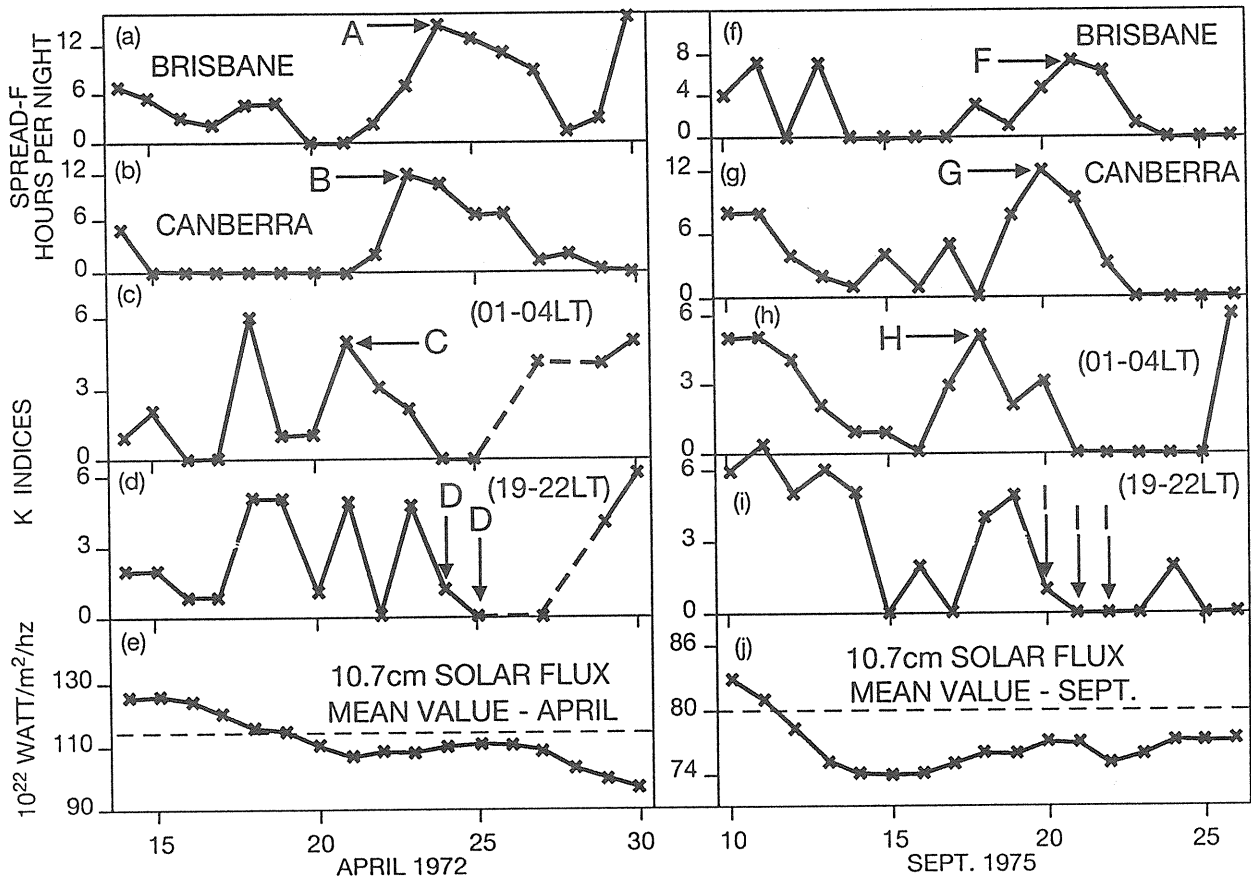
FIGURE 2. Two examples of enhanced spread-F occurrence at Brisbane and Canberra following geomagnetic-field changes.
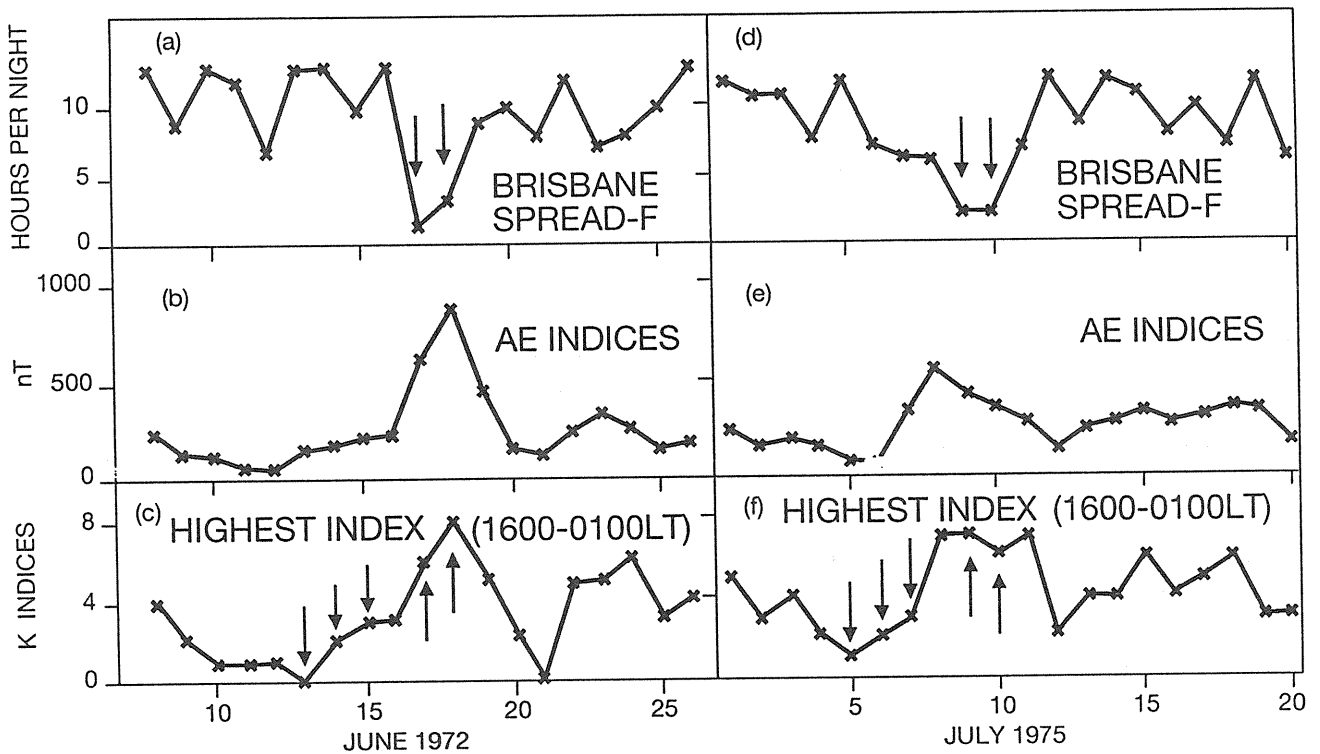
SPREAD-F - AE INDICES - K INDICES

FIGURE 3. Two examples of suppressed spread-F occurrence following geomagnetic-field changes.

The literature on the forecasting of ionospheric conditions seems to be mainly concerned with ionospheric parameters particularly foF2 (Ivanov-Kholodny and Mikhailov, 1986; Houminer et al., 1993). However this present paper (and the papers to which it refers) has been concerned specifically with short-term forecasting of mid-latitude ionospheric disturbance conditions. Concerning ionospheric parameters it should be noted that during the passage of MS-TIDs which produce disturbance conditions, there are changes to foF2 and h'F (Bowman, 1990) over short time intervals.

Conclusions

Apart from the 3 day delays in mid-latitude spread-F occurrence, which have been explained in other ways, it is proposed here that UA-NPD changes due to geomagnetic activity at specific local times, are effective in modifying spread-F occurrence levels after delays of a few hours. This modification occurs relative to spread-F occurrence levels due (it seems likely - Bowman, 1992) to the semi-annual and sunspot-cycle variations in the UA-NPD levels, as is illustrated by the dashed lines in Figure 1. Short-term forecasting appears a possibility.

References

Bowman, G. G., Latitude dependence of the time delay in spread-F occurrence following geomagnetic activity, **J. Atmos. Terr. Phys.**, 41, 999-1004, 1979.

Bowman, G. G., Spread-F occurrence in mid- and low-latitude regions related to various levels of geomagnetic activity **J. Atmos. Terr. Phys.**, 44, 585-589, 1982.

Bowman, G. G., Some effects of geomagnetic activity and ionospheric height rises on mid-latitude spread-F occurrence, **J. Atmos. Terr. Phys.**, 46, 55-64, 1984.

Bowman, G. G., A review of some recent work on mid-latitude spread-F occurrence as detected by ionosondes, **J. Geomag. Geoelectr.**, 42, 109-138, 1990.

Bowman, G. G., Delayed ionospheric absorption events following enhanced geomagnetic activity, **Indian J. Radio Space Phys.**, 21, 73-79, 1991a.

Bowman, G. G., Delayed mid-latitude spread-F occurrence following enhanced geomagnetic activity, **Indian J. Radio Space Phys.**, 21, 80-88 1991b.

Bowman, G. G., Upper atmosphere neutral-particle density variations compared with spread-F occurrence rates at locations around the world, **Ann. Geophysicae**, 10, 676-682, 1992.

Bowman, G. G., The influence of the upper-atmosphere neutral particle density on the occurrence of equatorial spread-F, **Ann. Geophysicae**, 11, 624-633, 1993a.

Bowman, G. G., Short-term delays in the occurrence of mid- latitude ionospheric disturbances following other geophysical and solar events, in press **J. Geomag. Geoelectr.** 1993b.

Bowman, G. G., Daytime and nighttime ionospheric disturbances and their delayed occurrence after geomagnetic activity, **Indian J. Radio Space Phys.**, 22, 1-10, 1993c.

Bowman, G. G., G. S. Dunne and D. W. Hainsworth, Mid-latitude spread-F occurrence during daylight hours, **J. Atmos.Terr. Phys.**, 49 165-176, 1987.

Dyson, P. L., G. P. Newton, and L. H. Brace, In situ measurements of neutral and electron density wave structure from the Explorer 32 satellite, **J. Geophys. Res.**, 75, 3200-3210, 1970.

Hines, C.O., The upper atmosphere in motion, **Quart. J.R.Met. Soc.**, 89, 1-42, 1963.

Houminer, Z., J. A. Bennett and P. L. Dyson, real-time ionospheric model updating **Electr. Electron. Eng. Aust.**, 13, 99-104, 1993.

Ivanov-Kholodny, G. S. and A. V. Mikhailov, The prediction of ionospheric conditions, **Geophysics and Astrophysics Monographs**, D. Reidel Publishing Coy, Dordrecht, 1986.

Jacchia, L. G., Atmospheric structure and its variations at heights above 200 km, Cospar International Reference Atmosphere (CIRA) 1965. **North-Holland Publishing Coy**. - Amsterdam, Appendix II, pp.293-313, 1965.

SOLAR CYCLE VARIATIONS AND LATITUDINAL DEPENDENCE ON THE MID-LATITUDE SPREAD-F OCCURRENCE AROUND JAPAN

Kiyoshi Igarashi and Hisao Kato
Communications Research Laboratory, Ministry of Posts and Telecommunications,
4-2-1 Nukui-kitamachi Koganei-shi, Tokyo 184 Japan

Abstract

Statistical results of spread-F occurrence probability are presented by using a long term ionospheric data base for five Japanese ionosonde stations from 1969 to 1989.

It is clearly shown that the spread-F occurrence probability is inversely correlated with sunspot number, especially manifesting at Akita. We found that the difference of spread-F occurrence between summer and winter strongly depends on solar cycles in northern mid-latitude stations for Wakkanai and Akita. Spread-F occurrences at lower latitude stations show different features, when compared with higher mid-latitude stations.

Introduction

A statistical study of spread-F occurrence has been made by many workers. Some recent work on mid-latitude spread-F occurrence is reviewed by Bowman (1990). Statistical results of spread-F occurrence over Japan were shown by Kasuya et. al.(1955) by using the data obtained at four stations for the period from 1949 to 1954. They found that occurrence of spread-F observed over Japan is more prevalent at night in the winter and summer solstices, especially during weak solar activity, and is also more frequent at the northern station. Shimazaki (1959) studied world-wide occurrence probability of spread-F based on the IGY data for the whole world. Thus, in mid-latitudes spread-F occurs more frequently in summer than in winter at stations in the Far East and South America. Bowman (1964) showed spread-F occurrence features by using the data over a 16 year period from 1947 to 1962 for Wakkanai, Akita and Yamagawa. This paper suggests that an inverse relationship between spread-F occurrence and the upper-atmosphere neutral particle density (UA-NPD) levels exists apparently, at least for the Japanese and Australian stations. Seasonal and solar cycle variations of spread-F at the equatorial anomaly crest zone were analyzed by using a long-term data base from 1960 to 1982 (Y.-N. Huang et al., 1987). They noted that frequency spread-F occurrence was much larger than range spread-F, except for equinoxes during high and medium solar activity.

In this report, we used the hourly values in a scaled ionospheric vertical sounding data set obtained at Wakkanai (43.39°N, 141.69°E geographic; 35.3°N, 206.5°E geomagnetic), Akita (49.73°N, 140.13°E geographic; 29.5°N, 205.9°E geomagnetic), Kokubunji (35.71°N, 139.49°E geographic ; 25.5°N, 205.8°E geomagnetic), Yamagawa (31.20°N, 130.62°E geographic; 20.4°N, 198.3°E geomagnetic) for the period from 1968 to 1989 and Okinawa (26.28°N, 127.81°E in geographic; 15.3°N, 196.0°E geomagnetic) for the period from 1972 to 1989.

Diurnal variations of spread-F occurrence

Diurnal variations of spread-F occurrence are shown in figure 1. The total occurrence numbers of spread-F from January to December are compared among five stations. During the solar maximum period in 1980, spread-F appears from 19 hr to 06 hr LT (LT=UT+9), and most frequently postmidnight. The spread-F occurrence number is larger in the solar minimum period than in the solar maximum period. Maximum occurrence period is around 02 hr LT. Of all the stations considered, spread-F occurs less frequently at Kokubunji and occurs more often at Akita. Although not prominant, there seems to be two peaks of spread-F occurrence at about 22-00 hr LT and 02-04 hr LT appearing at Akita and Kokubunji during the solar
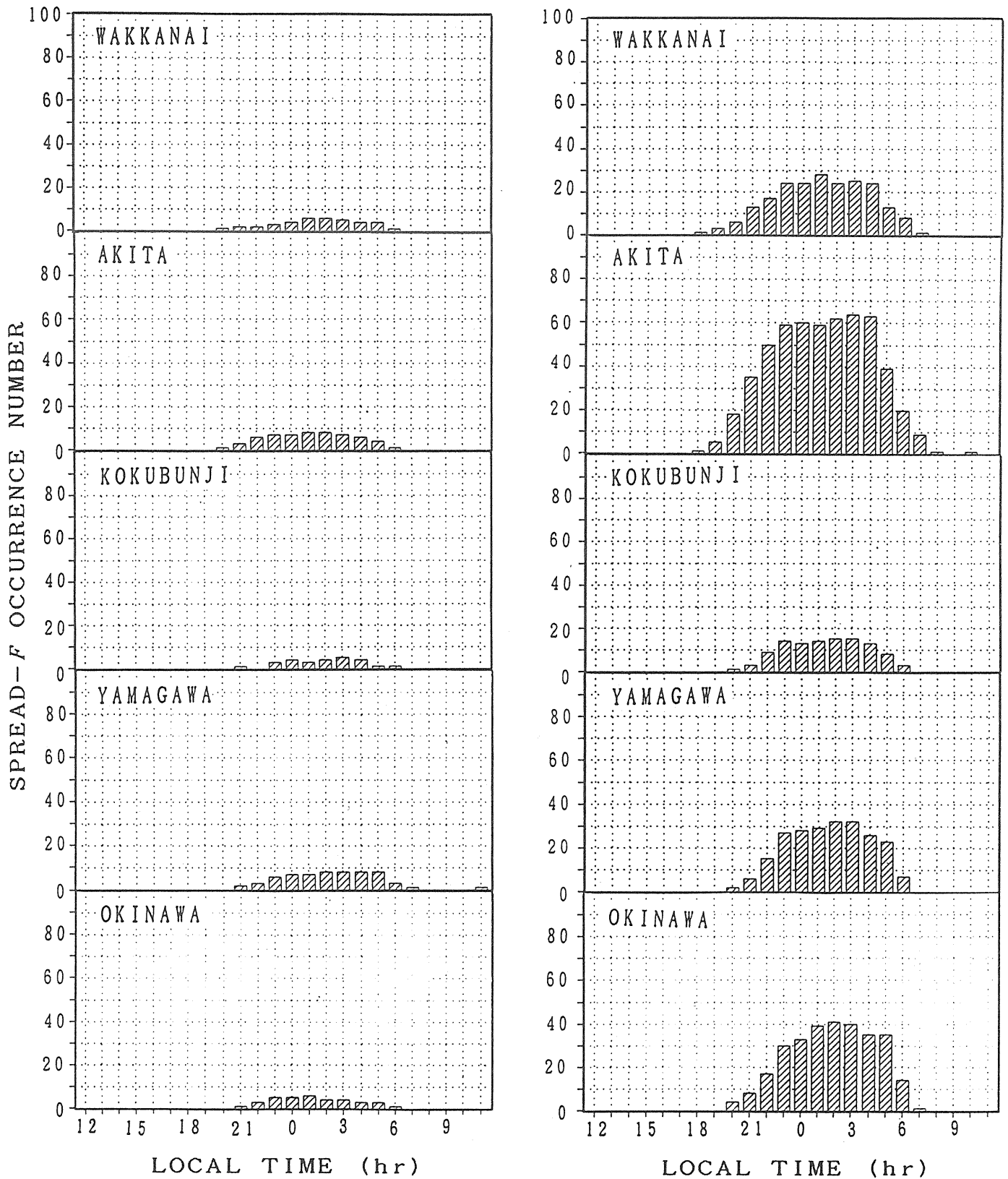
Figure 1. Local time dependence of spread-F occurrence number for a solar maximum period (1980) and a solar minimum period (1986) for the Japanese stations, Wakkanai, Akita, Kokubunji, Yamagawa and Okinawa.

minimum period. One peak of spread-F occurence at 01-03 hr LT is seen at Wakkanai, Yamagawa and Okinawa during the solar minimum period. During the solar maximum period two peaks of spread-F occurrence are seen only at Kokubunji, and the occurrence peak for Okinawa shifts from around 02 hr LT to around local midnight.

Solar cycle and seasonal variations of spread-F occurrence

Figure 2 shows solar cycle variations of spread-F occurrence probability at 02hr LT in Akita. Spread-F occurrence probability for Akita is anti-correlated with the monthly mean of sunspot number. Remarkable spread-F occurrence peaks appear from June to August and from December to February. During the first solar minimum period, spread-F occurrence in summer is larger than in winter. In 1983, 1985 and 1986 spread-F occurrence in summer is lower than in winter. Using limited ionogram data, Shimazaki (1959) concluded that in mid-latitude, the spread-F occurs more frequently in summer than in winter at stations in the Far East. But our results show that the difference in spread-F occurrence between summer and winter varies with solar activity. These results for solar cycle and seasonal variations of mid-latitude spread-F occurrence might be related in terms of the way UA-NPD changes, which was proposed by Bowman (1964, 1992).
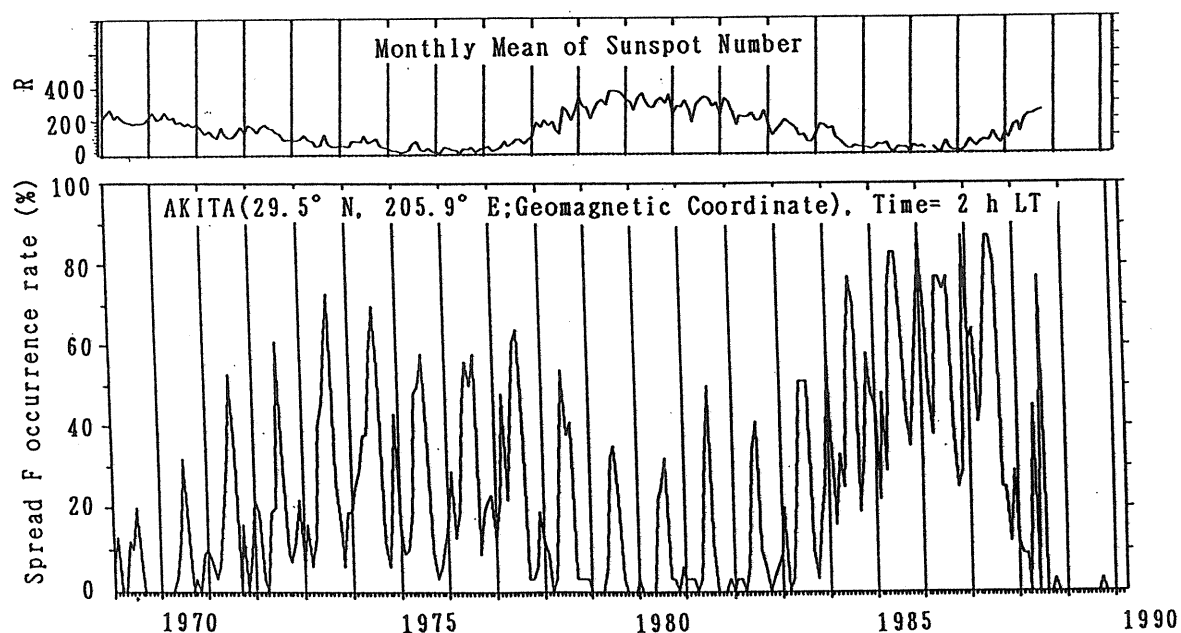
Figure 2. Solar cycle variations of spread-F occurrence probability at 02 hr LT (LT=UT+9) for Akita.

Latitudinal dependence in solar cycle variations of spread-F occurrence

In Figure 3 the spread-F occurrence rates at the five Japanese ionosonde stations are compared. As the occurrence of range type spread-F is rare in Japanese ionosonde data, except for Yamagawa and Okinawa, range and frequency spread-F types are not separated in this analysis. The spread-F occurrence rates for both Wakkanai and Akita show similar occurrence patterns. During a period of sunspot minimum around 1986, spread-F occurrence in winter is larger than in summer. But in other periods, spread-F occurrence in summer is larger than in winter. Spread-F occurrence for Kokubunji shows smooth variations during the increasing or decreasing phase of sunspot numbers. The 75 % peak occurrence of spread-F for Yamagawa during sunspot minimum in 1986 is larger than the 30 % peak occurrence during sunspot minimum in 1976. Spread-F occurrence for Okinawa shows distinctly large occurrence of 90% during sunspot minimum period in 1987. During sunspot maximum period around 1980, spread-F occurrence for Okinawa is lower than 20% occurrence probability.
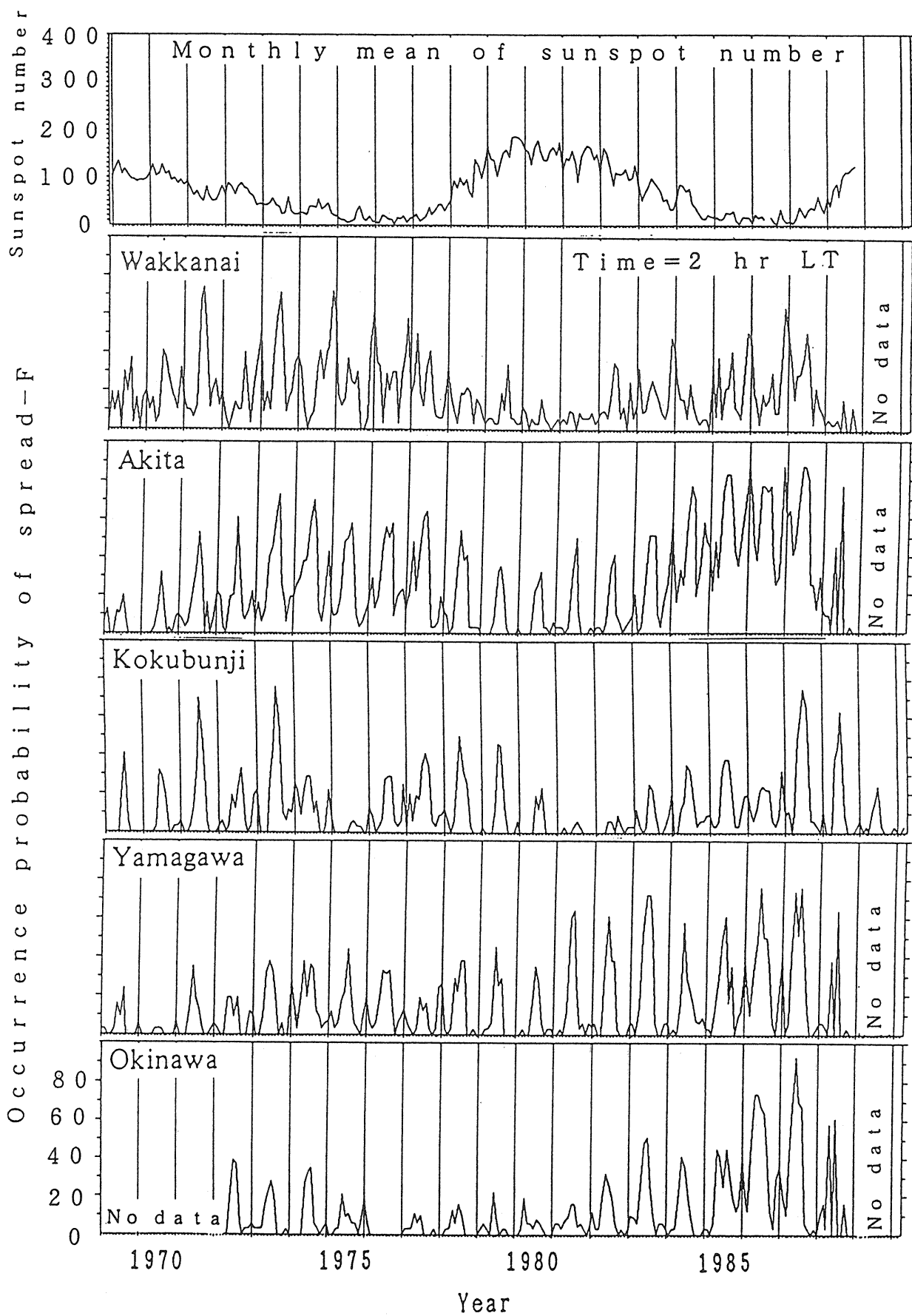
Figure 3. Latitudinal dependence of spread-F occurrence probability from 1969 to 1989 for five Japanese ionosonde stations.

Conclusions

A long term ionosonde data base for five Japanese ionosonde stations from 1969 to 1989 was used to study solar cycle variations and the latitudinal dependence of mid-latitude spread-F occurrence probability. Several features of solar cycle variations, local time dependence, and latitudinal dependence of the spread-F occurrence probability are summarised as follows;

(1) Spread-F occurrences are inversely correlated with sunspot number, especially at Akita.

(2) Remarkable occurrence peaks appear from June to July in summer and from December to January in winter.

(3) The difference of spread-F occurrence between summer and winter also depends on solar cycles at specific latitude(Akita and Wakkanai). This is different from the results of Shimazaki(1965) who found that in mid-latitudes spread-F occurs more frequently in summer than in winter at stations in the Far East.

(4) Maximum occurrence of spread-F appears in postmidnight from 00 hr LT to 05 hr LT.

(5) Spread-F occurrence probability depends strongly on the latitude of the station. Spread-F occurrence rates at lower latitude stations show different features, when compared with higher latitude stations.

Acknowledgments

References

Bowman G. G., Spread-F in the ionosphere and the neutral particle density of the upper atmosphere, **Nature**, Vol 201, No. 4919, 564-566, 1964

Bowman G.G., A review of some recent work on mid-latitude spread-F occurrence as detected by ionosondes, **J.Geomag.Geoelectr.**, 42, 109-138, 1990.

Bowman G. G., Upper atmosphere neutral-particle density variations compared with spead-F occurrence rates at locations around the world. **Ann. Geophysicae**, 10, 676-682, 1992.

Huang Yinn-Nien, Kang Cheng and Wen-Ter Huang, Seasonal and solar cycle variations of spread F at the equatorial anomaly crest zone, **J. Geomag. Geoelectr.**, 39, 639-657, 1987.

Kausya Isao, Katano Seizo and Shoji Taguchi,On the occurrence of spread echoes in the F region over Japan, **J. Radio Res. Labs.**, 2, 329-339, 1955.

Shimazaki T., A statistical study of world-wide occurrence probability of spread-F, **J.Radio Res.Labs.**, 6, 669-687, 1965.

INTERNATIONAL REFERENCE IONOSPHERE (IRI) IN CHINA

Cao Chong Dai Kailiang Quan Kunhai
China Research Institute of Radiowave Propagation Xinxiang, Henan, 453003, China
Shen Changshou
Department of Physics, Beijing University, Beijing, 100871, China

Abstract

There are four Chinese groups working on the International Reference Ionosphere (IRI). Their main works are comparisons of the IRI with ionospheric data observed in China and checking of the IRI available for the Chinese region. The compared results are shown in this paper. The CRIRP group has used the ionospheric data of nine ionosonde stations (Manzhouli, Changchun, Wulumuqi, Beijing, Lanzhou, Lhasa, Chongqing, Guangzhou, Haikou) during the 21st solar cycle. The compared parameters are foF2, M(3000)F2, foF1, hmE, and bottomside profile, and TEC (Xinxiang). It is indicated that there is a considerable systematic error when the IRI-86 is used in Southern China, especially during the solar maximum. The IRI is improving the use of ionospheric data observed in the Asia-Oceania region. The revised model is called the China Reference Ionosphere (CRI) and it is more accurate than the IRI for use in and around China.

Introduction

The four Chinese groups working on the International Reference Ionosphere (IRI) belong to the China Research Institute of Radiowave Propagation (CRIRP)[1-9]; Beijing University [10-12]; Wuhan Institute of Physics, Academia Sinica [13-14]; and the Center for Space Science and Applied Research, Academia Sinica [15], respectively. They have mainly compared the ionospheric data observed in China during the 21st and 22nd solar cycles with the IRI and checked the IRI available for the China region. Tables 1 and 2 list the associated ionospheric observatories, and the duration of observed data, comparative parameters and associated ionosonde stations.

Based on the statistical analyses of a large number of observed data and understanding of the IRI, the CRIRP group puts forward an improved IRI for use in China and the Asia-Oceania region. The revised model is called China Reference Ionosphere (CRI)[7].

Comparisons of foE, foF1 and foF2

The major task has been comparisons of the monthly median foE, foF1 and foF2 measured in China with results calculated from the IRI [3,5,6,8,9,10,11,13,14]. Results show that for any time, including both solar maximum and minimum activity periods, there is a good agreement between the measured and calculated foE and foF1. The relative deviations are less than 5% in most cases [5,10,11,13,14]. Therefore, the foE and foF1 predicted by the IRI is applicable to the China region.

The situation with foF2 and M(3000)F2 is very different from that for foE and foF1. Quan et. al. [3] have analysed the ionospheric data observed at nine Chinese ionosonde stations during the 21st solar activity cycle, and compared results with others predicted from the IRI. They have found that there are considerable systematic deviations in the predictions for low latitude regions (for example, Guangzhou and Haikou in Southern China) and some mid latitude regions (for example, Lanzhou) when using the IRI model.

Here we define the absolute deviation of foF2 monthly median as:

$$E = \Delta foF2 = foF2(\,meas\,) - foF2(\,cal\,)$$

Table1. Geographic positions of associated ionosonde stations

Station	Code	latitude	longitude
Manzhouli	(MZ)	49°35 'N	117°27 'E
Changchun	(CC)	43° 50'N	125°16'E
Wulumuqi	(WL)	43°45'N	87°38'E
Beijing	(BJ)	40°00'N	116°18'E
Lanzhou	(LZ)	6°04'N	103°52'E
Xinxiang	(XX)	35°18'N	113°51'E
Wuchang	(WC)	30°30'N	114°24'E
Lhasa	(LS)	29°38'N	91°10'E
Chongqin	(CQ)	29°30'N	106°25'E
Guangzhou	(GZ)	23°09'N	113°21'E
Haikou	(HK)	20°00'N	110°20'E

*Faraday rotation measurement

Here we define the absolute deviation of foF2 monthly median to be

$$\Delta foF2 = E,$$

$$E = \Delta foF2 = (foF2 \, (meas) - foF2 \, (cal)) \qquad (1)$$

The (cal) represents the values calculated from the IRI model, and (meas) represents the values measured by ionosonde. The relative deviation is

$$D(\%) = \frac{\Delta foF2}{foF2(cal)} \qquad (2)$$

The average deviation is

$$\delta = \frac{1}{n} \sum \Delta foF_2 \qquad (3)$$

and the

standard deviation is

$$\sigma = \sqrt{\frac{1}{n-1}\sum(\Delta foF_2)^2}\qquad(4)$$

Table 2. Details of comparisons of observed data with the IRI

Number of reference	Associated stations	Comparative parameters	Duration of data
[1]	MZ, BJ, FZ, MZ, XX	profile, TEC	March,1976,1978,1980, Feb, 1982, March, 1983
[2]	MZ, XX, HK	profile, TEC	August, 1982
[3]	MZ , CC, ML, BJ, LZ, LS, CQ, GZ, HK	foF2 M(3000)F2	1977-1986
[4]	WC	profile	1968
[5]	MZ, CC, WL, BJ, LZ, LS, CQ, GZ, HK	foF2, M(3000)F2, foE, foF1, hmE, profile, TEC	1977-1986
[6] / [8]	MZ, CC, WL, BJ, LZ, CQ, GZ, HK	foF2 , M(3000)F2	1977-1986
[9]	XX, WC	TEC, foF2	1982-1989
[10]	MZ, WL, WC, CQ, HK	foE, foF1, foF2	1965-1976
[11]	MZ, WL , CC, BJ, CQ, GZ, HK	foE, foF1, foF2	1968-1970, 1974-1976
[13] / [14]	MZ, BJ, WC, CQ ,GZ	foE, foF1, foF2	1965-1975
[15]	Xi'an (34°N,108°45'E)	TEC	Apr 1978-, Dec.1979

Results for 1977-1986 [3] show that the maximum foF2 average deviation δ occurred at Haikou, Guangzhou and Lanzhou, with values of +0.6MHz,+0.5MHz and -0.5MHz respectively, $|\delta| \le 0.2$MHz at other stations. Maximum values appeared at Haikou and Guangzhou, and they are 1.5MHz and 1.2MHz respectively, with $\sigma \le 0.9$MHz at other stations. Quan etal [3] have also noted that the relative deviations are in the limits$\pm15\%$ for the typical mid latitude stations (except Lanzhou station), but for low latitude stations Guangzhou and Haikou, they are larger. The maximum relative deviation reached 77% at Haikou. During sunset and sunrise periods the relative deviations were D>50% for most Chinese stations.

In summary, for the relative deviations of foF2 at all stations, night values are larger than day values, winter values are larger than summer values, and low latitude region values are larger than at mid latitudes. Other authors [10-14] provide similar conclusions.

Comparisons of TEC and density profiles

Dai [15] has compared the TEC measured at Xi'an during 1978-1979 with that predicted by the IRI-79. It is shown that the predicted values are much lower than measured in Spring.

Dai and Ma [9] have compared the predicted TEC monthly median values by IRI-86 and IRI-90 with the monthly median values observed at Xinxiang by receiving VHF signals from the ETS-II satellite from 1982 to 1989. The compared results indicate that the model predicted TEC values fit the measured values quite well. Normally, the predicted values are a little larger than the measured values. The predicted TEC accuracy of the IRI-90 is better than the IRI-86. During the high solar activity period, the IRI TEC appears to have a different behaviour from that observed. In the Winter and Spring seasons, the IRI TEC is much less (by nearly 50%) than the observed daytime TEC, especially near noon.

A comparison between bottomside electron density profiles deduced from Wuchang ionograms and from the IRI-86 has shown that the IRI hmE is usually lower than measured values, and the sub peak half-thickness is larger than the measured values. Both profiles fit very well in the daytime, but are not good at night [4,7].

Shen [12] has introduced the atmospheric and ionospheric models MSIS-86 and IRI-86, and deduced the thermospheric wind system, the spatial distribution and temporal variation of collision frequency and ionospheric conductivities. The empirical parameters of MSIS-86 and IRI-86 have been used to deduce the three dimensional distribution of ionospheric conductivity and thermospheric wind system by Shen et al.[16]. The thermospheric wind system, height-integrated conductivity, electrostatic potential and ionospheric current density are compared with observed data and the results deduced from model calculation. There is a good agreement between them.

China Reference Ionosphere

Based on the statistical results of observed data from 39 ionosonde stations (sited in regions from 65°N to 40°S and from 60°E to 150°E) over many years, Sun [17] has produced a method of predicting the ionospheric F2 layer in the Asia-Oceania Region (AOR). When the IRI-90 applies to region of China, using the AOR mapping instead of the CCIR coefficients or the URSI coefficients, the revised IRI model, called the China Reference Ionosphere, can provide more accurate predicted values of ionospheric parameters for the China region and around China [6,7,8,9]. The CRI is different from the IRI on the following two points:

(1)   hmE equals 115km;

(2)   When R12≤60 for latitudes≤40°, the occurrence of the F1 layer is considered in all seasons, and not as the IRI stipulates with no F1 appearance in Winter.

The values of TEC calculated using both the CRI and IRI have been compared with observations at Xinxiang based on Faraday rotation measurements from 1983 to 1989 [5,9], also with foF2 values predicted with observations at Wuchang based on ionograms [5,9]. The CRI give more accurate TEC and foF2 values than the IRI in the China region.

Conclusion

The IRI available for the China region is more realistic in Northern China (mid latitude region) than in Southern China (low latitude region). The prediction accuracy of foE and foF1 is much better than for

foF2. For foF2, in the low latitude region, there are considerable systematic deviations. The CRI is a computerised model, revised from the IRI-90 with substitution of some empirical formulas and assumptions based on the observations made in the China region. The CRI gives more accurate representation of the ionosphere for China and around China than the IRI.

References

[1] Wang Weiping (1987), The main ionospheric parameters obtained by using International Reference Ionosphere IRI-79, **Chinese Journal of Radio Science**, 2-1, pp62-69.

[2] Wang Weiping (1988),The reliability analysis of the ionospheric parameters over China Obtained by using International Reference Ionosphere, **International Symposium on Radio Propagation** (ISRP'88, Beijing), pp173-176.

[3] Quan Kunhai, Dai Kailing, Luo Fagen and Liu Ruiyuan (1992), Comparison of observed foF2 and M(3000)F2 with International Reference Ionosphere (IRI-86), **Chinese Journal of Radio Science**, 7-1,pp53-61.

[4] Luo Fagen, Dai Kailiang, Quan Kunhai and Liang liping (1992), Comparison between subpeak electron density profiles deduced from ionograms and the International Reference Ionosphere IRI-86), **Chinese Journal of Radio Science**, 7-3 pp42-48.

[5] Dai Kailiang, Quan Kunhai, Luo Fagen and Liu Ruiyuan (1993), Comparison of IRI with osphere observed in China, **Advanced Space Res**,13-3,pp57-59.

[6] Dai Kailiang, Luo Fagen, Quan Kunhai and Liu Ruiyuan (1992), Comparison of the Asia Oeania region F2 layer prediction with the CCIR method, **Chinese Journal of Space Science**, 12-2, p153-156.

[7] Liu Ruiyuan,Quan Kunhai,Dai Kailiang,Luo Fagen, Sun Xianru and Li Zhongqin (1993),Study of the Reference Ionosphere in Chinese Region, **International Symposium on Radio Propagation**, ISRP'93, Beijing.

[8] Dai Kailiang, Quan Kunhai and Liu Ruiyuan (1993), Comparative study of modelled foF2 with the observations in China, **International Symposium on Radio Propagation**, ISRP'93,Beijing.

[9] Dai Kailiang and Ma Jianming (1993), Comparison of Total Electron Content predicted using IRI with the data observed in China, **J Atmos. Terr. Phys.**, in press.

[10] Chen Zhongsheng and Shen Changshou (1990). Some comparisons between the IRI-86 with the ionospheric data of China, **Publications of Yumcan Observatory**, supplement, pp115-127.

[11] Shen Changshou and Zi Minjun (1990), A statistical comparison between critical frequencies predicted by IRI-86 and observed in China, **Publications of Yunnan Observatory**,supplement,pp103-114.

[12] Shen Changshou (1990), An additional application of MSIS-86 and IRI-86, **Chinese Journal of Space Science**, 10-1,pp50-60.

[13] Liang Shangqi(1990), A comparison of the main ionospheric parameters over China with IRI, **Chinese Journal of Space Science**, 10-2, pp135-140.

[14] Lian Shangqi (1990), The deviation of IRI from the ionospheric parameters observed over East Asia, **Publications of Yunnan Observatory**, supplement, pp128-134.

[15] Dai Yueqin (1986),A test of International Reference Ionosphere IRI-79 using ionospheric electron content data, **Chinese Journal of Space Science**, 6-2, pp144-146.

[16] Shen Changshou, Li Qing and Jiao Weixin (1992), A stude of the ionospheric dynamo by using empirical model parameters, **Chinese Journal of Space Science**, 12-2, pp102-110.

[17] Sun Xianru (1987), A method of predicting the ionospheric F2 layer in the Asia Oceania Region, **Journal of China Institute of Communications** 8-6, pp37-45.

MONTHLY AVERAGE BEHAVIOUR AND OSCILLATION OF DERIVED IONOSPHERIC DRIFTS

Shun-rong Zhang   Xin-yu Huang   Yuan-zhi Su
Wuhan Institute of Physics, Chinese Academy of Sciences,
P.O.Box 72003, Wuhan 430072, P. R. CHINA

Abstract

With the help of servo model, plasma drifts near F2 peak derived from ionosonde data for 1986, 1987 (low solar activity) and 1982 (high solar activity) are obtained over 4 East Asian stations. The general pattern of the drift is "W"-shaped for the diurnal curve, and superimposed with collapse at about 3LT, which is extremely obvious for March 1982. Possibly, the ionospheric F2 layer dynamo is responsible for the collapse of the drift. A case study of the vertical drift spectra is also carried out. The results show obvious 2.1-day oscillation over the low latitude station, Okinawa, and it seems to provide evidence for the modulation of the electric field by planetary waves, which may eventually modify the oscillation of the ionospheric characteristics.

Introduction

Current investigations indicate that existing ionosonde data obtained with relatively low costs and good time and geographical coverage can be used efficiently to estimate the global features of the thermospheric wind within the ionospheric F2 region. This research was originated from the study of wind effect on the ionospheric F2 peak. According to theory, for example, servo model (Rishbeth, 1967; Rishbeth et al, 1978), a vertical plasma drift approximately modifies the balance height, established by the balance between the photochemical loss and diffusion. Two major approaches to deriving neutral wind were developed by Buonsanto (1986), Buonsanto et al (1989) and Miller et al (1986) respectively. The method of Buonsanto et al uses the complete formulae suggested by Rishbeth et al (1978). In this approach, besides ionospheric data, namely foF2 and hmF2, the neutral density and temperature and also O^+ - O collision frequency are needed so that appropriate balance heights can be obtained. The other approach expresses the changes in the F2 layer peak in terms of a linear wind-induced drift, and employs a theoretical ionospheric model, from which the linear coefficient can be obtained at various neutral winds by a linear regression. Following this approach, several empirical formulae for the linear coefficients have been established for the equatorial, mid-latitude and high latitude regions (Forbes et al, 1992, and the references therein). In this paper, the Buonsanto et al method is used.

Comparing mid-latitudes, which is the case Buonsanto and other researchers have focused on (Buonsanto et al, 1989; Buonsanto, 1990), the lower mid-latitude is a much more complicated case, where E x B drift becomes more important for the vertical motion of ionization while wind-induced drift still plays a significant role. It is impossible, of course, to discriminate between each component, if there is no further information available. However, by using data from several stations, with different latitude along approximately the same longitude, the relative importance may be determined. Accordingly, we will be able to gain insight into some ionospheric phenomena, as will be discussed in this paper, for the chain of 4 East Asia ionosonde stations. The derived vertical drifts will be given as a function of month, season and solar activity over these locations.

Ionospheric oscillations characterised by the fluctuations in foF2 and hmF2 is another interesting subject. The few observations available for studying plasma drift, seem insufficient to reveal the mechanism of the ionospheric oscillation. The great advantage of derived vertical drifts from ionosonde data is that it makes it possible to obtain the variation for any time scale depending only upon the availability of the ionospheric data. We thus display a case study of the spectral structure obtained with an FFT for the vertical drift in a full month (December 1981) for a mid-latitude and a low latitude station, with emphasis on the tidal and 2-day wave components. This is different from Buonsanto's work (1991), where a Fourier decomposition of the mean daily variations for each month concerned at mid-latitudes is carried out.
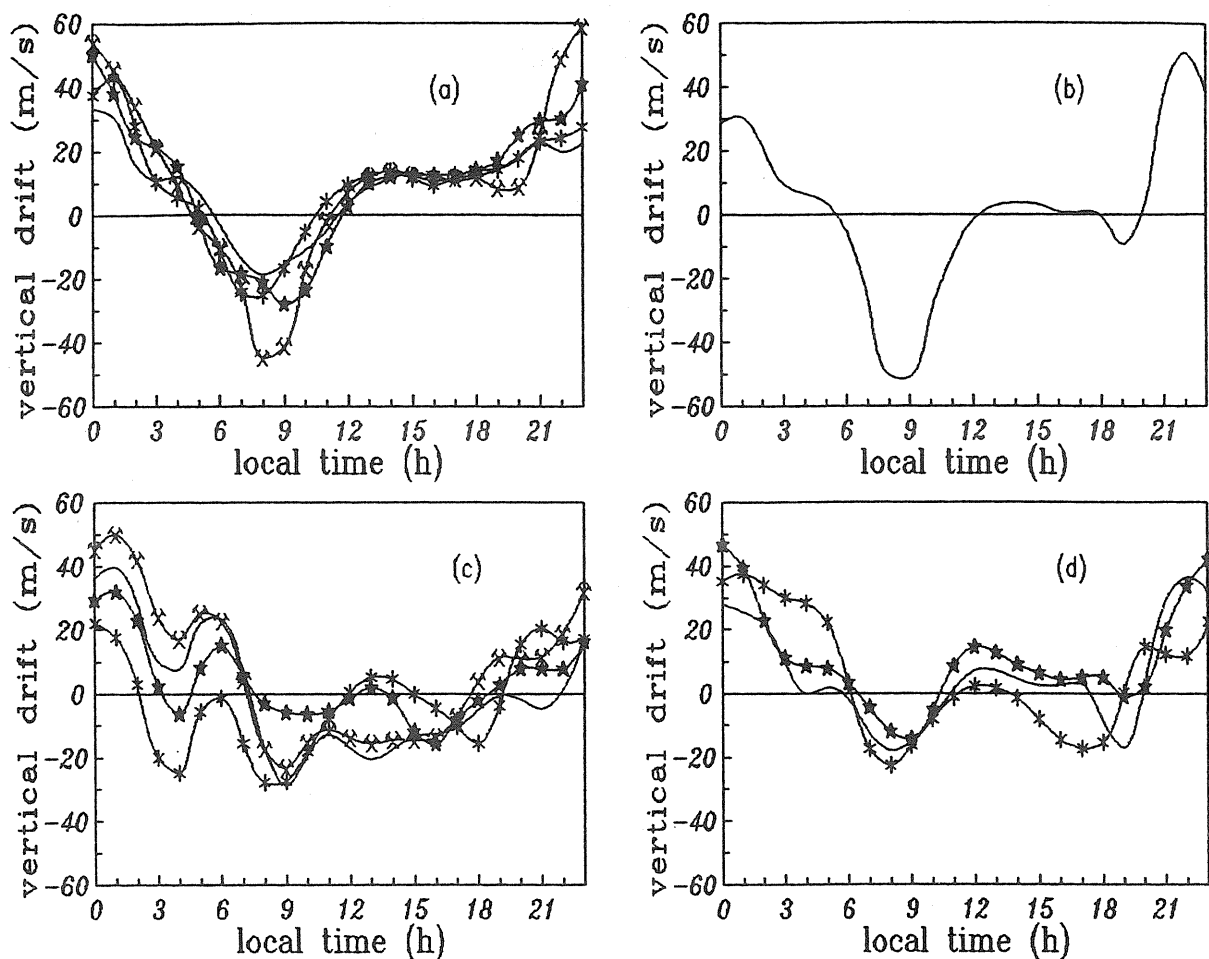
Figure 1. Diurnal variations of vertical drifts over Wuchang for a full year between 1986 - 87.
The months of data are displayed using four line types:

[i]   thin line   [iii]   line with stars
[ii]   line with asterisks   [iv]   line with crosses

The four figures are:

1[a] summer type   (May [ii], June [i], July [iii], August[iv])
1[b] autumn type   (September [i])
1[c] winter type   (October [ii], November [iii], December [i], January [iv])
1[d] spring type   (February [ii], March [i], April [iii])

Station	Geographic Latitude.	Geographic Longitude.	Geomagnetic Latitude	Dip
Wakkanai	45.4° N	141.7° E	35.3° N	59.3°
Yamagawa	31.2° N	130.6° E	20.4° N	43.8°
Wuchang	30.5° N	114.4° E	19.2° N	44.5°
Okinawa	26.3° N	127.8° E	15.3° N	36.4°

Table 1 Locations of Ionosonde Stations

128
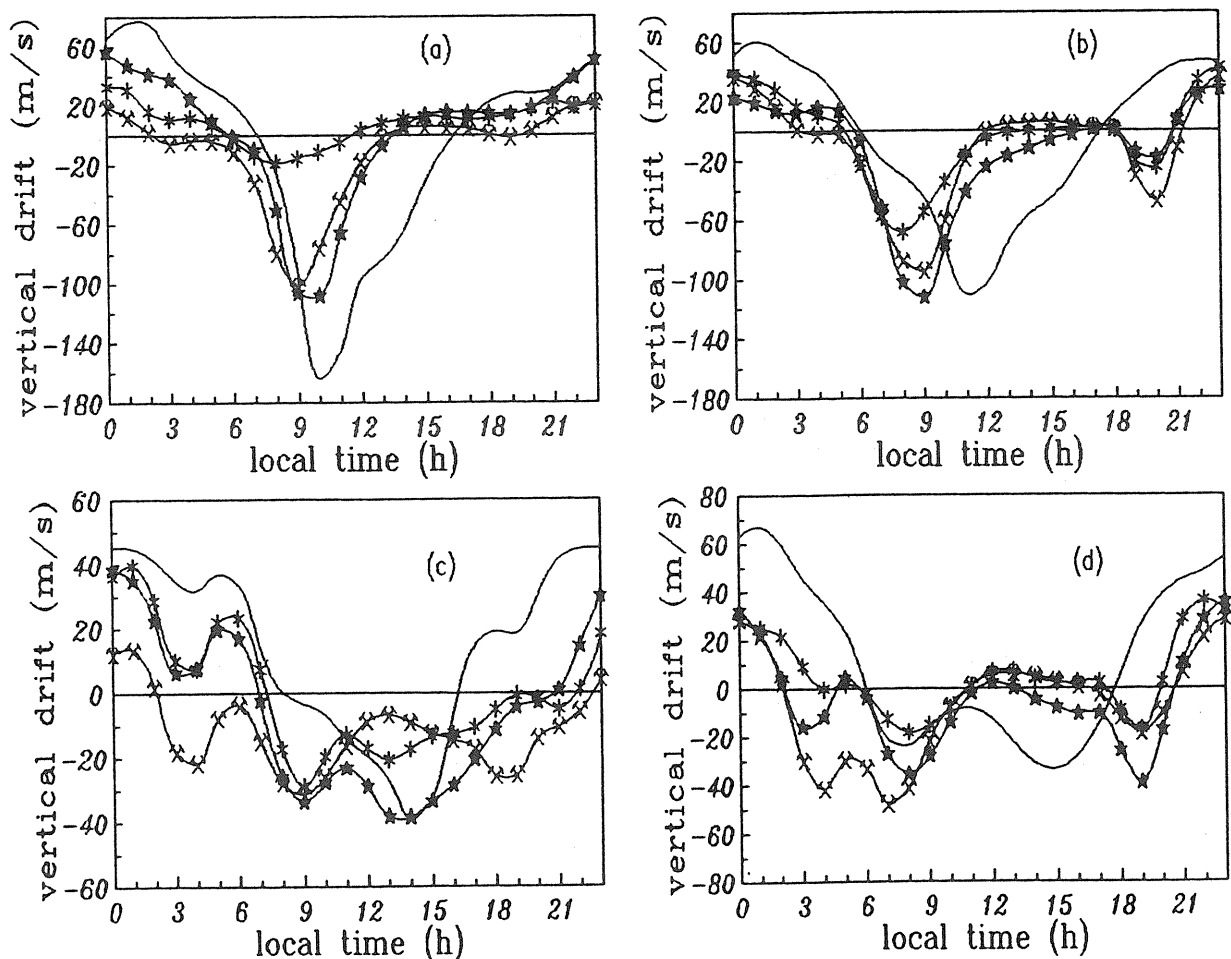
Figure 2. Diurnal variation of vertical drifts over 4 East Asian stations, at low solar activity, for four months:

2[a]	June 1986		2[c]	December 1986
2[b]	September 1985		2[d]	March 1987

The stations displayed using four line types

[i]	thin line	Wakkanai	[iii]	line with stars	Yamagawa
[ii]	line with asterisks	Wuchang	[iv]	line with crosses	Okinawa

Method and Data

The basic equation is the so-called "servo equation" (Rishbeth et al, 1978), and the related parameters are from the paper of Buonsanto et al (1989), except that the factor of O^+ - O collision frequency is assumed to be 1 instead of 1.7. This technique suffers from the shortcoming of assuming an equilibrium situation in the ionosphere for the period between sunrise and pre-noon, which might be unrealistic, as has been recently pointed out, Titheridge (1993). According to Titheridge's model study the servo balance height differs from the calculated one with more complete processes included, implying the occurrence of a non-equilibrium ionosphere. However, further work should be done to estimate the extent to which this off-equilibrium behaviour may cause significant errors in the derived vertical drift. The position of the stations is listed in table 1.

Morphology of Monthly Mean Drifts

Month-to-month and seasonal features for low solar activity

Fig 1 shows the local time vertical drifts for a full year over Wuchang. "W" shaped or its variant curves can be found. Generally, double peaks, a pre-noon one and an afternoon one occur at 8-10h and 15-18h, while 4

types can be identified and each of them corresponds to a different season. In summer, only a pre-noon peak occurs, and in autumn an additional afternoon one occurs with a small amplitude. The fluctuations dominate the winter curves. For spring, double peaks with nearly the same amplitude are clear. For the other 3 Japanese stations, similar variations can be found. These results are approximately identical to the MU radar observations of the meridional wind in trend (Oliver et al, 1990). It should be noted that the evening enhancement of the vertical drift, which is frequently observed near the low latitudes and equatorial areas (Goel et al, 1990, and the references therein), is not obvious here, even at Okinawa, whose geomagnetic latitude is 15.3°; instead, the collapse is at dawn (about 3LT or later) followed by the increasing at °5-°6LT of vertical drifts.

Latitudinal variations of abnormal drifts

Yamagawa and Okinawa have similar longitude but differ by 5 degrees in latitude, while Yamagawa and Wuchang have similar latitude but differ by 14 degrees in longitude. From Fig. 2(a) and (b), the variation for the stations with similar longitude, Yamagawa and Okinawa, is similar, and differs from Wuchang, suggesting a longitudinal dependence of the vertical drift. Since these 3 stations are located at the northern crest of the equatorial ionization anomaly (EIA), the longitudinal effects on the EIA may have to be considered, as Wakkanai is another pattern not only in amplitude but in phase, and this may be due to the obvious gap of the geographical position. It should also be noted that there exists a large downward drift at about 09h for the stations with similar longitude (Fig 2(a), (b)). This may be partly explained by the non-equilibrium in the ionosphere (Titheridge, 1993). The result for Wuhang is somewhat different at this time, suggesting a possible longitudinal difference for the ionospheric equilibrium condition.

The collapse is more noticeable in December and March under low solar activity, as shown in Fig. 2(b) and (c). The abnormal drift is much more obvious for high solar activity, as shown in Fig.3. When the collapse can be observed in all months concerned, of which March is particularly dominant, the maximum of downward drifts appears at °2LT for the first half of the year and °3LT for the other half. This behaviour becomes more pronounced, with decreasing latitude, and may an E x B contribution. These characters coincide with the evening increase in vertical drifts over some low latitudes and equatorial areas (Goel et al, 1990 and the references therein). It seems reasonable to assume a similar mechanism for the morning "collapse" as for the evening "enhancement", providing the sufficient loads (resistances) between E and F region along the line of force and also between two sides of the terminator occur under appropriate geophysical conditions. In this context, the polarized electric field may contribute to the collapse at dawn , which is driven by the east-west neutral wind and coupled with the ionospheric E region along the magnetic force lines, and is the widely accepted interpretation of the evening enhancement (Rishbeth, 1981).

Spectra of Vertical Drifts: A Case Study

A case study is carried out so as to gain an insight into the spectral structure for the vertical plasma drifts. Two sets of data are selected in the period of December 1-31,1982. For this month, the median of sunspot number R is 138, Ap index is 10, Ottawa 10.7cm solar emission flux is 201 s.f.u., and the daily Ap and F107 were obtained from the Solar Geophysical Data. The sampling interval is 1 point per hour, and the width of the Hamming window is 1024 hours.

foF2 and hmF2 Spectra

For the foF2 spectra at the 2 stations (not shown here), 24, 12, 8 and 6h components can be found with the strongest peak at 24h. The amplitude decreases as the period becomes short for Wakkanai, but it remains nearly unchanged for Okinawa. As for the hmF2 spectra (not shown here), it is much more abundant at Okinawa than at Wakkanai. Besides the tidal components, a weak peak at about 48h can be seen for Okinawa. The above results are summarized as table 2.
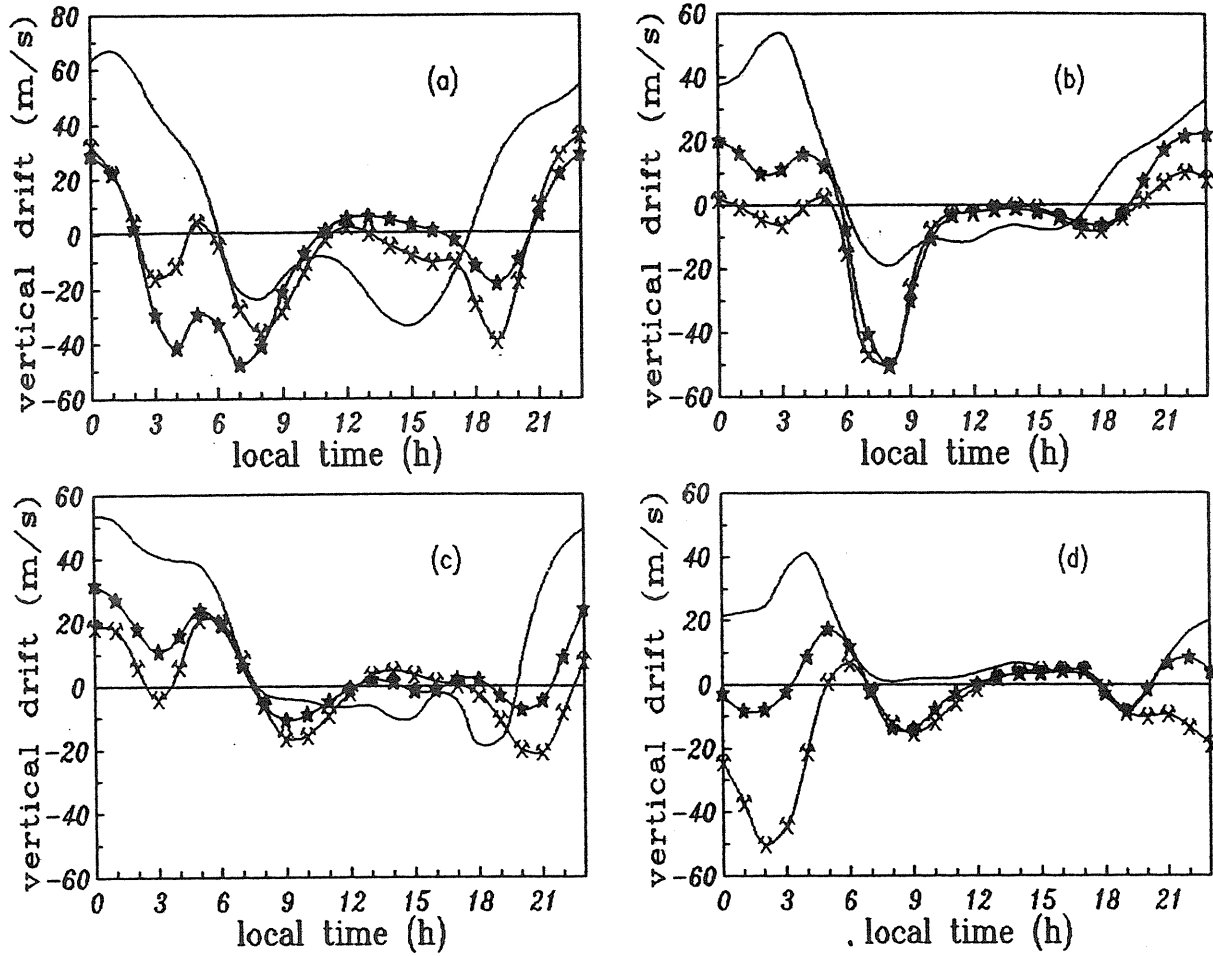
Figure 3 Same as Fig.2, except over 3 Japanese stations under high solar activity (1982)
(a) June   (b) September   (c) December   (d) March
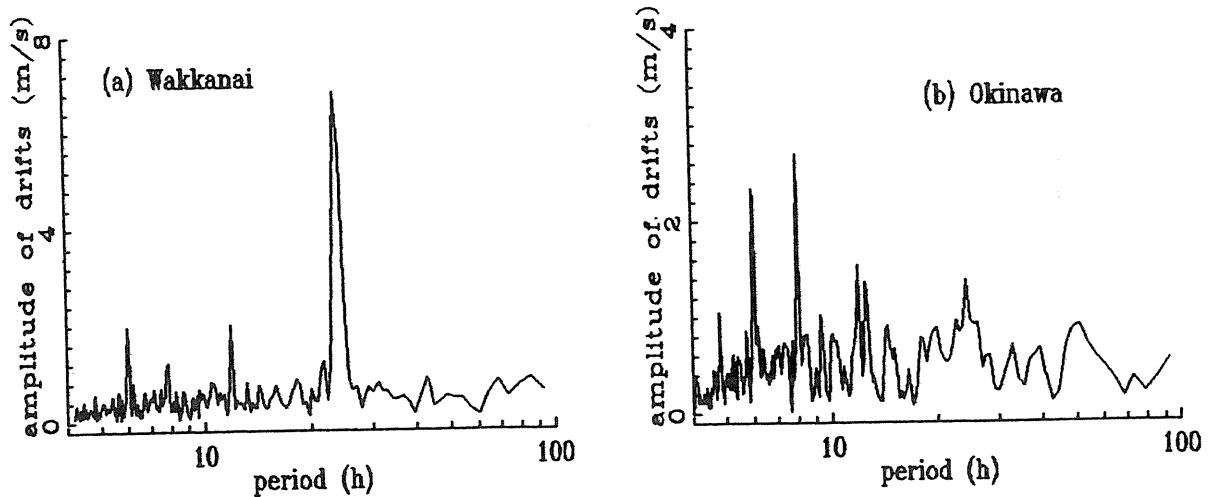
Figure 4 The spectrum for vertical drifts
(a) Wakkanai   (b) Okinawa

131

Spectra for Vertical Drifts

We pay special attention to the drift spectrum. At Wakkanai, as shown in Fig.4 (also see table 2), peaks at °6h and °12h with similar amplitude are stronger than at °8h; and the 24h component is the strongest. Components with periods greater than 24h are not obvious. At Okinawa, the strongest peak is at 8h, and the peak at 6h is also very strong; diurnal and semi-diurnal components are nearly the same in amplitude. Most important of all, a 52h (2.1 days) component can be seen. Deduced drifts contain the contribution of wind-and E x B induced drifts, however, firstly, the mid-latitude station Wakkanai does not show a 2-day component, instead, the low latitude Okinawa does; secondly, current observations in the thermosphere do not reveal the similar neutral wind oscillation with a planetary wave period of 2.1 days, therefore, it seems reasonable to ascribe the 2-d oscillation of the vertical drift to the contribution of E x B.

Table 2 Periods and Normalized Amplitude

Station	Period (hours)	6	8	12	24	48/52
Wakkanai	foF2	0.09	0.16	0.32	1	
	hmF2	0.17	0.08	0.33	1	
	drift	0.35	0.22	0.36	1	
Okinawa	foF2	0.18	0.16	0.19	1	0.15
	hmF2	0.77	1	0.74	0.99	0.69
	drift	0.86	1	0.57	0.51	0.34

Note: normalized amplitude = amplitude / Max. amplitude

As it is well known that there exists in the middle atmosphere a west-ward planetary wave frequently observed in summer and with the period of 2.1d. Chen (1992) suggested that the electric field modulated by this 2-day wave in the ionospheric dynamo region may couple into the F2 layer along the force line, and may produce the 2-day oscillation of the ionospheric characteristics through E x B drift to lift the F2 layer plasma and diffusion along the force line above the equatorial anomaly regions. If the electric field modulated by planetary waves is true, then the E x B drift, with 2-day period, should be valid on a global scale, however the ionospheric movement in the vertical direction induced by this drift may only be pronounced at the region where the dip is small, corresponding to low latitudes and equatorial areas. Our results indicate that the modulated field is likely to be present even in winter, and the related drift may act as a local source to produce the 52h component in the spectrum for the low latitude station Okinawa.

Summary

From the above discussions, we conclude that, (1) the general pattern of vertical drift induced by wind and E x B is "W"-shaped in the ionospheric F2 region over these 4 East Asia stations; and the collapse at about 3LT on the diurnal drift curve is obvious, and it is extremely marked over Okinawa for March under high solar activity conditions. This phenomenon may be caused by the polarized electric field within the F2 region; (2) a case study for the spectral structure of vertical drifts shows that the 2.1-day component, besides the usual tidal

component, is very clear over Okinawa, and it supports the assumption that a modulated electric field by planetary wave may actually emerge and result in the 2.1-day oscillation of the ionospheric characteristics.

Acknowledgement

References

Banks P. M. and G. Kockarts 1973 Aeronomy, **Academic Press**, New York

Buonsanto, M.J. 1986 .**J. Atmos. Terr. Phys**, 48, 365-373

Buonsanto M. J. 1990 **J. Atmos. Terr. Phys.**, 52 223-240

Buonsanto M. J. 1991 **J. Geophys. Res.**, 96, 3711-3724

Buonsanto M. J., J.E. Salah, K. L. Miller 1989 **J. Geophys. Res.**, 94, 987-997

Chen P. R. 1992 **J. Geophys. Res.**, 97, 6343-6357

Farley D. T., E. Bonelli, B. G. Fejer 1986 **J. Geophys. Res.**, 91,13723-13728

Forbes J. M., D. N. Anderson, I. Batista 1992 **Adv. Space Res.**, 6, (6)293-(6)301

Goel M. K., S. S. Singh and B. C. N. Rao 1990 **J. Geophys. Res.**, 95, 6237-6246

Miller K. L. and P. G. Richards 1986 **J. Geophys. Res.**, 91,4531-4535

Rishbeth H., S. Ganguly and J. C. G. Walker 1978 **J. Atmos. Terr. Phys.**, 40, 767-784

Rishbeth H. 1981 **J. Atmos. Terr. Phys.**, 43, 387

Rishbeth H. 1967 **J. Atmos. Terr. Phys.**, 29, 225-238

Oliver, W. L., S. Fukao, T. Takam et al 1990 **J. Geophys. Res.** 95, 7683-7692

Titheridge J. E. , 1993 **J. Atmos. Terr. Phys**, 48, 365-373.

Use of ground-based and satellite data for an improved procedure for testing the accuracy of ionospheric maps

P A Bradley and M I Dick

Rutherford Appleton Laboratory, Chilton, Didcot, Oxon OX11 0QX, UK

Abstract

Present methods of testing the accuracy of empirical maps of ionospheric characteristics, made from past measurements of ground-based vertical-incidence sounders, employ the same data from the same locations. A new method is proposed leading to a figure-of-merit of relative accuracy by which different mapping methods can be compared, making use of various other measurement and theoretical data sets. Proposals are made for using appropriate weighting factors to allow comparisons involving a mix of different types of measurement data.

Introduction

Planners of HF radio propagation circuits and assessors of the effects of the ionosphere on Earth-space links need long-term models of the height distributions of electron density for input to ray-tracing routines. These models have anchor points determined from predicted values of the standard vertical-incidence ionospheric characteristics given by empirical expressions fitted to past measurement data sets. The morphology of the regular E and, to a lesser extent, the F1-layer characteristics is governed by simple formulae in terms of solar-zenith angle, epoch of the solar cycle and latitude but the F2 layer exhibits more detailed structure and the most commonly used global maps of foF2 and M(3000)F2 are those generated by the Jones-Gallet numerical mapping procedure [1]. In this technique median measured data for each month of reference low and high sunspot numbers are separately mapped in terms of harmonic orthogonal Fourier functions and associated sets of numerical coefficients to give time-of-day, latitude and longitude variations. The numerical coefficients for the separate ionospheric characteristics are determined with different orders of harmonics. The maximum harmonic orders and sets of coefficients adopted (typically 988 coefficients for each month in the case of foF2) should be those for which the rms residuals between the mapped and measured values attain a lower limit.

The Radiocommunication Sector (former CCIR) of the International Telecommunication Union has adopted a set of such maps [2] based on data from some 160 measurement stations collected over the years 1954-58 and 1964. Reference values are given for twelve-monthly smoothed sunspot numbers R_{12} = 0 and 100, with an assumed linear variation in terms of R_{12} up to R_{12} = 150 and complete saturation for higher R_{12}. An example of one map of the set showing F2(ZERO)MUF = foF2 + 0.5 MHz for R_{12} = 100 is given in Figure 1. Although these maps have proved useful they suffer from a number of limitations, principal amongst which are (i) the measured data are non-uniform in geographical position and no specialised method has been produced to eliminate this potential bias, (ii) ocean regions are filled by assuming we understand the physics of the F region and by generating data given in terms of synthesised 'screen-point' values chosen to ensure that the harmonic functions remain stable in these regions and (iii) it is now possible in principle to augment old measurements with more recently collected data.

The 1984 Florence URSI General Assembly established Working Group G5, tasked to produce a new set of foF2 maps, took account of more recent vertical-sounding and satellite measurement data and applied latest thermospheric wind theory to aid in the geographical smoothing [3]. Following Rush et al [4], sets of coefficients were generated from up to 50 years of vertical-sounding data collected at the Australian Ionospheric Prediction Service, including data from the most recent years. The same maximum harmonic orders as the CCIR maps were retained to preserve software compatibility and new maps were published [5]. The URSI Working Group compared their maps and the CCIR maps with some 250,000 monthly median hourly vertical-sounding measurements. Mean differences for the separate months in both cases

JUIN - JUNE - JUNIO; 12h; R₁₂ = 100; EJF (4000) F2 (MHz)
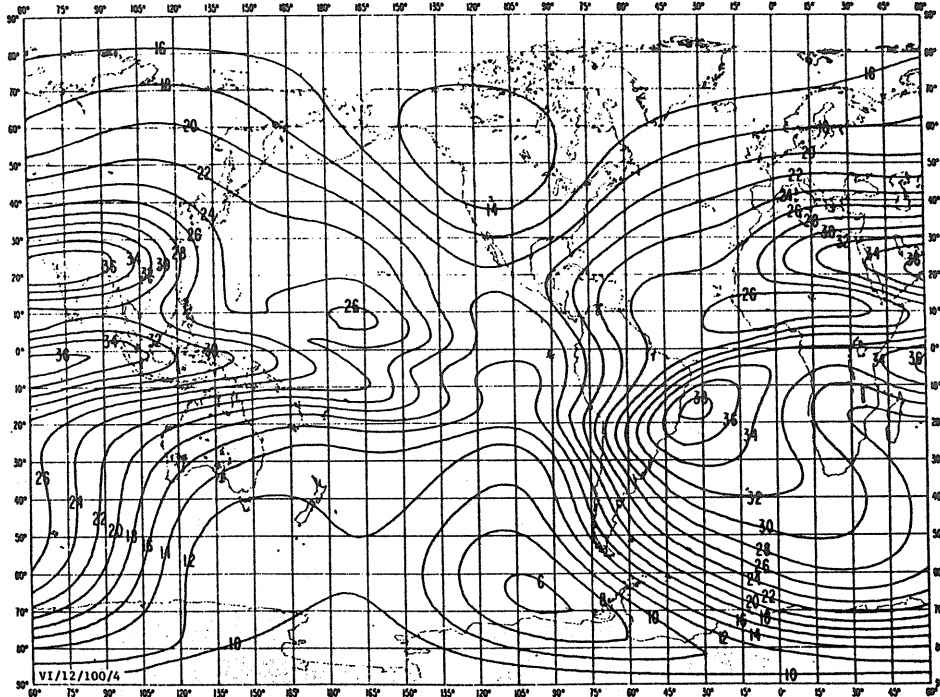
Figure 1: Sample CCIR map of predicted monthly median F2(ZERO)MUF, (MHz) for June at 12 UT with R_{12} = 100. [2]

were generally less than 0.2 MHz and standard deviations in the range 1.1-1.5 MHz. Differences for the URSI maps were marginally less than those for the CCIR maps, but despite the large data samples many of the test data were the same as those involved in the maps. In particular, to reproduce the greater ocean structure there was degrading of the fit at the measurement locations. This means that if the same criteria had been applied to the URSI maps in choosing the maximum orders of harmonics, these orders would undoubtedly have been greater than in the CCIR case, resulting in a reduction in residuals. In retrospect, noting that one of the present authors was a member of the URSI group, the decision to retain the same orders, whilst numerically convenient, turns out to have been a mistake. An additional consideration is that the method of comparison did not allow testing at the screen points.

Despite these efforts, the CCIR community would not adopt these as a replacement for the maps already in use and the position remains unchanged. Although there are no international efforts under way to generate further global maps, some studies are in train to produce improved regional maps, in particular in limited geographical areas [6]. This points to a need to review the adopted map-testing procedure. This present paper makes proposals through the use of appropriate weighting factors to allow comparisons involving a mix of different types of measurement data.

In the comparison of different types of empirical map, the question arises how to balance accuracy and complexity of approach with a reluctance to change from existing procedures. The solution has to depend on the application. Where extreme day-to-day variability exists, how accurate does the predicted median need to be? For telecommunications planning, for example, the requirements are likely to be less stringent than in following long-term ionospheric changes, perhaps related to global warming or secular drifts in the Earth's magnetic field. Ultimately the adopted approach involves subjective factors. Here we address only accuracy considerations. The aim is to formulate a figure-of-merit for the maps giving their overall relative accuracy's, rather than to quote a separate accuracy figure for the different places and times. The criteria to apply in assembling a measurement data base for map testing is also considered.

135
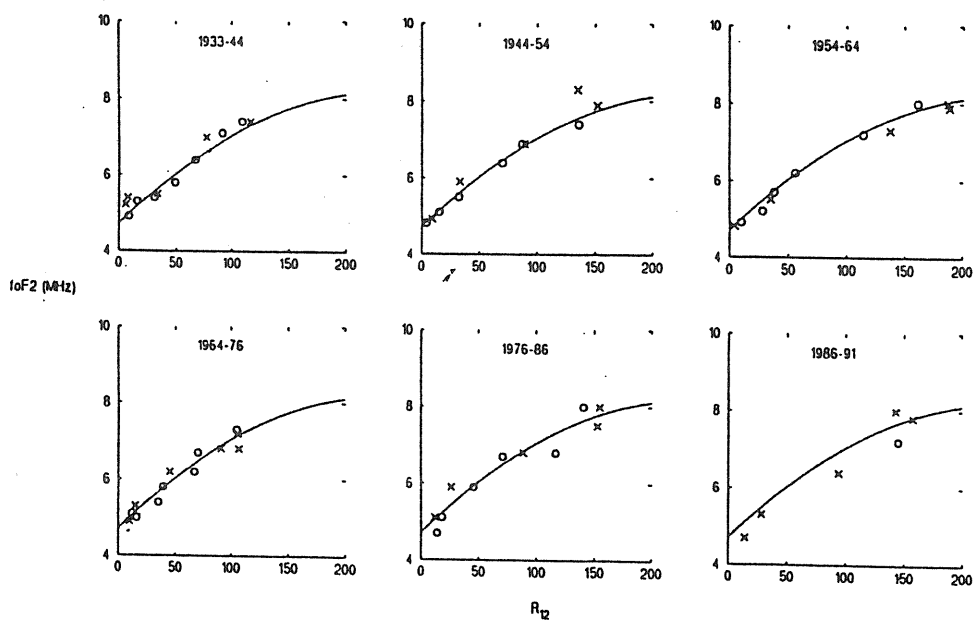
Figure 2: Variation with R_{12} of monthly median noon foF2 for Slough measurements in June for different solar cycles. (Crosses indicate data collected on the rising half cycles and circles on the downgoing half cycles). The solid curves in each case are the same, as derived from parabolic regression analysis applied to the full data set over all cycles.

Data availability

Earlier tests used only vertical-sounding data, resulting in two particular problems. The same measurement data should not be used for map generation as for map testing and ideally half the data should be applied in each role. However, in the real situation where vertical-sounding data locations are sparse, there is a tendency to employ as many as possible for map generation. This leaves an inadequate number of locations for testing, or means that greater weight is given to those locations selected for testing than those used in making the maps. In fact, the testing is undertaken with test data for the same locations as those used in map generation. Hence the accuracy's in other world areas where the maps are determined by interpolation/extrapolation procedures or theory, and may well be least accurate, are not tested. This then points to the value of examining the availability for testing using data sets from other types of measurements as shown in Table 1.

We need to consider the epochs for which data are needed. Many groups have examined the sunspot-cycle variations of monthly median foF2 for different stations and some workers [7, 8] have noted differences on the upwards and downgoing legs of a given cycle, leading to a so-called 'hysteresis effect'. Nonetheless, Bradley [9], from an examination of Slough foF2 and M(3000)F2 data since 1932, the longest sequence of available measurements, has concluded that changes between cycles and differences on the rising and falling half cycles are irregular and small in comparison with the scatter. Figure 2 is an example from these earlier results in which noon monthly median foF2 for June is shown plotted as a function of smoothed sunspot number R_{12} and displayed separately for the different solar cycles. Also given is the same curvilinear best-fit line over the whole period drawn through the data points for each cycle. Agreement is good in all cycles supporting the contention that any measurement data for any past epoch may be used for map testing.

The data used should be temporally distributed as uniformly as possible to incorporate all times-of-day, seasons and solar epochs. Testing also should cover the full geographical regions that are mapped. Vertical-sounding data cover a wide range of different years and months. This suggests the need to

136

1978,342   △UT=02H:283.00.00.00 (3204)-42.00.00.00 (4816)
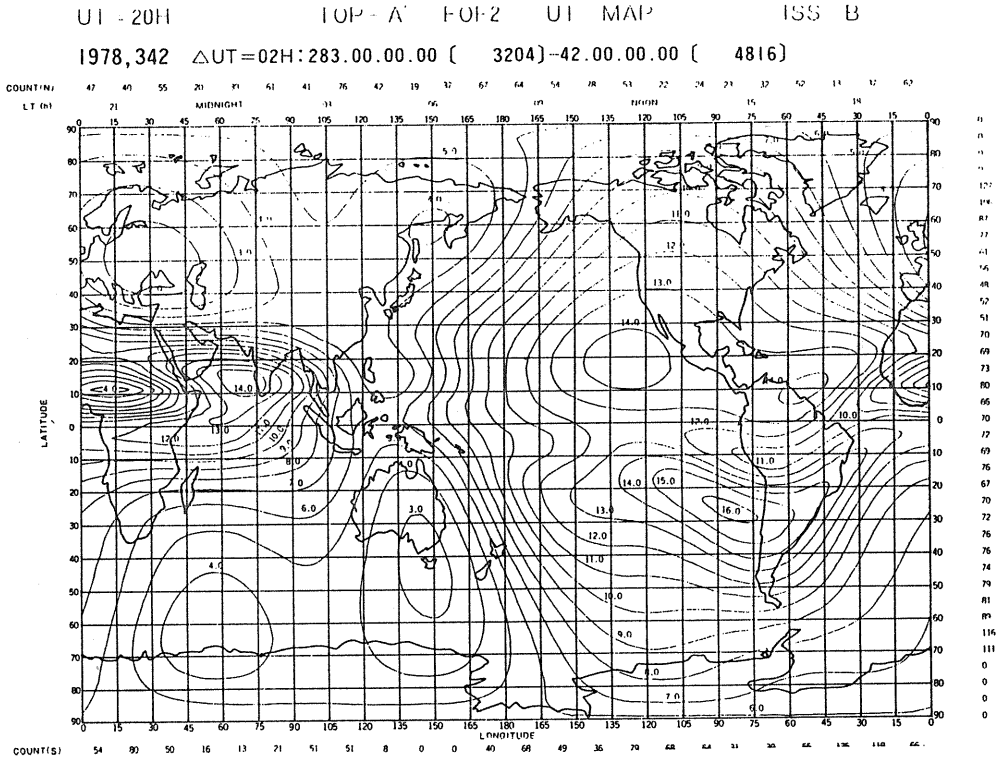
Figure 3:   foF2 map for 20UT over the period October 1978 to March 1979 determined from the ISS-b topside-sounder satellite. Contours are given at 1 MHz increments with the highest values exceeding 15 MHz.

UT=20H   TOP-A'   FOF2   OBSERVED   POINTS   ISS-B   (ALL)
1978,282 △UT=02H:223.00.00.00(2533)-346.00.00.00(3876)
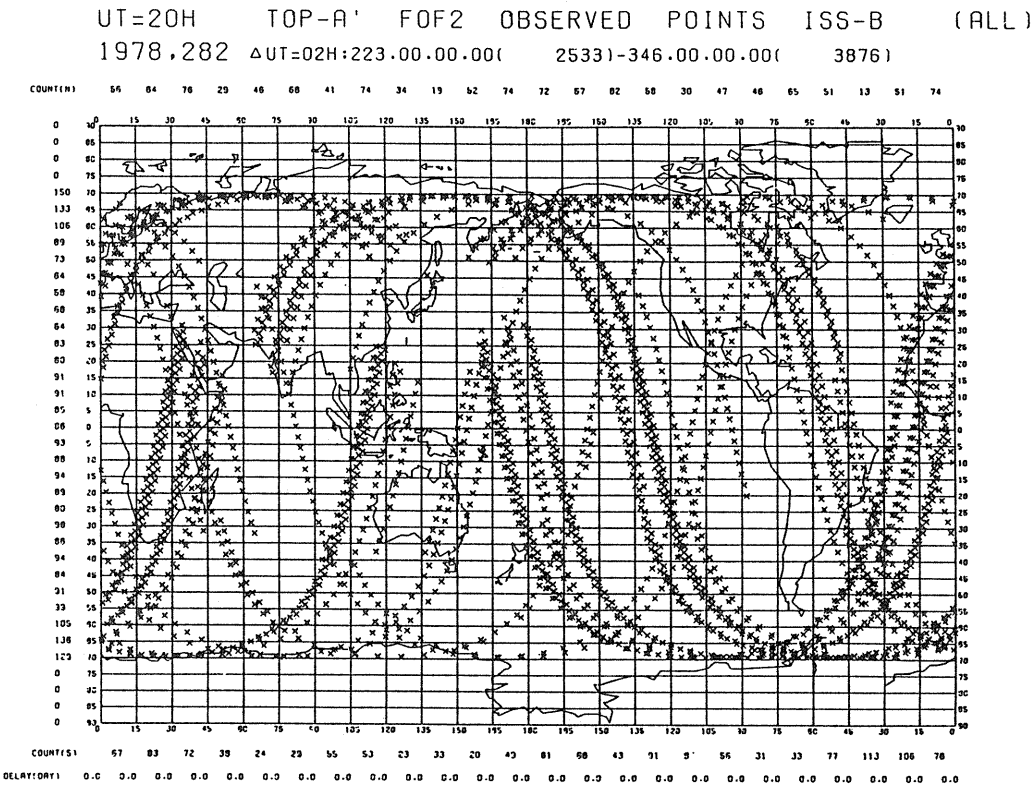
Figure 4: Tracks of the ISS-b satellite and locations of data points (crosses) used in the construction of the foF2 map for August - December, 1978.

137

weight the test data sample to provide a uniform assessment, using as many data as feasible in map testing without compromising map generation. Weighting is particularly important if limited additional measurements are made in new areas specifically for map testing.

Whereas vertical-incidence ionosondes are irregularly distributed geographically, polar-orbiting satellites offer the possibility of uniform area testing. A difficulty lies in the temporal coverage of the satellite data and in the significance of the information obtained. A most valuable data set is that provided by the Japanese ISS-b topside-sounder satellite from which constant UT maps have been constructed seasonally by combining the data for the separate orbits (Figure 3). Tests of Rush et al [5] for 65,000 data points over six separate seasons in 1978/79 resulted in rms differences of 19.2-24.5% for the CCIR maps in comparison with 16.7-21.7% for the URSI maps. There was a tendency for the CCIR residuals to be smaller over land and for the URSI residuals to be appreciably less over the Pacific Ocean. However, it should be noted that the ISS-b measured seasonal data sets each consist of around 65,000 data points, or only some 2,700 values for each UT hour. Yet, for example, with comparisons made on a 5° latitude-longitude grid this would provide just 2-3 samples per geographical cell (Figure 4), which is a gross under sampling. So there are sampling problems in using topside sounder or other satellite data that need to be compensated with appropriate weighting factors.

Bilitza [10] has reviewed the availability of satellite sounder and direct probe data. Figure 5 taken from his survey shows the lifetimes and heights of relevant satellites. Topside-sounder data were collected from the Alouette and ISIS series of satellites but synoptic data sets of foF2 were never published and the raw measurements are understood no longer to be available. Other topside soundings were collected aboard Intercosmos 19 and Cosmos 1809 satellites. At present these data are stored in original form, some with hard copy. A sample of topside height profiles has been generated [Pulinets et al, 11]. Interpretation of direct satellite plasma-probe data creates additional problems as reviewed by King [12]. Besides knowing
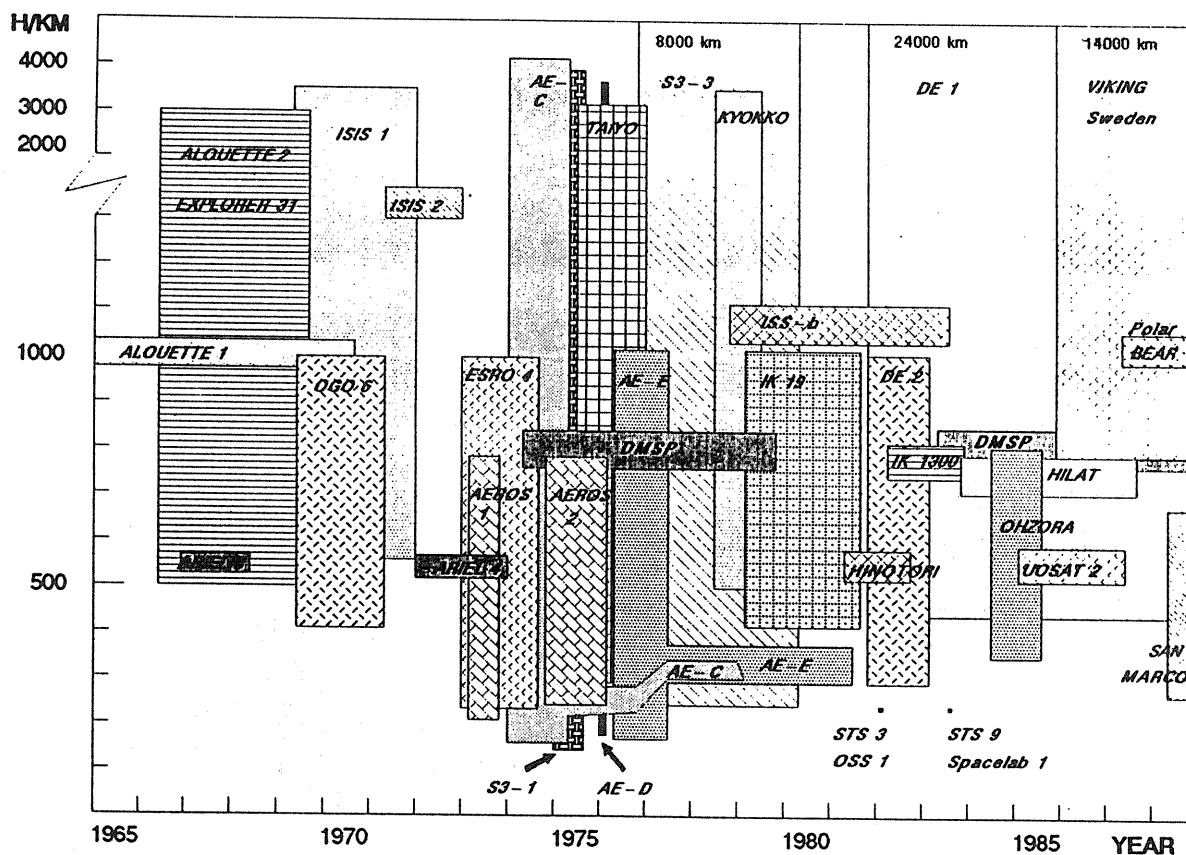
Figure 5: Altitude/time chart of ionospheric satellite measurement data [from Bilitza, 10].

the laws of extrapolation to the F2-layer peak height there are additional uncertainties in estimating that height itself. Nonetheless Kutiev and Stankov [13] have developed extrapolation techniques and applied these subject to varying approximations.

Total electron content (TEC) data exist with significant geographical coverage around each ground-based measuring site. With TEC given as the product of equivalent slab thickness and maximum plasma density and with slab thickness showing much less spatial structure than foF2, the use of an appropriate slab thickness model would enable measured TEC to be converted to corresponding foF2. To the best of the authors' knowledge this has not yet been done, perhaps because hitherto there has been no motivation. However, this possibility should be considered.

Normally incoherent-scatter radar measurements do not give absolute peak electron densities but rather relative values that are to be calibrated in terms of nearby foF2 vertical-sounding measurements. On the other hand they do yield the heights of peak densities. Empirical formulae are available (Dudeney and Kressman [14]) to relate peak height to corresponding M(3000)F2 with acceptable accuracy. Although the numbers of incoherent scatter sounders distributed throughout the world are relatively low and although these do not usually make synoptic measurements, the quantities of data that exist are considered sufficient to be of value in global map testing.

Anderson [15] has pioneered the use of semi-empirical ionospheric models in which relatively simple empirical expressions are formulated to approximate to the results of full calculations based on equations of continuity and momentum. By normalising to ground-based measurements, it is possible to use the theory to give absolute values in neighbouring regions. This technique generates considerably more ionisation structure over the oceans than is given by conventional polynomial smoothing procedures. The question arises whether it is valid to test maps using data based on the same theory as went into their generation. This is an important point, since it is over the oceans that existing maps are least accurate.

Methods exist for inverting oblique-incidence ionograms to equivalent mid path electron-density profiles [16,17], thereby yielding associated foF2 and M(3000)F2 values. However, not all ionograms are suitable for inversion because there is insufficient visible trace or because of spread effects. The assumption is usually made that there is a concentric ionosphere so that for path lengths beyond about 3000 km and for
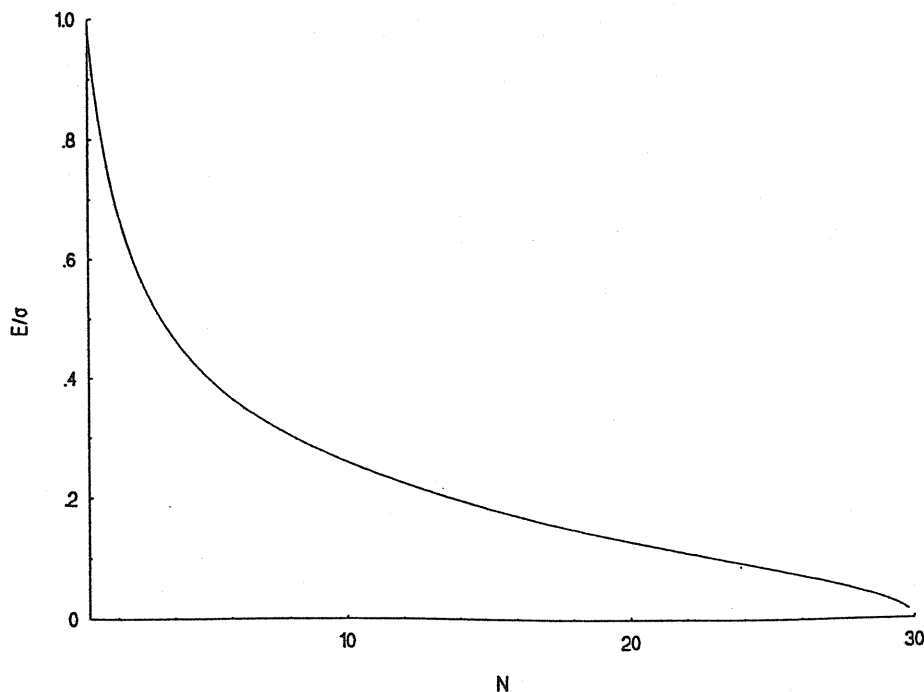
Figure 6: Ratio of standard error of sample (E) to population standard deviation (σ) as a function of number of days sampled (N).

multiple-hop propagation, procedures cannot meaningfully be applied. Inversion methods tend to be complicated so that automated implementations are complex. This means that few reliable data are available using these techniques.

We recommend the establishment of a test data set composed of as may of the above types of data as are feasible.

Weighting factors

Typically the testing data base consists of different data sets of unequal size, have different accuracy's related to the techniques and monthly sampling and cover different geographical areas. In some cases these areas will overlap, whereas other regions are relatively sparsely served (see Table 1). Any means of reconciling these separate factors is subjective. The proposals presented here apply to the combination of any number of such different test data sets where these varying considerations are taken into account by means of appropriate weighting factors. Suggestions are offered for values of the weighting factors.

TABLE 1 - Relative quantities of available test data, their inherent accuracy's, monthly sampling and numbers of locations for which they apply

Data Source	Quantity	Inherent Accuracy	Monthly Sampling	Numbers of Locations
Routine vertical ionosondes	Much	Good	Good	Many
Temporary ionosondes	Little	Good	Poor	Few
Satellite probe	Medium	Medium	Medium	Many
Topside sounder	Medium	Good	Medium	Many
TEC	Medium	Medium	Medium	Medium
Incoherent scatter	Little	Good	Medium	Few
Theory	Infinite	Poor	Perfect	Infinite
Oblique ionograms	Little	Medium	Poor	Few

Weighting factors need to take account of inherent data usefulness from a location standpoint; the daily sampling and accuracy. In formulating numerical values for the weighting factors the dominant influences are reviewed.

location

If test data relate to nearby locations at the same time eg two adjacent ionosondes or measurements along a satellite track, then the weighting should be diminished in inverse proportion to the quantities of such data. On the other hand, as separation increases the data sets become independent and should have full weighting. According to Edwards et al, [18] the correlation distance for foF2 fluctuations about the monthly median is typically some 500 km in a N-S direction and 1000 km E-W. Other ionospheric characteristics vary over comparable or enlarged distances. So it is proposed to define an array with each element corresponding to a geographical area of size 5° in latitude by 10° in longitude where the number of such elements depends on the extent of the region mapped. For a given epoch, all test data, within an element, are weighted by the number of other values within that element for that epoch. Satellite data will

be quantised to one value at the centre of the area for each time. Thus $W_{location}$ is the weighting factor for location and

$$W_{location} = 1/S \qquad (1)$$

for S sets of data

daily sampling

Sampling accuracy effects on estimates of the monthly median value derived from a limited number of daily samples can be assessed [19] assuming a normal law of variation of the daily values. The standard error E for a sample of D days drawn from a population of standard deviation σ is determined as:

$$E = \sigma \sqrt{\frac{1}{D} - \frac{1}{30}} \qquad (2)$$

This equation states (Figure 6) that E tends to zero as the sample size rises to 30 days. E remains relatively low for sample sizes exceeding 5-10 days, but increases for smaller samples. It is appropriate to adopt a weighting factor which is the inverse of the standard error with a limiting maximum of 10: i.e.

$$W_{sampling} = \frac{1}{\sqrt{\frac{1}{D} - \frac{1}{30}}} < 10 \qquad (3)$$

accuracy

Somewhat arbitrarily an accuracy weighting factor, $W_{accuracy}$, is proposed and values are given in Table 2.

TABLE 2 -Proposed values of $W_{accuracy}$

Data Source	$W_{accuracy}$	Reason
Fixed vertical ionosondes	1	arbitrary
Temporary ionosondes	1	same as above
Topside sounder	1	data availability?
Satellite probe	0.7	some interpretation problems
TEC	0.7	slab height model needed
Incoherent scatter radar	1	limited data sets
Theory	0.5	depend on complexity of approval
Oblique ionograms	0.7	some interpretation problems

Now suppose for a given time period and element there are n_i test data values of type i each derived from D days of sampling. Then the overall weight factor associated with these can be taken as:

with the separate terms given as above.

Proposed procedure

For a uniform set of N test data values, each of equal weight, the figure-of-merit F is taken as the standard deviation between the test data and mapped values -

$$F = \sqrt{\frac{1}{N-1}\left[\sum_N (T-M)^2 - \frac{1}{N}\left(\sum_N (T-M)\right)^2\right]} \qquad (5)$$

where   T = test data value

M = mapped value

The map with lowest F is taken as the best. If the test data, for example, are daily values and the mapped figures are regarded as monthly medians, then equation (5) provides an indication of the accuracy of the maps on a given day. In the present application it is assumed that the test data are estimates of the monthly median values so F is a smoothed figure having relative rather than absolute significance.

Equation. (5) can be extended to the case where the separate data have different weights. Suppose there are C classes of data composed of N_c values with weighting W_c. Then we have that -

$$F = \sqrt{\frac{1}{(\sum_c W_c)-1}\sum_c \frac{W_c}{N_c-1}\left[\sum_{N_c} (T-M)^2 - \frac{1}{N_c}\left(\sum_{N_c} (T-M)\right)^2\right]} \qquad (6)$$

Equation (6) applies where the separate classes correspond to different data sources and test locations and the respective values to the various times-of-day, season and solar epoch encompassed within the test.

Conclusions

The problems of limited sampling and associated significance of comparison results, as for example in the case of use of topside-sounder data cited above, highlighted the need to adopt a procedure, of the type described, for future mapping accuracy assessments. Future work will apply the above procedure to test various alternative mapping methods [eg 20-23] being developed under EEC project COST 238 (PRIME) [6]. Consideration might also be given to a reassessment of the existing URSI and CCIR maps by this approach.

Acknowledgments

References

1. Jones, W.B., and Gallet, R.M., 1962 'Methods for applying numerical maps of ionospheric characteristics', **J Res NBS-D,66D**, 649-662.
2. CCIR Report 340, 'CCIR atlas of ionospheric characteristics', **ITU**, Geneva, 1990.
3. Rush, C.M., PoKempner, M., Anderson, D.N., Stewart, F.G., and Perry, J., 1983 'Improving ionospheric maps using theoretically derived values of foF2', **Radio Sci**, 18, 95-107.
4. Rush, C.M., PoKempner, M., Anderson, D.N. ,Perry, J., Stewart, F.G., and Reasoner, R., 1984 'Maps of foF2 derived from observations and theoretical data', **Radio Sci**, 19, 1083-1097.
5. Rush, C.M., Fox, M., Bilitza, D., Davies, K., McNamara, L., Stewart, F., and PoKempner, M., 1989 'Ionospheric mapping: an update of foF2 coefficients', **Telecomm. J**, 56, 179-182.

6. Bradley, P.A., 1993 'COST-PRIME (Prediction and retrospective ionospheric modelling over Europe)', INAG 59, 12-16, WDC-A Boulder, Colorado 80203, USA.

7. Mikhailov, A.V., 1993 'On the dependence of monthly median foF2 on solar activity indices', **Advances in Space Research**, 13(3), 71-74.

8. Adler, N.O., Ezquer, R.G. and Manzano, J.R., 1993 'On the relationship between ionospheric characteristics and solar indices', **Advances in Space Research**. 13(3), 75-78.

9. Bradley, P.A., 1993 'A study of the differences in foF2 and M(3000)F2 between solar cycles', Proceedings of the PRIME COST 238 Workshop, **Wissenschaftlicher Bericht** 2, 67-77, Karl-Franzens Universitat, Graz, Austria.

10. Bilitza, D., 1989 'The worldwide ionospheric data base', National Space Science Data Center, **WDC-A Report** 89-03, Goddard Space Flight Center, Washington DC.

11. Pulinets, S.A., Karpachev, A.T. and Shoya, L.D., 1993 'The role of topside sounding in modelling the topside of the ionospheric F-region: the present situation and future possibilities', Proceedings of the PRIME COST 238 Workshop, **Wissenschaftlicher Bericht** 2, 29-37, Karl-Franzens Universitat, Graz, Austria.

12. King, J.W., 1973 'The determination of foF2 and hmF2 from satellite-borne probe data', **Telecomm J**, 40, 364-368.

13. Kutiev, I., and Stankov, S., 1992, 'Satellite data for use in the ionospheric mapping', Proceedings of the PRIME/URSI joint Workshop on 'Data validation of ionospheric models and maps (VIM),' **Memoria**, COST 238TD(93)001, 100-104.

14. Dudeney, J.R., and Kressman, R.I., 1986, 'Empirical models of the electron concentration of the ionosphere and their value for radio communications purposes', **Radio Sci**, 21, 319-330.

15. Anderson, D.N., 1993 'Global ionospheric modelling', Modern Radio Science, **Oxford Science Publication**, Oxford, UK, 159-188.

16. Gething, P.J.D., 1969 'The calculation of electron density profiles from oblique ionograms', **J Atmosph Terr Phys**, 31, 347-354.

17. Krasheninnikov, I.V. and Liannoy, B.E., 1990 'Estimation of the true ionospheric height profile', **J Atmosph Terr Phys**, 52(2), 113-117.

18. Edwards, W.R., Rush, C.M., and Miller, D.M., 1975 'Studies on the development of an automated objective ionospheric mapping technique', **Air Force Surveys in Geophysics** No 302, AFCRL-TR-75-0124, Air Force Cambridge Research Laboratories, Bedford, Mass 01730, USA.

19. CCIR Report 253, 'Measurements of sky-wave signal intensities at frequencies above 1.6 MHz', ITU, Geneva, 1990.

20. Zolesi, B., Cander, Lj.R., and De Franceschi, G., 1991 'Mapping of some ionospheric characteristics over a restricted area using SIRM', Seventh International Conference on Antennas and Propagation, **IEE Conference Publication** 333, 512-515.

21. De Santis, A., De Franceschi, G., Zolesi, B., Pau, S., and Cander, Lj.R., 1992 'Regional mapping of the critical frequency of the F2 layer by spherical cap harmonic expansion', **Ann. Geophysicae**, 9, 401-406.

22. Singer, W., and Taubenheim, J., 1990 'Application of the expansion into empirical orthogonal functions to ionospheric characteristics', **Advances in Space Research**, 10(11), 59-64.

23. Teryokhin, Yu.L., and Mikhailov, A.V., 1992 'A new approach to solving the problem of a spatial approximation of the field of observed foF2 values', **Geomag and Aeronomy**, 32(2), 205-210.

OBLIQUE IONOSPHERIC SOUNDING WITH AN ANALYSIS OF SIGNAL LEVELS

Donat V. Blagoveshchensky
State Academy of Aerospace Instrumentation
67 Bolshaya Morskaya Str., St. Petersburg, RUSSIA, 190000
(FAX: (7)+812 315-77-78)

Vladimir M. Vystavnoi
Arctic and Antarctic Research Institute
38 Bering Str.. St. Petersburg, RUSSIA, 199397
(FAX: (7)+812 352-26-88)

Abstract

HF radio signal propagation conditions were analysed on a sub auroral radio path, Moscow-Dixon, using the signal intensity. Regular changes in the redistribution of signal amplitudes during substorms and the influence of the main ionisation trough are described.

Introduction

The behaviour of the ionosphere and HF wave propagation parameters and their possible changes can be described using ionospheric oblique sounding (IOS) data. With the help of this method the maximum observed frequency (MOF), the maximum useable frequency (MUF), the lowest observed frequency (LOF), the number of propagation modes and the signal delays can be determined. In the Arctic and Antarctic Research Institute there is a system allowing ordinary IOS ionograms to show, in addition, the distribution of signal levels for every mode in the range of radio frequencies from 3.5 to 27.5 MHz (Blagoveshchensky and Vystavnoi, 1991). The signal level is displayed as the vertical extent of the oblique ionogram trace. Thus, the value of the IOS equipment is enhanced by the new parameter.

Examples of IOS ionograms, with signal levels, for three geophysical conditions for high latitudes are shown in Figures 1, 2 and 3. Experimental investigations were conducted on the high-frequency radio path Moscow-Dixon, with a length of 2,700 km. The measuring equipment and receiving and transmitting antenna characteristics were taken into account (Vystavnoi 1978). Data for winter (beginning of 1978) were analysed and the following problems were considered:

a)   signal amplitude behaviour was described for ionospheric disturbances during periods of magnetospheric substorms and magnetic storms,

b)   the influence of the main ionisation trough on the character of signals at the reception point was described.

Main Results and Discussion

In contrast to the earlier analysis of IOS ionograms during substorms and magnetic storms (Blagoveshchensky and Zherebtsov, 1987; Blagoveshchensky et al., 1992) where only the MOF, MUF and LOF were examined, the present investigation is concerned with variations in signal amplitude over the frequency range from 3.5 to 27.5 MHz, i.e. over the oblique sounding range. The ionograms studied were recorded during the winter nighttime in medium solar activity conditions. Ionograms recorded during periods of substorms, magnetically quiet periods and also continuous, gradual commencement storm periods were compared. Using all the data for winter, 1978, general features in the signal amplitude variations were revealed which can be observed in ionograms such as Figures 1, 2 and 3 which are typical of the different geophysical conditions. The sequence of ionograms, showing time delay (distance) versus frequency, during

144

a single intense substorm is presented in the first figure. The second figure shows quiet conditions and the third is a sequence of ionograms during a storm of medium intensity. The ionograms were recorded between 14 to 21 UT on the 10th (Figure1), 11th (Figure2) and 12th (Figure3) of February 1978.

During the substorm (Figure 1), compared to the quiet period (Figure 2), the following is observed. The substorm is characterised by the AE index and the abrupt onset of the substorm occurs at 18 UT, this time being referred to as T = 0. About 4 hours before, at 14 UT, the signal amplitude begins to increase, mainly in the high-frequency range. Three hours before T = O, at 15 UT in both Figures 1 and 2, there is a considerable increase in HF signal level in part of the frequency range, extending to low frequencies. Two hours before T = O, at 16 UT, the whole frequency range is characterised by a raised signal level compared with the quiet period. Such regularity in amplitude variations is caused, most probably, by normal ionisation at the upper ionospheric layers and then particle precipitation in the lower ionospheric layers. Consequently, the signals are stronger near the MUF than through the whole frequency range when precipitation increases. Directly before T = 0, at 17 UT, the signal amplitude through the whole range corresponds to the quiet level. Immediately after T = 0, the signal gradually becomes weaker and during the substorm it becomes extraordinarily small, because of the increasing absorption starting at 18 UT and continuing through 19 and 20 UT. By the end of the substorm, the reflection picture is similar to the corresponding quiet period, at 21 UT.

A longer storm, of medium intensity with a gradual commencement is presented in Figure 3, and is characterised by the following features. Here also, 3 hours before T = 0 (16 UT in Figure3), the signal becomes intense in the lower part of the HF frequency range, and the intensity of the signal also increases in the lower frequency range, then 1 hour before T = 0, the intensity approaches the corresponding quiet period levels at 14 and 15 UT. After T = 0, the signal is absorbed in the low-frequency region and is absent from ionograms at 17 to 21 UT. However, as the comparison shows most clearly, the indicated effects of increasing signal intensity and absorption and its disappearance are displayed more clearly for a single impulsive substorm than for the gradual commencement storm.

The Influence of the Main Ionisation Trough

In quiet conditions (Figure2), on average, the path intersects the trough from 18 UT and onwards through the night. The character of the reflected signal becomes ill defined; here and there diffuse without definite regularities. The frequency range with the intense signals is limited to only a few megahertz. The maximum observed frequencies do not exceed 8-9 MHz. Since the average reflection point of the path has a corrected geomagnetic latitude $\Theta=59.6°$, during the night in the absence of a disturbance, this point will never extend into the northern boundary of the trough or the auroral zone. That is why the picture of reflections observed on ionograms during the entire night remains approximately identical to the 19-21 UT period in Figure 2.

During disturbances, the situation changes. First of all, when the disturbance intensity increases, the average reflection point of the path intersects the trough earlier, for example, at 17 UT in Figure 3. In the second place, the average reflection point of the path extends into the northern boundary of the trough, beginning from 19 UT. Reflections maintain a stable maximum signal character and lie in the range 10 to 14 MHz. Ionograms show diffuse structure from 19 UT (Figure 3) because the signal is reflected from the equatorial boundary of the diffuse precipitation zone, which forms the poleward edge of the main ionisation trough. At 20 UT the signal becomes intense and pronounced. After 21 UT, diffuse reflection structure is obtained again before the transition of the average reflection point of the path from the northern boundary of the trough into the auroral activity zone.

Conclusion

(i) New data about the redistribution of signal levels during the growth phase of a pre-midnight substorm, with sharp onset, were shown. About 3-4 hours before the moment of onset, parameterised by the AE-index at T = O, there is a signal intensification at frequencies approximately from 15 MHz to 25 MHz.

Two hours prior to T = O there is a more intense increase in signal level at frequencies less than 15 MHz, i. e., in the low-frequency part of the oblique ionogram.

(ii) The influence of the main ionisation trough on the Moscow to Dixon path at first appears to show diffuse signals. Then there are steady reflections from the northern wall of the trough. Once again there are diffuse signals. The range of steady reflections falls in the range of a few megahertz and its temporal position is determined by the disturbance level.

References

1. Blagoveshchensky D.V., Bystavnoi V.M. Investigation of the oblique sounding signal structure on high-latitude radio tone. **Studies on Geomagnetism, Aeronomy and Solar Physics**, Moscow. Nauka, v.93, pp. 92-100, 1991.

2. Vystavnoi V.M. Two Methods of Amplitude Characteristics Investigation of Ionosphere Oblique Sounding Signals. Trudy AANII, Leningrad, **Gidrometeoizdat**. v.351, pp.45-52, 1978.

3. Blagoveshchensky, D.V., Zherebtsov, G.A. High-Latitude Geophysical Phenomena and Prediction of HF Radio Channels, Moscow. **Nauka**, p.272, 1987.

4. Blagoveshchensky, D.V. et al. High Latitude Ionospheric Phenomena Diagnostics by HF Radio Wave Propagation Observations. **Radio Sci.**, v.27, N 2, pp. 267-274, 1992.

Figure 1   Sequence of ionograms during a single intensive substorm

147
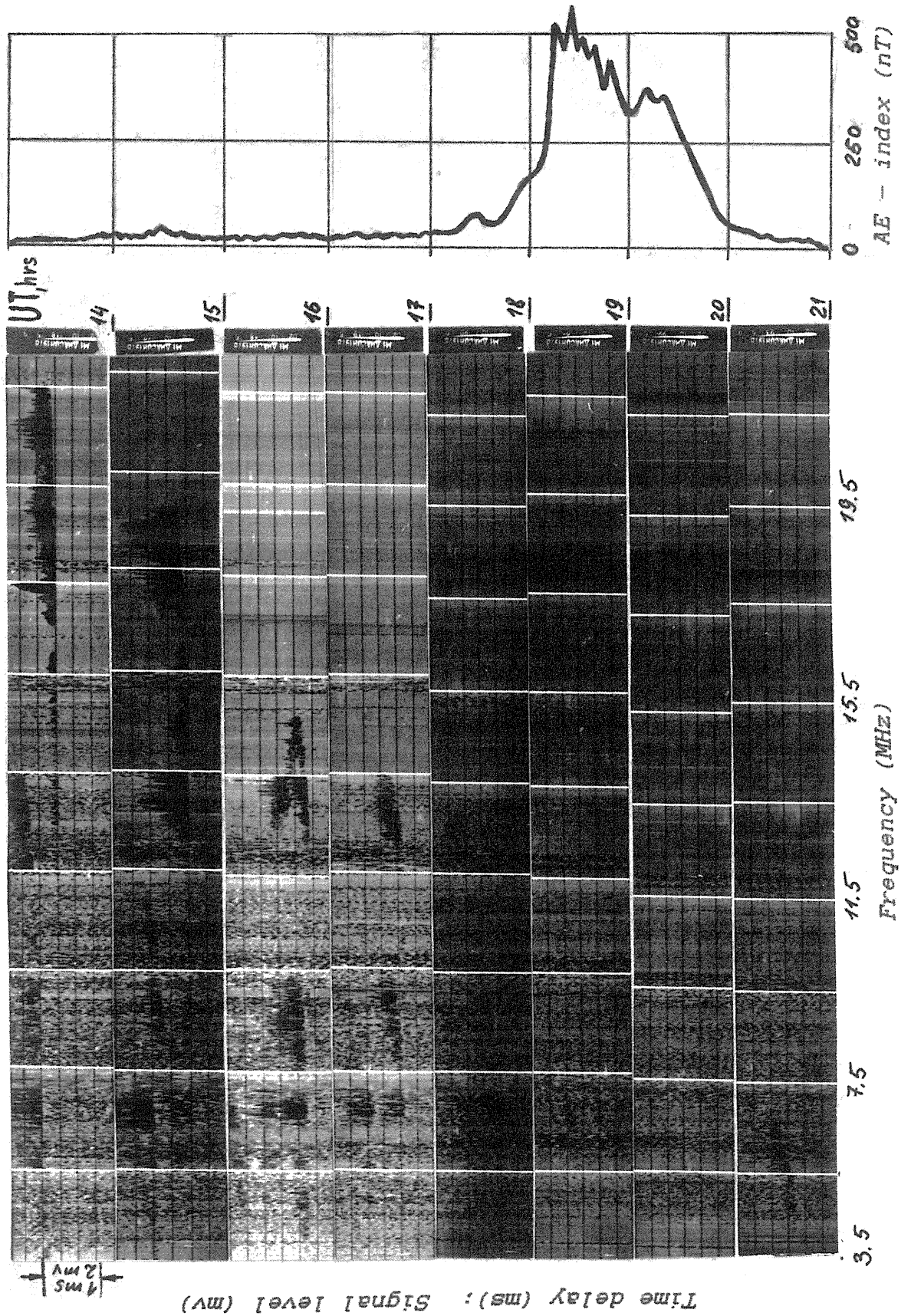
Figure2   Sequence of ionograms in quiet conditions
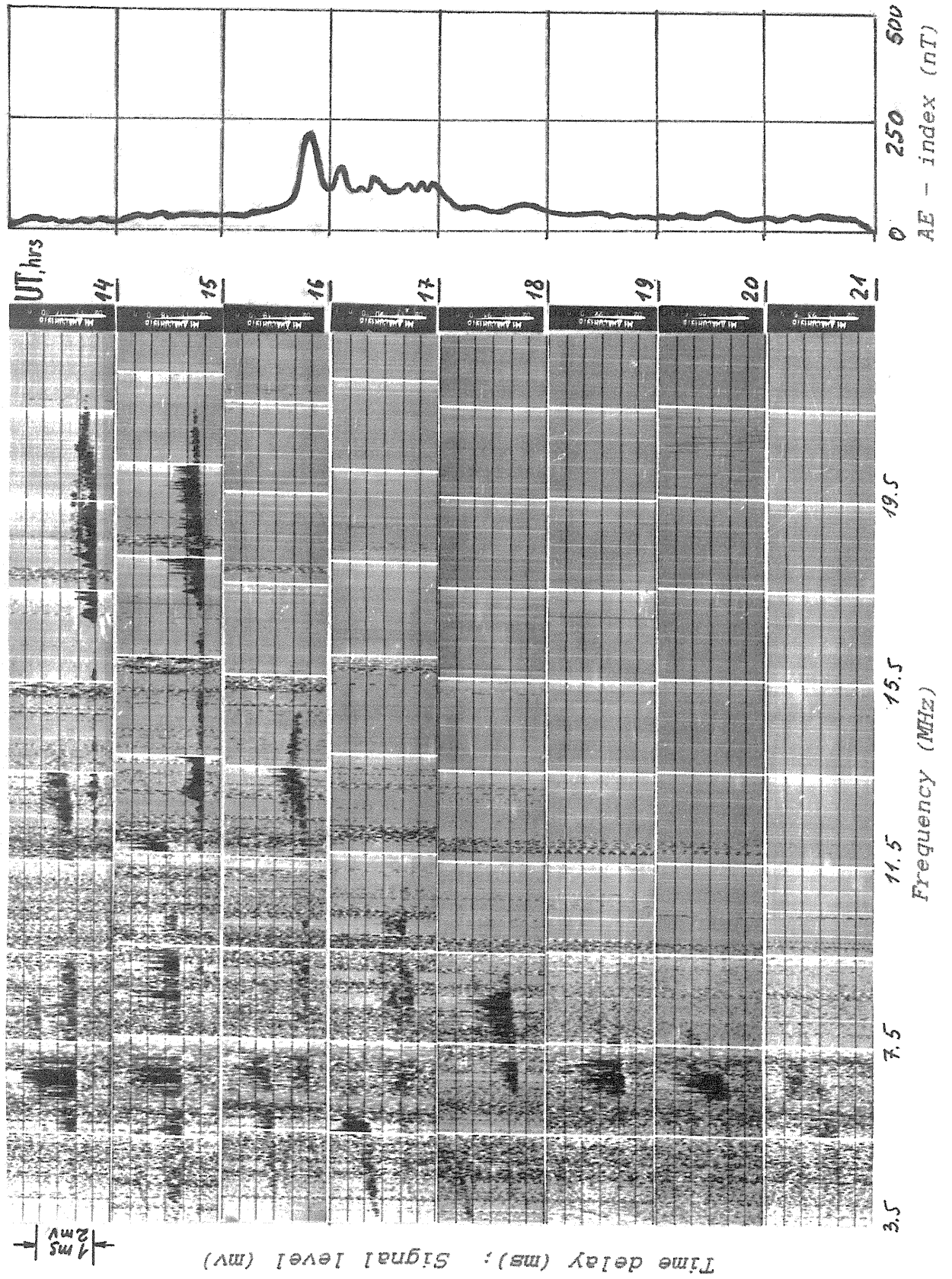
Figure3 Sequence of ionograms during a medium intensity storm.
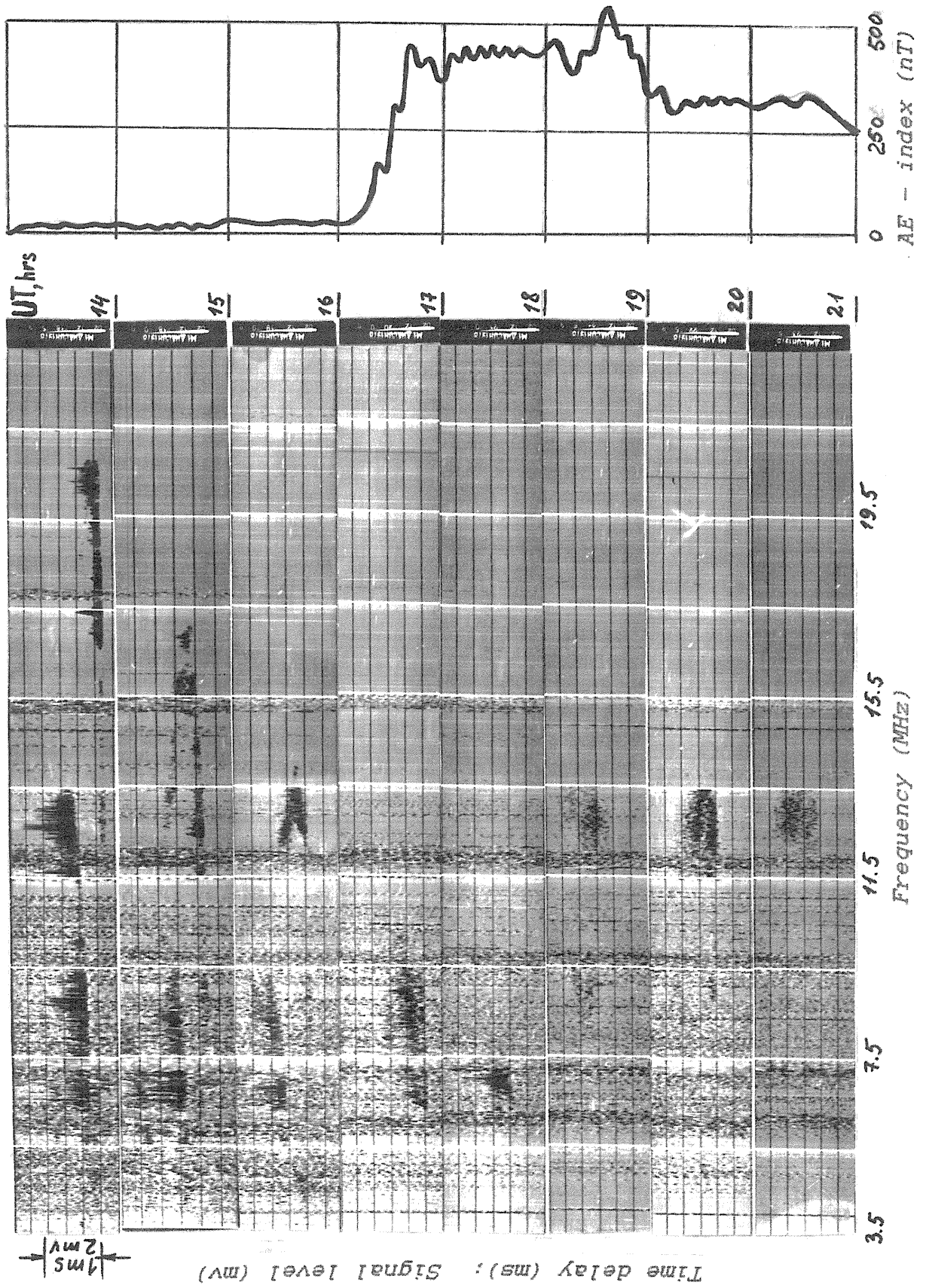
TRANSIONOSPHERIC RADIO SOUNDING AND NH-PROFILE DETERMINATION

N.P. Danilkin,
Fedorov Institute for Aplied Geophysics, 9, Rostokinskaya, Moscow, 129226,
Russia ,
phone/ fax(095) 2889502, telex: 411914 ZEMLA SU , e-mail:
geophys@sovamsu.sovusa.com
C.L. Tolsky
Jet Infosystems, PB 45, Moscow, 103006, Russia,
phone (095)9721182, fax (095)9720791, e-mail: costya@jet.msk.su

Introduction.

The first papers on transionospheric sounding (TIS) were published nearly twenty years ago. Nevertheless western scientists had little information about this method, its apparatus and results. This paper contains brief descriptions of the TIS-method, ionograms and Nh-profile results.

Transionospheric sounding.

TIS applies to radio waves passing through the ionosphere at frequencies above the penetration frequency.

Direct TIS uses a transmitter on board a satellite and a ground-based receiver. A ground-based ionosonde
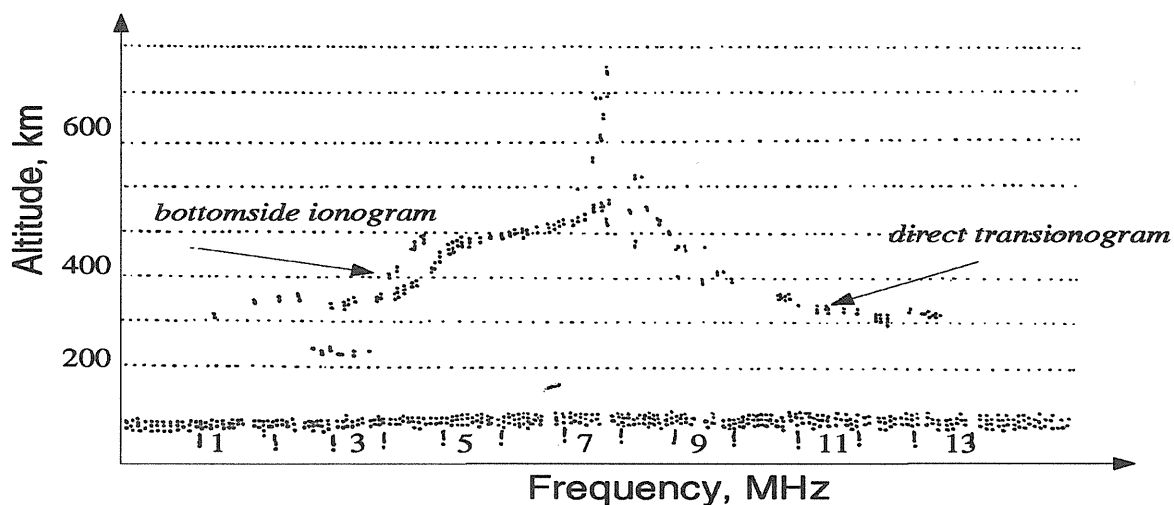
FIGURE 1
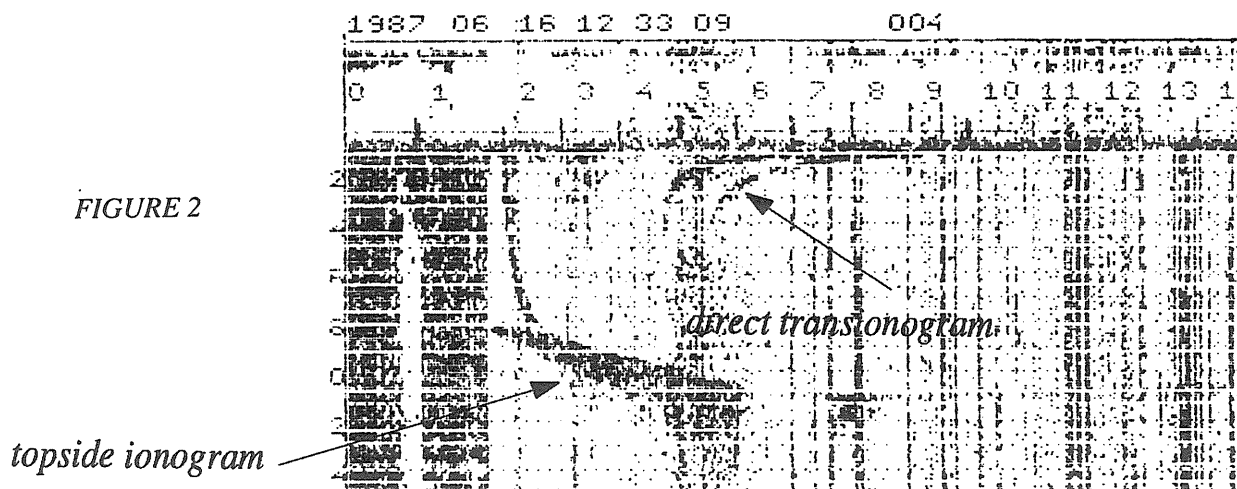
FIGURE 2

topside ionogram

can be used as the receiver. In this case the transionogram and botomside ionogram can be observed together (see Figure 1). The other way to obtain the direct transionogram is to use the special receiver. In this case the transionogram can be single or combined with topside ionogram (see Figure 2).
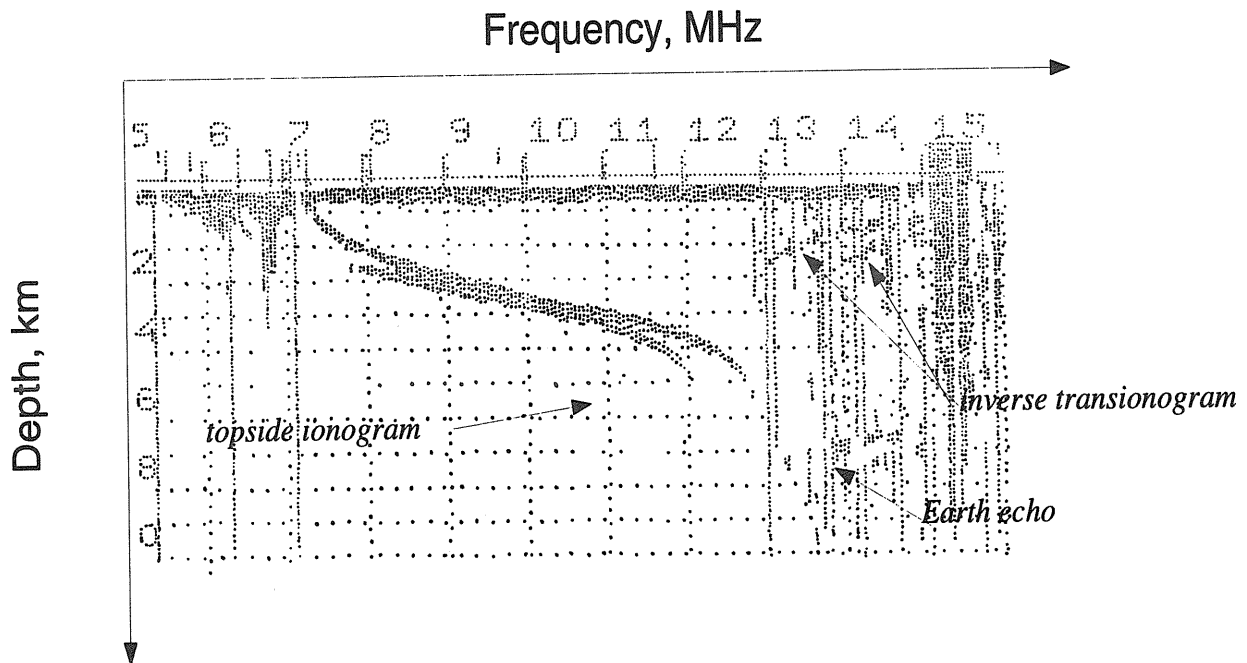
FIGURE 3

In the case of inverse TIS, a ground-based transmitter and an on-board receiver are used. Usually the inverse transionogram is combined with the topside ionogram. Figure 3 shows an example of this ionogram.

The Earth echo is often seen on the satellite ionogram. To obtain this kind of ionogram we do not need any equipment besides the satellite ionosonde. This kind of transionogram was obtained before the TIS was proposed.

To obtain the direct and inverse transionogram it is necessary to synchronise the transmitter and receiver. During experiments on "Intercosmos-19" and "Cosmos-1809" the high frequency radio pulses of telemetry were used for synchronisation.

The Nh-profile determination.

To determinate Nh-profile it is necessary to solve the equation

$$p'(f) = \int_{\Xi} \mu' \left(N, f, \frac{r}{r} \right) ds \tag{1}$$

where Ξ is the trajectory of radio wave,

p' is group path,

μ' is group refraction index,

N is electron density,

f is frequency,

$\frac{r}{r}$ is radius-vector.

There are two unknown objects in this equation: Nh-profile and the radio wave trajectory. In the case of vertical TIS (Earth echo) the trajectory is known and can be considered as a vertical line. That is why all

known methods of Nh-profile calculation using TIS solve this problem for the vertical TIS case. Non-vertical TIS is not less accurate for electron density profile determination but TIS is still useful for this purpose in regions where are no ground-based stations.

In the case of vertical TIS the equation (1) can be transformed to the next form.

$$p'(f) = \int_{o}^{hs} \mu'(h)dh \qquad (2)$$

where h_s is the satellite altitude.

FIGURE 4

altitude, km (y-axis, 150 to 550)

electron density, $10^6 cm^{-3}$ (x-axis, 0 to 20)

Earth echo

Incoherent scatter
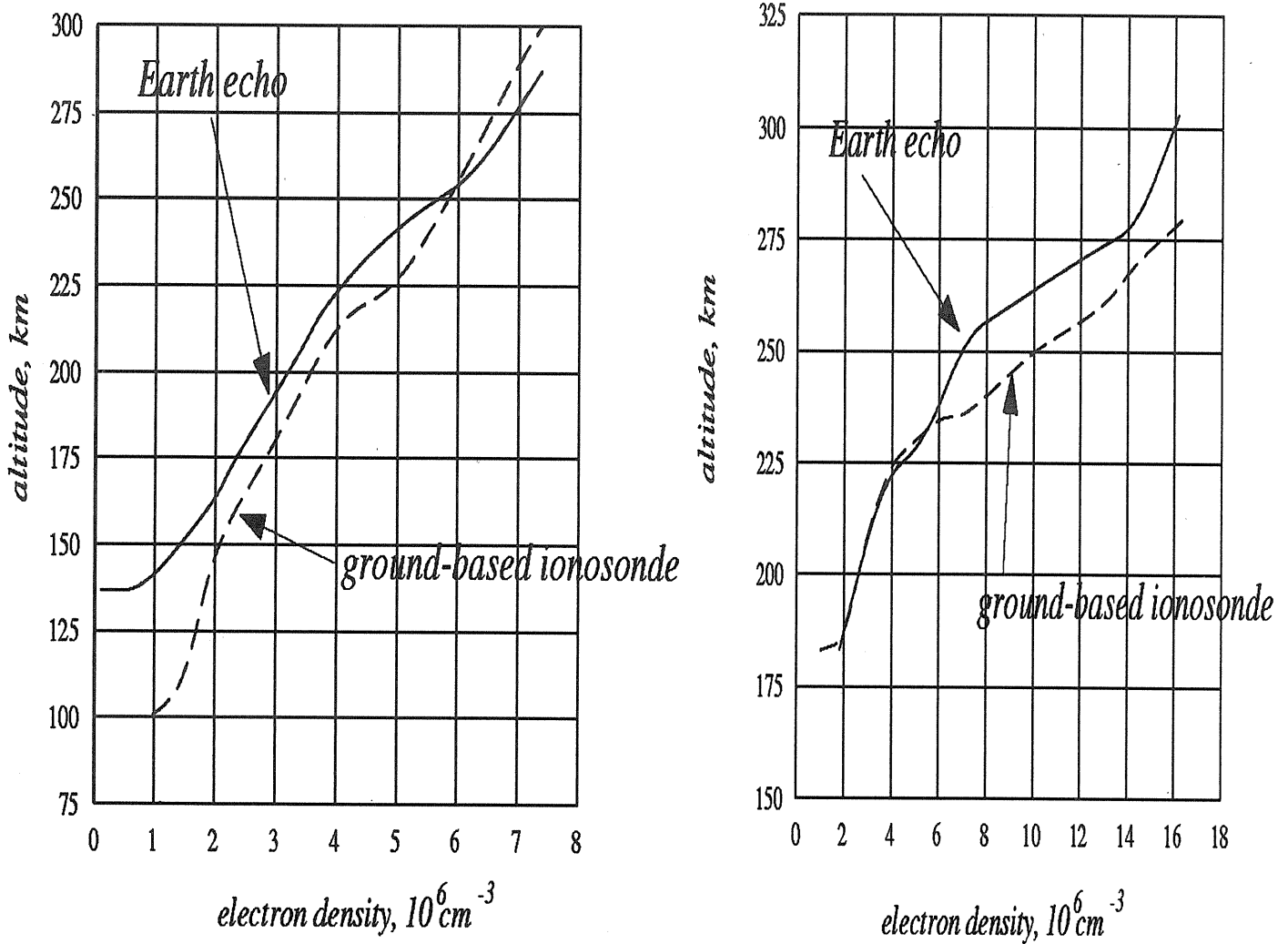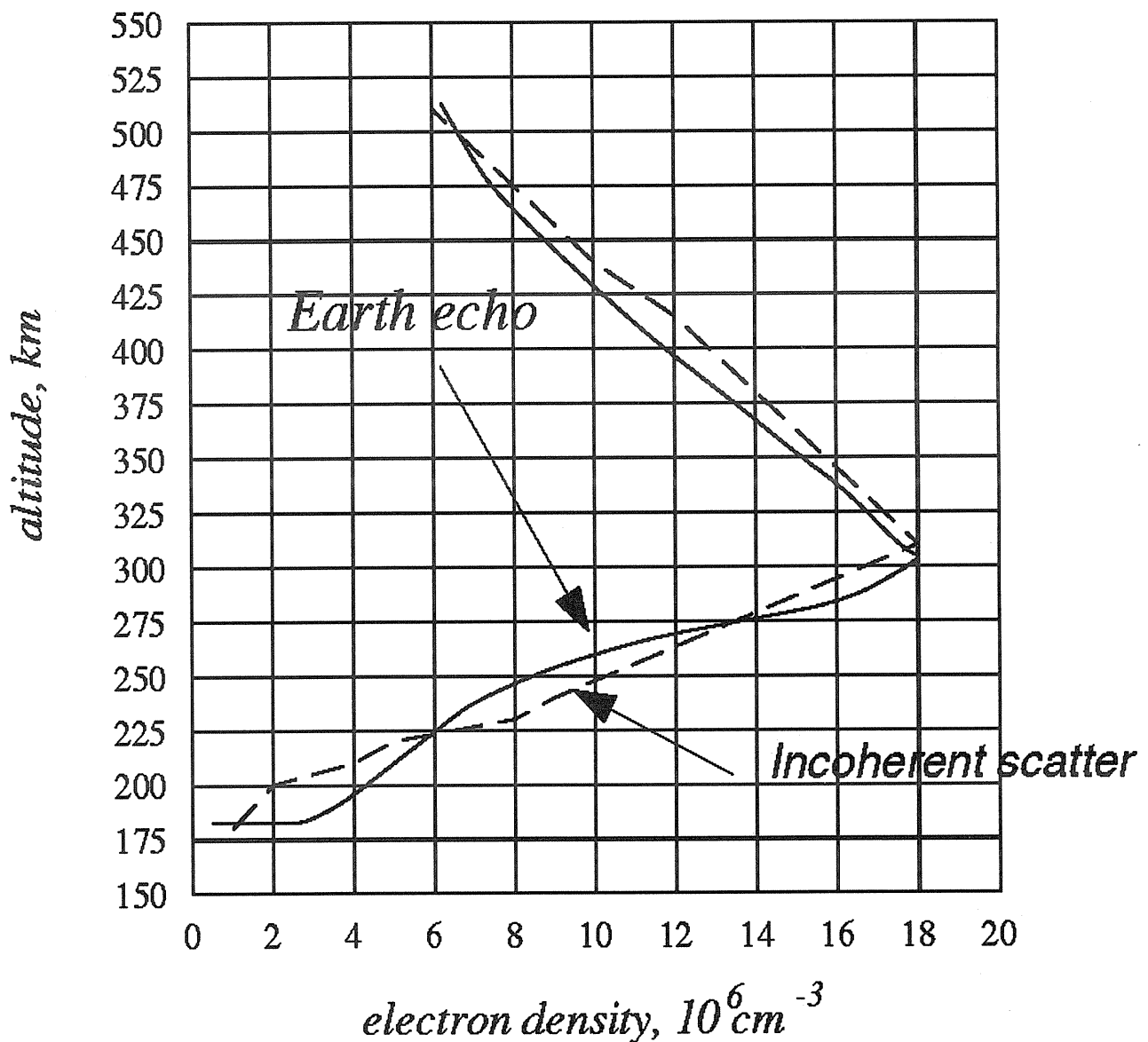
Figure 5.

By considering bottomside and topside Nh-profiles monotone the equation (2) can be changed to:

$$p'(f) = \int_0^{N\max} \mu'(n)\frac{dz}{dn}dn \qquad (3)$$

where N_{max} is maximum electron density,
z is a range between two layers with identical electron density.

Equation (3) (like equations (1) and (2)) is an ill-posed problem, so the regularization method must be used to find solutions. Good results have been obtained by using L-pseudoconversion. Figure 4 shows bottomside Nh-profiles determined by ground-based ionosonde and by satellite one. The comparison of Nh-profiles obtained by on-board ionosonde and incoherent scatter is presented in Figure 5. The results presented in these figures show that the Earth echo can be used for determining electron density. Although the assurance of this method is worse than topside and botomside sounding, it may be useful for ionospheric measuring in regions where other methods are not available.

The single ionospheric irregularities detection

To detect single ionospheric irregularities non-vertical (direct or reverse) TIS should be used. The detection of irregularities is based on the fact that radio waves with different frequencies have different trajectories. That is why when the radio pulses, having frequencies in the narrow band, traverse the irregularity there is a "bay" on the transionogram in this frequency band. Analysis of these frequency bands, for different satellite positions, makes it possible to detect the irregularity location. The method is
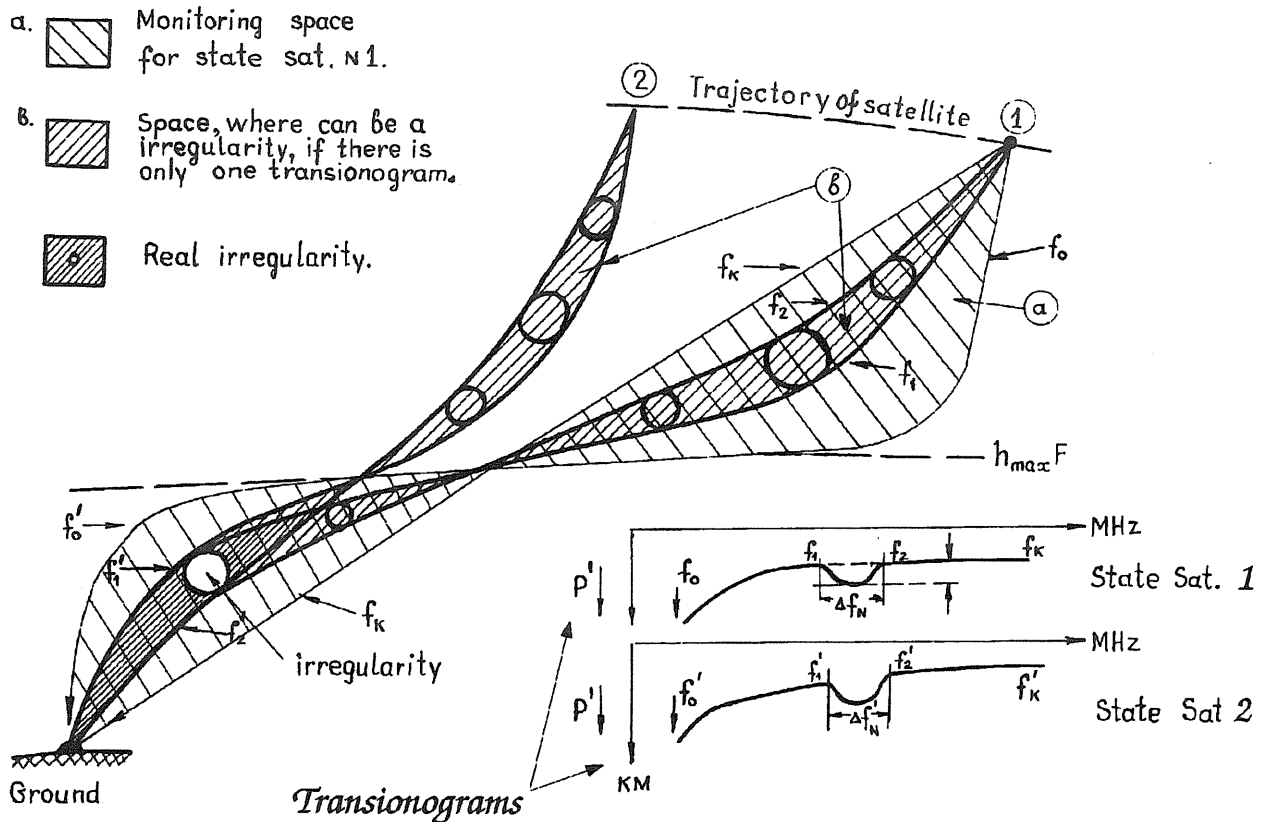
illustrated by diagram on Figure 6.

Conclusion.

We have shown that TIS is a continuation of well-known methods of ionosphere radio sounding: vertical, oblique and topside. This method can be used to obtain ionospheric data that could not be obtained by other methods.

IONOSONDE NETWORKS AND STATIONS
AUTHOR INDEX

UAG SERIES OF REPORTS

Fewer than four UAG Reports are published at irregular intervals each year. Copies of these publications may be purchased through the NATIONAL GEOPHYSICAL DATA CENTER, Solar-Terrestrial Physics Division (E/GC2) 325 Broadway, Boulder, Colorado 80303, USA. Please note that some reports are available on microfiche only at $4.00 a copy and that a $10.00 handling charge will be added. In this case orders must include check or money order payable in U.S. currency to Commerce, NOAA/NGDC.

UAG- 1 IQSY NIGHT AIRGLOW DATA, by L.L. Smith, F.E. Roach, and J.M. McKennan, ESSA Aeronomy Laboratory, Boulder, CO, July 1968, 305 pp.

UAG- 2 A REEVALUATION OF SOLAR FLARES, 1964-1966, by Helen W. Dodson and E. Ruth Hedeman, McMath-Hulbert Observatory, University of Michigan, Pontaic, MI, August 1968, 28 pp.

UAG- 3 OBSERVATIONS OF JUPITER'S SPORADIC RADIO EMISSION IN THE RANGE 7.6-41 MHZ, 6 JULY 1966 THROUGH 8 SEPTEMBER 1968, by James W. Warwick and George A. Dulk, University of Colorado, Boulder, CO, October 1968, 35 pp.

UAG- 4 ABBREVIATED CALENDAR RECORD 1966-1967, by J. Virginia Lincoln, Hope I. Leighton and Dorothy K. Kropp, ESSA [now NOAA], Aeronomy and Space Data Center, Boulder, CO, January 1969, 170 pp.

UAG- 5 DATA ON SOLAR EVENT OF MAY 23, 1967, AND ITS GEOPHYSICAL EFFECTS, compiled by J. Virginia Lincoln, World Data Center A, Upper Atmosphere Geophysics, ESSA [now NOAA], Boulder, CO, February 1969, 120 pp.

UAG- 6 INTERNATIONAL GEOPHYSICAL CALENDARS 1957-1969, by A.H. Shapley and J. Virginia Lincoln, ESSA Research Laboratories [now NOAA], Boulder, CO, March 1969, 25 pp.

UAG- 7 OBSERVATIONS OF THE SOLAR ELECTRON CORONA: FEBRUARY 1964 - JANUARY 1968, by Richard T. Hansen, High Altitude Observatory, NCAR, Boulder, CO, and Kamuela, HI, October 1969, 12 pp.

UAG- 8 DATA ON SOLAR-GEOPHYSICAL ACTIVITY OCTOBER 24 - NOVEMBER 6, 1968, Parts 1 and 2, compiled by J. Virginia Lincoln, World Data Center A, Upper Atmosphere Geophysics, ESSA [now NOAA], Boulder, CO, March 1970, 312 pp, (includes Parts 1 and 2).

UAG- 9 DATA ON COSMIC RAY EVENT OF NOVEMBER 18, 1968, AND ASSOCIATED PHENOMENA, compiled by J. Virginia Lincoln, World Data Center A, Upper Atmosphere Geophysics, ESSA [now NOAA], Boulder, CO, April 1970, 109 pp.

UAG-10 ATLAS OF IONOGRAMS, edited by A.H. Shapley, ESSA Research Laboratories [now NOAA], Boulder, CO, May 1970, 243 pp.

UAG-11 [Superseded by UAG-30]

UAG-12 SOLAR-GEOPHYSICAL ACTIVITY ASSOCIATED WITH THE MAJOR GEOMAGNETIC STORM OF MARCH 8, 1970, Parts 1, 2 and 3, compiled by J. Virginia Lincoln and Dale B. Bucknam, World Data Center A, Upper Atmosphere Geophysics, ESSA [now NOAA], Boulder, CO, April 1971, 466 pp, (includes 3 parts).

UAG-13 DATA ON THE SOLAR PROTON EVENT OF NOVEMBER 2, 1969, THROUGH THE GEOMAGNETIC STORM OF NOVEMBER 8-10, 1969, compiled by Dale B. Bucknam and J. Virginia Lincoln, World Data Center A, Upper Atmosphere Geophysics, ESSA [now NOAA], Boulder, CO, May 1971, 76 pp.

UAG-14 AN EXPERIMENTAL, COMPREHENSIVE FLARE INDEX AND ITS DERIVATION FOR 'MAJOR' FLARES, 1955-1969, by Helen W. Dodson and E. Ruth Hedeman, McMath-Hulbert Observatory, University of Michigan, Pontiac, MI, July 1971, 25 pp.

UAG-15 [Superseded by UAG-30]

UAG-16 TEMPORAL DEVELOPMENT OF THE GEOPHYSICAL DISTRIBUTION OF AURORAL ABSORPTION FOR 30 SUBSTORM EVENTS IN EACH OF IQSY (1964-65) AND IASY (1960), by F.T. Berkey, University of Alaska, Fairbanks, AK; V.M. Driatskiy, Arctic and Antarctic Research Institute, Leningrad, USSR; K. Henriksen, Auroral Observatory, Tromso, Norway; D.H. Jelly, Communications Research Center, Ottawa, Canada; T.I. Shchuka, Arctic and Antarctic Research Institute, Leningrad, USSR; A. Theander, Kiruna Geophysical Observatory, Kiruna, Sweden; and J. Yliniemi, University of Oulu, Oulu, Finland, September 1971, 131 pp, $4.00 (microfiche only).

UAG-17 IONOSPHERIC DRIFT VELOCITY MEASUREMENTS AT JICAMARCA, PERU (JULY 1967 - MARCH 1970), by Ben B. Balsley, NOAA Aeronomy Laboratory, Boulder, CO, and Ronald F. Woodman, Jicamarca Radar Observatory, Instituto Geofisico del Peru, Lima, Peru, October 1971, 45 pp, $4.00 (microfiche only).

UAG-18   A STUDY OF POLAR CAP AND AURORAL ZONE MAGNETIC VARIATIONS, by K. Kawasaki and S.-I. Akasofu, University of Alaska, Fairbanks, AK, June 1972, 21 pp.

UAG-19   REEVALUATION OF SOLAR FLARES 1967, by Helen W. Dodson and E. Ruth Hedeman, McMath-Hulbert Observatory, University of Michigan, Pontiac, MI, and Marta Rovira de Miceli, San Miguel Observatory, Argentina, June 1972, 15 pp.

UAG-20   [Superseded by UAG-30]

UAG-21   PRELIMINARY COMPILATION OF DATA FOR RETROSPECTIVE WORLD INTERVAL JULY 26 - AUGUST 14, 1972, by J. Virginia Lincoln and Hope I. Leighton, World Data Center A for Solar-Terrestrial Physics, NOAA, Boulder, CO, November 1972, 128 pp.

UAG-22   AURORAL ELECTROJET MAGNETIC ACTIVITY INDICES (AE) FOR 1970, by Joe Haskell Allen, National Geophysical and Solar-Terrestrial Data Center, Boulder, CO, November 1972, 146 pp.

UAG-23   U.R.S.I. HANDBOOK OF IONOGRAM INTERPRETATION AND REDUCTION, Second Edition, November 1972, edited by W.R. Piggott, Radio and Space Research Station, Slough, UK, and K. Rawer, Arbeitsgruppe fur Physikalische Weltraumforschung, Freiburg, GFR, November 1972, 324 pp.

UAG-23A   U.R.S.I. HANDBOOK OF IONOGRAM INTERPRETATION AND REDUCTION, Second Edition, Revision of Chapters 1-4, edited by W.R. Piggott, Radio and Space Research Station, Slough, UK, and K. Rawer, Arbeitsgruppe fur Physikalische Weltraumforschung, Freiburg, GFR, November 1972, 135 pp.

UAG-24   DATA ON SOLAR-GEOPHYSICAL ACTIVITY ASSOCIATED WITH THE MAJOR GROUND LEVEL COSMIC RAY EVENTS OF 24 JANUARY AND 1 SEPTEMBER 1971, Parts 1 and 2, compiled by Helen E. Coffey and J. Virginia Lincoln, World Data Center A for Solar-Terrestrial Physics, NOAA, Boulder, CO, December 1972, 462 pp, (includes Parts 1 and 2).

UAG-25   OBSERVATIONS OF JUPITER'S SPORADIC RADIO EMISSION IN THE RANGE 7.6-41 MHZ, 9 SEPTEMBER 1968 THROUGH 9 DECEMBER 1971, by James W. Warwick, George A. Dulk and David G. Swann, University of Colorado, Boulder, CO, February 1973, 35 pp.

UAG-26   DATA COMPILATION FOR THE MAGNETOSPHERICALLY QUIET PERIODS FEBRUARY 19-23 AND NOVEMBER 29 - DECEMBER 3, 1970, compiled by Helen E. Coffey and J. Virginia Lincoln, World Data Center A for Solar-Terrestrial Physics, NOAA, Boulder, CO, May 1973, 129 pp.

UAG-27   HIGH SPEED STREAMS IN THE SOLAR WIND, by D.S. Intriligator, University of Southern California, Los Angeles, CA, June 1973, 16 pp.

UAG-28   COLLECTED DATA REPORTS ON AUGUST 1972 SOLAR-TERRESTRIAL EVENTS, Parts 1, 2 and 3, edited by Helen E. Coffey, World Data Center A for Solar-Terrestrial Physics, NOAA, Boulder, CO, July 1973, 932 pp.

UAG-29   AURORAL ELECTROJET MAGNETIC ACTIVITY INDICES AE(11) FOR 1968, by Joe Haskell Allen, Carl C. Abston and Leslie D. Morris, National Geophysical and Solar-Terrestrial Data Center, Boulder, CO, October 1973, 148 pp.

UAG-30   CATALOGUE OF DATA ON SOLAR-TERRESTRIAL PHYSICS, prepared by NOAA Environmental Data Service, Boulder, CO, October 1973, 317 pp. Supersedes catalogs UAG-11, 15 and 20.

UAG-31   AURORAL ELECTROJET MAGNETIC ACTIVITY INDICES AE(11) FOR 1969, by Joe Haskell Allen, Carl C. Abston and Leslie D. Morris, National Geophysical and Solar-Terrestrial Data Center, Boulder, CO, February 1974, 142 pp.

UAG-32   SYNOPTIC RADIO MAPS OF THE SUN AT 3.3 MM FOR THE YEARS 1967-1969, by Earle B. Mayfield, Kennon P. White III, and Fred I. Shimabukuro, Aerospace Corp., El Segundo, CA, April 1974, 26 pp.

UAG-33   AURORAL ELECTROJET MAGNETIC ACTIVITY INDICES AE(10) FOR 1967, by Joe Haskell Allen, Carl C. Abston and Leslie D. Morris, National Geophysical and Solar-Terrestrial Data Center, Boulder, CO, May 1974, 142 pp.

UAG-34   ABSORPTION DATA FOR THE IGY/IGC AND IQSY, compiled and edited by A.H. Shapley, National Geophysical and Solar-Terrestrial Data Center, Boulder, CO; W.R. Piggott, Appleton Laboratory, Slough, UK; and K. Rawer, Arbeitsgruppe fur Physikalische Weltraumforschung, Freiburg, GFR, June 1974, 381 pp.

UAG-35   [Superseded by UAG-92]

UAG-36	AN ATLAS OF EXTREME ULTRAVIOLET FLASHES OF SOLAR FLARES OBSERVED VIA SUDDEN FREQUENCY DEVIATIONS DURING THE ATM-SKYLAB MISSIONS, by R.F. Donnelly and E.L. Berger, NOAA Space Environment Laboratory; Lt. J.D. Busman, NOAA Commissioned Corps; B. Henson, NASA Marshall Space Flight Center; T.B. Jones, University of Leicester, UK; G.M. Lerfald, NOAA Wave Propagation Laboratory; K. Najita, University of Hawaii; W.M. Retallack, NOAA Space Environment Laboratory and W.J. Wagner, Sacramento Peak Observatory, October 1974, 95 pp.
UAG-37	AURORAL ELECTROJET MAGNETIC ACTIVITY INDICES AE(10) FOR 1966, by Joe Haskell Allen, Carl C. Abston and Leslie D. Morris, National Geophysical and Solar-Terrestrial Data Center, Boulder, CO, December 1974, 142 pp.
UAG-38	MASTER STATION LIST FOR SOLAR-TERRESTRIAL PHYSICS DATA AT WDC-A FOR SOLAR-TERRESTRIAL PHYSICS, by R.W. Buhmann, World Data Center A for Solar-Terrestrial Physics, Boulder, CO; Juan D. Roederer, University of Denver, Denver, CO; and M.A. Shea and D.F. Smart, Air Force Cambridge Research Laboratories, Hanscom AFB, MA, December 1974, 110 pp.
UAG-39	AURORAL ELECTROJET MAGNETIC ACTIVITY INDICES AE(11) FOR 1971, by Joe Haskell Allen, Carl C. Abston and Leslie D. Morris, National Geophysical and Solar-Terrestrial Data Center, Boulder, CO, February 1975, 144 pp.
UAG-40	H-ALPHA SYNOPTIC CHARTS OF SOLAR ACTIVITY FOR THE PERIOD OF SKYLAB OBSERVATIONS, MAY 1973 MARCH 1974, by Patrick S. McIntosh, NOAA Space Environment Laboratory, Boulder, CO, February 1975, 32 pp.
UAG-41	H-ALPHA SYNOPTIC CHARTS OF SOLAR ACTIVITY DURING THE FIRST YEAR OF SOLAR CYCLE 20 OCTOBER 1964 AUGUST 1965, by Patrick S. McIntosh, NOAA Space Environment Laboratory, Boulder, CO, and Jerome T. Nolte, American Science and Engineering, Inc., Cambridge, MA, March 1975, 25 pp.
UAG-42	OBSERVATIONS OF JUPITER'S SPORADIC RADIO EMISSION IN THE RANGE 7.6-80 MHZ, 10 DECEMBER 1971 THROUGH 21 MARCH 1975, by James W. Warwick, George A. Dulk and Anthony C. Riddle, University of Colorado, Boulder, CO, April 1975, 49 pp.
UAG-43	CATALOG OF OBSERVATION TIMES OF GROUND-BASED SKYLAB-COORDINATED SOLAR OBSERVING PROGRAMS, compiled by Helen E. Coffey, World Data Center A for Solar-Terrestrial Physics, NOAA, Boulder, CO, May 1975, 159 pp.
UAG-44	SYNOPTIC MAPS OF SOLAR 9.1 CM MICROWAVE EMISSION FROM JUNE 1962 TO AUGUST 1973, by Werner Graf and Ronald N. Bracewell, Stanford University, Stanford, CA, May 1975, 183 pp.
UAG-45	AURORAL ELECTROJET MAGNETIC ACTIVITY INDICES AE(11) FOR 1972, by Joe Haskell Allen, Carl C. Abston and Leslie D. Morris, National Geophysical and Solar-Terrestrial Data Center, Boulder, CO, May 1975, 144 pp, $4.00 (microfiche only).
UAG-46	INTERPLANETARY MAGNETIC FIELD DATA 1963-1964, by Joseph H. King, National Space Science Data Center, NASA Goddard Space Flight Center, Greenbelt, MD, June 1975, 382 pp.
UAG-47	AURORAL ELECTROJET MAGNETIC ACTIVITY INDICES AE(11) FOR 1973, by Joe Haskell Allen, Carl C. Abston and Leslie D. Morris, National Geophysical and Solar-Terrestrial Data Center, Boulder, CO, June 1975, 144 pp, $4.00 (microfiche only).
UAG-48	[Superseded by UAG-48A]
UAG-48A	SYNOPTIC OBSERVATIONS OF THE SOLAR CORONA DURING CARRINGTON ROTATIONS 1580-1596 (11 OCTOBER 1971 - 15 JANUARY 1973), [Re-issue of UAG-48 with quality images], by R.A. Howard, M.J. Koomen, D.J. Michels, R. Tousey, C.R. Detwiler, D.E. Roberts, R.T. Seal, and J.D. Whitney, U.S. Naval Research Laboratory, Washington, DC; and R.T. Hansen and S.F. Hansen, C.J. Garcia and E. Yasukawa, High Altitude Observatory, NCAR, Boulder, CO, February 1976, 200 pp. Supersedes UAG-48.
UAG-49	[Superseded by UAG-92]
UAG-50	HIGH-LATITUDE SUPPLEMENT TO THE URSI HANDBOOK ON IONOGRAM INTERPRETATION AND REDUCTION, edited by W.R. Piggott, British Antarctic Survey, c/o Appleton Laboratory, Slough, UK, October 1975, 294 pp.
UAG-51	SYNOPTIC MAPS OF SOLAR CORONAL HOLE BOUNDARIES DERIVED FROM HE II 304A SPECTROHELIOGRAMS FROM THE MANNED SKYLAB MISSIONS, by J.D. Bohlin and D.M. Rubenstein, U.S. Naval Research Laboratory, Washington, DC, November 1975, 30 pp.

UAG-70　　　　ANNOTATED ATLAS OF H-ALPHA SYNOPTIC CHARTS FOR SOLAR CYCLE 20 (1964-1974) CARRINGTON SOLAR ROTATIONS 1487-1616, by Patrick S. McIntosh, NOAA Space Environment Laboratory, Boulder, CO, February 1979, 327 pp.

UAG-71　　　　MAGNETIC POTENTIAL PLOTS OVER THE NORTHERN HEMISPHERE FOR 26-28 MARCH 1976, A.D. Richmond, NOAA Space Environment Laboratory, Boulder, CO; H.W. Kroehl, National Geophysical and Solar-Terrestrial Data Center, Boulder, CO; M.A. Henning, Lockheed Missiles and Space Co., Aurora, CO; and Y. Kamide, Kyoto Sangyo University, Kyoto, Japan, April 1979, 118 pp.

UAG-72　　　　ENERGY RELEASE IN SOLAR FLARES, PROCEEDINGS OF THE WORKSHOP ON ENERGY RELEASE IN FLARES, 26 FEBRUARY - 1 MARCH 1979, CAMBRIDGE, MASSACHUSETTS, U.S.A., edited by David M. Rust, American Science and Engineering, Inc., Cambridge, MA; and A. Gordon Emslie, Harvard-Smithsonian Center for Astrophysics, Cambridge, MA, July 1979, 68 pp, $4.00 (microfiche only).

UAG-73　　　　AURORAL ELECTROJET MAGNETIC ACTIVITY INDICES AE(11-12) FOR JANUARY - JUNE 1975, by Joe Haskell Allen, Carl C. Abston, J.E. Salazar and J.A. McKinnon, National Geophysical and Solar-Terrestrial Data Center, NOAA, Boulder, CO, August 1979, 114 pp, $4.00 (microfiche only).

UAG-74　　　　ATS-6 RADIO BEACON ELECTRON CONTENT MEASUREMENTS AT OOTACAMUND, INDIA, OCTOBER - JULY 1976, by S.D. Bouwer, K. Davies, R.F. Donnelly, R.N. Grubb, J.E. Jones and J.H. Taylor, NOAA Space Environment Laboratory, Boulder, CO; and R.G. Rastogi, M.R. Deshpande, H. Chandra and G. Sethia, Physical Research Laboratory, Ahmedabad, India, March 1980, 58 pp.

UAG-75　　　　THE ALASKA IMS MERIDIAN CHAIN: MAGNETIC VARIATIONS FOR 9 MARCH - 27 APRIL 1978, by H.W. Kroehl and G.P. Kosinski, National Geophysical and Solar-Terrestrial Data Center, Boulder, CO; S.-I. Akasofu, G.J. Romick, C.E. Campbell and G.K. Corrick, University of Alaska, Fairbanks, AK; and C.E. Hornback and A.M. Gray, NOAA Space Environment Laboratory, Boulder, CO, June 1980, 107 pp.

UAG-76　　　　AURORAL ELECTROJET MAGNETIC ACTIVITY INDICES AE(12) FOR JULY - DECEMBER 1975, by Joe Haskell Allen, Carl C. Abston, J.E. Salazar and J.A. McKinnon, National Geophysical and Solar-Terrestrial Data Center, NOAA, Boulder, CO, August 1980, 116 pp.

UAG-77　　　　SYNOPTIC SOLAR MAGNETIC FIELD MAPS FOR THE INTERVAL INCLUDING CARRINGTON ROTATIONS 1601-1680, MAY5, 1973 - APRIL 26, 1979, by J. Harvey, B. Gillespie, P. Miedaner and C. Slaughter, Kitt Peak National Observatory, Tucson, AZ, August 1980, 66 pp.

UAG-78　　　　THE EQUATORIAL LATITUDE OF AURORAL ACTIVITY DURING 1972-1977, by N.R. Sheeley, Jr. and R.A. Howard, E.O. Hulbert Center for Space Research, U.S. Naval Research Laboratory, Washington, DC and B.S. Dandekar, Air Force Geophysics Laboratory, Hanscom AFB, MA, October 1980, 61 pp.

UAG-79　　　　SOLAR OBSERVATIONS DURING SKYLAB, APRIL 1973 - FEBRUARY 1974, I. CORONAL X-RAY STRUCTURE, II. SOLAR FLARE ACTIVITY, by J.M. Hanson, University of Michigan, Ann Arbor, MI; and E.C. Roelof and and R.E. Gold, The Johns Hopkins University, Laurel, MD, December 1980, 43 pp.

UAG-80　　　　EXPERIMENTAL COMPREHENSIVE SOLAR FLARE INDICES FOR 'MAJOR' AND CERTAIN LESSER FLARES, 1975-1979, compiled by Helen W. Dodson and E. Ruth Hedeman, The Johns Hopkins University, Laurel, MD, July 1981, 33 pp.

UAG-81　　　　EVOLUTIONARY CHARTS OF SOLAR ACTIVITY (CALCIUM PLAGES) AS FUNCTIONS OF HELIOGRAPHIC LONGITUDE AND TIME, 1964-1979, by E. Ruth Hedeman, Helen W. Dodson and Edmond C. Roelof, The Johns Hopkins University, Laurel, MD, August 1981, 103 pp.

UAG-82　　　　INTERNATIONAL REFERENCE IONOSPHERE - IRI 79, edited by J. Virginia Lincoln and Raymond O. Conkright, National Geophysical and Solar-Terrestrial Data Center, NOAA, Boulder, CO, November 1981, 243 pp.

UAG-83　　　　SOLAR-GEOPHYSICAL ACTIVITY REPORTS FOR SEPTEMBER 7-24, 1977 AND NOVEMBER 22, 1977, Parts 1 and 2, compiled by John A. McKinnon and J. Virginia Lincoln, World Data Center A for Solar-Terrestrial Physics, NOAA, Boulder, CO, February 1982, 553 pp.

UAG-84　　　　CATALOG OF AURORAL RADIO ABSORPTION DURING 1976-1979 AT ABISKO, SWEDEN, by J.K. Hargreaves, C.M. Taylor and J.M. Penman, Environmental Sciences Department, University of Lancaster, Lancaster, UK, July 1982, 69 pp.

UAG-85　　　　[Superseded by UAG-91]

UAG-86　　　　[Superseded by UAG-92]

UAG-87   CHANGES IN THE GLOBAL ELECTRIC FIELDS AND CURRENTS FOR MARCH 17-19, 1978, FROM SIX IMS MERIDIAN CHAINS OF MAGNETOMETERS, by Y. Kamide, Kyoto Sangyo University, Kyoto, Japan; H.W. Kroehl, National Geophysical Data Center, NOAA, Boulder, CO; and A.D. Richmond, NOAA Space Environment Laboratory, Boulder, CO, November 1982, 102 pp.

UAG-88   NUMERICAL MODELING OF IONOSPHERIC PARAMETERS FROM GLOBAL IMS MAGNETOMETER DATA FOR THE CDAW-6 INTERVALS, by Y. Kamide, Kyoto Sangyo University, Kyoto, Japan; H.W. Kroehl, National Geophysical Data Center, NOAA, Boulder, CO; and B.A. Hausman, National Geophysical Data Center, NOAA, Boulder, CO, November 1983, 197 pp.

UAG-89   ATMOSPHERIC HANDBOOK: ATMOSPHERIC DATA TABLES AVAILABLE ON COMPUTER TAPE, by V.E. Derr, NOAA Environmental Research Laboratories, Boulder, CO, July 1984, 56 pp.

UAG-90   EXPERIENCE WITH PROPOSED IMPROVEMENTS OF THE INTERNATIONAL REFERENCE IONOSPHERE (IRI): CONTRIBUTED PAPERS, MAINLY FROM THE URSI-COSPAR WORKSHOP HELD IN BUDAPEST IN 1980, edited by K. Rawer, University of Freiburg, Federal Republic of Germany, and C.M. Minnis, International Union of Radio Science (URSI), Brussels, Belgium, May 1984, 233 pp.

UAG-91   COMBINED CATALOG OF IONOSPHERE VERTICAL SOUNDINGS DATA, compiled by Raymond O. Conkright and Marcus O. Ertle, National Geophysical Data Center, NOAA, Boulder, CO, December 1984, 174 pp.

UAG-92   INTERNATIONAL CATALOG OF GEOMAGNETIC DATA, compiled by C.C. Abston, National Geophysical Data Center, NOAA, Boulder, CO; N.E. Papitashvili, Academy of Sciences of the USSR, World Data Center B2, Moscow, USSR; and V.O. Papitashvili, IZMIRAN, Moscow Region, USSR, August 1985, 291 pp. Supersedes UAG-35, 49, and 86.

UAG-93   IONOGRAM ANALYSIS WITH THE GENERALIZED PROGRAM POLAN, by J.E. Titheridge, University of Auck land, New Zealand, December 1985, 194 pp.

UAG-94   THE SOLAR MAGNETIC FIELD--1976 THROUGH 1985: AN ATLAS OF PHOTOSPHERIC MAGNETIC FIELD OBSERVATIONS AND COMPUTED CORONAL MAGNETIC FIELDS FROM THE JOHN M. WILCOX SOLAR OBSERVATORY AT STANFORD, by J. Todd Hoeksema and Philip H. Scherrer, Center for Space Science and Astrophysics, Stanford University, Stanford, CA, January 1986, 370 pp.

UAG-95   SUNSPOT NUMBERS: 1610-1985, (based on THE SUNSPOT-ACTIVITY IN THE YEARS 1610-1960, by Prof. M. Waldmeier, Copyright 1961, Swiss Federal Observatory, Zurich, Switzerland), revised by John A. McKinnon, National Geophysical Data Center, NOAA, Boulder, CO, January 1987, 112 pp.

UAG-96   SOLAR-GEOPHYSICAL ACTIVITY REPORTS FOR STIP INTERVAL XV, 12-21 February 1984 Ground Level Event, AND STIP INTERVAL XVI, 20 April - 4 May 1984 Forbush Decrease, compiled by Helen E. Coffey and Joe H. Allen, National Geophysical Data Center, NOAA, Boulder, CO, July 1987, 418 pp.

UAG-97   NUMERICAL MODELING OF POLAR IONOSPHERIC ELECTRODYNAMICS FOR JULY 23-24, 1983, UTILIZING IONOSPHERIC CONDUCTANCES DEDUCED FROM DMSP X-RAY IMAGES, by B.-H. Ahn, Kyungpook National University, Taegu, Korea; E. Friis-Christensen, Division of Geophysics, Danish Meteorological Institute, Copenhagen, Denmark; D.J. Gorney, Space Sciences Laboratory, The Aerospace Corporation, Los Angeles, CA; Y. Kamide, Kyoto Sangyo University, Kyoto, Japan; and H.W. Kroehl, National Geophysical Data Center, NOAA, Boulder, CO, April 1988, 133 pp.

UAG-98   TYPE II SOLAR RADIO BURSTS RECORDED AT WEISSENAU 1966-1987, by H.W. Urbarz, Astronomical Institute of Tubingen University, Weissenau Station, 7980 Rasthalde, Ravensburg, GFR, February 1990, 86 pp.

UAG-99   PROCEEDINGS OF THE WORKSHOP ON GEOPHYSICAL INFORMATICS, MOSCOW, AUGUST 14-18, 1988, edited by J.H. Allen, National Geophysical Data Center, NOAA, Boulder, CO; and V.A. Nechitailenko, Soviet Geophysical Committee, Academy of Sciences of the USSR, Moscow, USSR, January 1991, 304 pp.

UAG-100   CATALOGUE OF SOLAR FILAMENT DISAPPEARANCES 1964-1980, by C.S. Wright, Electronics Research Laboratory, Defence Science and Technology Organisation, Salisbury, South Australia 5108, Australia, February 1991, 62 pp.

UAG-101   ATLAS OF STACKPLOTS DERIVED FROM SOLAR SYNOPTIC CHARTS, Evolution of Large-Scale Magnetic Fields and Coronal Holes from H-alpha Synoptic Charts: 1966-1987, by P.S. McIntosh, NOAA Space Environment Laboratory, Boulder, CO; and E.C. Willock and R.J. Thompson, IPS Radio and Space Services, West Chatswood, New South Wales 2057, Australia, October 1991, 188 pp.

UAG-102   CATALOGUE OF CORONAL HOLES 1970-1991, A.Sanchez Ibarra, Centro de Investigacion en Fisica, Universidad de Sonora, Hermosillo, Sonora, Mexico; and M. Barraza-Paredes, Centro de Investigacion en Astronomia Solar, CIAS, Hermosillo, Sonora, Mexico, October 1992, 64 pp.

UAG-103   GEOMAGNETIC POLAR CAP (PC) INDEX, S. Vennerstrøm and E. Friis-Christensen, Division of Geophysics, Danish Meteorological Institute, Copenhagen, Denmark; O.A. Troshichev and V.G. Andresen, Department of Geophysics, Arctic and Antarctic Research Institute, St. Petersburg, Russia, April 1994, 274 pp.